Saint-Petersburg State University

On the rights of the manuscript

Titov Vladimir Borisovich

General three body problem in the shape space

Scientific speciality 1.3.1.

Space physics, astronomy

Dissertation for the degree

Doctor of Physical and Mathematical Sciences

Saint Petersburg — 2024

Contents

Стр.

Стр.

Introduction

The three-body problem is a challenge with a centuries-old history and remarkable achievements, but it has yet to receive a complete analytical solution, despite the efforts of outstanding mathematicians and astronomers. The history of the problem can be traced back to ancient times, but in its modern form, it has been known since the time of Newton, or perhaps Kepler. There is a certain analogy between the three-body problem and Fermat's Last Theorem. Both problems are easily formulated. Their formulations can be understood by a high school student. However, despite the simple and transparent formulations, finding their solutions is extremely difficult. Proving Fermat's theorem took more than 350 years. For three and a half centuries, the search for a proof led to new heights in mathematics. This is very similar to the role of the three-body problem in mathematics. Of course, the three-body problem, in addition to its theoretical significance, also has purely practical applications. An analytical solution would allow for the construction of more accurate theories of the motion of celestial bodies (both artificial and natural). This is a practical task; in the absence of a solution, perturbation methods have been developed that allow predicting the positions of celestial bodies with very high accuracy. Similar to Fermat's theorem, the search for a solution to the three-body problem led to the development of entire branches of mathematics: the theory of functions of a complex variable, dynamical systems, chaos. Euler, Lagrange, Laplace, Hamilton, Poincaré, ... – this list can be a list of the greatest mathematicians and, with the same right, a list of the greatest astronomers. Fermat's Last Theorem was proven three and a half centuries after its formulation. The three-body problem, despite the greatest achievements, has not received a final solution in almost three and a half centuries. At the beginning of the 20th century, Karl Sundman [67—69] found a general analytical solution to the three-body problem (with non-zero angular momentum) in the form of everywhere convergent series. Unfortunately, this magnificent theoretical result does not provide any knowledge about the properties of the solutions, as these

series converge extremely slowly. In some sense, Sundman's result is simply a theorem on the existence of an (analytical) solution to the three-body problem.

Without knowing the complete solution, we can nevertheless study the properties of these solutions. These properties are certainly a consequence of the properties of the equations of motion (symmetries, properties of the force function, etc.). If the system is closed, then the amount of motion is conserved, and we have for the center of mass of the system $\mathbf{r}_{\text{cm}} = \frac{\sum_{i=1}^{n} m_i \mathbf{r}_i}{M} = \mathbf{C}_1 t + \mathbf{C}_0$, ($\mathbf{C}_0$ and $\mathbf{C}_1$ are constant vectors). For closed systems, the kinetic moment is also conserved: $\sum_{i=1}^{n} m_i \, \mathbf{r}_i \times \dot{\mathbf{r}}_i = \mathbf{J}$. For a conservative system, the total energy $T + \Pi = h = \text{const}$ is also conserved.

At the end of the XIX-th century, Bruns and Poincaré proved that there are no other first integrals, except for the already known ten classical ones. Bruns proved that there are no other algebraic integrals in terms of coordinates and velocities, and shortly after, Poincaré proved that there are no other analytical integrals. Thus, we have only ten classical first integrals, which are obtained when we consider closed, conservative systems, regardless of the form of the potential function, taking into account only its general properties. This is sufficient to solve the two-body problem but insufficient if the number of bodies $N \geqslant 3$.

Let us list them again:

1. The first six integrals, the integrals of the amount of motion, have been known since the time of Galileo: the center of mass of a closed system of bodies (i.e., a system of bodies not acted upon by external forces) moves in a straight line uniformly.
2. If the moment of external forces (relative to a fixed center) is zero, then the kinetic moment of the system of bodies is constant, which gives three more integrals.
3. In a conservative system, the total energy is constant, and thus, we have a total of ten integrals.

From the ten classical first integrals, important properties of the solutions to the N-body problem are derived. Using another general property of the potential function,

namely homogeneity, the Lagrange-Jacobi identity was obtained, from which important consequences are derived. Here are some of them:

- If the constant of energy for the N-body system is negative, then at least one of the mutual distances is bounded.
- If the constant of energy for the N-body system is non-negative, then at least one of the bodies must move away to an infinitely large distance (from the barycenter of the system).
- If a collision of all N bodies at one point occurs, it will happen in a finite amount of time.
- For the simultaneous collision of N bodies at one point in the space, the angular momentum (or the constant of areas) of the system must be zero.

It should be emphasized that all the listed (and many other) properties of the three-body problem, as well as the first integrals, are derived from the most general properties of the equations of motion and are valid for any N. For $N = 3$, another property can be obtained: if the angular momentum is zero, then the motion is planar.

Let us look at the first integrals of the problem from another perspective. According to Noether's theorem, each integral corresponds to a group of transformations of the space $\mathbb{R}^3$. For our problem, the first group of integrals (Galilean) corresponds to the translation (movement) of space, the integral of angular momentum corresponds to the group of rotations, and the energy integral (autonomous system, potential does not depend on time) corresponds to the time shift.

Thus, we can seek solutions as a class of invariance with respect to a certain group of transformations. In the two-body problem, for example, such a class is the conic section, defined by size and shape (semi-axis and eccentricity), all sections that can be obtained from one of its representatives through rotation. All orbits of the class can be considered as one orbit of the two-body problem. Other groups can also be used, for example, in the works [80—82], a two-parameter group of translations in the (two-dimensional) velocity space is used. In the three-body problem, symmetry was implicitly used by Lagrange, who sought (a particular) solution defined by three mutual distances. Lagrange's equilateral triangular solution represents a class of congruent

(equilateral) triangles. The importance of considering the configuration of the three bodies was noted by A. Poincaré (see [53]), and this work is discussed in detail in [15]; useful references can be found in the works of A. Chenciner [1; 11; 12; 14; 110], Marchal [97], and Saari [40; 41; 55—57; 100]. Lagrange's solution [29] and the collinear solution found by Euler [19] a few years earlier remained the only known exact partial solutions to the three-body problem for more than two hundred years. The next partial solution to the three-body problem with equal masses was discovered in 2000 and is also associated with a certain group of symmetry. It becomes desirable to consider the solutions to the three-body problem in a space invariant with respect to groups of transformations that map the solutions of the three-body problem into (generally speaking, other) solutions of the problem. As it turns out, if we factorize the configuration space by such groups (translation group and rotation group), we can study the orbits of the three-body problem in such a factorized space. This space first appeared in the three-body problem in the work of J. Lemaitre, and later, at the end of the last century and the beginning of the 21st century, it became known as the *shape space* [24]. In the planar three-body problem, this is the space of congruent triangles of the configuration of three bodies; in the spatial problem, the orientation of the plane of the three bodies must also be added.

The dimension of the phase space of the general three-body problem is 18: 3 bodies $\times$ (3 coordinates of position plus 3 coordinates of velocity). By considering barycentric systems, we can reduce the dimension to 12, and by restricting ourselves to the planar problem, to 8. The dimension of the configuration space in this case is 4. Such a configuration space can be reduced to a three-dimensional space, where it is easier to visualize, for example, regions of possible motion and surfaces bounding these regions, similar to the regions built by V. G. Golubev [94]. A point in such a space represents a class of congruent triangles, considering that the center of mass of the three bodies at the vertices of this triangle is placed at the barycenter; such a point determines both the size and shape of the triangle, and knowing the motion of this point, we can easily obtain the positions of all three bodies by quadrature.

The goal of this dissertation is to present the solutions of the three-body problem in shape space, study the properties of the solutions in this space, and determine the region of possible motion of the three-body problem. Considering the problem in shape space allows investigating various properties that give an understanding of the general properties of the problem. In the planar three-body problem, the shape space is three-dimensional. Therefore, the three-body problem in this space simplifies and allows the natural visualization of the solutions. The obtained regions of possible motion have a clear appearance, and the constructed degenerate orbits allow for a simple analysis of their properties.

To achieve this goal, it was necessary to solve the following **problems**:

1. Derive formulas for transforming the initial rectangular coordinates of the three bodies into the coordinates of the shape space and consider special points in this space.
2. Calculate periodic orbits that are then used to study the properties of these orbits in shape space.
3. Determine the regions of possible motion and zero-velocity surfaces in shape space.
4. Regularize the equations of motion in shape space for degenerate cases.
5. Obtain examples of degenerate orbits and examine their properties.

The relevance of the proposed work follows from the relevance of the three-body problem, the solution of which would have not only theoretical significance as the solution to a problem that has fascinated astronomers and mathematicians for over three centuries, but also practical significance for constructing theories of celestial motion, astronautics, etc. The obtained results provide a new perspective on the solutions of the three-body problem.

Evaluation of results. The main results of the dissertation research were presented in reports at international conferences:

– “Few-Body Problem: Theory and Computer Simulations”, Turku, 2005,
– “CelMec-V” (Celestial Mechanics-V), Viterbo, Italy, 2009,
– “CelMec-VI” (Celestial Mechanics-VI), Viterbo, Italy, 2013,

– “CelMec-VII” (Celestial Mechanics-VII), Viterbo, Italy, 2017,
– “8-th Polyakhovskie readings”, Saint Petersburg, 2018,
– “9-th Polyakhovskie readings”, Saint Petersburg, 2021,
– “Triple Evolution and Dynamics 3” (Evolution and Dynamics of Triple System-3), USA (online), 2021,
– “PCA-2022” (Polynomial Computer Algebra-2022), Saint Petersburg, 2022,
– “CelMec-VIII” (Celestial Mechanics-VIII), Италия (online), 2022,
– “PCA-2023” (Polynomial Computer Algebra-2023), Saint Petersburg, 2023,
– “PCA-2024” (Polynomial Computer Algebra-2024), Saint Petersburg, 2024.

Publications. The main results on the topic of the dissertation are presented in:

1. *Titov V. B.* Groups of transformations of phase trajectories in the two-body problem // Astronomiya i geodeziya. – 1985. – T. 13. – C. 11–21.

2. *Titov V. B.* Isoenergetic transformations in the two-body problem // Leningradskii Universitet Vestnik Matematika Mekhanika Astronomiia. – 1986. – C. 116–118.

3. *Titov V. B.* On a geometric method for determining an unperturbed orbit from observations using group transformations // Kinematics and physics of celestial bodies. – 1987. – Vol. 3, № 4, p. 26–29 (in russian).

4. *Titov V.* Symmetrical periodic orbits in the three body problem - the variational approach
   Few-Body Problem: Theory and Computer Simulations. – University of Turku, Finland, 2006. – C. 9.

5. *Титов В. Б.* Periodic orbits of general three body problem with zero angular moment // Nonlinear dynamics. – 2012. – T. 8, № 2. – C. 377–389.

6. *Titov V.* Three-body problem periodic orbits with vanishing angular momentum // Astronomische Nachrichten. – 2015. – T. 336, № 3. – C. 271-275.

7. *Orlov V. V.,, Titov V. B., Shombina L. A.* Periodic orbits in the free-fall three-body problem // Astronomy Reports. – 2016. – T. 60, № 12. – C. 1083–1089.

8. *Titov V.* Some solutions of the general three body problem in form space // 8th Polyakhov's Reading. Vol. 1959 / ed. by E. Kustova [et al.]. – United State: American Institute of Physics, 2018.

9. *Kholshevnikov K. V. [et all]* A Problem Found in the Position Shift Norm of a Celestial Body in Dynamical Astronomy // Astronomy Reports. – 2020. – V. 64, № 4. – P. 369–373.

10. *Kholshevnikov K. V. [et all]* Deflecting an Asteroid with a Low-Thrust Tangential Engine to the Orbit // Astronomy Reports. – 2020. – V. 64, № 9. – P. 785–794.

11. *Kholshevnikov K. V, Titov V. B.* Minimal Velocity Surface in a Restricted Circular Three-Body Problem // Vestnik St. Petersburg University, Mathematics, 2020, V. 53, No. 4, pp. 473–479.

12. *Titov V.* Some properties of Lemaitre regularization: Collinear trajectories // Astronomische Nachrichten. – 2021. – T. 342, № 3. – C. 588–597.

13. *Titov V.* Some properties of Lemaitre regularization. II isosceles trajectories and figure-eight // Astronomische Nachrichten. – 2022. – T. 343, № 3. – e14006.

14. *Titov V.* The regions of possible motion in the general three bodies problem // Zap. nauchn. sem. POMI. – 2022. – V. 517. – P. 225–249 (in russian).

15. *Titov V.* Zero-Velocity Surface in the General Three-Body-Problem // Vestnik St. Petersburg University, Mathematics, 2023, V. 56, No. 1, pp. 125–133.

Personal contribution. The author performed works 1-6, 8, 12-15. In work 7, the author formulated the problem in shape space and supervised the computational part carried out by graduate student L. Shombina. V. V. Orlov linked this work with his approach to the three-body problem, implemented in his works and those of his students. In work 9, K. V. Kholshevnikov provided general guidance. The author derived and verified the formulas using computer algebra. Work 10 is a continuation of the previous work, where the derived formulas are applied to the specific task of deflecting an asteroid using a low-thrust engine. Work 11 is devoted to the minimal velocity

surfaces in the restricted three-body problem. The idea of using averaging belongs to K. V. Kholshevnikov; the author conducted the analysis of the resulting surfaces and calculated these surfaces in the Pluto-Charon-satellite system.

Reliability The reliability of the obtained results is confirmed by agreement with the results of other authors and the results of numerical integration.

Scientific novelty:

1. Invariant configurations in the shape space of the general three-body problem were obtained for the first time.
2. Projections of the found periodic orbits onto the shape sphere and their properties were considered for the first time.
3. For the first time, regions of possible motion are constructed in the form space of the planar general three body problem.
4. The minimal velocities regions in a restricted three-body problem averaged over the longitude of the primary bodies were constructed for the first time.
5. New degenerate orbits of the three-body problem were obtained, showing the chaotic nature of such orbits.

The volume and structure of the work. The dissertation consists of introduction, 5 chapter, conclusion and 2 appendices. The full volume of the dissertation is 177 page, including 67 figure and 11 table. The bibliography contains 110 titles.

The introduction briefly describes the problem statement and solution methods.

The first chapter deals with the reduction by translations and rotations, thus introducing the shape space. The geometric properties of the shape space are considered, and the equations of motion are derived.

The second chapter is devoted to finding periodic solutions using the variational method. The solution is sought in the form of trigonometric series by minimizing the action functional. Three symmetries from the list of planar three-body problem symmetries are taken as the model: simple choreography (only one orbit – the figure-eight), 2-1 choreographies (where two masses must be equal), and linear symmetry (where all masses differ from each other). The obtained solutions are analyzed.

In the third chapter, the regions of possible motion in the planar three-body problem are constructed. Such regions are well known in the two-body problem and the circular restricted three-body problem. If the problem is not circular, it can be simplified by averaging over the angular variable of the primary bodies. However, even in the general three-body problem, regions of possible motion can be constructed if we consider the motion in shape space, where this problem has only three dimensions. Such zero-velocity surfaces in shape space are constructed for different values of masses.

The fourth chapter deals with Lemaitre's regularization, which will be used in the next chapter for analyzing degenerate trajectories. The regularized shape space is analyzed.

The fifth chapter examines degenerate trajectories: collinear and isosceles. For each case, a parameterization is constructed that allows the equations of motion for these degenerate cases, free from singularities, to be written and numerically solved, followed by analysis.

The conclusion lists the solved problems.

Appendix A contains listings of models used in the search for periodic solutions in Chapter 2.

Appendix B shows the resulting orbits. Fourier series expansions of the coordinates of the problem in a rotating coordinate system and the initial coordinates and velocities in the barycentric coordinate system are provided.

Main scientific results

1. Zero-velocity surfaces and regions of possible motion for the general three-body problem in shape space were firstly constructed [50; 104; 105].
2. The general planar three-body problem is firstly consistently considered in shape space. The formulas for the transition to shape space coordinates are given [84; 85; 103]. In this space, the geometric properties of trajectories and their special points, including Euler and Lagrange points, are studied, allowing motion with invariant configuration to be obtained. The equations of motion and first integrals in shape space are derived [104; 105].

3. The properties of some orbits in the Lemaitre-regularized shape space were firstly investigated and described [84; 85].
4. Degenerate (collinear and isosceles) trajectories in the regularized shape space were firstly numerically obtained, showing their chaotic nature [84; 85].
5. Using the variational approach [78; 83; 103], new periodic orbits were found. The projections of the obtained orbits onto the shape sphere is analyzed for the first time.
6. New special cases are investigated and described. In these cases symmetry either gives simple results (see, for example, [81], the two-body problem), or significantly simplifies the analysis of the problem, in [109] the averaging over the longitudes of the primaries allows you to build surfaces of minimum velocity; using the averaging method makes it possible to solve the purely pragmatic problem of deflecting an asteroid from an orbit of collision with the Earth [98; 107].

In the work [50], the author is responsible for setting the problem in the space of forms and directing the computational part of the work. At work [98] K. V. Kholshevnikov owns the general management. The author has performed the derivation and verification of formulas using computer algebra. Work [107] is a continuation of the previous work. The work [105] is devoted to surfaces of minimum velocity in a limited three-body problem. The idea to use averaging belongs to K. V. Kholshevnikov, the author owns the analysis of the resulting surfaces, the calculation of these surfaces in the Pluto–Charon–Sputnik system.

Concepts to be defended:

1. Geometric properties of the solutions to the general planar three-body problem in shape space, motion with invariant configuration in this space. Equations of motion in the considered shape space.
2. Periodic orbits of the general three-body problem, obtained by the variational method using symmetry groups (dihedral group, 2-1 choreography symmetry, and linear symmetry). All orbits obtained by the variational method were verified by numerical integration.

3. Regions of possible motion in the general planar three-body problem. Minimal velocity surfaces in the restricted circular three-body problem, averaged over the longitude of the primary bodies.
4. Pre-images of the equator, isosceles configuration meridian, and figure-eight orbits in Lemaitre's regularization. Parameterizations of degenerate cases (isosceles and collinear configurations) on the shape sphere, leading to singularity-free equations of motion.
5. Degenerate (collinear and isosceles) trajectories in the regularized shape space, obtained by numerical integration, and their properties, including the chaotic aspects of degenerate trajectories.

Chapter 1. Shape Space in the Three-Body Problem

For the N-body problem, we have 10 classical integrals, 9 of which are related to translation and rotation symmetries. However, Even for $N = 2$, these symmetries transform conic sections (ellipses, parabolas, or hyperbolas) into conic sections with the same eccentricity, i.e., into orbits of the same shape regardless of size. For the two-body problem, it is not difficult to find transformations that map any orbit of the problem into any other orbit. Since Hamilton, we know that the orbits of the two-body problem in velocity space (Hamilton called them *hodographs*) are circles or parts of cicles if the orbit is hyperbolic or parabolic (see, for example, [8]). Any translation, rotation, or scaling transforms a conic section into a conic section, and, consequently, the orbit of the two-body problem into another orbit.

In Fig. 1.1, the hodographs of the two-body problem in the velocity space u,v are shown. The line of apsides in the coordinate space x,y remains directed along the abscissa axis of this space. In the left part, all circles have two common points, the foci of the Apollonius circles $(-k,0)$ and $(k,0)$, and, hence, the semi-major axis is μ/k^2. In the right part, for $e > 1$, the foci of the Apollonius circles are located at points $(0, -k)$ and $(0,k)$.

Based on delatations, rotations, and translations in velocity space, a group of transformations can be constructed that map the solutions of the two-body problem x,y,u,v into solutions x',y',u',v' of the two-body problem [80; 81]:

$$
\begin{aligned}
x' &= \frac{d(x\cos\gamma - y\sin\gamma)}{1 + x\beta - y\alpha}\,, y' = \frac{d(x\sin\gamma + y\cos\gamma)}{1 + x\beta - y\alpha}\,,\\
u' &= d^{-1/2}((u+\alpha)\cos\gamma - (v+\beta)\sin\gamma),\\
v' &= d^{-1/2}((u+\alpha)\sin\gamma + (v+\beta)\cos\gamma).
\end{aligned}
$$

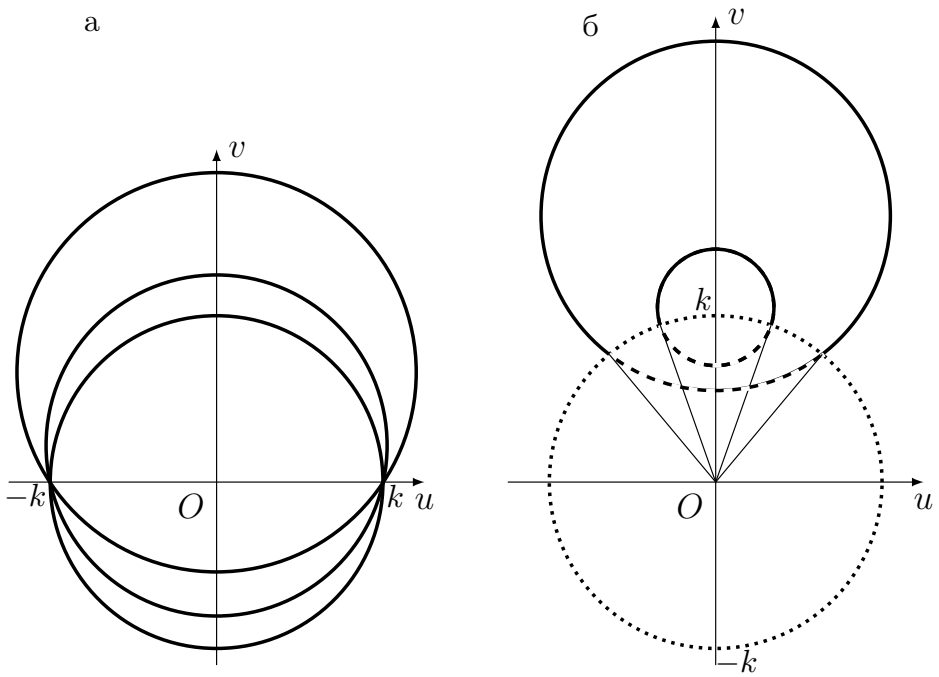

Figure 1.1 – Hodographs of velocities of the two-body problem (orbit in the velocity space), details are in the text

Here d, γ, α, β are the parameters of the group transformations; x, y, u, v are the coordinates and velocities of the points of the original orbit, i.e.,

$$\begin{pmatrix} x' \\ y' \\ u' \\ v' \end{pmatrix} = g(d,\gamma,\alpha,\beta) \begin{pmatrix} x \\ y \\ u \\ v \end{pmatrix} = g_1(d)g_2(\gamma)g_3(\alpha)g_4(\beta) \begin{pmatrix} x \\ y \\ u \\ v \end{pmatrix},$$

g_1 and g_2 are one-parameter groups of scalings and rotations respectively, and g_3 and g_4 are groups of translations along the coordinate axes in velocity space. The group multiplication law is:

$$\begin{aligned} &g(d,\gamma,\alpha,\beta) = g(d_2,\gamma_2,\alpha_2,\beta_2) \cdot g(d_1,\gamma_1,\alpha_1,\beta_1) \\ &d = d_1 d_2, \quad \gamma = \gamma_1 + \gamma_2, \\ &\alpha = \alpha_1 + (\alpha_2 \cos\gamma_1 + \beta_2 \sin\gamma_1)\, d_1^{1/2}, \\ &\beta = \beta_1 + (-\alpha_2 \sin\gamma_1 + \beta_2 \cos\gamma_1)\, d_1^{1/2}. \end{aligned}$$

It is easy to obtain transformations that leave the energy constant invariant [81]. Clearly, for negative energy constants h, any transformation that maps a circle into a

circle while preserving the length of the chord passing through the origin perpendicular to the diameter will suffice, in which case $e < 1$. If we fix the line of apsides, the resulting circles represent a family of Apollonius circles on the left side of Fig. 1.1. For positive h ($e > 1$), the corresponding trajectories represent a family of Apollonius circles on the right side of Fig. 1.1.

The considered group can be used to determine the parameters of the group transformation from observations [82] (and, consequently, the elements of the orbit). It is easy to identify a subgroup whose transformations would change only the shape of the orbits, i.e., the eccentricity e and the semi-major axis a. Thus, all orbits with the same shape (e) and size (a) can be considered identical, and the properties of the classes of such orbits can be studied. The dimension of the space of such orbits will be smaller (in this case, it is equal to two), and studying the properties in such a space will be simpler.

If the two-body problem has a complete solution that allows determining the properties of the solutions, then in the three-body problem, the complete solution is unknown, and any simplification of the problem may be useful in studying the properties of its solutions.

1.1 Reduction the Order of System

So, to investigate a complicated problem, it is necessary to simplify it in some way. For example, by reducing the problem to a lower-dimensional problem. A trivial reduction to a lower dimension is achieved if we limit ourselves to a planar problem. Any properties of the solutions of the planar problem will allow us to make progress in solving the spatial problem.

For further reduction of our problem to a problem of lower dimensionality, known relations and symmetries can be used. According to Noether's theorem, each first integral corresponds to a group of transformations.

If we consider only the integrals of momentum and angular momentum, then the groups of transformations are the translation group and the rotation group.

1.1.1 Scale symmetry

Let us start with another well-known symmetry group of the N problem – scale symmetry. This symmetry is a simple consequence of the uniformity of the potential function of degree -1 and the uniformity of the kinetic energy of degree 2:

If the functions $\mathbf{r}_i(t)$, $\mathbf{v}_i(t)$, $i = 1, \ldots, N$, represent the solution to the N-body problem, then the solution to the problem is also

$$\begin{aligned} \boldsymbol{\rho}_i(t) &= \lambda \mathbf{r}_i(\lambda^{-3/2} t) \\ \dot{\boldsymbol{\rho}}_i(t) &= \lambda^{-1/2} \mathbf{v}_i(\lambda^{-3/2} t), \end{aligned} \tag{1.1}$$

with

$$\begin{aligned} h' &= \lambda^{-1} h \\ J' &= \lambda^{1/2} J, \end{aligned} \tag{1.2}$$

where h is the energy constant, J is the angular momentum, and $\lambda \in \mathbb{R}^+$ is any positive real number. This symmetry, essentially discovered by Kepler, is valid for any number of bodies. Thus, having a solution for h, we obtain a solution for any value of the energy constant of the same sign, which allows us to limit ourselves to just three values of the energy constant, for example, $h = -1/2, 0, 1/2$. In fact, any three values can be chosen. If the energy is negative, one could choose $h = -1$. The value $h = -1/2$ has a slight advantage in some problems: as we will see later, if the radius of the shape sphere is chosen to be $1/2$, then under a certain stereographic projection, the equator of the shape sphere maps to a unit circle, which is very convenient in many cases.

1.1.2 Reduction by Translations. Jacobi Coordinates

Let us return to symmetry groups, starting with translations. Invariance under translations allows us to choose a system with the origin at the barycenter:

$$\sum_{i=1}^{N} m_i \mathbf{x}_i = 0. \tag{1.3}$$

Condition (1.3) allows reducing the dimensionality of the problem by 2 (in the spatial case by 3). Another way to eliminate translations, used by Legendre, is to use mutual distances as variables. In this case, the spatial problem will require two additional variables responsible for the orientation of the plane of the three bodies.

Using (1.3) directly gives the equations of relative motion, but by reducing the dimensionality of the problem, we obtain asymmetric expressions with a disturbing function that varies for each body. To eliminate this drawback, Jacobi coordinates are used in celestial mechanics (Fig. 1.2): the coordinates of each subsequent body are measured from the center of mass of all the previous ones. This construction works for any number of N bodies. For three bodies, we have:

$$\begin{aligned} \mathbf{Q}_1 &= \mathbf{r}_2 - \mathbf{r}_1, \\ \mathbf{Q}_2 &= \mathbf{r}_3 - \frac{m_1\mathbf{r}_1 + m_2\mathbf{r}_2}{m_1 + m_2}, \end{aligned}$$

From the three vectors $\mathbf{r}_i$, we obtained two: $\mathbf{Q}_1$ and $\mathbf{Q}_2$, assuming

$$\mathbf{Q}_3 = \frac{m_1\mathbf{r}_1 + m_2\mathbf{r}_2 + m_3\mathbf{r}_3}{m_1 + m_2 + m_3} = 0,$$

and thus, considering the motion of $\mathbf{r}_i$ in the barycentric coordinate system, we can easily write the inverse transformation to obtain $\mathbf{r}_i$, $i = 1,2,3$ from the known $\mathbf{Q}_1$, $\mathbf{Q}_2$ (and $\mathbf{Q}_3 \equiv 0$):

$$\begin{aligned} \mathbf{r}_1 &= -\tfrac{m_2}{m_1+m_2}\mathbf{Q}_1 - \tfrac{m_3}{M}\mathbf{Q}_2 + \mathbf{Q}_3, \\ \mathbf{r}_2 &= \tfrac{m_1}{m_1+m_2}\mathbf{Q}_1 - \tfrac{m_3}{M}\mathbf{Q}_2 + \mathbf{Q}_3, \\ \mathbf{r}_3 &= \tfrac{m_1+m_2}{M}\mathbf{Q}_2 + \mathbf{Q}_3. \end{aligned} \tag{1.4}$$

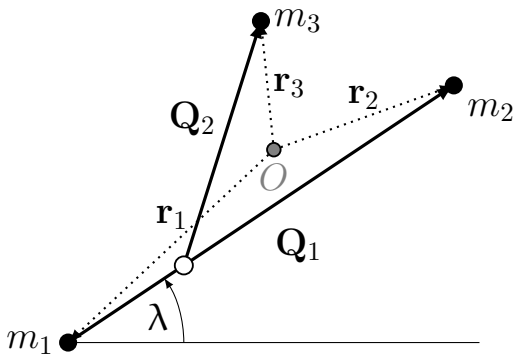

Figure 1.2 – Jacobi coordinates, λ is the angle of the direction $m_1 - m_2$ relative to the fixed axis

In the space of Jacobi coordinates, we can obtain the mutual distances r_{ij}:

$$\begin{aligned} r_{12} &= |\mathbf{Q}_1|\,, \\ r_{13} &= \left|\mathbf{Q}_2 + \frac{m_2}{m_1+m_2}\mathbf{Q}_1\right|, \\ r_{23} &= \left|\mathbf{Q}_2 - \frac{m_1}{m_1+m_2}\mathbf{Q}_1\right|, \end{aligned}$$

the kinetic energy T, the Lagrangian L, and the angular momentum J:

$$\begin{gathered} T = \frac{1}{2}(m_1\dot{\mathbf{r}}_1^2 + m_2\dot{\mathbf{r}}_2^2 + m_3\dot{\mathbf{r}}_3^2) = \frac{1}{2}\left(\mu_1\dot{\mathbf{Q}}_1^2 + \mu_2\dot{\mathbf{Q}}_2^2\right), \\ L = T(\dot{\mathbf{Q}}_1,\dot{\mathbf{Q}}_2) + V(\mathbf{Q}_1,\mathbf{Q}_2), \\ J = \mu_1\mathbf{Q}_1 \times \dot{\mathbf{Q}}_1 + \mu_2\mathbf{Q}_2 \times \dot{\mathbf{Q}}_2. \end{gathered} \tag{1.5}$$

Here, $\mu_1 = m_1m_2/(m_1+m_2)$, $\mu_2 = m_3(m_1+m_2)/(m_1+m_2+m_3)$, and the potential function V is easily expressed through Q_1, Q_2.

Symmetry among the bodies seems to be violated since we start constructing Jacobi coordinates by choosing a specific body. This is justified in planetary problems where the central body (the Sun) has a mass significantly greater than the masses of the other bodies. In the general three-body problem, this is not the case, but the next reduction makes all the bodies have equal right.

1.1.3 Reduction by Rotations. Hopf Transformation

Now, let us move on to the next symmetry, which is related to the integral of angular momentum, i.e., the conservation of the angular momentum vector–symmetry under rotations (in two-dimentional or three-dimensional space).

The sphere in the space of Jacobi coordinates $(\mathbf{Q}_1,\mathbf{Q}_2)$ is $\mathbb{S}^3$, and, by eliminating rotations, we obtain $\mathbb{S}^2$. Thus, we naturally arrive at the classical Hopf transformation ($\mathcal{S}^1 \hookrightarrow \mathcal{S}^3 \to \mathcal{S}^2$).

We will consider $\mathbf{Q}_1$, $\mathbf{Q}_2$ as points in complex space, $\mathbf{Q}_1, \mathbf{Q}_2 \in \mathbb{C}$. Then, following Hopf, we can introduce new variables:

$$\begin{aligned} \xi_1 &= \frac{1}{2}\mu_1|\mathbf{Q}_1|^2 - \frac{1}{2}\mu_2|\mathbf{Q}_2|^2, \\ \xi_2 + i\xi_3 &= \sqrt{\mu_1\mu_2}\,\mathbf{Q}_1\bar{\mathbf{Q}}_2. \end{aligned} \tag{1.6}$$

The right-hand side of the first equation is real, and the right-hand side of the second equation is a complex number. Thus, we obtain three real variables: ξ_1, ξ_2, and ξ_3.

The inverse transformation is:

$$\begin{aligned} \mathbf{Q}_1 &= \begin{pmatrix} 1 \\ \operatorname{tg}\lambda \end{pmatrix} \sqrt{\sqrt{\xi_1^2+\xi_2^2+\xi_3^2}+\xi_1}/(\sqrt{2\mu_1}\sqrt{1+\operatorname{tg}^2\lambda}), \\ \mathbf{Q}_2 &= \begin{pmatrix} \xi_2 - \xi_3\operatorname{tg}\lambda \\ \xi_2\operatorname{tg}\lambda + \xi_3 \end{pmatrix} /(\sqrt{2\mu_2}\sqrt{\sqrt{\xi_1^2+\xi_2^2+\xi_3^2}+\xi_1}\sqrt{1+\operatorname{tg}^2\lambda}), \end{aligned} \tag{1.7}$$

The three-dimensional space $\Xi = (\xi_1,\xi_2,\xi_3)$ is the space of oriented congruent triangles. Each point in this space represents a class of such oriented congruent triangles. This space is called the *shape space*, and it is in this space that we will study the properties of the solutions of the three-body problem.

In this space, we can obtain the expression for the moment of inertia I:

$$\begin{aligned} I &= m_1|\mathbf{r}_1|^2 + m_2|\mathbf{r}_2|^2 + m_3|\mathbf{r}_3|^2 \\ &= \frac{(m_1m_2r_{12}^2 + m_1m_3r_{13}^2 + m_2m_3r_{23}^2)}{(m_1+m_2+m_3)} = \\ &= \mu_1|\mathbf{Q}_1|^2 + \mu_2|\mathbf{Q}_2|^2 = \\ &= \sqrt{\xi_1^2+\xi_2^2+\xi_3^2}. \end{aligned} \tag{1.8}$$

Thus, the *distance from the origin to a point in the shape space is equal to the moment of inertia*. Note that the moment of inertia plays an important role in the qualitative study of the N-body problem. The well-known Lagrange-Jacobi identity states:

$$\ddot{I} = 2(2T - V) = 2(T + h) = 2(V + 2h). \tag{1.9}$$

In our case, this equation is the Lagrange equation for the variable ρ ($\rho = \sqrt{\xi_1^2 + \xi_2^2 + \xi_3^2} = I$). It will be discussed in section 1.3. Many qualitative conclusions about the solutions of the 3-body (N-body) problem directly follow from the identity (1.9). They are discussed in the next chapter.

1.2 Geometric Properties and Special Points

Let us consider the geometric properties of the shape space.

In the XX-th and XXI-th centuries, the shape sphere was used by Chenciner and Montgomery [16] to prove the existence of the famous figure-eight orbit. Shape space is now used to study various aspects of the three-body problem [11; 22—24; 47], including the search for new choreographies [18; 25; 26; 70—73], regularization [44; 45; 50; 78; 79], and other aspects [27].

Let us introduce spherical coordinates ρ,φ,θ in the space Ξ. It is natural to consider the coordinate ρ as the size of the triangle, and φ,θ as angular variables defining its shape. Then the coordinate ρ, as follows from (1.8), coincides with the moment of inertia. In the shape space, all properties related to the moment of inertia of the system are naturally associated with the size of the triangle. The square root of ρ can be taken as the size of the triangle as well, matching the unit of measurement with the unit of length. In any case, points on a sphere of fixed radius, for example, $\rho = 1$ or $\rho = 1/2$, will correspond to the shape of the triangle. Such a sphere is called the *shape sphere*, and the entire shape space is a cone over this sphere with the apex at the triple collision point $(0,0)$. Thus, a point in the shape sphere represents a class of similar triangles,

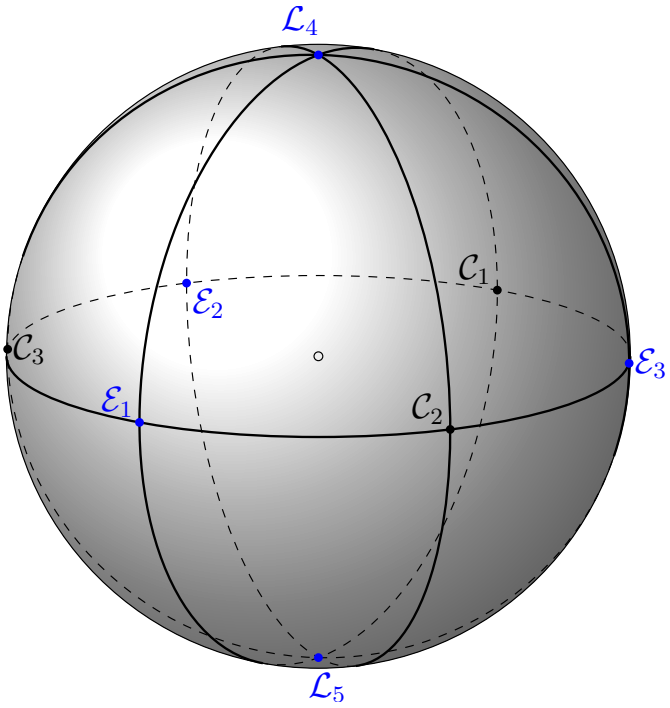

Figure 1.3 – Shape sphere, $\mathcal{C}_i$ are double collision points, $\mathcal{E}_i$ are Eulerian collinear configurations

and all points on a ray in the shape space emanating from the origin represent similar configurations of three bodies, differing only in size.

In Fig. 1.3, the shape sphere is depicted. For clarity and illustration of the properties of various points on the shape sphere, it is assumed that $m_1 = m_2 = m_3$. In the case of unequal masses, the positions of the points will change, and this will be indicated.

From the second equation (1.6), it is clear that the equator of the shape sphere (the plane $\xi_3 = 0$) corresponds to collinear configurations ($\mathbf{Q}_1 \times \mathbf{Q}_2 = 0$). Thus, all double collision points lie on the equator for any mass values. In Fig. 1.3, these points are $\mathcal{C}_1$, $\mathcal{C}_2$, and $\mathcal{C}_3$. Note that due to rotational symmetry, it does not matter where we choose the origin of the angle φ. In the figure, it is chosen such that the point $\mathcal{C}_3$ (collision of bodies m_1 and m_2) corresponds to the value $\varphi = \pi$. Then, for the collision of m_1 and m_3 ($\mathcal{C}_2$) in the case of equal masses, $\varphi = -\pi/3$, and for the collision of m_2 and m_3 ($\mathcal{C}_1$), $\varphi = \pi/3$. In the case of equal masses, the points diametrically opposite to the points $\mathcal{C}_i$ correspond to Eulerian configurations $\mathcal{E}_i$, and the poles $\mathcal{L}_4$ and $\mathcal{L}_5$ correspond to Lagrangian equilateral configurations. The meridians passing through the poles and one of the double collision points also pass through the corresponding Eulerian point.

The points on this meridian correspond to isosceles configurations. If only two masses are equal, then only one meridian corresponds to isosceles configurations.

In the case of unequal masses, collinear configurations, both Eulerian and double collision configurations, of course, remain on the equator but shift from the positions shown in Fig. 1.3. Moreover, the points corresponding to Lagrangian configurations cease to be poles, although they remain symmetric with respect to the equator.

Let us express the mutual distances in terms of ξ_1, ξ_2, ξ_3:

$$\begin{aligned}
r_{12}^2 &= \frac{m_1+m_2}{2m_1m_2}(\sqrt{\xi_1^2+\xi_2^2+\xi_3^2}+\xi_1) \\
r_{13}^2 &= \frac{m_1+m_3}{2m_1m_3}\sqrt{\xi_1^2+\xi_2^2+\xi_3^2} \\
&\quad +\frac{m_2m_3-m_1(m_1+m_2+m_3)}{2m_1m_3(m_1+m_2)}\xi_1+\frac{\sqrt{m_1m_2m_3(m_1+m_2+m_3)}}{m_1m_3(m_1+m_2)}\xi_2 \\
r_{23}^2 &= \frac{m_2+m_3}{2m_2m_3}\sqrt{\xi_1^2+\xi_2^2+\xi_3^2} \\
&\quad +\frac{m_1m_3-m_2(m_1+m_2+m_3)}{2m_2m_3(m_1+m_2)}\xi_1-\frac{\sqrt{m_1m_2m_3(m_1+m_2+m_3)}}{m_2m_3(m_1+m_2)}\xi_2
\end{aligned} \tag{1.10}$$

From here, we easily obtain the expressions for the rays of double collisions:

$$\begin{aligned}
c_{12}&=\frac{m_1+m_2}{2m_1m_2}\,R\,\big(-1,0,0\big)^T, \\
c_{13}&=\frac{m_1+m_3}{2m_1m_3}\,R\left(-\frac{m_2m_3-m_1(m_1+m_2+m_3)}{(m_1+m_2)(m_1+m_3)},-\frac{2\sqrt{m_1m_2m_3(m_1+m_2+m_3)}}{(m_1+m_2)(m_1+m_3)},0\right)^T, \\
c_{23}&=\frac{m_2+m_3}{2m_2m_3}\,R\left(-\frac{m_1m_3-m_2(m_1+m_2+m_3)}{(m_1+m_2)(m_2+m_3)},\quad\frac{2\sqrt{m_1m_2m_3(m_1+m_2+m_3)}}{(m_2+m_3)(m_1+m_2)},0\right)^T,
\end{aligned} \tag{1.11}$$

here $R\in\mathbb{R}^+$ is any positive real number. The expressions in parentheses give us the coordinates of the double collision points on the shape sphere. In the case of equal masses, the double collision points are evenly distributed along the equator.

The double collision points (1.11) can be transformed into three equidistant points $\pm 2\pi/3$, π by performing a fractional linear transformation. Such a transformation maps the unit circle to the unit circle, and thus it can be represented as

$$z=\lambda\frac{w-a}{1-\bar{a}w} \tag{1.12}$$

where

$$
\begin{aligned}
a &= \frac{m_1^2 m_2 + m_1 m_2^2 - m_2^2 m_3 - m_1^2 m_3 - i\,(m_2 - m_1)\,\sqrt{m_1 m_2 m_3 (m_1 + m_2 + m_3)}}{(m_1 + m_2)\,\left(\sqrt{3 m_1 m_2 m_3 (m_1 + m_2 + m_3)} + m_1 m_2 + m_1 m_3 + m_2 m_3\right)} \\
\lambda &= \Big(2(m_1 + m_2)\,\sqrt{3 m_1 m_2 m_3 (m_1 + m_2 + m_3)} \\
&\qquad + m_2^2 m_3 + 6 m_1 m_2 m_3 + m_1^2 m_3 + 2 m_1 m_2^2 + 2 m_1^2 m_2 \\
&\quad + i\,(m_2 - m_1)\,(2\,\sqrt{m_1 m_2 m_3 (m_1 + m_2 + m_3)} + \sqrt{3}\,m_2\,m_3 + \sqrt{3}\,m_1\,m_3)\Big) \Big/ \\
&\quad \Big(2(m_1 + m_2)\,(\sqrt{3 m_1 m_2 m_3 (m_1 + m_2 + m_3)} + m_1 m_2 + m_1 m_3 + m_2 m_3)\Big)
\end{aligned}
$$

of course, $|\lambda| = 1$.

Eulerian points are not so easily derived and will be considered in the next section. The formulas for the rays of the Lagrangian points $L_{4,5}$ can be easily obtained from the condition $r_{12} = r_{13} = r_{23}$:

$$
L_{4,5} = \frac{R}{m_1 m_2 + m_1 m_3 + m_2 m_3}
\begin{pmatrix}
\dfrac{m_1 m_2 (m_1 + m_2) - m_3 (m_1^2 + m_2^2)}{m_1 + m_2} \\
\dfrac{(m_1 - m_2)\sqrt{m_1 m_2 m_3 (m_1 + m_2 + m_3)}}{m_1 + m_2} \\
\pm\sqrt{3 m_1 m_2 m_3 (m_1 + m_2 + m_3)},
\end{pmatrix} \tag{1.13}
$$

For $R = 1$, we have two points on the shape sphere, symmetric relative to the equatorial plane.

It is clear that in the case of equal masses, the Eulerian points are equidistant from each other by an angle of $2\pi/3$. However, if the masses are unequal, the Eulerian points are obviously unevenly spaced, and the Lagrangian points $L_{4,5}$ are not located at the poles. We can transform the Eulerian points into three equidistant points, placing the Lagrangian points at the poles, using the transformation (1.12).

Indeed, with a fractional linear transformation, we can map the Eulerian points to three equidistant points, placing the Lagrangian points at the poles. This could be useful in certain applications, but in the problems we consider, the resulting expressions become much more complicated, and therefore, the corresponding transformation was not performed.

1.2.1 Eulerian Points

Let us consider spherical coordinates in the space Ξ:

$$\begin{aligned} \xi_1 &= \rho\cos\varphi\cos\theta, \\ \xi_2 &= \rho\sin\varphi\cos\theta, \\ \xi_3 &= \rho\sin\theta, \end{aligned} \tag{1.14}$$

The unit of measurement for the variable ρ is the square of the unit of length multiplied by the unit of mass, as ρ is the moment of inertia of the three bodies. In these coordinates, the mutual distances can be written as

$$\begin{aligned} r_{12}^2 &= \frac{m_1+m_2}{2m_1m_2}\,\rho(1+\cos\varphi\cos\theta), \\ r_{13}^2 &= \frac{m_1+m_3}{2m_1m_3}\,\rho(1-\cos(\varphi-\varphi_{13})\cos\theta), \\ r_{23}^2 &= \frac{m_2+m_3}{2m_2m_3}\,\rho(1-\cos(\varphi-\varphi_{23})\cos\theta). \end{aligned} \tag{1.15}$$

Here, the expressions for the cosines and sines of φ_{ij} are obtained from (1.11) for the coordinates of the double collision ij on the shape sphere. For the potential function V, we have

$$V(\rho,\theta,\varphi) = \frac{1}{\sqrt{\rho}}\left(\frac{\nu_{12}}{\sqrt{1+\cos\theta\cos\varphi}} + \frac{\nu_{13}}{\sqrt{1-\cos\theta\cos(\varphi-\varphi_{13})}} + \frac{\nu_{23}}{\sqrt{1-\cos\theta\cos(\varphi-\varphi_{23})}}\right) = \frac{1}{\sqrt{\rho}}\,D(\theta,\varphi), \tag{1.16}$$

where $\nu_{ij} = \sqrt{2}(m_im_j)^{3/2}/\sqrt{m_i+m_j}$. Note that the potential function separates into two factors, one depending only on the size of the system (moment of inertia) and the other only on the shape of the triangle.

Let us try to find configurations that can remain unchanged [79], $\theta = \text{const}$, $\varphi = \text{const}$. Thus, we will look for critical points of D, that is,

$$\begin{aligned} \frac{\partial D(\varphi,\theta)}{\partial\theta} &= 0, \\ \frac{\partial D(\varphi,\theta)}{\partial\varphi} &= 0 \end{aligned}$$

In this case, the size of the configuration may change, but the shape remains unchanged, meaning that the triangle of the three bodies remains similar over time.

Let us first consider collinear configurations. The partial derivative with respect to θ has a factor $\sin\theta$ and, therefore, is zero for all points on the equator. To compute the partial derivative with respect to φ, and to eliminate the radicals in the expression (1.16), it is necessary to fix the order of the bodies. Let, for example, body m_3 be located between m_1 and m_2. The equatorial plane of the space Ξ is shown in Fig. 1.4 ($m_1 = m_2 = 3/5, m_3 = 9/5$):

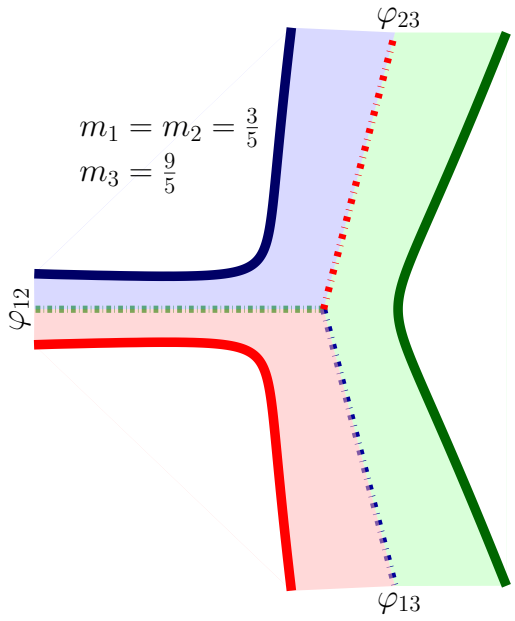

Figure 1.4 – Three-body location on the equatorial plane

In Fig. 1.4, the possible motion region is shown as well, more precisely, its equatorial plane cross-section. The region is bounded by zero-velocity curves. These curves will be defined below, while the double collision lines have already been determined: the green dashed-dotted line represents the collision line of bodies m_1 and m_2, the blue line represents the collision line of bodies m_1 and m_3, and the red line represents the collision line of bodies m_2 and m_3. The green shaded area corresponds to the order m_1-m_3-m_2, the blue shaded area to m_1-m_2-m_3, and the red shaded area to m_2-m_1-m_3. For the considered order m_1-m_3-m_2, the mutual distances for points on the equator

can be written as:

$$\begin{aligned} r_{12} &= \sqrt{\rho}\sqrt{\frac{m_1+m_2}{2m_1m_2}}\cos\varphi/2, \\ r_{13} &= \sqrt{\rho}\sqrt{\frac{m_1+m_3}{2m_1m_3}}\sin(\varphi-\varphi_{13})/2, \\ r_{23} &= -\sqrt{\rho}\sqrt{\frac{m_2+m_3}{2m_2m_3}}\sin(\varphi-\varphi_{23})/2, \end{aligned} \tag{1.17}$$

then

$$D(0,\varphi)=\frac{1}{\sqrt{2}}\left(\frac{\nu_{12}}{\cos\varphi/2}+\frac{\nu_{13}}{\sin(\varphi-\varphi_{13})/2}-\frac{\nu_{23}}{\sin(\varphi-\varphi_{23})/2}\right),$$

and

$$\frac{\partial D(0,\varphi)}{\partial\varphi}=\frac{1}{\sqrt{8}}\left(\nu_{12}\frac{\sin\varphi/2}{\cos^2\varphi/2}-\nu_{13}\frac{\cos(\varphi-\varphi_{13})/2}{\sin^2(\varphi-\varphi_{13})/2}+\nu_{23}\frac{\cos(\varphi-\varphi_{23})/2}{2\sin^2(\varphi-\varphi_{23})/2}\right).$$

Denominators in the last expression equal zero only at the double collision points, which obviously cannot have an unchanging configuration. The expression $\partial D(0,\varphi)/\partial\varphi=0$ is equivalent to the expression

$$\begin{aligned} 0 = {} & m_1^{5/2}m_2^{5/2}\sqrt{(m_1+m_3)(m_2+m_3)}(m_1+m_2+m_3)^2\operatorname{tg}^5\varphi/2+ \\ & +2m_1^2m_2^2(m_2-m_1)\sqrt{m_3(m_1+m_3)(m_2+m_3)}(m_1+m_2+m_3)^{3/2}\operatorname{tg}^4\varphi/2+ \\ & +m_1^{3/2}m_2^{3/2}m_3\sqrt{(m_1+m_3)(m_2+m_3)}(m_1+m_2+m_3) \\ & (2m_2m_3+2m_1m_3+m_2^2-4m_1m_2+m_1^2)\operatorname{tg}^3\varphi/2+ \\ & +m_1m_2(m_2-m_1)m_3^{3/2}\sqrt{(m_1+m_3)(m_2+m_3)(m_1+m_2+m_3)} \\ & (3m_2m_3+3m_1m_3+m_2^2+m_1^2)\operatorname{tg}^2\varphi/2+ \\ & +\sqrt{m_1m_2(m_1+m_3)(m_2+m_3)}m_3^2 \\ & (3(m_1+m_2)(m-1^2+m-2^2)m_3+2(m_1^2+m_2^2)^2+m_1m_2(4m_2^2+m_1m_2+4m_1^2))\operatorname{tg}\varphi/2+ \\ & +(m_2-m_1)(m_1+m_2)(m_2^2+m_1m_2+m_1^2)m_3^{5/2}\sqrt{(m_1+m_3)(m_2+m_3)(m_1+m_2+m_3)} \end{aligned}$$

The value $\varphi=\pi$ corresponds to a double collision and has already been excluded from consideration. The real root of this equation will give us the desired point. Let us reduce the equation to a known fifth-degree polynomial concerning the ratio $z=r_{13}/r_{23}$. From (1.17) we have:

$$z=r_{13}/r_{23}=-\frac{\sqrt{m_1m_2(m_1+m_2+m_3)}\operatorname{tg}\varphi/2+m_2\sqrt{m_3}}{\sqrt{m_1m_2(m_1+m_2+m_3)}\operatorname{tg}\varphi/2-m_1\sqrt{m_3}}$$

Expressing $\mathrm{tg}\,\varphi/2$ in terms of z from this equation, we obtain a fifth-degree polynomial:

$$(m_3{+}m_2)z^5{+}(2m_3{+}3m_2)z^4{+}(m_3{+}3m_2)z^3{-}(m_3{+}3m_1)z^2{-}(2m_3{+}3m_1)z{-}(m_3{+}m_1) \tag{1.18}$$

The single positive root of this polynomial determines the ratio z, and thus the angle φ corresponding to the unchanging collinear configuration is calculated from

$$\mathrm{tg}\,\frac{\varphi}{2} = \frac{\sqrt{m_3}(m_1 z - m_2)}{\sqrt{m_1 m_2 (m_1 + m_2 + m_3)}(z+1)}\,.$$

For another order, for example, m_1-m_2-m_3, we get the same polynomial, but the masses in its coefficients need to be cyclically permuted. There are three such permutations, and thus we have three unchanging collinear configurations.

1.2.2 Lagrangian Points

Now let us consider the case $\theta \neq 0$.

$$\begin{aligned}
\frac{\partial D(\theta,\varphi)}{\partial\theta} &= \frac{\sin\theta}{2}\left(\nu_{12}\frac{\cos\varphi}{(1+\cos\varphi\cos\theta)^{3/2}} - \nu_{13}\frac{\cos(\varphi-\varphi_{13})}{(1-\cos(\varphi-\varphi_{13})\cos\theta)^{3/2}}\right.\\
&\qquad\left. - \nu_{23}\frac{\cos(\varphi-\varphi_{23})}{(1-\cos(\varphi-\varphi_{23})\cos\theta)^{3/2}}\right)\\
\frac{\partial D(\theta,\varphi)}{\partial\varphi} &= \frac{\cos\theta}{2}\left(\nu_{12}\frac{\sin\varphi}{(1+\cos\varphi\cos\theta)^{3/2}} - \nu_{13}\frac{\sin(\varphi-\varphi_{13})}{(1-\cos(\varphi-\varphi_{13})\cos\theta)^{3/2}}\right.\\
&\qquad\left. - \nu_{23}\frac{\sin(\varphi-\varphi_{23})}{(1-\cos(\varphi-\varphi_{23})\cos\theta)^{3/2}}\right)
\end{aligned} \tag{1.19}$$

It can be verified by direct computation that the points (1.13) are the desired critical points.

Thus, the critical points of the function D coincide with the Euler and Lagrange points. In the form space, if interpreted as a cone over the shape sphere, the Lagrange and Euler points are rays through the corresponding points on the form sphere.

Both collinear and triangle critical points are commonly referred to as Lagrangian points. In the shape space, they naturally separate into Eulerian collinear points (the

corresponding solutions were discovered by Euler in 1767 [19]), which are thus located on the equator, and equilateral points (solution given by Lagrange in 1772 [29]). It should be noted that in the form space, the directions of the rays for both configurations depend on the values of the masses of the bodies.

1.2.3 Motion with Invariant Configuration

In the previous section, conditions were derived under which the configuration of the three bodies remains unchanged (up to similarity), i.e., $\theta = \text{const}$, $\varphi = \text{const}$. These are the Eulerian L_1, L_2, L_3 and the Lagrangian L_4, L_5 configurations. In this case, the potential function has a simple form:

$$V = \frac{C_1}{\sqrt{\rho}},$$

and the Lagrange–Jacobi identity (1.9) becomes:

$$\ddot{I} = 2\left(\frac{C_1}{\sqrt{I}} + 2h\right),$$

where C_1 is a constant determined by the position of the invariant configuration; i.e., ultimately only by the masses of the three bodies. Using the well-known variable substitution $r^2 = I$ and the time transformation $\frac{dt}{d\tau} = r = \sqrt{I}$, we get

$$r'' = 2hr + C_1,$$

where $'$ denotes differentiation with respect to the variable τ, and h is the constant of the energy integral (1.23) derived in the next section. The solution to this equation for $h < 0$ is evidently

$$r = \sqrt{I} = A\cos(n\tau - \vartheta) - \frac{C_1}{2h}, \quad n = \sqrt{-2h}.$$

A and ϑ are integration constants.

1.3 Equations of Motion

The expression for the kinetic energy T in Jacobi coordinates is well known (1.5). To write the expression for T in the shape space, we use the transformation (1.7), obtaining

$$T = \frac{\dot{\xi}_1^2+\dot{\xi}_2^2+\dot{\xi}_3^2}{8\sqrt{\xi_1^2+\xi_2^2+\xi_3^2}} + \frac{\xi_3^2\dot{\xi}_2^2+\xi_2^2\dot{\xi}_3^2}{8\sqrt{\xi_1^2+\xi_2^2+\xi_3^2}(\sqrt{\xi_1^2+\xi_2^2+\xi_3^2}+\xi_1)^2} - \frac{\xi_2\dot{\xi}_2\xi_3\dot{\xi}_3}{4\sqrt{\xi_1^2+\xi_2^2+\xi_3^2}(\sqrt{\xi_1^2+\xi_2^2+\xi_3^2}+\xi_1)^2} + \frac{\dot{\lambda}^2\sqrt{\xi_1^2+\xi_2^2+\xi_3^2}}{2} + \frac{\dot{\lambda}(\xi_2\dot{\xi}_3-\xi_3\dot{\xi}_2)}{2(\sqrt{\xi_1^2+\xi_2^2+\xi_3^2}+\xi_1)} \quad (1.20)$$

The force function V depends only on the mutual distances, which do not depend (1.10) on the angle $lambda$. Thus, λ is a cyclic variable. Interestingly, the conjugate momentum to the variable λ:

$$\frac{\partial T}{\partial \dot{\lambda}} = \sqrt{\xi_1^2+\xi_2^2+\xi_3^2}\,\dot{\lambda} + \frac{\xi_2\dot{\xi}_3-\xi_3\dot{\xi}_2}{2(\sqrt{\xi_1^2+\xi_2^2+\xi_3^2}+\xi_1)} \quad (1.21)$$

matches the constant angular momentum J, as can be verified by substituting the inverse transformation for $\mathbf{Q}_1$ and $\mathbf{Q}_2$ (1.7) into the expression (1.5). Thus, λ is a cyclic variable of the problem, and the angular momentum J is its conjugate momentum. Therefore, we can use Routh's method of eliminating cyclic coordinates by defining the Routh function R [99]:

$$\begin{aligned} R &= T+V-J\dot{\lambda} = \\ &= \frac{\dot{\xi}_1^2+\dot{\xi}_2^2+\dot{\xi}_3^2-4J^2}{8\sqrt{\xi_1^2+\xi_2^2+\xi_3^2}} + \frac{J(\xi_2\dot{\xi}_3-\xi_3\dot{\xi}_2)}{2\sqrt{\xi_1^2+\xi_2^2+\xi_3^2}(\sqrt{\xi_1^2+\xi_2^2+\xi_3^2}+\xi_1)} + V \end{aligned}$$

Knowing the solution of the problem, i.e., the functions $\xi_1(t)$, $\xi_2(t)$, $\xi_3(t)$, we can find the function $\lambda(t)$ from the quadrature

$$\lambda(t) = \int_0^t \frac{J - \dfrac{\xi_2\dot{\xi}_3-\xi_3\dot{\xi}_2}{(2\sqrt{\xi_1^2+\xi_2^2+\xi_3^2}+\xi_1)^2}}{\sqrt{\xi_1^2+\xi_2^2+\xi_3^2}}d\tau.$$

Next, it is convenient to replace the coordinates ξ_1, ξ_2, ξ_3 with their spherical analogs:

$$\begin{aligned}\xi_1 &= \rho\cos\varphi\cos\theta,\\ \xi_2 &= \rho\sin\varphi\cos\theta,\\ \xi_3 &= \rho\sin\theta.\end{aligned}$$

In these coordinates, the Routh function is written as

$$R=\frac{\dot\rho^2+\rho^2\dot\theta^2+\rho^2\cos^2\theta\dot\varphi^2-4J^2}{8\rho}+\frac{J(\sin\varphi\dot\theta-\cos\varphi\dot\varphi\cos\theta\sin\theta)}{2(1+\cos\varphi\cos\theta)}+\frac{D(\varphi,\theta)}{\sqrt{\rho}}\,, \quad (1.22)$$

and the generalized energy integral is:

$$\frac{\dot\rho^2+\rho^2\dot\theta^2+\rho^2\cos^2\theta\dot\varphi^2+4J^2}{8\rho}-\frac{D(\varphi,\theta)}{\sqrt{\rho}}=h. \quad (1.23)$$

The fact that the kinetic energy is represented as the sum of a quadratic form relative to the positional velocities ξ_i, $i=1,3$, and a quadratic form relative to the generalized impulses p_λ (in this case, only one term $p_\lambda = J$ is present), was demonstrated by Routh.

The equations of motion for the positional variables are the Lagrange equations with the Routh function as the Lagrangian. For ρ, we obtain the equation:

$$\frac{d}{dt}\left(\frac{\partial R}{\partial\dot\rho}\right)-\frac{\partial R}{\partial\rho}=0,$$

From the Routh function (1.22), using the integral (1.23), we obtain:

$$\ddot\rho=\frac{2D(\varphi,\theta)}{\rho^{3/2}}+4h,$$

which coincides with the Lagrange-Jacobi identity (1.9) ($\ddot I = 2(V+2h)$).

The force function (1.16) has already been obtained. Knowing the expression for the kinetic energy, we can derive the Hamiltonian. The conjugate momenta are:

$$\begin{aligned}
p_{\xi_1} = \frac{\partial T}{\partial \dot{\xi}_1} &= \frac{\dot{\xi}_1}{4\sqrt{\xi_1^2+\xi_2^2+\xi_3^2}}\,, \\
p_{\xi_2} = \frac{\partial T}{\partial \dot{\xi}_2} &= \frac{\dot{\xi}_2}{4\sqrt{\xi_1^2+\xi_2^2+\xi_3^2}} + \frac{\xi_3(\dot{\xi}_2\xi_3 - \dot{\xi}_3\xi_2)}{4\sqrt{\xi_1^2+\xi_2^2+\xi_3^2}(\sqrt{\xi_1^2+\xi_2^2+\xi_3^2}+\xi_1)^2} \\
&\quad - \frac{\xi_3\dot{\lambda}}{2(\sqrt{\xi_1^2+\xi_2^2+\xi_3^2}+\xi_1)}\,, \\
p_{\xi_3} = \frac{\partial T}{\partial \dot{\xi}_3} &= \frac{\dot{\xi}_3}{4\sqrt{\xi_1^2+\xi_2^2+\xi_3^2}} - \frac{\xi_2(\dot{\xi}_2\xi_3 - \dot{\xi}_3\xi_2)}{4\sqrt{\xi_1^2+\xi_2^2+\xi_3^2}(\sqrt{\xi_1^2+\xi_2^2+\xi_3^2}+\xi_1)^2} \\
&\quad + \frac{\xi_2\dot{\lambda}}{2(\sqrt{\xi_1^2+\xi_2^2+\xi_3^2}+\xi_1)}\,, \\
p_\lambda = \frac{\partial T}{\partial \dot{\lambda}} &= \sqrt{\xi_1^2+\xi_2^2+\xi_3^2}\dot{\lambda} + \frac{\xi_2\dot{\xi}_3 - \xi_3\dot{\xi}_2}{2(\sqrt{\xi_1^2+\xi_2^2+\xi_3^2}+\xi_1)}\,.
\end{aligned} \tag{1.24}$$

The Hamiltonian ($p_\lambda = J$) is:

$$\begin{aligned}
H = 2\sqrt{\xi_1^2+\xi_2^2+\xi_3^2}\,(p_{\xi_1}^2 + p_{\xi_2}^2 + p_{\xi_3}^2) \\
+ \frac{p_\lambda^2}{\sqrt{\xi_1^2+\xi_2^2+\xi_3^2}+\xi_1} - 2p_\lambda\,\frac{p_{\xi_2}\xi_3 - p_{\xi_3}\xi_2}{\sqrt{\xi_1^2+\xi_2^2+\xi_3^2}+\xi_1} - V(\xi_1,\xi_2,\xi_3)
\end{aligned} \tag{1.25}$$

In spherical coordinates $\rho,\varphi,\theta,\lambda$, the Hamiltonian is:

$$\begin{aligned}
H = 2\rho p_\rho^2 + 2\frac{p_\varphi^2}{\rho\cos^2\theta} + 2\frac{p_\theta^2}{\rho} + \frac{p_\lambda^2}{\rho(1+\cos\varphi\cos\theta)} \\
+ 2p_\lambda\frac{p_\varphi\cos\varphi\sin\theta - p_\theta\sin\varphi\cos\theta}{\rho\cos\theta(1+\cos\varphi\cos\theta)} - V(\rho,\varphi,\theta).
\end{aligned} \tag{1.26}$$

Having described the shape space and some of its properties, we can now proceed to study the properties of trajectories in this space.

Chapter 2. Symmetric Periodic Orbits in the Three-Body Problem: A Variational Approach

In the year 2000, more than two centuries after the discovery of particial solutions by Euler [19] and Lagrange [29], Chenciner and Montgomery [16] proved the existence of another particial solution, the so-called figure-eight orbit. This orbit was first found numerically ten years earlier [48], but Chenciner and Montgomery mathematically rigorously proved the existence of the figure-eight. In their proof, they used the variational method with constraints imposed by symmetry. Thr>ee bodies of equal mass move along a single orbit shaped like a figure-eight, with a phase shift of one-third of the period $T/3$.

The solution of Euler's equations $\mathbf{q}_i(t)$ with the Lagrangian $L(\mathbf{q}_i,\dot{\mathbf{q}}_i,t)$ is a stationary extremal of the Hamiltonian action functional:

$$\mathcal{A} = \int_{t_1}^{t_2} L(\mathbf{q}_i,\dot{\mathbf{q}}_i,t)\,dt. \tag{2.1}$$

In the case of the three-body problem, and if there are no collisions in the solution, we can seek the minimizer of the functional (2.1).

To find a periodic solution to the three-body problem, it is sufficient to find a (local) minimizer of the action functional in the space of 2π-periodic functions. Periodic solutions with a period different from 2π can be found using the scale symmetry (1.1).

The orbit constructed by Chenciner and Montgomery was indeed the minimizer of the action functional. Following the article [16], a large number of works followed, dedicated to the use of the variational method for finding particial solutions to the N-body problem. Many orbits (for three and more bodies) were constructed by C. Simó [63; 64], and a number of trajectories with zero angular momentum for 3 bodies were found in [72].

In the seventies, the orbits of the general three-body problem were investigated numerically in [74] (the Pythagorean problem), [5; 6; 52] (periodic orbits), [20; 21] and others, but in later works, symmetry begins to play a significant role in the search for periodic solutions (see, for example, [10; 13; 17; 49; 54]). Taking into account

the constraints imposed by symmetry, one can obtain, using the variational approach, a lot of periodic orbits.

If we find the minimizer of the functional $\mathcal{A}$ numerically, we obtain not only the initial conditions for the periodic orbit but also the entire solution as a function, for example, in the form of trigonometric series. Therefore, obtaining solutions in the form of functions is very useful.

We will seek the solution in the form

$$\begin{aligned} x_j(t) &= C_x^0 + \sum_{k=1} C_{xk}^j \cos\, kt + S_{xk}^j \sin\, kt \\ y_j(t) &= C_y^0 + \sum_{k=1} C_{yk}^j \cos\, kt + S_{yk}^j \sin\, kt, \end{aligned} \tag{2.2}$$

where j is the number of the body.

Of course, to find the solution, we must determine the coefficients C_x^0, C_{xk}^j, S_{xk}^j, C_y^0, C_{yk}^j, S_{yk}^j. Let us limit the number of terms considered, say, by the number n. For simple periodic orbits, the number of terms in the series (2.2) turns out to be small: in cases with the considered symmetries, for $|C_{x,y_k}^j| < 10^{-7}$ and $|S_{x,y_k}^j| < 10^{-7}$, it is sufficient to consider $k < 20$. By using symmetry, we can reduce the number of determined variables C_x^0, C_{xk}^j, S_{xk}^j, C_y^0, C_{yk}^j, S_{yk}^j, since some of the coefficients are identically zero, and some are related by known relations. Moreover, some symmetries exclude collisions, and symmetries that lead to collisions are not considered, as the variational approach is inapplicable in such cases.

We are considering an inertial space; therefore, we can seek functions x_j, y_j only for two bodies $j = 1,2$, and obtain the coordinates of the third body from the condition $0 = m_1\mathbf{r}_1 + m_2\mathbf{r}_2 + m_3\mathbf{r}_3$, or seek the solution in Jacobi coordinates.

All the determined solutions have a period of 2π, but the obtained minimizer solutions, due to the scale symmetry (1.1), cover all planar solutions of the three-body problem.

Barutello et al. [2] showed that all finite symmetry groups of the Lagrangian action functional in the planar three-body problem contain only ten elements. The authors proved the following theorem:

Theorem (Barutello, Ferrario, Terracini)**.** *Let G be the symmetry group of the Lagrangian action functional of the 3-body problem. Then G is either associated with collisions, fully non-coercive, homographic, or, up to rotation of the coordinate system, one of the symmetry groups listed in Table 1 (RCP stands for Rotating Circle Property, and HGM stands for Homographic Global Minimizer).*

Table 1 – Symmetry groups of the planar three-body problem (from [2])

Name	$\lvert G\rvert$	*type R*	*act. type*	*trans. dec.*	RCP	HGM
Trivial	1	yes		$1+1+1$	yes	yes
Line	2	yes	brake	$1+1+1$	(no)	no
$2-1$ Choreography	2	yes	cyclic	$2+1$	yes	no
Isosceles	2	yes	brake	$2+1$	no	yes
Hill	4	yes	dihedral	$2+1$	no	no
3 Choreography	3	yes	cyclic	3	yes	yes
Lagrange	6	yes	dihedral	3	no	yes
C_6	6	no	cyclic	3	yes	no
D_6	6	no	dihedral	3	yes	no
D_{12}	12	no	dihedral	3	no	no

Table 1 can serve as a basis for searching for periodic solutions to the planar three-body problem. By choosing a symmetry group, one can impose conditions on the coefficients of the trigonometric series to ensure the symmetry of this group, and then determine the minimizer within this class of symmetric functions; according to the principle of symmetric criticality by Palais [51], the found minimizer will be a minimizer in the class of all functions, i.e., a solution to the problem.

Let us limit ourselves to only a few groups from the list in Table 1, considering the symmetries of $2-1$ choreographies, linear symmetry, and the dihedral D_{12} symmetry, which by the way gives the same solutions as D_6.

The third column, *type R*, means the following: for any angular velocity ω, the corresponding group is a symmetry group for the Lagrangian functional in the rotating coordinate system. If the group does not possess this property, then the angular momentum of all equivariant trajectories is zero.

Thus, we will search for periodic orbits where the coefficients of the trigonometric series expansions of the coordinates are subject to conditions ensuring that the resulting solutions satisfy the conditions of the considered symmetry [83].

2.1 Simple Choreography – The Figure-Eight

Let us start with the figure-eight. This orbit, discovered numerically by C. Moore and whose existence was rigorously proven by A. Chenciner and R. Montgomery, is a so-called *simple choreography*: all three bodies move along the same trajectory, each phase-shifted by one-third of the period. Thus, the figure-eight is associated with the dihedral group D_{12}. The solution remains unchanged when shifted by $\pi/3$, reflected relative to the axes, and when the masses are permuted (i.e., all masses must be equal). Since the group is not of type *R*, the angular momentum is zero. As it turned out [65], this orbit possesses an important and unexpected property for an orbit with zero angular momentum: it is stable.

So, we have one trajectory along which the masses move with a shift of $T/3$. Therefore, the series (2.2) can be written as

$$\begin{aligned} x_j(t) &= \sum_k \left[C_{xk}\cos k(t+2(j-1)\pi/3) + S_{xk}\sin k(t+2(j-1)\pi/3)\right], \\ y_j(t) &= \sum_k \left[C_{y_k}\cos k(t+2(j-1)\pi/3) + S_{y_k}\sin k(t+2(j-1)\pi/3)\right], \end{aligned} \tag{2.3}$$

Thus, we only need to determine the set of coefficients C_{xk}, S_{xk}, C_{y_k}, and S_{y_k} for just one expansion of x and y. In this case, we determine the coordinates of the third body from the same series as for the first one (shifted by $4\pi/3$), not from the condition of the center of mass being stationary. However, this condition must be satisfied, i.e., $x_1(t) + x_2(t) + x_3(t) = 0$ and $y_1(t) + y_2(t) + y_3(t) = 0$,

hence:

$$\begin{aligned} C_{xk}\left(\cos kt+\cos k(t+2\pi/3)+\cos k(t+4\pi/3)\right) = \\ = C_{xk}\left(3-4\sin^2 2k\pi/3\right)\,\cos(kt+2k\pi/3)=0, \\ S_{xk}\left(\sin kt+\sin k(t+2\pi/3)+\sin k(t+4\pi/3)\right) = \\ = S_{xk}\left(3-4\sin^2 2k\pi/3\right)\,\sin(kt+2k\pi/3)=0 \end{aligned}$$

Therefore, for the center of mass to remain at the origin, the coefficients of the trigonometric series (2.3) must satisfy the condition:

$$C_{xk}=S_{xk}=0 \text{ for } k=3m, m=0,\ldots$$

The dihedral symmetry D_{12} implies symmetry with respect to the axes, meaning we can seek the expansions (2.3) only in terms of sines (the trajectory passes through the origin, forming an Eulerian configuration), thus, we will look for the trajectory in the form:

$$\begin{aligned} x(t) &= \sum_{\substack{k=1\\k\neq 3m}}^{N} S_{xk}\,\sin\,k\,t, \\ y(t) &= \sum_{\substack{k=1\\k\neq 3m}}^{N} S_{yk}\,\sin\,k\,t, \\ x_j(t) &= x\left(t+\frac{2\pi(j-1)}{3}\right), \quad j=1,2,3, \\ y_j(t) &= y\left(t+\frac{2\pi(j-1)}{3}\right), \quad j=1,2,3. \end{aligned}$$

Thus, to determine the figure-eight solution while maintaining harmonics up to order N in the expansions, it is necessary to find $4N/3$ variables.

Returning to the action functional (2.1). Minimizing the function $f(x_1,\ldots,x_n)$ is the primary task of linear programming

$$\min f(\xi_1,\ldots,\xi_n), \quad i=1,\ldots,n \tag{2.4}$$

$$g_j(\xi_1,\ldots,\xi_n)=0, \quad j=1,\ldots,m \tag{2.5}$$

$$g_k(\xi_1,\ldots,\xi_n)\leqslant 0, \quad k=m+1,\ldots,l \tag{2.6}$$

with constraints g_i. If the number of variables n and/or the number of constraints l is large enough, this becomes a complex problem even for linear functions f and g_i. In the case of linear functions, however, the problem is solvable, i.e., algorithms have been developed to find solutions or prove that no solutions exist, and these algorithms aim to minimize resource requirements.

The problem (2.4) has many variations depending on the properties of the task being solved: for example, large-scale systems, nonlinear optimization with linear constraints, global optimization, integer optimization, etc. Besides the linear case, the problem has a solution if the functions f and g_i are *convex*, i.e.,

$$f(a\xi_1 + b\xi_2) > af(\xi_1) + bf(\xi_2)$$

Unfortunately, the Lagrangian of the N-body problem and the action functional are not convex functions. Nevertheless, some methods developed for convex functions often yield good results in general problems, including the N-body (three-body) problem. However, since these methods do not guarantee results in the general case, all obtained solutions need to be verified.

Various algorithms have been developed for finding solutions to problem (2.4): different variants of gradient methods, the interior point method, Newton's method, etc. The diversity of applications and solution methods for optimization problems has stimulated the creation of a formal language for describing problem (2.4), which can then be solved using programs that implement one method or another, the so-called "solvers". In this work, the LOQO solver, created by R. Vanderbei [86], was used to find the "minimizer" of the considered problem using the interior point method. The widely-known AMPL (A Mathematical Programming Language) was used to formulate the problem. In the work [87], the author of LOQO provides an example model for finding periodic solutions, but the initial values of the coefficients of these solutions are chosen randomly. The description of the model for the eight-figure can be found in the appendix A.1, here we will outline the main steps. First of all, the parameters are set:

– the number of bodies N (only the three-body problem solutions are sought, so N is always 3, but the number of bodies is specified as a parameter);
– the number of terms retained in the Fourier series n, the remaining terms are discarded, usually this number is within two to three dozen; this number determines the number of unknowns to be determined, generally equal to $2(N-1)(2n+1)$ (in the three-body problem $4(2n+1)$), which ultimately determines the complexity of the problem;
– the number of nodes m used for calculating the integral (action functional), the integral is calculated by the simplest rectangle method, since solutions without double collisions are sought, and the accuracy can be increased by increasing this parameter m, which does not significantly affect the efficiency of the calculations; all quantities are calculated on a grid of m equally spaced moments.

With the symmetries considered for a particular orbit, the number of Fourier series coefficients can be greatly reduced, for example, for the figure-eight, $4(2n+1)$ Fourier series terms are reduced to only $4n/3$. The problem is fully determined by the structure of the coefficients, which is set in the model, for example, for the figure-eight:

```
set C3X := {1..n} diff {3..n by 3}; # defines the set of indices
var x {i in Bodies, t in Times} =
     sum{k in C3X} as[k]*sin(k*theta[i,t]);
var y {i in Bodies, t in Times} =
     sum{k in C3Y} bs[k]*sin(k*theta[i,t]);
```

Here, `theta[i,t]` are the time moments for the i-th body (with a shift of $2\pi/3$). Based on the given coordinates `x[i]` and `y[i]`, we define the action functional `A` (having previously defined the kinetic energy and potential function), and finally set the objective function:

```
minimize A: sum {t in Times} (K[t] - P[t])*dt;
# at the initial moment the first point is on the x-axis
subject to inity1 : y[1,0] = 0;
```

With the given parameters and initial values for `as[k]`, `bs[k]`, we start solving the problem:

```
option solver loqo;
option loqo_options "verbose=2 timing=1 iterlim=120";
solve;
```

The specified initial values for `as[k]` and `bs[k]`, as a rule, do not correspond to the solution of the problem under consideration. The result of solving (in this case, the LOQO ”solver” works with the specified parameters, for example, `iterlim` determines the maximum number of iterations in the search for a solution) are the values `as[k]` and `bs[k]`, such that the objective function (the action functional) takes a locally minimal value if such a solution is found. For each choice of initial coefficient values, this solution is, of course, unique, but with different initial values, we can obtain different solutions. Moreover, for the same orbit, different sets of coefficients corresponding to the minimum of the functional represent different solutions to the variational problem but not necessarily different trajectories. A shift along the trajectory represents another solution to the variational problem but the same orbit, or a rotation of the trajectory around the center of mass by any angle also gives another solution to the variational problem but the same orbit.

With the given constraint (`subject to inity1 : y[1,0] = 0;`), we obtain an orbit where the first point lies at the origin at the initial moment. In all the figures of this chapter, the initial points of each orbit are marked with a white circle, and to show the direction of motion, the positions of the bodies after a short period of time are shown with a colored circle (the colors correspond to the respective orbit). Since in the case of the eight-shaped orbit, all three bodies move along the same path, each body is shown

only for one-third of the period. Depending on the given initial values, the orbits will form a family of solutions, five of which are shown in Figure 2.1.

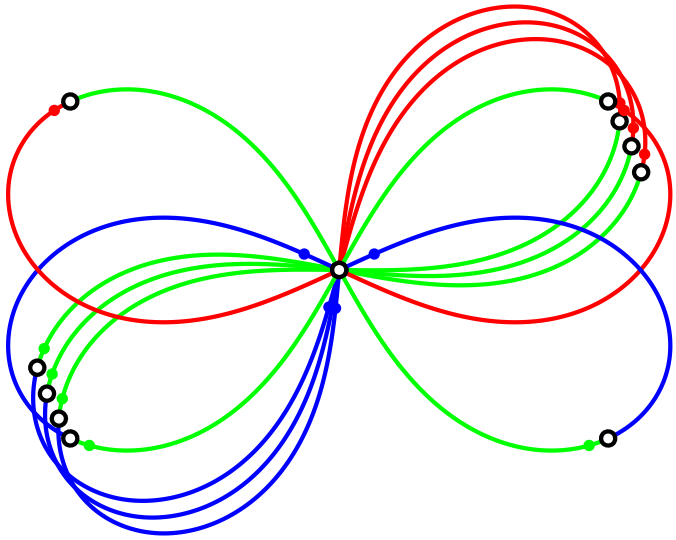

Figure 2.1 – Family of “figure-eight’s” orbits with the given constraint

To avoid such duplication of solutions, one can either set a more adequate structure for the coefficients and/or define additional constraints, for example,

```
# all points at the initial moment are on the x-axis
subject to inity1 : y[1,0] = 0;
subject to inity2 : y[2,0] = 0;
```

In this case, the bodies are in syzygy, i.e., on a single line. This constraint, as proven by Montgomery [46], holds for any orbit of the three-body problem with zero angular momentum (except for the Lagrange solution where all bodies are at the vertices of an equilateral triangle) and fixes the positions of the bodies on the x-axis at the initial moment. Although this constraint reduces the number of solutions, it is still obvious that we can obtain four different solution variants, differing by the branch of the eight along which the first body moves. In particular, if we replace $t \rightarrow -t$, the motion will occur in the opposite direction. Of course, with additional constraints, one can obtain a single orbit, but with the considered symmetry, we always obtain the same orbit characterized by the value of the action functional $A = 24.37193$ or the energy constant $h = -1.29297$. The constant of the kinetic moment (areas) is 0.

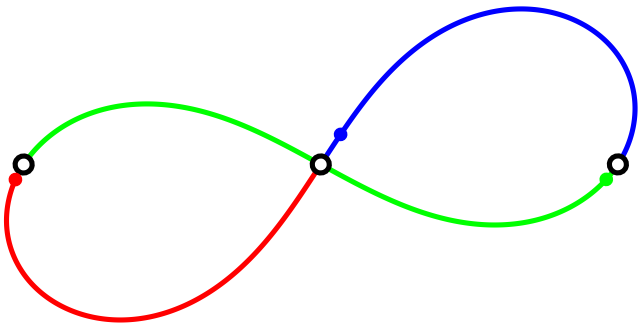

Figure 2.2 – The figure-eight orbit – solution of the problem (2.4)

For the eight (i.e., for the given model and initial parameter values), we obtain the following result (only terms with amplitude >0.0001 are shown):

$$\begin{aligned} x(t) &= 0.4082\sin t + 0.1973\sin 2t + 0.0326\sin 4t - 0.0094\sin 5t - 0.0022\sin 7t \\ &\quad -0.0017\sin 8t - 0.0005\sin 10t + 0.0002\sin 11t, \\ y(t) &= -0.6409\sin t + 0.1256\sin 2t + 0.0208\sin 4t + 0.0148\sin 5t + 0.0034\sin 7t \\ &\quad -0.0011\sin 8t - 0.0003\sin 10t - 0.0002\sin 11t - 0.0001\sin 13t. \end{aligned}$$

2.2 $2-1$ Choreographies

Now let us consider another symmetry: $2-1$ choreographies. The corresponding cyclic group is a group of type R (see Table 1), and orbits that minimize the action functional in the rotating coordinate system in the space of paths equivariant with respect to the group are the desired minimizers. According to Palais' principle [51], minimizers in the space of equivariant paths will be minimizers in the space of all paths, and thus, solutions to the problem.

Thus, the desired coordinate functions determine the coordinates of the bodies in a certain system, which we will call the primary system. To obtain the coordinates in the inertial system, we need to rotate the found coordinates by an angle $\omega\, t$. If ω is a rational number, we obtain a periodic orbit; if not, a conditionally periodic orbit. The search for periodic orbits in a rotating system is well known, see, for example, [3]. For a group of type R, such orbits should appear in almost any uniformly rotating system.

In the case of $2-1$ choreographies, two bodies of equal mass move along the same trajectory with a phase shift of π. The model of the problem is provided in Appendix A.2. In this model, the series for the coordinates in the rotating system are sought in the general form (2.2). When computing the action functional, the coordinates (and velocities) in the inertial coordinate system are used, and constraints are set so that all three initial points lie on the x-axis.

For $2-1$ configurations, the two points moving in the rotating coordinate system along the same trajectory must have equal masses. In the results presented below, the masses are taken as $m_1 = m_2 = 0.95, m_3 = 1.1$. One $2-1$ orbit we know from Euler's time, it is the collinear solution of the three-body problem, found by Euler in 1767: the third point is in the middle between the two equal masses, then choosing appropriate velocities, we can obtain a collinear solution as Euler did. This solution, of course, is also obtained as a minimizer of the action functional using the `2-1.mod` model. Such solutions are not provided further as the analytical solution is known.

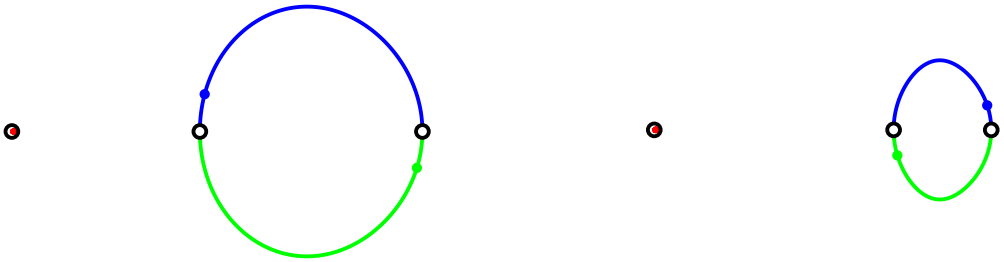

Figure 2.3 – Two 2-1 orbits in the rotating coordinate system ($\omega = 1/2$).

2.2.1 Angular velocity $\omega = 1/2$

Thus, in the rotating coordinate system with an angular velocity $\omega = 1/2$, we seek an orbit where two bodies of equal mass move with a half-period lag (π), and the position of the third body is determined by the condition of the barycenter's immobility. Figure 2.3 shows two different orbits in the base (rotating) coordinate

system: two bodies in the primary system move along one orbit, but this is not always the case in the inertial system (an example of such an orbit can be seen in Figure 2.6 on the left). For all orbits with 2-1 symmetry, the orbits of the bodies with equal masses are drawn in blue and green, and the orbit of the third body is shown in red.

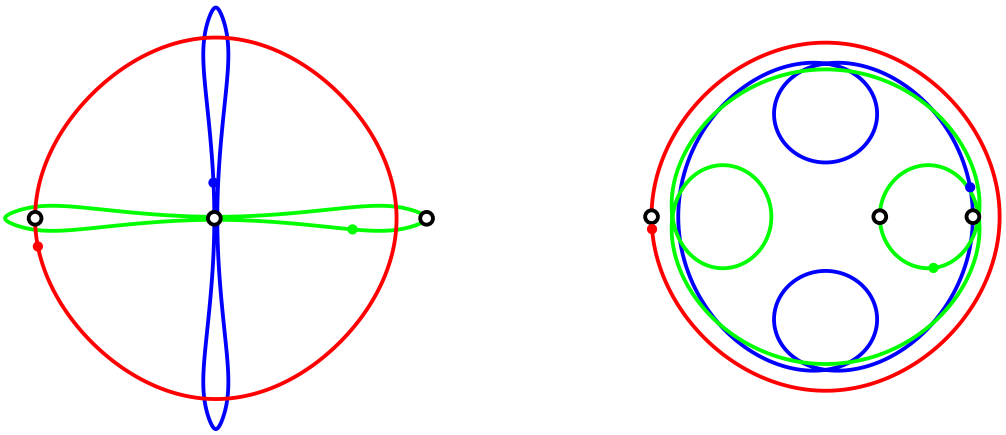

Figure 2.4 – Two 2-1 orbits in the inertial coordinate system ($\omega = 1/2$).

The same orbits in the inertial system are shown in Figure 2.4. For these orbits, minimizer solutions were obtained: for the left orbit:

$$\begin{aligned} x(t) &= 0.8613454 - 0.8866\cos t + 0.0129\cos 2t - 0.0009\cos 3t + \\ &\quad +0.0006\cos 4t + 0.0001\cos 5t + 0.0001\cos 6t, \\ y(t) &= 0.9902\sin t + 0.0056\sin 2t - 0.0051\sin 3t + 0.0005\sin 4t + 0.0003\sin 5t. \end{aligned}$$

and for the right:

$$\begin{aligned} x(t) &= 0.8360497 + 0.3582\cos t + 0.0063\cos 2t + 0.0275\cos 3t + \\ &\quad +0.0002\cos 4t + 0.0031\cos 5t + 0.0004\cos 7t + 0.0001\cos 9t, \\ y(t) &= 0.9794\sin t - 0.0061\sin 2t - 0.0274\sin 3t - 0.0002\sin 4t + 0.0031\sin 5t + \\ &\quad +0.0004\sin 7t + 0.0001\sin 9t. \end{aligned}$$

Naturally, there is a desire to classify these orbits. The period of all orbits is fixed, equal to 2π and set by the model, as we are seeking a solution in the form of trigonometric series. In this case, the energy constant will differ. By using the scaling symmetry, we can bring it to a fixed value $h = -1/2$, but we will identify the orbits by the value of the action functional (and, of course, by the value of

the angular velocity ω). For the two given orbits, the values of the action functional are $A = 13.13826$ and $A = 17.61955$ respectively. Before moving to other values of ω, note that replacing, for example, $\omega = 1/2$ with $\omega = 3/2$ will lead to the same orbits, resulting in a rotation by an integer number of turns. However, we can change the model by considering Fourier series starting from some term $\mathbf{k}$:

$$\mathbf{r}(t) = \sum_{k=\mathbf{k}}^{N} \begin{pmatrix} \mathbf{C}_j \\ \mathbf{S}_j \end{pmatrix} \begin{pmatrix} \cos \\ \sin \end{pmatrix} j\,t,$$

Such orbits (along with orbits obtained for other values of ω) will be considered below.

2.2.2 Angular velocity $\omega = 1/5{,}2/5$

Let us consider orbits for $\omega = 1/5$ and $2/5$.

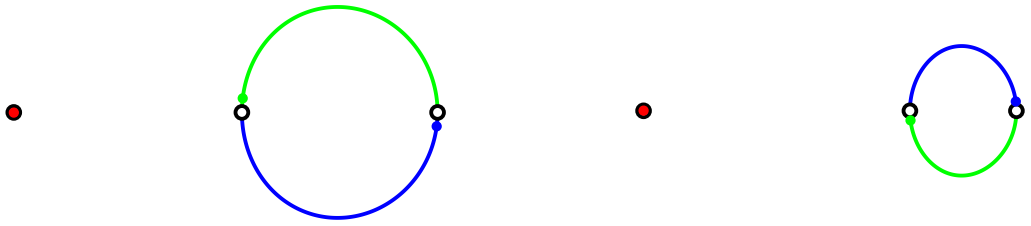

Figure 2.5 – 2-1-orbits: $\omega = 2/5$.

Figure 2.5 shows the orbits for $\omega = 2/5$ in the rotating coordinate system. Figure 2.6 shows these same orbits in the inertial coordinate system. Again, orbits can be identified by the value of the action functional. Of course, these values will differ.

If we take the rotational speed of the base system (in which the Fourier expansions are sought) to be half as much, $\omega = 1/5$, we get the orbits shown in Figure 2.7.

The pairs of orbits in Figures 2.4, 2.6, and 2.7 differ in the direction of rotation of the equal masses: on the left, the motion is retrograde, on the right, it is direct. Naturally, the value of the action functional and the energy constants in the pair differ. Such pairs

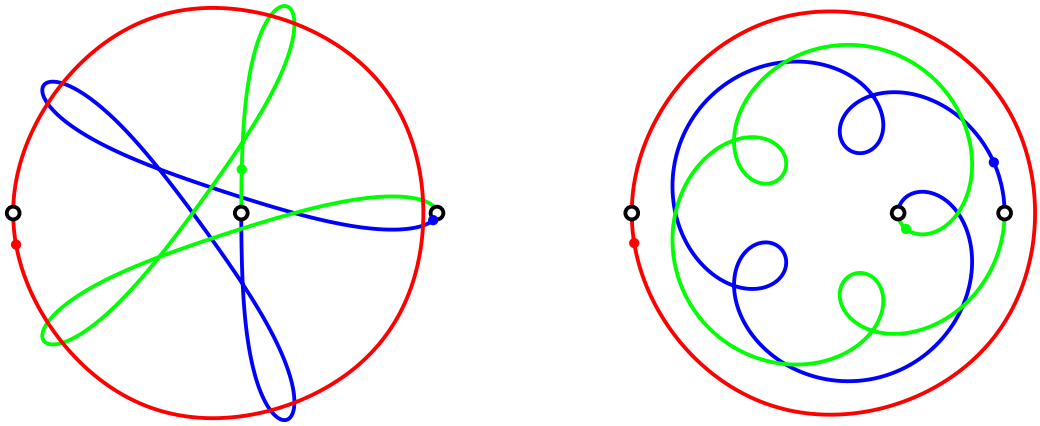

Figure 2.6 – 2-1-orbits: $\omega = 2/5$.

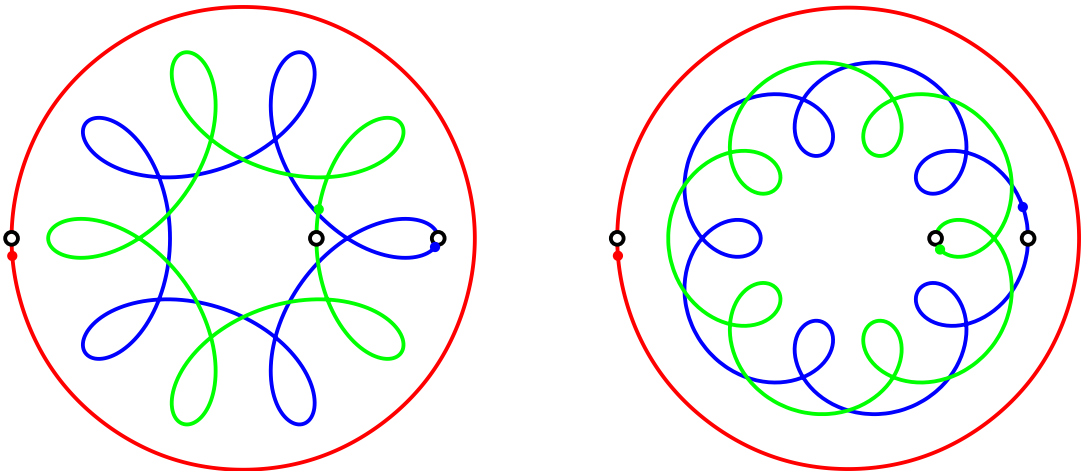

Figure 2.7 – 2-1-orbits: $\omega = 1/5$.

are found for other values of ω as well (see, for example, the two left orbits in Figures 2.8 and 2.9, pairs of orbits in Figures 2.10 and 2.11).

As minimizer solutions, we can obtain solutions whose trajectories coincide but differ only in the direction of motion along them. Naturally, this is a time-reversal symmetry, $t \to -t$, but we consider such trajectories to be the same. Time-reversal symmetry in the used models also leads to another effect: considering the values of the angular velocity of the rotating system, for example, $\omega = 3/5$, leads to the same trajectories as $\omega = 1 - 3/5 = 2/5$, as a result of the superposition of time reversal and the replacement $\omega' = 1 - \omega$ when rotating the base system. The same applies when replacing ω with $\omega = n + \omega$, where n is any integer. For this reason, when

searching for minimizer solutions in the considered way, it is natural to consider only $\omega \leqslant 1/2$.

2.2.3 Angular velocity $\omega = 1/3$

Let's also consider the orbits obtained for $\omega = 1/3$.

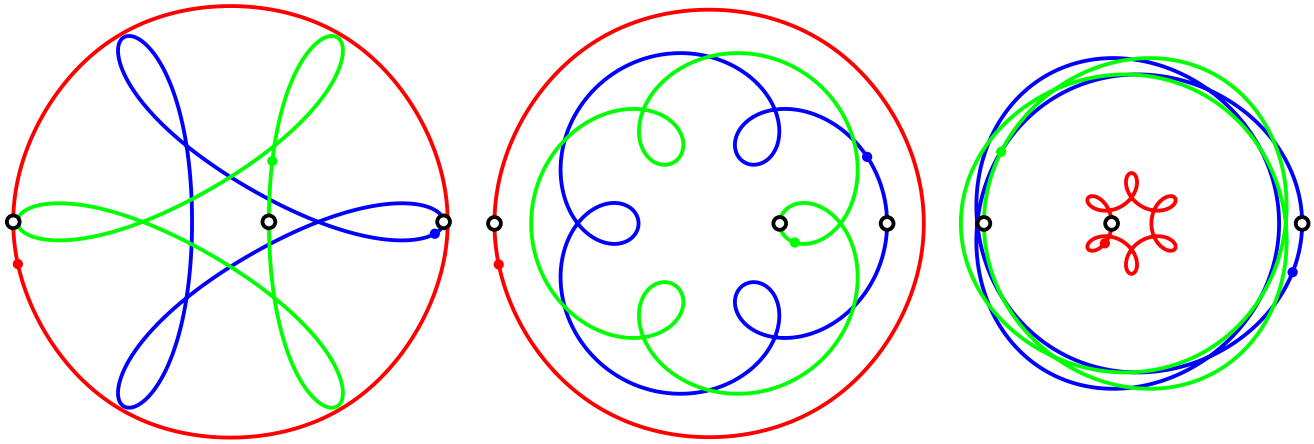

Figure 2.8 – 2-1 orbits: $\omega = 1/3$.

2-1 choreographies require only two masses to be equal, which move along one trajectory in the base system, while the third mass can differ from the other two. An example with masses $m_1 = m_2 = 1.05; m_3 = 0.9$ is shown in Fig. 2.9, which presents three such orbits for $\omega = 1/3$.

Note that a slight change in masses does not change qualitatively the trajectories.

2.2.4 Orbits with tight binaries

All the orbits considered so far have comparable mutual distances. Let us try to obtain hierarchical orbits in the same way, where a tight binary revolves around a distant third component. Thus, the frequency of revolution in the binary is significantly higher than the frequency of the binary itself relative to the third body. Such trajectories

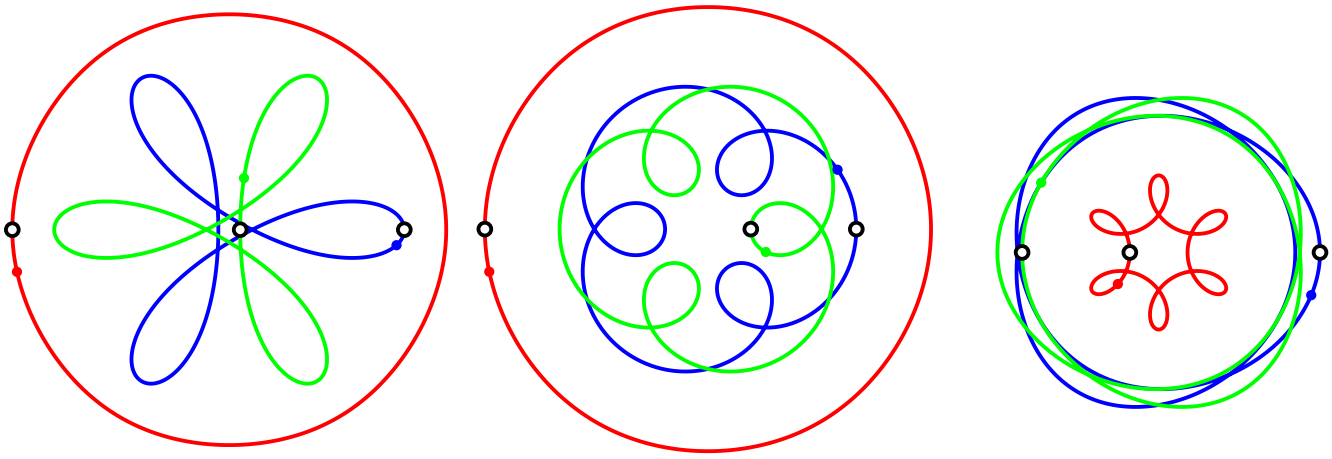

Figure 2.9 – 2-1 orbits ($m_1 = m_2 = 1.05$; $m_3 = 0.9$): $\omega = 1/3$.

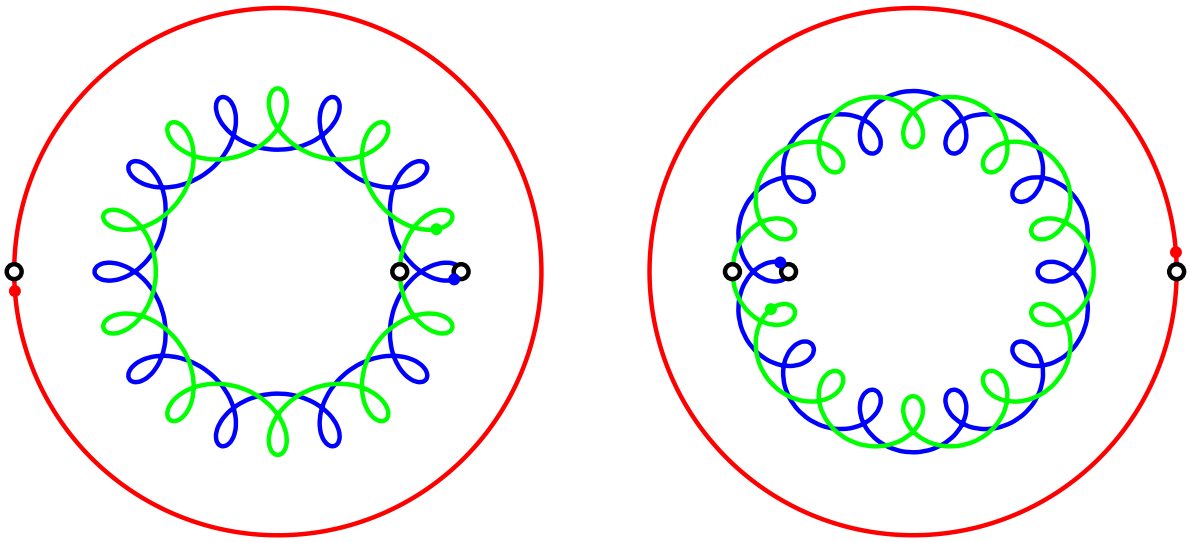

Figure 2.10 – 2-1 orbits: Equal masses form a tight binary, $\omega = 1/3, k = 5$.

can be obtained if we set the initial harmonics to zero in the Fourier expansion for the coordinates of the pair, starting the expansion, for example, with terms having the tern kt, where k is an integer greater than one. In Fig. 2.10, trajectories are shown whose expansions start with terms $k = 5$.

In Fig. 2.11, the orbits are shown, whose Fourier expansions start with $k = 3$.

Once again, note that in Figs. 2.10 and 2.11, the motion of the tight pair in the left figure is retrograde, while in the right figure, it is direct.

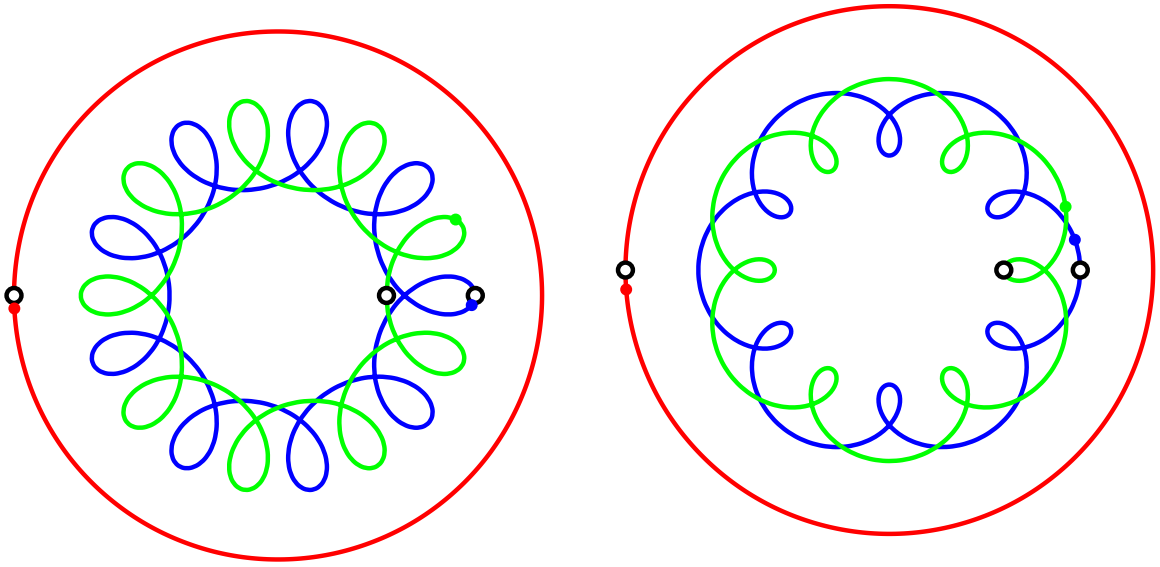

Figure 2.11 – 2-1 orbits: Equal masses form a tight binary, $\omega = 1/3, k = 3$.

It is obvious that the larger the value of k, the tighter the pair and the more distant the third component. In real hierarchical triple systems, the inner pair is much tighter, and it can be assumed that k is at least on the order of several tens, if not much more.

The same approach allows us to find trajectories for various rational values of ω.

In Table 2, the considered orbits with 2-1 symmetry are presented. Each row contains values for the action functional, the constant of energy, the constant of angular momentum, the value of ω, the ranges of the system size (moment of inertia), the number of the figure with the orbit, and either a «+» or «−»: «+» if the orbits remain stable for a long time (on the order of several thousand periods) or «−» otherwise. The last three rows show the same values for slightly modified masses $m_1 = m_2 = 1.05$, $m_3 = 0.9$.

All solutions are listed in Table 2, and their full descriptions (series and initial conditions) are provided in Appendix B.

Table 2 – Orbits with 2-1 symmetry

$m_1 = m_2 = 0.95$, $m_3 = 1.1$						
A	E	$\lvert C\rvert$	ω	$[I_{\min}, I_{\max}]$	Fig	Stab
10.61083	-0.562922	1.73204	1/5	[3.38488, 3.97924]	2.7l	+
11.87886	-0.630193	1.34061	1/3	[2.59540, 2.68433]	2.8l	+
12.41405	-0.658586	1.22094	2/5	[2.39094, 2.50262]	2.6l	+
12.43822	-0.850687	3.17929	1/5	[3.27315, 3.30845]	2.7r	+
13.13826	-0.697007	1.09433	1/2	[2.19634, 2.34595]	2.4l	+
14.90941	-0.790968	2.76171	1/3	[2.39013, 2.45279]	2.8c	+
16.03507	-0.850687	2.61695	2/5	[2.12957, 2.21161]	2.6r	+
16.57031	-0.879082	2.44831	1/3	[1.83954, 1.90829]	2.8r	-
17.61955	-0.934746	2.43060	1/2	[1.83522, 1.95725]	2.4r	-
19.78460	-1.049610	1.57727	1/3	[2.28883, 2.30208]	2.11l	+
21.89957	-1.161810	2.58582	1/3	[2.26047, 2.27089]	2.11r	+
25.74992	-1.366082	1.65989	1/3	[2.22605, 3.34307]	2.10l	+
27.53447	-1.460752	2.51159	1/3	[2.21422, 2.21935]	2.10r	+
$m_1 = m_2 = 1.05$, $m_3 = 0.9$						
12.20094	-0.647280	0.98928	1/3	[2.52298, 2.61020]	2.9l	+
15.79177	-0.837779	2.68412	1/3	[2.27099, 2.33355]	2.9c	+
16.61662	-0.881539	2.33447	1/3	[1.81034, 1.93278]	2.9r	-

2.3 Testing the obtained solutions. Isosceles symmetry

As noted in the previous section, nonlinear programming methods guarantee a solution to the minimization problem if the considered functions are convex. Otherwise, the problem's solution is not guaranteed. Therefore, each resulting solution needs to be tested. The simplest test is to check the conservation of the integrals of motion, the energy integral h and the angular momentum integral J. Naturally, since we represent the solution with truncated Fourier series, the calculated values of the integrals should fluctuate slightly around their mean values. In all the solutions presented above, these fluctuations (relative deviations of the constants from their mean values, $\delta h/\bar{h}$

and $\delta J/\bar{J}$) do not exceed $2 \cdot 10^{-7}$ and decrease with increasing the order of the trigonometric polynomials used in the model and the accuracy of the integral calculation when determining the action functional. Solutions with constant fluctuations exceeding 10^{-5}, for example, for the 2-1 choreography with $\omega = 1/2$, are not presented. The simplest test is numerical integration. From the obtained solution, we know the initial conditions (at any moment), and by integrating the equations of motion over one period (2π), we should obtain a closed trajectory.

The condition of isosceles symmetry according to [2] is that at moments 0 and π, the configuration of the three bodies forms an isosceles triangle with the vertex on a line relative to which the trajectories of the bodies are symmetric. The "figure-eight" orbit certainly possesses this property, and the dihedral symmetry is significantly stricter than isosceles symmetry. In the case considered here, only the equality of the two masses $m_1 = m_2$ is required, and the trajectory will not be a simple choreography. We will look for trajectories in the form

$$\begin{aligned}
x_1(t) &= \sum_{k=1} C_{2k-1} \cos{(2k-1)\,t} + S_{2k-1} \sin{(2k-1)\,t} \\
y_1(t) &= b_0 + \sum_{k=1} C_{2k} \cos{2k\,t} + S_{2k} \sin{2k\,t} \\
x_2(t) &= \sum_{k=1} C_{2k-1} \cos{(2k-1)\,t} - S_{2k-1} \sin{(2k-1)\,t} \\
y_2(t) &= -b_0 - \sum_{k=1} C_{2k} \cos{2k\,t} + S_{2k} \sin{2k\,t}
\end{aligned} \tag{2.7}$$

To determine the Fourier series expansion of the solution up to the N-th harmonic inclusively, it is necessary to determine $2N + 1$ coefficients. We consider trajectories in the barycentric coordinate system, and this gives us the expansions for the coordinates of the third body.

The description of such a model is given in Appendix A.3. Attempts to construct an orbit with such symmetry using the variational method [78; 103] were unsuccessful. The resulting "solution" is not an actual solution: the fluctuation of the integrals' values is about $\sim 10^{-3}$ or more. Numerical integration yields trajectories near to closed ones but are not actually closed. An example of such a trajectory is shown in Fig. 2.12. In this example, $m_1 = m_2 = 1.0$ (red and green curves) and $m_3 = 0.97$ (blue curve).

The red curve is a reflection of the green one relative to the x-axis, and the blue curve is symmetric relative to this axis. For comparison, the classic figure-eight is drawn with a dashed line.

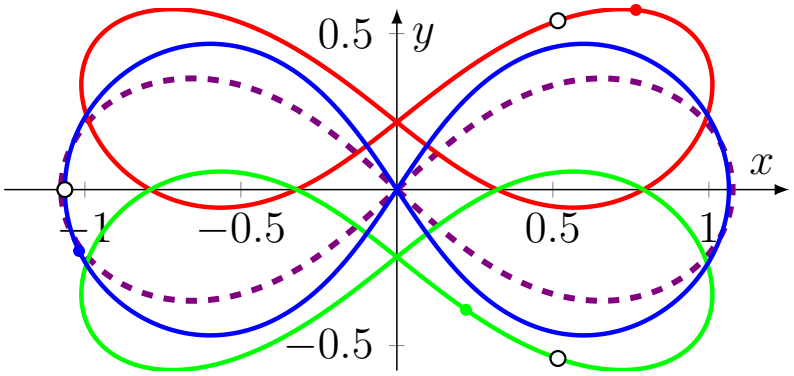

Figure 2.12 – “Solution” with isosceles symmetry.

Thus, with the model A.3 and the solver used, it is not successful in determining the trajectory. This is a consequence of the non-convexity of our action functional. The ten groups of symmetries [2] do not include symmetry groups associated with collisions. Such isosceles symmetry orbits with double collisions will be considered in Chapter 5, Section 5.2.

2.4 Linear Symmetry

The condition of linear symmetry according to [2] is that at moments 0 and π, the masses are collinear on a certain line, let it be the x-axis, in some initial plane, which rotates with angular velocity $\omega \notin \mathbf{Z}$. In the case of linear symmetry, the bodies can have arbitrary masses. The task model is presented in Appendix A.4. The series for

coordinates in the rotating system are sought in the form:

$$\begin{aligned} x_1(t) &= a_1 + \sum_{k=1} C_{1,k} \cos\, k\,t, \\ y_1(t) &= \sum_{k=1} S_{1,k} \sin\, k\,t, \\ x_2(t) &= a_2 + \sum_{k=1} C_{2,k} \cos\, k\,t, \\ y_2(t) &= \sum_{k=1} S_{2,k} \sin\, k\,t. \end{aligned} \tag{2.8}$$

When calculating the action functional, the coordinates (and velocities) in the inertial coordinate system are used, and the constraints are set so that all three initial points lie on the x-axis.

All three masses can be different. Let us first consider masses that differ slightly from each other, for example, $m_1 = 0.99$, $m_2 = 1.01$, $m_3 = 1.0$. Cyclic permutation of the masses leads to slightly different orbits, which are almost indistinguishable from each other. In the figures provided (Fig. 2.13 and onwards), the orbit of the smaller mass is shown in red, the orbit of the larger mass in green, and the orbit of the third body in blue.

2.4.1 Angular velocity $\omega = 1/2$

In the case of linear symmetry, the masses can be arbitrary, unlike the symmetries considered earlier (in the choreography, all masses must be equal, while in the 2-1 choreography and in the isosceles symmetry, two masses must be equal). Let's see how the orbits change with varying masses, for example, the last (right) orbit in Fig. 2.13. The orbits with different masses are shown in Fig. 2.14.

All the orbits shown in Fig. 2.14 are indeed orbits of the three-body problem, as confirmed by numerical integration. Moreover, integrating over 1 000 periods results in the same orbits, and integrating over 10 000 periods yields the same orbits, albeit slightly blurred. Thus, unlike the figure-eight, the orbits in Fig. 2.14 are not sensitive

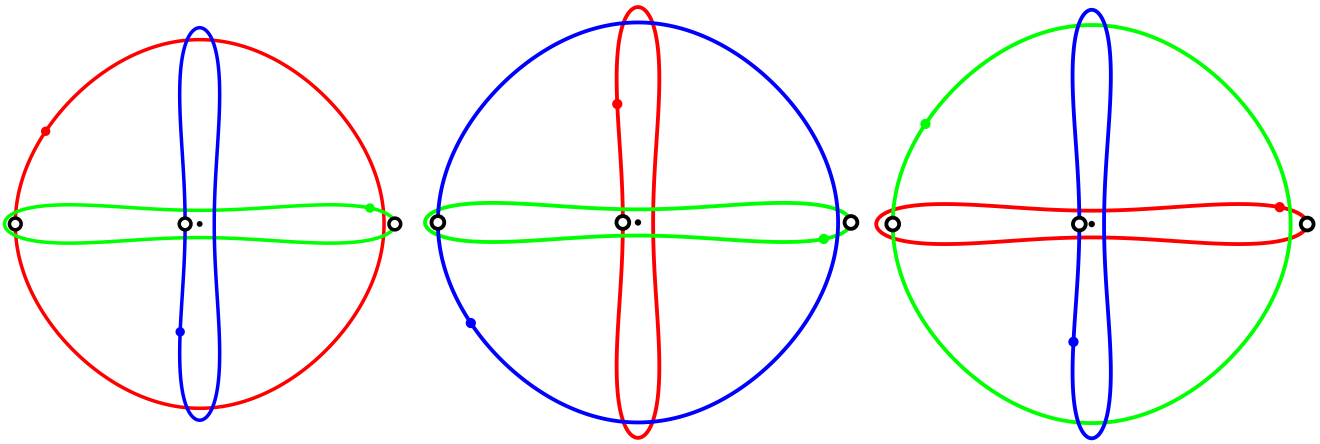

Figure 2.13 – Three orbits with linear symmetry corresponding to cyclic permutation of masses m_1, m_2, m_3 ($\omega = 1/2$).

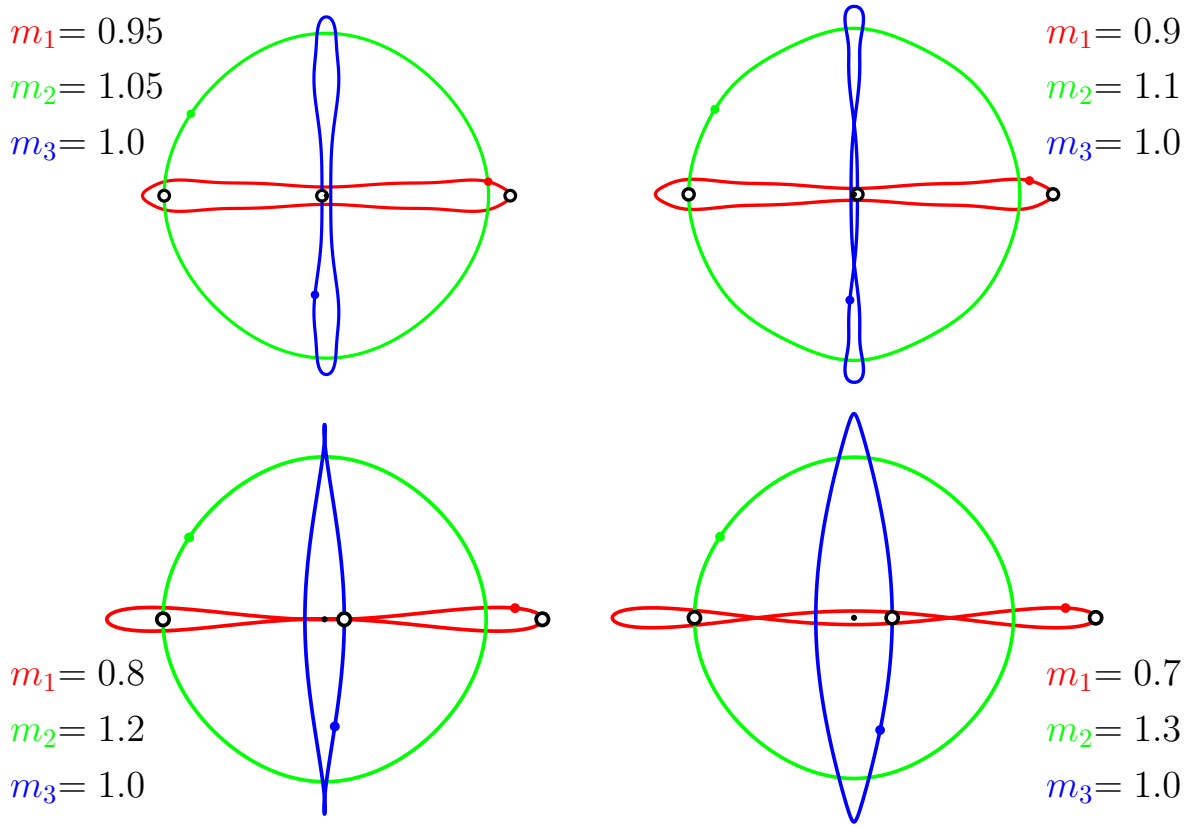

Figure 2.14 – The last orbit of Fig. 2.13 with different mass values, ($\omega = 1/2$).

to variations in masses within a wide range and maintain “stability” over a long period. Over intervals of about 10 000 periods, the orbits remain in a confined region, periodic and do not significantly “drift” from the initial orbit, as essentially the rotation of points relative to each other is absent (although the angular momentum is not zero).

Let's now return to the orbits obtained with different values of ω, with the initial masses $m_1 = 0.99$, $m_2 = 1.1$, $m_3 = 1.0$.

2.4.2 Angular velocity $\omega = 1/4$

Fig. 2.15 shows three different orbits obtained for $\omega = 1/4$.

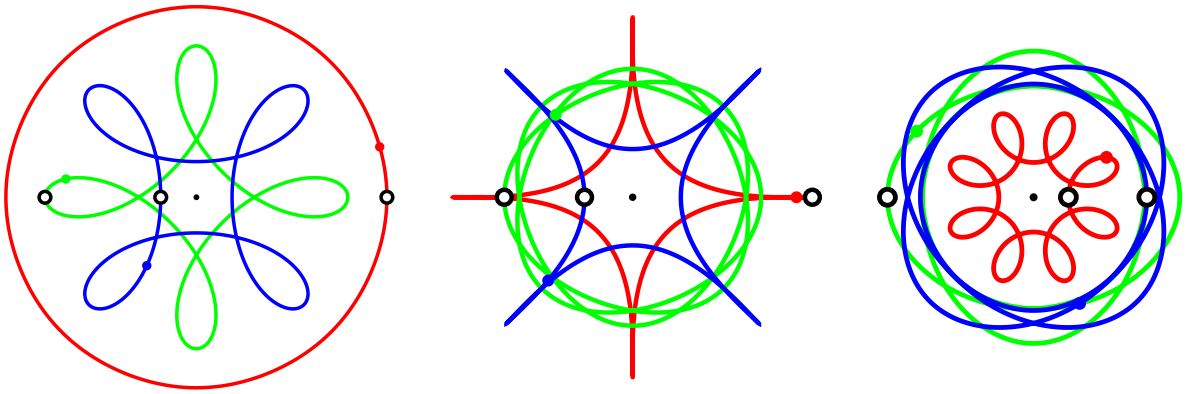

Figure 2.15 – Three orbits with $\omega = 1/4$.

If, as in the case shown in Fig. 2.13, we cyclically permute the masses on the left orbit of Fig. 2.15, we will also obtain similar orbits. Numerical integration of the left orbit in Fig. 2.15 over a long period (about 10 000 periods) shows that the orbit maintains its shape. Numerical integration of the middle orbit in Fig. 2.15 over one period yields the same orbit, with energy and angular momentum constants preserved to an accuracy of $6 \cdot 10^{-6}$ and $3 \cdot 10^{-6}$ respectively. However, even by the second period, the orbit breaks down, indicating that the middle orbit is very sensitive to initial conditions, and 5-6 significant figures are not sufficient to achieve a periodic orbit. The same can be said for the right orbit, although the energy and angular momentum constants are preserved (to an accuracy of $4 \cdot 10^{-6}$ and $1 \cdot 10^{-6}$), the orbit is extremely sensitive to initial conditions, and by the first period, the result of numerical integration significantly diverges from the right orbit shown in Fig. 2.15.

2.4.3 Angular velocity $\omega = 1/3$

The orbits obtained for $\omega = 1/3$ are shown in Fig. 2.16.

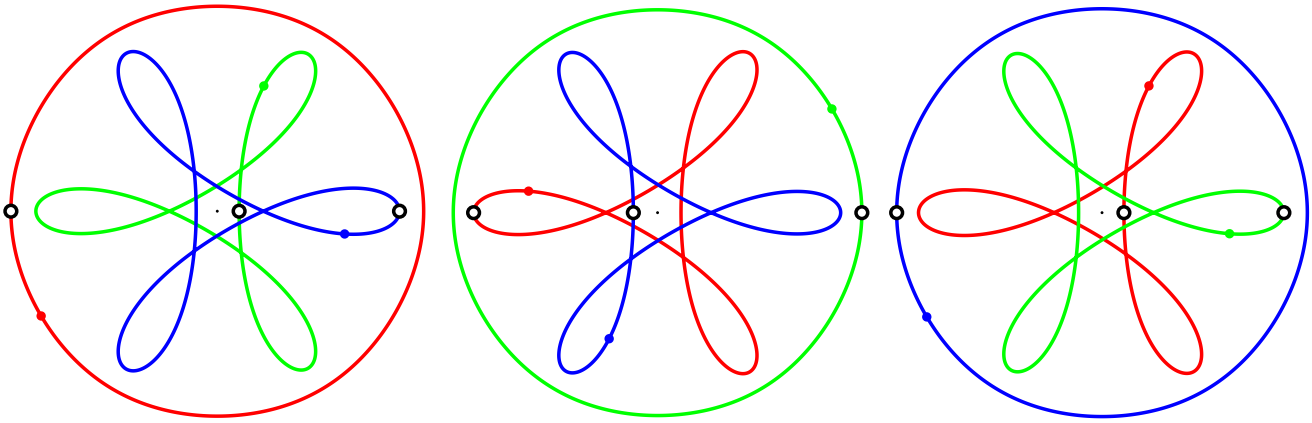

Figure 2.16 – Three orbits with linear symmetry corresponding to the cyclic permutation of masses m_1, m_2, m_3 ($\omega = 1/3$).

As with the case of $\omega = 1/2$, numerical integration over a span of 10 000 periods yields similar orbits.

In Fig. 2.17, periodic orbits are shown, for which numerical integration beyond one period causes the bodies to deviate from the orbit. The two left orbits

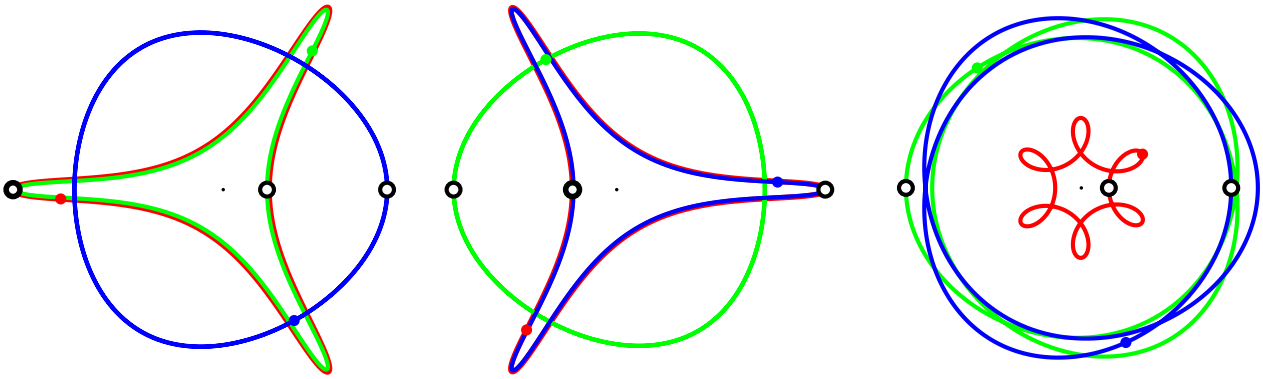

Figure 2.17 – Three unstable orbits with linear symmetry, $m_1 = 0.99$, $m_2 = 1.01$, $m_3 = 1.0$ ($\omega = 1/3$).

differ slightly from each other because their masses are slightly different. Naturally, the orbit with the third cyclic permutation of masses is also similar to these

two orbits, and it is not shown here. Numerical integration for one period results in orbits that do not differ from these orbits, but integrating over several periods alters the original orbit, causing the triangular orbits of the two bodies to slowly rotate. Numerical integration of the initial conditions for the rightmost orbit in Fig. 2.17 results in an open orbit even after one period, although the deviation is small, and refining the initial conditions can achieve greater accuracy.

In Fig. 2.18, the orbits are shown where two particles (red and blue) move around each other, while the third (green) rotates around the first two. In this case, the constancy of energy and angular momentum fluctuates very little (about 10^{-7} and $2 \cdot 10^{-8}$ in the first case and about $4 \cdot 10^{-8}$ and $2 \cdot 10^{-8}$ in the second). On the right, the result of numerical integration for the middle orbit over a span of 500 periods is shown. It can be seen that the orbits only shift around the origin, remaining qualitatively the same as on the (one-period) middle plot.

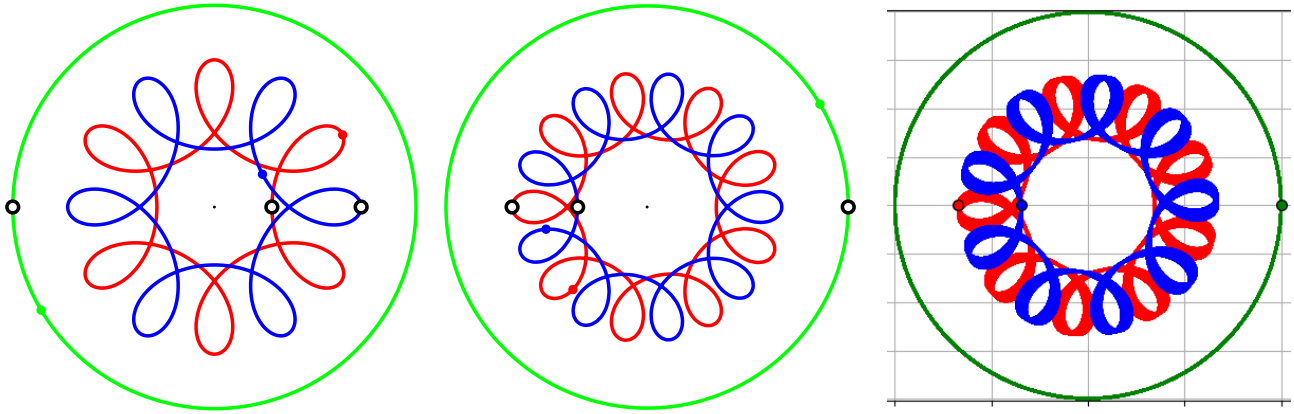

Figure 2.18 – Orbits with tight binaries, $m_1 = 0.99$, $m_2 = 1.01$, $m_3 = 1.0$ ($\omega = 1/3$).

In Tables 3 and 4, the considered orbits with linear symmetry are presented. Each row contains the values of the action functional, constant of energy, constant of angular momentum, value of ω, intervals of system size variation (moment of inertia), the figure number with the orbit, and a "$+$" or "$-$" indicating whether the orbits remain stable over a long time (on the order of several thousand periods) or not.

In Table 4, for different values of m_1 ($m_1 + m_2 + m_3 = 3$, $m_3 = 1$) and for $\omega = 1/2$, the action functional A, constant energy E, absolute value of the area constant $|J|$, the interval of inertia moment I, and the corresponding figure number are provided.

Table 3

$m_1 = 0.99$, $m_2 = 1.01$, $m_3 = 1.0$						
A	E	$\|J\|$	ω	$[I_{\min}, I_{\max}]$	Fig	Stab
11.42286	-0.606002	1.36301	1/4	[2.94098,3.00409]	2.15l	+
12.04740	-0.639135	1.19429	1/3	[2.57062,2.65947]	2.16c	+
12.06332	-0.639979	1.17690	1/3	[2.56697,2.65581]	2.16r	+
12.07962	-0.640844	1.15915	1/3	[2.56338,2.65206]	2.16l	+
13.15385	-0.697833	0.92132	1/2	[2.20208,2.35139]	2.13l	+
13.15566	-0.697930	0.93926	1/2	[2.20200,2.35145]	2.13c	+
13.15748	-0.698026	0.95484	1/2	[2.20195,2.35150]	2.13r	+
14.08066	-0.747002	0.85327	1/3	[2.08666,2.31026]	2.17l	-
14.09948	-0.748001	0.86909	1/3	[2.08357,2.30697]	2.17c	-
14.55725	-0.772286	0.88706	1/4	[2.08071,2.34630]	2.15c	-
16.64808	-0.883208	1.19288	1/3	[1.82682,1.92875]	2.17r	-
16.76479	-0.889400	1.37020	1/3	[2.31341,2.33911]	2.18l	+
17.80747	-0.944715	2.06327	1/4	[1.64193,1.85856]	2.15r	-
20.59152	-1.09242	1.45497	1/3	[2.23074,2.24393]	2.18c	+

Table 4

m_1	$m_1 + m_2 = 2$, $m_3 = 1.0$, $\omega = 1/2$				
	A	E	$\|J\|$	$[I_{\min}, I_{\max}]$	Fig
0.99	13.15748	-0.698026	0.95484	[2.20195,2.35150]	2.13r
0.95	13.15312	-0.697795	1.01964	[2.20000,2.35627]	2.14
0.9	13.12580	-0.696348	1.09648	[2.19456,2.35000]	2.14
0.8	12.99779	-0.689554	1.23654	[2.17368,2.32511]	2.14
0.7	12.77091	-0.677518	1.35872	[2.13912,2.28344]	2.14

2.5 Periodic Orbits in the Shape Space

Now, let us look at how the found orbits appear in the shape space. From Tables 2–4, we can see that in almost all cases, the moment of inertia changes insignificantly, usually within a few percent. This means that we can limit the visualization of these orbits to the shape sphere, or even more simply, in the space of angular coordinates (φ,θ).

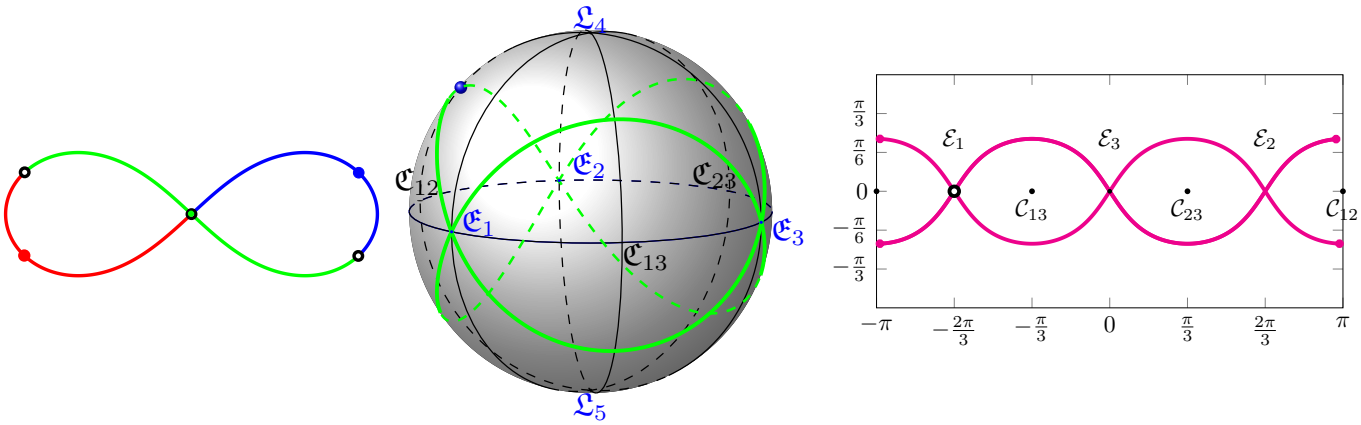

Figure 2.19 – The figure-eight in the inertial system, on the shape sphere, and in the plane (φ,θ)

In Fig. 2.19, the trajectory of the figure-eight is shown in the inertial space, on the shape sphere, and in the (φ,θ) plane. On the left image (inertial coordinate system), the initial positions are marked by small black circles: the three bodies are in one of the Eulerian configurations ($\mathcal{C}_1$). After one-sixth of the period, the bodies are again in (another) Eulerian configuration, with the positions marked by colored circles on the left image. On the shape sphere (middle image), the point moves along the green trajectory, sequentially passing through the Eulerian configurations $\mathcal{C}_1, \mathcal{C}_2, \mathcal{C}_3, \mathcal{C}_1, \mathcal{C}_2, \mathcal{C}_3$, or in reverse order, as the equations of motion are time-reversible. Each Eulerian point is passed twice per period. In the φ,θ plane (right image), the motion starts at the point $\mathcal{C}_1$. Pairs of points with $\varphi = -\pi$ and $\varphi = \pi$ and the same θ values should be identified, so the motion in the φ,θ plane will exactly correspond to the motion on the shape sphere.

Now let us consider the periodic orbits obtained for the $2-1$ symmetry. We will plot these trajectories on the φ,θ plane. For example, we will choose trajectories obtained for different values of ω: $1/2$ (left orbit in Fig. 2.4), $2/5$ (left orbit in Fig. 2.6),

and $1/3$ (left orbit in Fig. 2.9). In the first two cases, $m_1 = m_2 = 0.95, m_3 = 1.1$, and in the last case, $m_1 = m_2 = 1.05, m_3 = 0.9$. In Fig. 2.20, the three indicated trajectories are shown on the φ,θ plane.

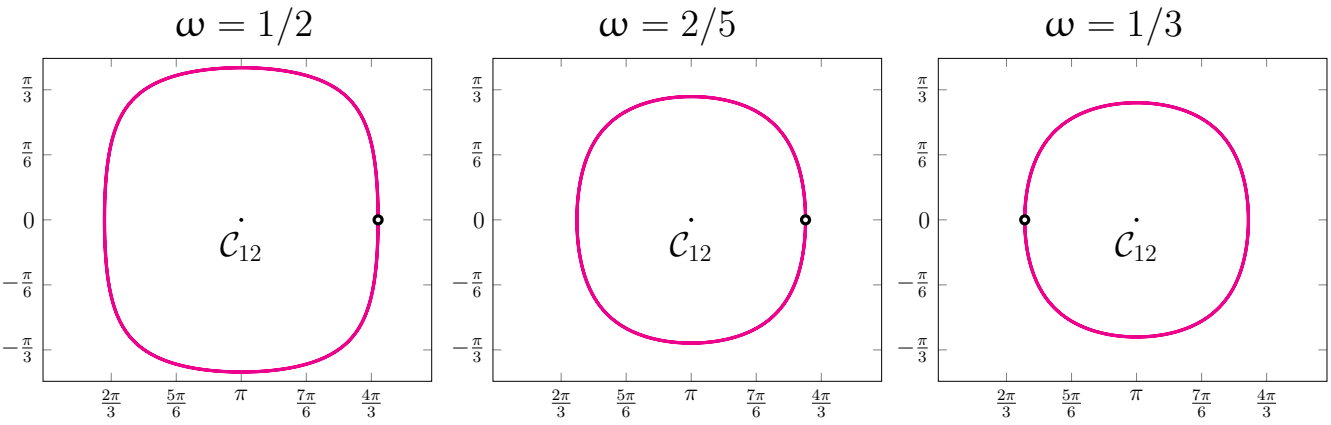

$5.462 \leqslant I \leqslant 5.580$ $\quad$ $6.446 \leqslant I \leqslant 6.518$ $\quad$ $5.462 \leqslant I \leqslant 5.580$

$(m_1 = m_2 = 1.05, m_3 = 0.9)$

Figure 2.20 – Periodic orbits with $2-1$ symmetry on the (φ,θ) plane

The considered trajectories represent closed curves, quasi-circles, with the point of double collision C_{12}, the collision point of equal masses, at their center. The size of the orbit decreases with decreasing ω.

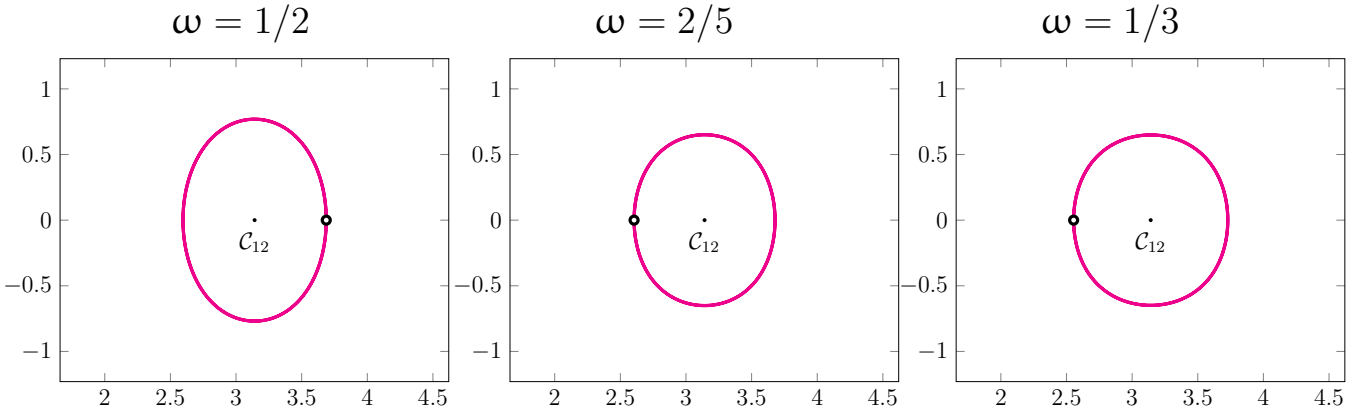

$3.967 \leqslant I \leqslant 4.154$ $\quad$ $5.352 \leqslant I \leqslant 5.457$ $\quad$ $6.275 \leqslant I \leqslant 6.341$

$(m_1 = m_2 = 1.05, m_3 = 0.9)$

Figure 2.21 – More periodic orbits with $2-1$ symmetry on the (φ,θ) plane

It is interesting to look at other orbits with $2-1$ choreography symmetry. In Fig. 2.21, three more orbits are shown: for $\omega = 1/2$, the right orbit from Fig. 2.4; for

$\omega = 2/5$, the right orbit from Fig. 2.6; and for $\omega = 1/3$ ($m_1 = m_2 = 1.05, m_3 = 0.9$), the middle orbit from Fig. 2.9.

It is obvious that qualitatively, these orbits shown in Fig. 2.21 do not differ from the orbits in Fig. 2.20: closed quasi-circles around the point of double collision $\mathcal{C}_{12}$, only the size of these orbits has slightly decreased.

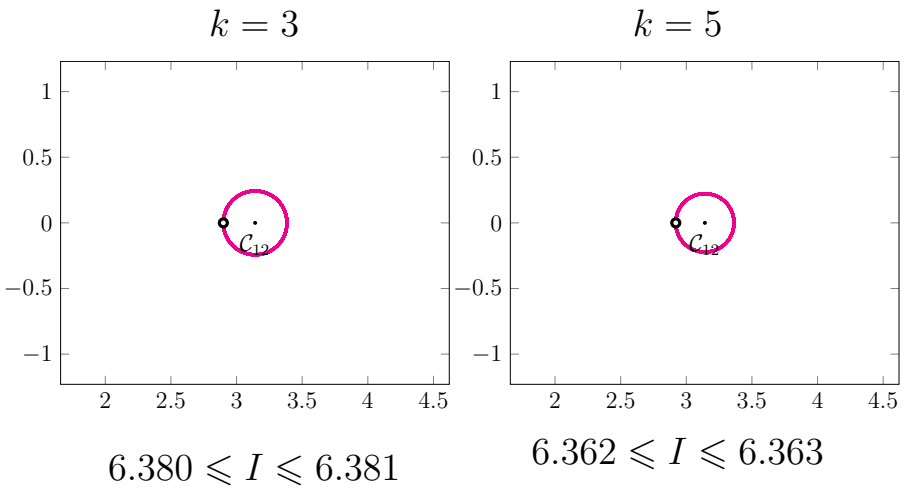

Figure 2.22 – Periodic orbits with tight binaries with $2-1$ symmetry on the (φ,θ) plane ($\omega = 1/3$)

In section 2.2, we also obtained orbits with tight binaries. Here is their depiction on the (φ,θ) plane. In this case, the size of the curves is small (and decreases with increasing k), the moment of inertia changes within very narrow limits, but at the center of the curves is the point of double collision $\mathcal{C}_{12}$.

The question arises: do all orbits represent curves with the double collision point $\mathcal{C}_{12}$ at their center? Of course, this point is different from the other two since $m_1 = m_2$, but let us look at other orbits from Table 2. Only two orbits from this table are closed curves with the Euler configuration point $\mathcal{E}_3$, opposite to the double collision point $\mathcal{C}_{12}$, at their center. These are the right orbit in Fig. 2.8 and the right orbit in Fig. 2.9; in fact, these orbits differ only slightly in their masses and both are unstable.

Now, let us consider orbits with linear symmetry. In this case, the masses can be arbitrary, and cyclic permutation of the masses gives us different orbits. If the masses differ only slightly, the orbits will be similar. In Fig. 2.13 of section 2.4, there are three orbits where the masses are cyclic permutations of $m_1 = 0.99$, $m_2 = 1.01$, $m_3 = 1.0$.

The masses differ very little, and therefore the orbits in Fig. 2.13 are very similar. But how do they look in shape space? As before, since the moment of inertia changes very little, it is sufficient to look at the orbits on the shape sphere, or on the (φ,θ) plane (Fig. 2.23).

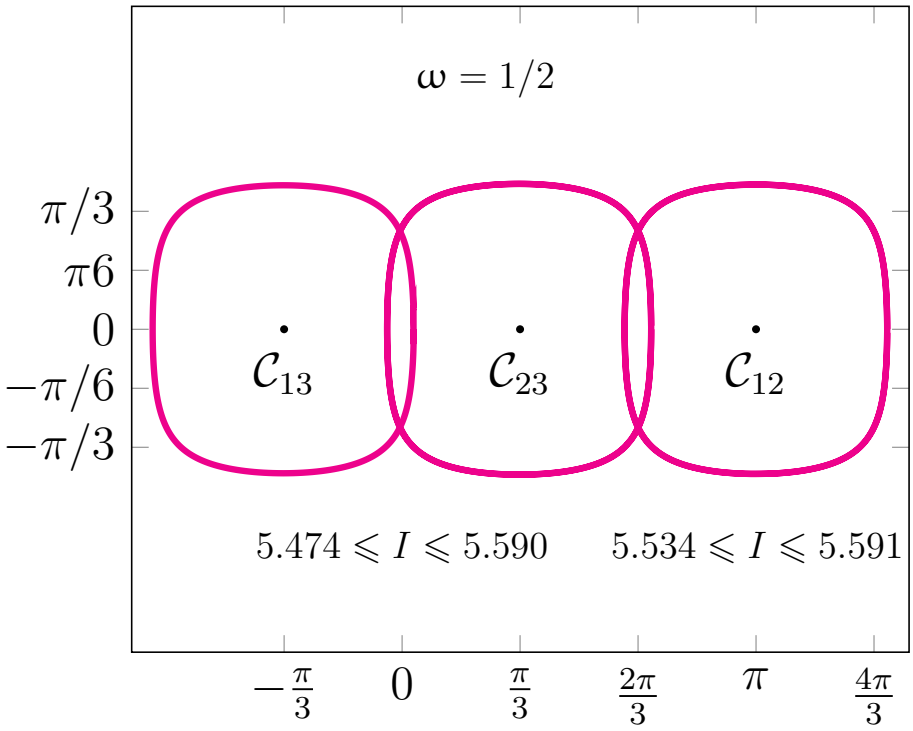

Figure 2.23 – Periodic orbits with line symmetry on the (φ,θ) plane, $\omega = 1/2$

The three orbits in Fig. 2.13 correspond to three very similar orbits on the (φ,θ) plane, but located in completely different places: centered at three different double collision points: $\mathcal{C}_{13}$, $\mathcal{C}_{23}$, and $\mathcal{C}_{12}$.

The same picture will be obtained for the three orbits shown in Fig. 2.16. In this case, $\omega = 1/3$, the orbits differ only by a cyclic permutation of the masses, and on the (φ,θ) plane we have:

Thus, both Fig. 2.23 and Fig. 2.24 show qualitatively the same picture: closed curves around the double collision points. The same pattern will remain for the mass values shown in Fig. 2.14, changing the size of the curve and its shape, but the qualitative picture will remain the same: closed curves around the corresponding double collision points $\mathcal{C}_{ij}$. Obviously, the picture will not change for the tight binary orbits shown in Fig. 2.18.

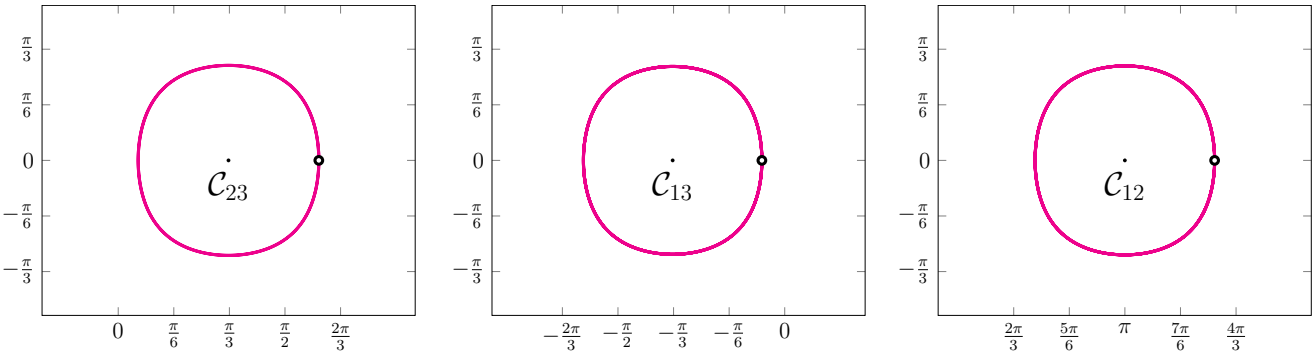

$7.471 \leqslant I \leqslant 7.520$ $7.508 \leqslant I \leqslant 7.557$ $7.489 \leqslant I \leqslant 7.538$

Figure 2.24 – Periodic orbits with line symmetry on the (φ,θ) plane, $\omega = 1/3$

As with the $2-1$ choreography symmetry orbits, among the orbits listed in Tables 3 and 4, there are also orbits with Euler configuration points $\mathcal{E}_i$ at their centers. The right orbits in Figs. 2.15 and 2.17 (around point $\mathcal{E}_3$), the middle orbit in Fig. 2.15 (around point $\mathcal{E}_2$), and the right orbit in Fig. 2.15 (around point $\mathcal{E}_1$) are such examples. These orbits are shown in Fig. 2.25. All of them are unstable.

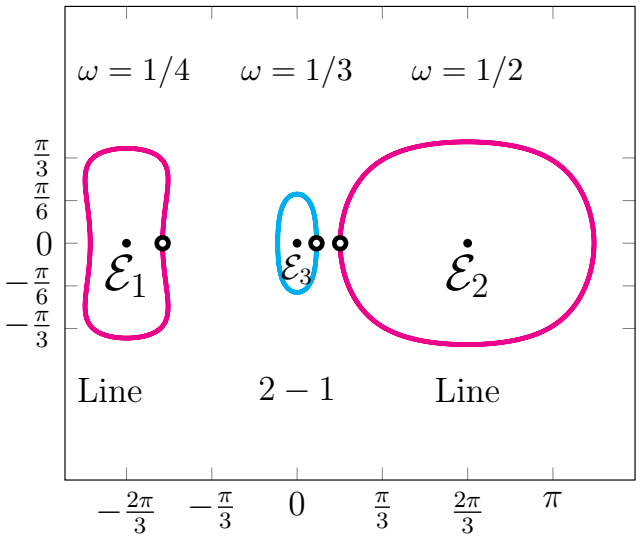

Figure 2.25 – Periodic orbits around $\mathcal{E}_i$ on the (φ,θ) plane

Thus, in the shape space, periodic orbits have a simple form.

Chapter 3. Regions of Possible Motion

At the end of the XIX-th century, Bruns and Poincaré proved that the 10 classical integrals of the three-body problem, listed in the introduction, are the only independent integrals of the problem. Later, Poincaré extended this statement to the N-body problem. Although K. Sundman constructed a general solution to the three-body problem in the case of non-zero angular momentum J in the form of convergent series, these series are of little use for studying the solution: their extremely slow convergence does not allow us to study the properties of the solutions or obtain these solutions in an acceptable form. For example, to obtain the coordinates of a well-known partial solution obtained by Lagrange, where the configuration of the three bodies forms an equilateral triangle, one would need to take $10^{80\,000}$ terms of the series, which is unlikely to ever become feasible.

Therefore, the qualitative study of the three-body problem is of great importance, particularly the investigation of the regions of possible motion of the problem.

In the two-body problem, the region of possible motion can be assessed from the energy integral:

$$T - V = \frac{\dot{\mathbf{r}}^2}{2} - \frac{1}{r} = h$$

For $h < 0$, this condition gives a circle outside of which motion is impossible (see Fig. 3.1 left). If we also consider the angular momentum integral,

$$\mathbf{r} \times \dot{\mathbf{r}} = \mathbf{J} = r^2\dot{\theta},$$

we obtain

$$\frac{2}{r} + 2h - \frac{J^2}{r^2} \geqslant 0$$

or

$$\begin{cases} r_{\min} \leqslant r \leqslant r_{\max}, & \text{if } h < 0, \\ r \geqslant r_{\min}, & \text{if } h \geqslant 0. \end{cases}$$

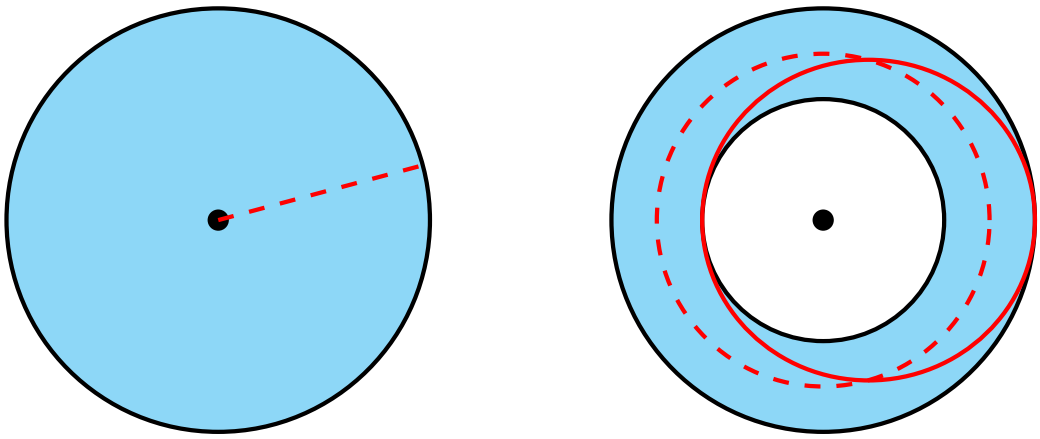

Figure 3.1 – Regions of possible motion for the two-body problem with energy $h < 0$ (left), with $h < 0$ and angular momentum $J \neq 0$ (right)

Thus, in the two-body problem, knowledge of two constants, energy and angular momentum, allows us to determine the region of possible motion, a disk as shown in Fig. 3.1 on the right. These regions are defined either in the space of relative coordinates or in the barycentric coordinate system.

For the N-body problem, the inequality derived by Lagrange is valid (see, for example, [90]),

$$J^2 = \left|\sum m_i(\mathbf{r}_i \times \mathbf{v}_i)\right|^2 \leqslant \left(\sum m_i|\mathbf{r}_i|\,|\mathbf{v}_i|\right)^2 \leqslant \left(\sum m_i\mathbf{r}_i^2\right)\left(\sum m_i\mathbf{v}_i^2\right) = I \cdot 2T. \quad (3.1)$$

In the planar three-body problem, the set of possible motions is $B = \{V + J^2/2I \leqslant h\}$, but in the spatial problem, the set of possible motions is only a subset of the set defined by the inequality, $B \subset \{V + J^2/2I \leqslant h\}$. In Fig. 3.2, the region of possible motion (blue) is included in the region B (cyan).

In the restricted circular three-body problem, the zero-velocity surface, which bounds the set of possible motions $\mathcal{B}$ of a body of zero mass, was introduced by J. Hill in 1878. Geometrically, the Hill surface is a projection of the 5-dimensional level surface of the Jacobi integral onto the 3-dimensional configuration space. The properties of $\mathcal{S}$ have been studied in detail; see, for example, [101; 102]. Several generalizations of this concept are known, both for the case when one of the bodies is not a point (see, for example, [109]) and for cases when the problem is not circular [95].

The regions of possible motion in the general three-body problem in Cartesian coordinates were investigated by V. G. Golubev in [93] and V. N. Thai in [106]. In these

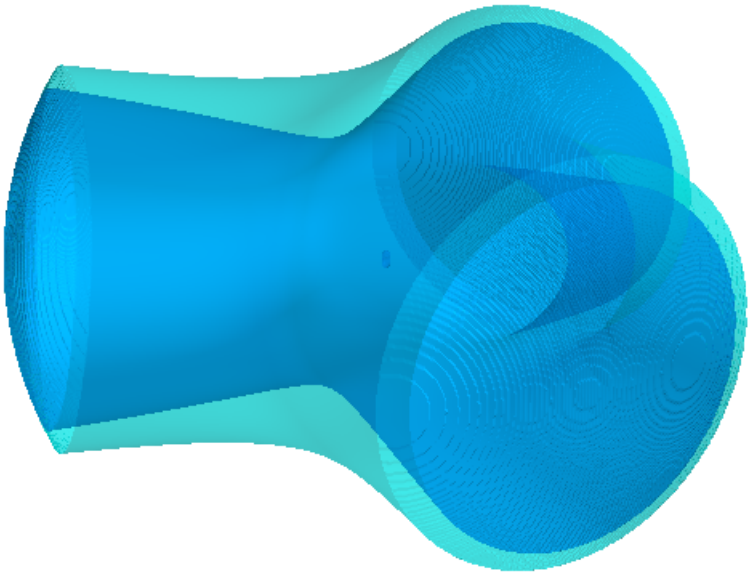

Figure 3.2 – The region of possible motion is included in the region $\{V + J^2/2I \leqslant h\}$

works, mutual distances are used as variables (in V. G. Golubev's work – relative mutual distances). These variables are related to the configuration of the three bodies, but in the shape space considered in this work, surfaces are constructed much more easily, and they are simple to draw.

To construct the region of possible motion, the integrals of motion are used. In the two-body problem, for example, the energy integral

$$T - U = \frac{\dot{\mathbf{r}}}{2} - \frac{1}{r} = h$$

yields

$$\frac{1}{r} + h \geqslant 0, \text{ или } \quad r \leqslant 2a = -\frac{1}{h}, \text{if } h < 0.$$

We assume the universal gravitational constant to be equal to 1, which can always be achieved by an appropriate choice of units (length, mass, time). In the case of $h \geqslant 0$, the region of possible motion coincides with the entire configuration space $\mathbb{R}^2$.

The region of possible motion will be even more restricted if we consider the angular momentum integral as well:

$$\mathbf{r} \times \dot{\mathbf{r}} = \mathbf{J} = r^2\dot{\psi}$$

Taking this integral into account, the energy integral can be written as

$$T - U = \dot{r}^2 + r^2\dot{\psi}^2 = \dot{r}^2 + \frac{J^2}{r^2} - \frac{1}{r} = h$$

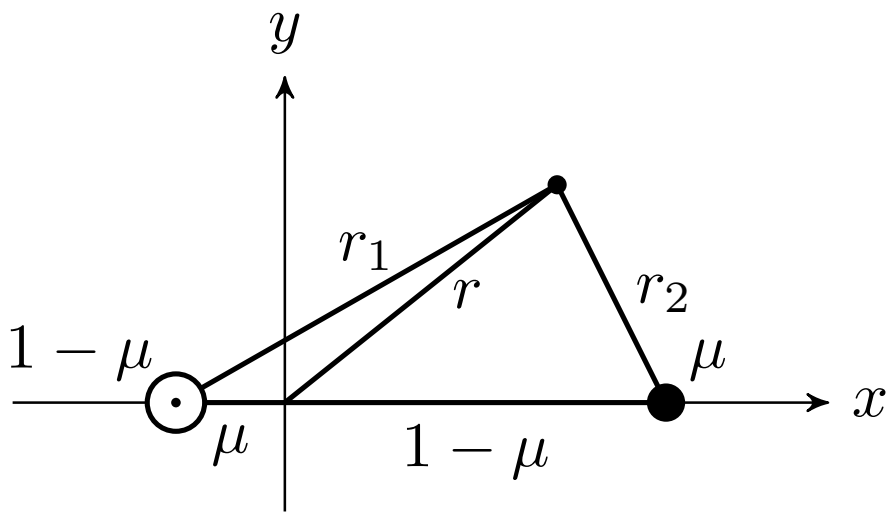

Figure 3.3 – Restricted three-body problem

For $h < 0$, we obtain

$$\frac{1}{r} + h - \frac{J^2}{r^2} \geqslant 0 \quad \rightarrow \quad 0 < r_1 \leqslant r \leqslant r_2$$

Thus, if we consider only the energy integral for $h < 0$, the region of possible motion is a disc of radius $2a$. If we also fix the value of the angular momentum integral J, the region of possible motion is a ring, where motion is possible between its boundaries. These boundaries are also included in the region of possible motion, and this connected region is compact.

In the circular restricted three-body problem (Fig. 3.3), the regions of possible motion are well studied and are determined by the Jacobi integral:

$$\dot{x}^2 + \dot{y}^2 + \dot{z}^2 - (x^2 + y^2) - 2\left(\frac{m_1}{r_1} + \frac{m_2}{r_2}\right) + C = 0,$$

where x,y,z are the coordinates of a point with negligible mass in the rotating coordinate system. In this system, the two bodies of masses m_1 and m_2 are fixed, the origin is at the barycenter, and the units of mass, length, and time are chosen such that the angular velocity of rotation is unity, the sum of the masses $m_1 + m_2 = 1$, and the distance between m_1 and m_2 is equal to unity. The zero-velocity surface is then defined by the equation

$$(x^2 + y^2) + 2\left(\frac{m_1}{r_1} + \frac{m_2}{r_2}\right) = C$$

and serves as the boundary of the region of possible motion. There is no second integral in this problem, but the Jacobi integral allows for the qualitative description of the motion of the body with negligible mass.

In the x,y plane, the regions of possible motion appear as shown in Fig. 3.4

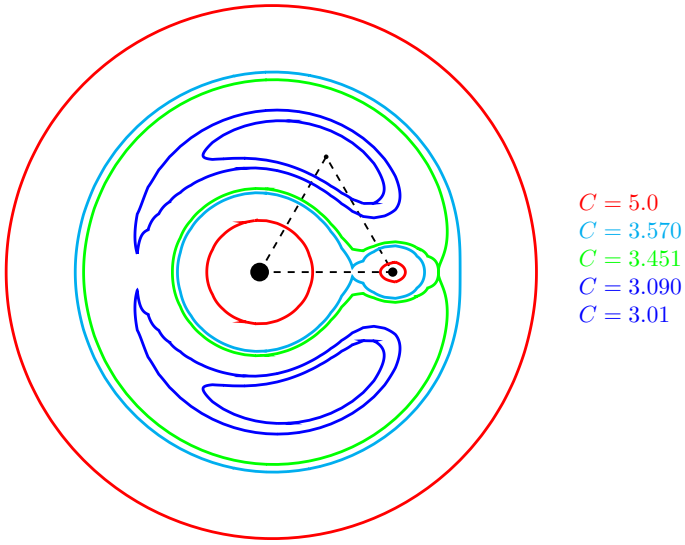

Figure 3.4 – Zero-velocity curves in the x,y plane

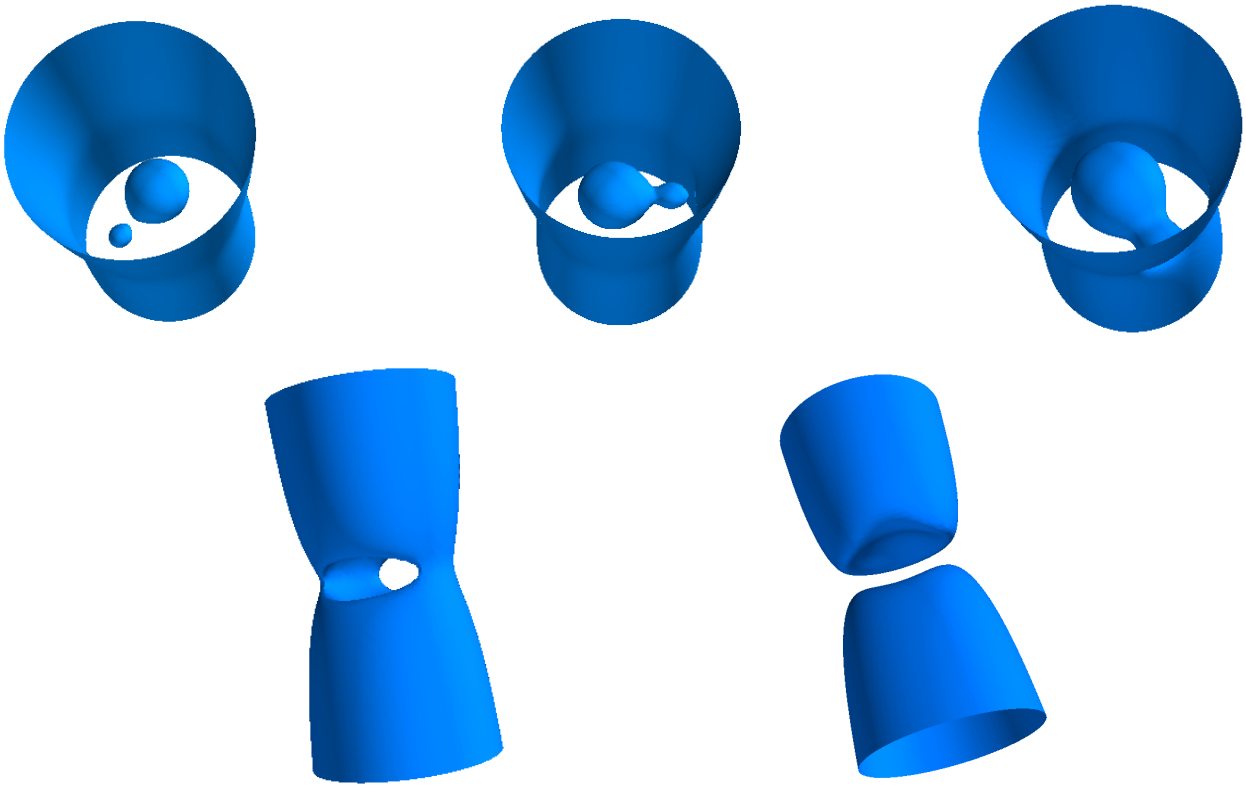

Figure 3.5 – Five types of Hill surfaces in the circular restricted three-body problem

Fig. 3.5 shows five topologically different types of zero-velocity surfaces (bounding the region of possible motion) depending on the value of the Jacobi constant C. The

first image, top left, corresponds to a relatively large value of C. The two quasi-spheres around the bodies m_1 and m_2 are compact, and motion is possible either inside these quasi-spheres (in which case the negligible mass body will always remain there, a situation described as Hill-stable motion) or outside the quasi-cylinder. With a decrease in C, as shown in the center top image, the two quasi-spheres merge at the Lagrange point L_1, and with further reduction of C, a dumbbell-shaped surface is formed. This surface is compact; a body of negligible mass will always remain inside it, but transfer from the vicinity of one massive body to another is possible. Further decrease in C causes the dumbbell-shaped surface to merge with the quasi-cylinder at the Lagrange point L_2, forming a single zero-velocity surface. This surface is homeomorphic to a cylinder. The region of possible motion is simply connected. With further decrease in C, the dumbbell-shaped surface merges with the quasi-cylinder at the Lagrange point L_3, forming a quasi-cylinder with a hole; motion is only possible outside this surface. Finally, with further reduction of C, the quasi-cylinder splits into two non-compact parts. For $C < C_*$, motion is possible throughout the entire configuration space.

Remark 1: In the two-body problem, the zero-velocity surface is constructed in a rectangular coordinate system centered on the (larger) body, while in the circular restricted three-body problem, it is constructed in a rotating coordinate system. In this coordinate system, the Hill surface is the zero-velocity surface.

Remark 2: The presence of the area integral significantly narrows the region of possible motion.

3.1 Minimum Velocity Surface in the Circular Restricted Three-Body Problem

Consider the averaged circular restricted three-body problem. Averaging introduces additional symmetry to the problem and, consequently, another integral (the area integral), which can be utilized in various problems.

In the work [98], the norm of the difference between the coordinates of the osculating and averaged motion in the problem of motion with a perturbing acceleration constant in the reference frame associated with the velocity vector is evaluated. Corresponding expansions are constructed with an accuracy up to e^4. The results of this work were used in [107] to assess the possibility of diverting a hazardous asteroid from a collision course with Earth using a low-thrust engine.

The Hill surfaces discussed in the previous section have been generalized by many authors, such as [95; 96; 106]. Here, we define the minimum velocity surface $\mathcal{S}$. Its use allows for much stricter constraints on the set of possible motions $\mathcal{T}$ of a zero-mass body. In particular, for typical parameter values, the surface $\mathcal{S}$ (and hence $\mathcal{T}$) is bounded and quite narrow, unlike the classical Hill surface, which always contains an unbounded subset. Of course, $\mathcal{S}$ exists only in the problem averaged over the longitudes of the primary bodies and thus possessing additional symmetry.

Thus, the bodies Q_1 and Q_2 with masses m_1 and m_2 ($0 < m_2 \leqslant m_1$) move in a circular orbit, i.e., they describe Keplerian circles around the barycenter O with an angular velocity (mean motion) n. The motion of the zero-mass body Q is considered in the barycentric system, whose xy-plane coincides with the plane of motion of the primary bodies m_1 and m_2. If we denote the distances Q_1Q_2, OQ_1, OQ_2, Q_1Q, Q_2Q, OQ as c, c_1, c_2, r_1, r_2, r, then according to the two-body problem formulas we have

$$c_1 = \frac{m_2}{m_1+m_2}c, \quad c_2 = \frac{m_1}{m_1+m_2}c, \quad c = c_1 + c_2\,, \quad n = \sqrt{\mathcal{G}(m_1+m_2)}c^{-3/2},$$

where $\mathcal{G}$ is the gravitational constant. The coordinates of the points Q_s as a function of time t can be set due to the choice of the initial epoch as

$$Q_1 = (-c_1\cos nt,\ -c_1\sin nt, 0), \qquad Q_2 = (c_2\cos nt, c_2\sin nt, 0).$$

The coordinates of the point Q are denoted here as $Q = (x,y,z)$.

The kinetic energy and the potential function per unit mass of the point Q in the field of the primary bodies are given by

$$T_m = \frac{v^2}{2}\,, \qquad V_m = V_1 + V_2\,, \qquad V_s = \frac{\mathcal{G}m_s}{r_s}\,, \qquad s = 1{,}2. \tag{3.2}$$

Here, v is the velocity of the point Q,

$$r_1^2 = (x+c_1\cos nt)^2+(y+c_1\sin nt)^2+z^2, \qquad r_2^2 = (x-c_2\cos nt)^2+(y-c_2\sin nt)^2+z^2.$$

The functions (3.2) have a period $P = 2\pi/n$ over time, so it is permissible to apply the averaging method to our dynamic system. Namely, we replace V,V_s with their average values W,W_s over the explicitly entered time. By definition,

$$W_1 = \frac{\mathcal{G}m_1}{P}\int_0^P \frac{dt}{r_1}. \tag{3.3}$$

The integral (3.3) has been known since the time of Gauss [89]. Let us represent r_1^2 in the form

$$r_1^2 = r^2 + c_1^2 + 2c_1(x\cos\omega t + y\sin\omega t) = r^2 + c_1^2 + 2c_1\sqrt{x^2+y^2}\cos(\omega t - \psi),$$

where ψ does not explicitly depend on time. Making the substitution in the integral (3.3) $nt - \psi = 2\tau$, we get

$$W_1 = \frac{\mathcal{G}m_1}{\pi}\int_{-\psi/2}^{\pi-\psi/2} \frac{d\tau}{r_1}.$$

The integrand has a period of π with respect to τ, so the integration limits can be replaced by 0 and π. As a result, we arrive at the complete elliptic integral

$$W_1 = \frac{\mathcal{G}m_1}{\pi}\int_{-\psi/2}^{\pi-\psi/2} \frac{d\tau}{r_1}. \tag{3.4}$$

Here,

$$k_1^2 = \frac{4c_1\sqrt{x^2+y^2}}{r^2 + c_1^2 + 2c_1\sqrt{x^2+y^2}}, \tag{3.5}$$

with

$$0 \leqslant k_1 \leqslant 1. \tag{3.6}$$

The equality on the left is achieved only on the z-axis (when $x^2 + y^2 = 0$), and on the right only on a special circle (when $x^2 + y^2 = c_1^2$, $z = 0$).

It is evident that W_2 is given by the formulas (3.4), (3.5), (3.6) with the substitution of index 1 by 2.

The system defined by the functions T_m, $W = W_1 + W_2$ is autonomous and depends on x,y only through $x^2 + y^2$. Therefore, it possesses two integrals: energy and angular momentum

$$W - \frac{v^2}{2} = h, \tag{3.7}$$

$$x\dot{y} - y\dot{x} = J. \tag{3.8}$$

Bounded motions are possible only with negative total energy of the body Q, in which case $h > 0$. We will consider only such motions.

Often, besides averaging over the longitudes of the primary bodies, averaging over the longitude of the body Q is also performed [88; 92], but this is not required for constructing the desired surfaces.

By the Cauchy–Bunyakovsky inequality from (3.8), we get

$$J^2 \leqslant (\dot{x}^2 + \dot{y}^2)(x^2 + y^2) \leqslant v^2(x^2 + y^2). \tag{3.9}$$

Hence, from the integral (3.7), it follows that $W \geqslant \frac{J^2}{2(x^2+y^2)} + h$, which is more conveniently written as

$$F(x,y,z) \geqslant 0 \tag{3.10}$$

where

$$F(x, y, z) = W - \frac{J^2}{2(x^2 + y^2)} - h. \tag{3.11}$$

The relationship (3.10) indicates that the point Q is always located in the region $\mathcal{T} \subset \mathbb{R}^3$, whose boundary $\mathcal{S} \subset \mathbb{R}^3$ is defined by the equation

$$F(x,y,z) = 0. \tag{3.12}$$

We will call $\mathcal{S}$ the *minimum velocity surface*.

Note. The boundedness of the closed set $\mathcal{T} \in \mathbb{R}^3$ is proven below, making it compact.

Properties of the minimum velocity curve. Let $\mathcal{T}^*$ and $\mathcal{S}^*$ denote the intersections of $\mathcal{T}$ and $\mathcal{S}$ with the xy plane. Our dynamical system allows for planar motions $z = 0$.

Table 5 – Values of k_s, W_s and F at key points.

r	0	c_1	c_2	∞
k_1^2	0	1	$\dfrac{4c_1c_2}{c^2}$	0
k_2^2	0	$\dfrac{4c_1c_2}{c^2}$	1	0
W_1	$\dfrac{\mathcal{G}m_1}{c_1}$	∞	$\dfrac{2\mathcal{G}m_1\mathbf{K}(k_1(c_2))}{\pi c}$	0
W_2	$\dfrac{\mathcal{G}m_2}{c_2}$	$\dfrac{2\mathcal{G}m_2\mathbf{K}(k_2(c_1))}{\pi c}$	∞	0
F	-∞	∞	∞	$-h$

Therefore, $\mathcal{T}^*$ with boundary $\mathcal{S}^*$ defines the compact region of possible motions if the initial position and velocity of the point Q lie in the xy plane.

The curve $\mathcal{S}^*$ is given by the same equation (3.12), where W and $F(x,y,0) = F^*(r)$ depend only on $r = \sqrt{x^2+y^2}$:

$$k_s^2 = \frac{4c_s r}{(r+c_s)^2}\,, \qquad W_s = \frac{2\mathcal{G}m_s\mathbf{K}(k_s)}{\pi(r+c_s)}\,, \qquad F^* = W_1 + W_2 - \frac{J^2}{2r^2} - h. \tag{3.13}$$

Table 5 provides the values of k_s, W_s, and F^* at key points, including the point at infinity.

The relationships (3.13) and the data from Table 5 allow us to establish the following properties of $\mathcal{T}^*$ and $\mathcal{S}^*$:

1. The sets $\mathcal{T}^*$ and $\mathcal{S}^*$ are bounded.
2. The portion of $\mathcal{S}^*$ lying within the circle $r < c_1$ consists of an odd number of circles and is therefore not empty (the function F depends only on x and y and changes sign in the interval $(-\infty,c_1)$). The same holds true for the region $r > c_2$.
3. The annulus $c_1 < r < c_2$ contains an even number of circles.

If

$$\min_{c_1<r<c_2}\left(W(r) - \frac{J^2}{2r^2}\right) > h, \tag{3.14}$$

this number is zero, and then $\mathcal{T}^*$ contains the annulus $c_1 \leqslant r \leqslant c_2$.

If inequality (3.14) is not satisfied, the corresponding part of $\mathcal{S}^*$ contains at least two circles.

Remark: To a multiple root of the equation $F^*(r) = 0$ corresponds a number of coinciding circles equal to the multiplicity.

Properties of the Minimum Velocity Surface Let us establish the main properties of $\mathcal{T}$ and $\mathcal{S}$ in the spatial case.

1. $\mathcal{S}$ and $\mathcal{T}$ are symmetric with respect to the xy plane.
2. $\mathcal{S}$ is a surface of revolution around the z-axis.
3. $\mathcal{S}$ and $\mathcal{T}$ are bounded.

   Indeed, if $r \to \infty$, then $k_s \to 0$, $W_s \to 0$, and $F \to -h$. Therefore, $\mathcal{S}$ and $\mathcal{T}$ do not contain points outside a sufficiently large radius sphere. Thus, the sets $\mathcal{S}$ and $\mathcal{T}$ are bounded and, consequently, compact.
4. The surface $\mathcal{S}$ consists of a finite number of non-intersecting and non-nested topological tori. The compact $\mathcal{T}$ consists of a finite number of non-intersecting topological full tori.

By property 2, a complete representation of the surface $\mathcal{S}$ is given by its section $\mathcal{S}_*$ in the xz plane.

Example. As an example, consider the system Pluto (Q_1) – Charon (Q_2) – a small external (relative to Charon) satellite (Q).

First, we introduce the system of units adopted in the restricted three-body problem:

unit of distance: $c = c_1 + c_2$;

unit of time: $\sqrt{c^3/(\mathcal{G}m_1 + \mathcal{G}m_2)}$.

In these units

$$c = \omega = 1, \qquad c_1 = \mathcal{G}m_2, \qquad c_2 = \mathcal{G}m_1,$$

and $\mathcal{T}$ and $\mathcal{S}$ are given by the relations (3.10, 3.12) with

$$F(x,y,z) = \frac{2c_2\mathbf{K}(k_1)}{\pi\sqrt{r^2+c_1^2+2c_1\sqrt{x^2+y^2}}} + \frac{2c_1\mathbf{K}(k_2)}{\pi\sqrt{r^2+c_2^2+2c_2\sqrt{x^2+y^2}}} - \\ - \frac{J^2}{2(x^2+y^2)} - h. \quad (3.15)$$

Note. The function (3.11) contains 6 parameters: m_1, m_2, c_1, c_2, J, h. There are only 3 independent parameters: c_1, J, h, as shown by the representation (3.15) taking into account $c_2 = 1 - c_1$.

Using the data from [76], we obtain the necessary parameter values:

$$c_1 = 0.10854, \qquad c_2 = 0.89146.$$

The constants h and J, which differ for various satellites, are listed in Table 6.

Table 6 – Values of h and J for the outer satellites.

Satellite	Styx	Nix	Kerberos	Hydra
h	0.22635	0.20274	0.16963	0.15086
J	1.49409	1.57688	1.72182	1.82464

Figure 3.6 shows the tori for Pluto's outer satellites. The satellites are located in the meridional sections of the corresponding tori, these sections are black circles. Separate sections are shown in Figures 3.7–3.10. The tori are highlighted in colors: cyan for Hydra, blue for Kerberos, green for Nix, and red for Styx. The x-axis passes through the initial positions of Pluto and Charon. The spatial structure of the surfaces is poorly visible due to the very small "thickness" of the tori, but since the surfaces of minimum velocity are surfaces of revolution, the full picture can be obtained by drawing meridional sections. These sections are shown in Figures 3.7–3.10. In these sections, the meridian is chosen so that the corresponding satellite is also located in it, which is marked on these figures with circles of the corresponding color. In the cases of Styx, Nix, and Kerberos, they are almost on their surfaces $\mathcal{S}$. This is explained by the fact that their orbits differ little from flat circular ones, so almost all the velocity moment falls on its z-component, i.e., on J. In other words, inequality (3.10) differs little from

equality. The black circle enclosing the section differs little from the section itself, thus the topological tori of the surfaces of minimum velocity are tori in the usual sense. As for the surfaces including Pluto and Charon, although they are always present, their sizes are so small (the semi-major axis of Charon's orbit is 20,000 km, from Table 7 we get at best 13 meters!!!) that they are not shown in the figures.

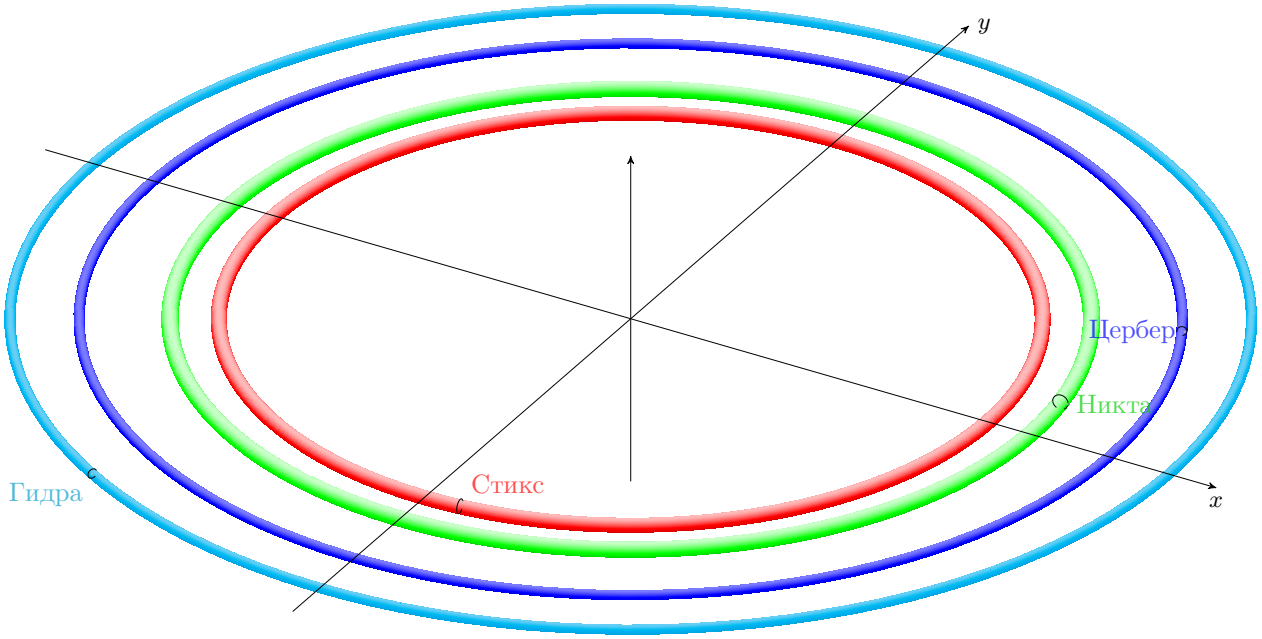

Figure 3.6 – Surfaces of S for four small moons of Pluto

Table 7 – Ring sizes around c_1 and c_2

	Half-width of the ring $c_1 = 0.10854$	Half-width of the ring $c_2 = 0.89146$	F value at the boundaries
Styx	$1.53253 \cdot 10^{-16}$	$6.7100 \cdot 10^{-7}$	$0.9 \cdot 10^{-5}$
Nix	$2.49513 \cdot 10^{-18}$	$1.9904 \cdot 10^{-8}$	$0.4 \cdot 10^{-6}$
Kerberos	$1.07711 \cdot 10^{-21}$	$1.9934 \cdot 10^{-11}$	$0.8 \cdot 10^{-6}$
Hydra	$2.91671 \cdot 10^{-24}$	$8.6971 \cdot 10^{-14}$	$0.3 \cdot 10^{-7}$

Note that the circle c_1 is contained within the layer between the two circles corresponding to the roots of the function $F^*(r)$. One root is smaller than c_1, the other is larger, but they differ from c_1 by amounts on the order of 10^{-16}, that is, they coincide with c_1 to within tens of meters. The same applies to c_2 (perhaps this is why larger planets sweep away debris). Thus, for $r < c_1$ we have one root $c_1 - 0$, between c_1 and

Table 8 – Sizes of the surfaces of minimum velocity for the outer satellites of Pluto (roots of $F^*(r)$, $r_* < r < r^*$)

	r_*	r^*
Styx	2.154184	2.234821
Nix	2.410331	2.497633
Kerberos	2.911059	2.965172
Hydra	3.278759	3.333529

c_2 there are two roots $c_1 + 0$ and $c_2 - 0$, and for $r > c_2$ we have three roots: $c_2 + 0$ and two roots that define the region of possible motion, although not very large. The sizes of the tori determined by the roots of the function $F^*(r)$ are given in Table 8. Table 7 also shows the half-widths of the possible motion rings that include the circles of Pluto ($c_1 = 0.10854$) and Charon ($c_2 = 0.89146$). The thickness of the largest ring (Styx, Charon's ring) is on the order of tens of meters!

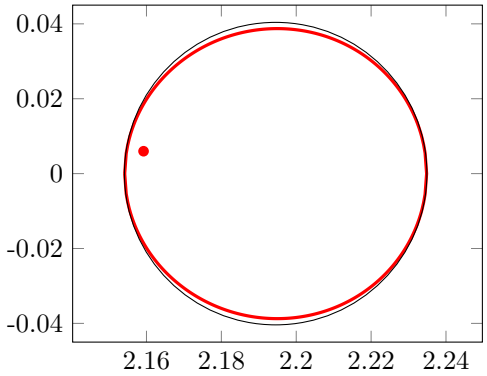

Figure 3.7 – Meridional section of the torus for Styx

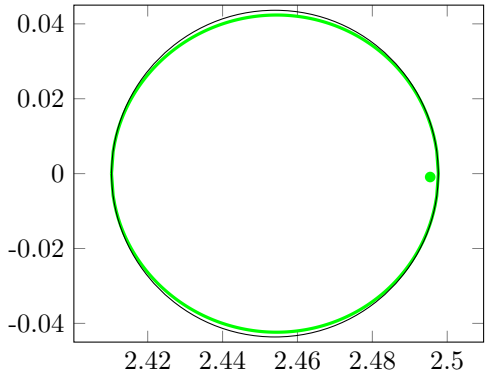

Figure 3.8 – Meridional section of the torus for Nix

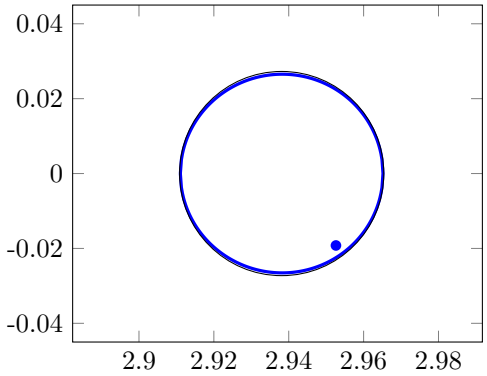

Figure 3.9 – Meridional section of the torus for Kerberos

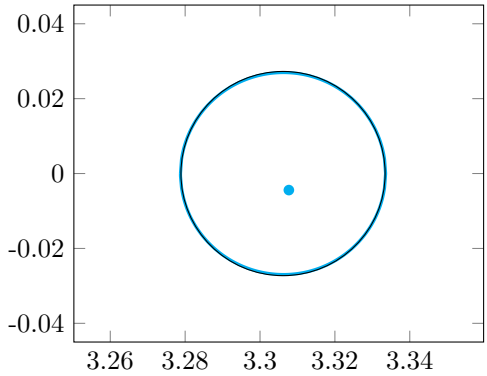

Figure 3.10 – Meridional section of the torus for Hydra

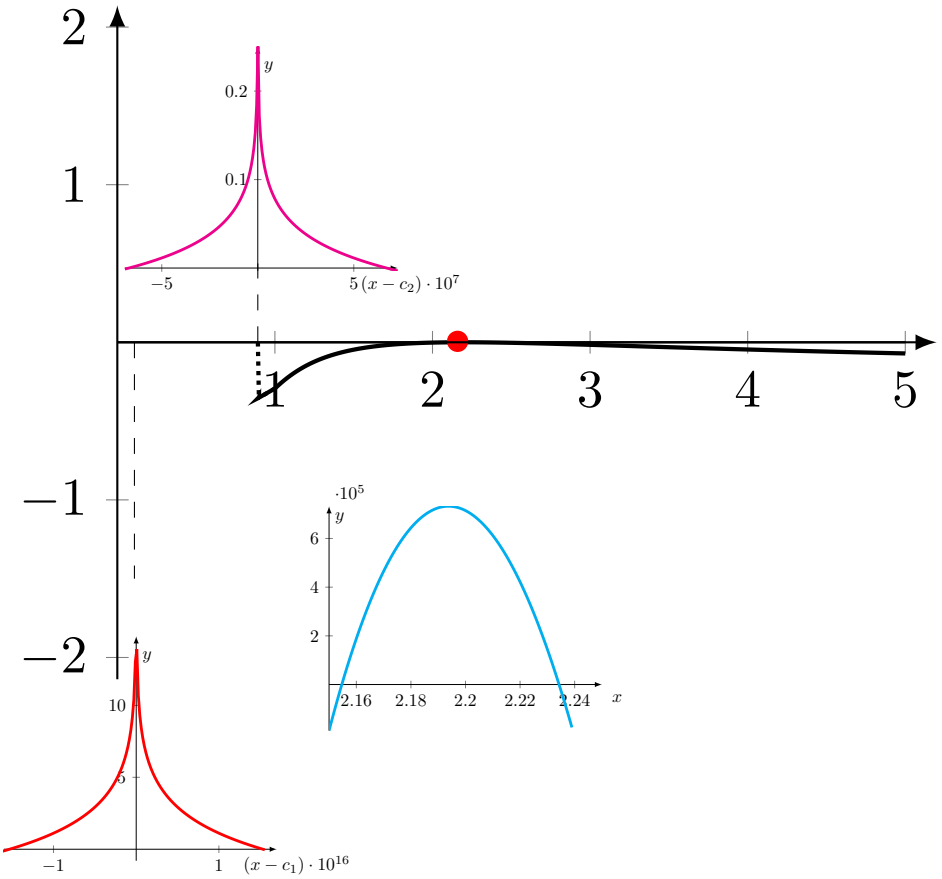

Figure 3.11 – The function $F^*(x)$ for Styx

On Figure 3.11 is shown the function $F^*(r)$ for Styx. Its roots determine the regions of possible motion $F^*(r) \geqslant 0$. In the interval $[0.9 - 5.0]$, there are only two roots, 2.154184 and 2.234821; in this interval, motion is possible. This segment is shown in an enlarged view in cyan color at the bottom right. The pair of roots enclosing c_2 has a half-width of about $6.67 \cdot 10^{-7}$, the half-width of the area containing the circle c_1 is even smaller $1.53 \cdot 10^{-16}$. The behavior of $F^*(r)$ in the vicinity of c_s is shown in an enlarged scale in the upper part (magenta color near c_2) and in the lower part of the figure (red color near c_1). Recall that $F^*(c_s) = \infty$. The other satellites (Nix, Kerberos, Hydra) have different constants h and J, but the behavior of the function $F^*(r)$ for them qualitatively remains the same.

The minimum velocity surface $\mathcal{S}$, and therefore the region $\mathcal{T}$, allows for significantly stricter constraints on the motion of a zero-mass body. However, it is important to note that these constraints are only valid within the framework of the averaged problem and, consequently, only apply over a limited period of time in real applications.

3.2 Region of Possible Motion in the General Planar Three-Body Problem

Despite the difficulty in finding a general solution to the three-body problem, significant progress has been made in understanding the properties and behaviors of these solutions. Besides the examples of restricted problems mentioned earlier, a number of properties are known for the general three-body (and N-body) problem. These results are related to the Lagrange–Jacobi identity and Sundman inequalities. Below are some findings concerning the general properties of solutions to the three-body (and N-body) problem. Most of these properties are based on the general characteristics of the functions under consideration, such as homogeneity, and are valid for any N. This section explores the properties of zero-velocity surfaces (regions of possible motion) in the general three-body problem in shape space [104; 105].

The simplest properties, formulated in [69; 91], are:

– *If $h < 0$, the smallest of the mutual distances remains bounded.* To prove this property, it is sufficient to consider the expression for the potential function V. Since $V = T - h \geqslant -h > 0$, we have

$$\sum_{i<j}^{n} \frac{m_i m_j}{r_{ij}} \geqslant \sum_{i<j}^{n} m_i m_j / \inf(r_{ij}) \geqslant -h \;\Rightarrow\; \inf(r_{ij}) \leqslant \left(\sum_{i<j}^{n} m_i m_j \right) / (-h).$$

The proof is straightforward and applies to any number N.

A similar property,

– *If $h \geqslant 0$, at least one of the system's points must move away from the barycenterrecede to an unbounded distance,* requires the use of the Lagrange–Jacobi identity (1.9) for proof and is also straightforward. Recall that the Lagrange–Jacobi identity coincides with the Lagrange equation for the variable ρ.

– *Collision of* all *bodies at a single point is impossible in finite time unless it occurs at an infinite time.*

– *Total collapse of the system cannot occur if the system's angular momentum is non-zero.*

– *If all three constants of areas are non-zero, given the initial conditions, it is possible to specify a positive lower bound for the two largest distances between the bodies.*

– *At a double collision,* ρ *and* $\dot{\rho}$ *(the moment of inertia and its derivative) remain continuous, along with* $r\dot{r}$ *(*r *being the smallest distance), although* $\dot{r}$ *is not continuous.*

– *Simple calculations show that* ρ *at a double collision has a local minimum. As* t *approaches the collision time,* ρ *tends to this limit, and* $\dot{\rho} = 0$.

Indeed, let the double collision of bodies P_1 and P_2 occur at time $t = 0$, with body P_3 located at a distance a from the collision point at the collision moment. In a sufficiently small vicinity of the collision, body P_3 can be considered fixed. The moment of inertia at the collision and at the moment before (or after) the collision is easily calculated (let δ denote the distance between bodies P_1 and P_2):

$$\begin{aligned} I_0 &= (m_1+m_2)m_3/(m_1+m_2+m_3)a^2, \\ I &= I_0 + \delta^2 m_1 m_2 \frac{(m_1-m_2)^2 + m_1m_3 + m_2m_3 - 4m_1m_2\sin^2\varphi}{(m_1+m_2)^2(m_1+m_2+m_3)} \geqslant I_0. \end{aligned}$$

Thus, the moment of inertia I, or the distance ρ, takes a minimum value, which implies that the trajectory of the solution of the three-body problem in the shape space always intersects the collision line orthogonally if a collision occurs.

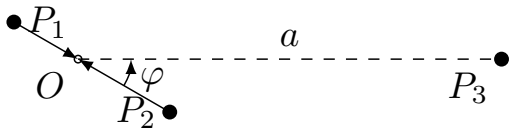

Figure 3.12 – Double collision at time t_0

The Sundman inequality is of great importance for the qualitative analysis of the solutions to the three-body problem. In the considered shape space, it is a simple consequence of the energy integral (1.23):

$$J^2 \leqslant \rho(\ddot{\rho} - 2h). \qquad J^2 \leqslant 2D(\varphi,\theta)/\sqrt{\rho} + 2h\rho. \tag{3.16}$$

Or, keeping the derivative of ρ in the expression for the energy integral, we obtain a stricter Sundman inequality:

$$J^2 + \frac{1}{4}\dot{\rho}^2 \leqslant \rho(\ddot{\rho} - 2h); \qquad J^2 + \frac{1}{4}\dot{\rho}^2 \leqslant 2D(\varphi,\theta)/\sqrt{\rho} + 2h\rho. \tag{3.17}$$

The zero-velocity surface ($\dot{\xi}_1^2 + \dot{\xi}_2^2 + \dot{\xi}_3^2 = 0$), i.e., the surface where the velocity of the triangle configuration change is zero, separates the region of possible motion from the region where motion is impossible.

If in the energy integral (1.23) we replace the variables ρ,φ,θ with the variables ξ_1,ξ_2,ξ_3, we obtain the equation of the surface in the form

$$V(\xi_1,\xi_2,\xi_3) + h - \frac{J^2}{2\sqrt{\xi_1^2 + \xi_2^2 + \xi_3^2}} = 0. \tag{3.18}$$

It is evident that the surface exists if $J^2/(2\rho) - h > 0$, which is always satisfied if $h < 0$.

The Sundman inequality (see, for example, [38; 40; 56; 69])

$$\frac{J^2}{2I} - V(\xi_1,\xi_2,\xi_3) - h \leqslant 0,$$

is a simple consequence of the energy integral (1.23), and conversely, the equation of the zero-velocity surface in shape space can be derived directly from the Sundman inequality. Note that the given inequality can also be satisfied when $h > 0$.

Let us start with the zero-velocity surface and the region of possible motion for $J = 0$. Figure 3.13 shows the zero-velocity surface for $m_1 = m_2 = m_3$.

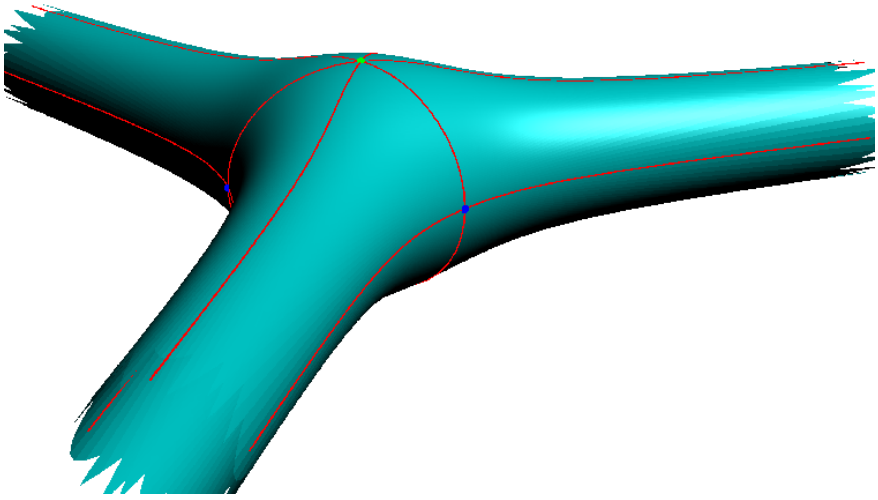

Figure 3.13 – Zero-velocity surface for $J = 0$

In this case, a triple collision is possible, and the origin, therefore, lies within the region of possible motion. As noted in 1.1.1, due to the scale symmetry, we can fix the value of the energy constant without loss of generality, for example, in the case of negative energy $h = -1/2$. Further, we will investigate the regions of possible motion with this value of h. Let us estimate the size of the region of possible motions, starting with the case of equal masses. In this case, the rays of double collisions in the space ξ_1,ξ_2,ξ_3 correspond to the three rays: $\lambda(-1,0,0)^T$, $\lambda(1/2,-\sqrt{3}/2,0)^T$, $\lambda(1/2,\sqrt{3}/2,0)^T$, while the collinear Euler configurations correspond to the rays $\lambda(1,0,0)^T$, $\lambda(-1/2,\sqrt{3}/2,0)^T$, $\lambda(-1/2,-\sqrt{3}/2,0)^T$; equilateral Lagrange configurations correspond to the poles $\lambda(0,0,\pm 1)^T$ in the case of equal masses (here $\lambda \in \mathbb{R}^+$ is an arbitrary number). It is evident that only in the case of equal masses are the Lagrange configurations located at the poles of the shape sphere. In the considered case, the zero-velocity surface and the region of possible motion are symmetric with respect to rotations by $2k\pi/3$. Let us consider the points of the zero-velocity surface in the positive direction of the z-axis: $(0,0,\xi_3)$. For $J = 0$ from (3.18) we have

$$V(0,0,\xi_3) = 3/\sqrt{\xi_3} = 1/2 \quad \rightarrow \quad \xi_3 = 36.$$

Thus, the region of possible motion includes the segment $[-36,36]$ of the z-axis. The origin can be excluded from this segment if we do not consider a triple collision. Note that the zero-velocity surface at the origin does not have physical meaning: it is not possible to speak of three bodies located at a single point with zero velocity, essentially it is one point with a mass equal to the sum of the masses of the three bodies.

Now consider the points on the surface in the positive direction of the x-axis (for $\xi_1 < 0$, the entire ray $(\xi_1,0,0)$ lies within the region of possible motion): From the equation (3.18) we have

$$V(\xi_1,0,0) = 1/\sqrt{2\xi_1} + 2/\sqrt{\xi_1/2} = 1/2 \quad \rightarrow \quad \xi_1 = 50.$$

If the masses are not equal, then in the case of zero angular momentum $J = 0$, the surface will not change qualitatively, but the positions of the Lagrangian and Eulerian points and the sizes of the branches will change. For example, for the Lagrangian

points (1.13):

$$r_{12} = r_{13} = r_{23} = \sqrt{m_1 + m_2 + m_3}\sqrt{\rho}/\sqrt{m_1m_2 + m_1m_3 + m_2m_3}\,,$$

the potential function takes the value

$$V = \frac{(m_1m_2 + m_1m_3 + m_2m_3)^{3/2}}{\sqrt{m_1 + m_2 + m_3}\sqrt{\rho}}\,. \tag{3.19}$$

A similar approach applies to the Eulerian points. If the masses are not equal, we obtain the Eulerian point (on the shape sphere, or the direction of the corresponding ray) as the root of the fifth-degree polynomial (1.18) and, consequently, the angle φ for this ray, and then the point on the equatorial plane corresponding to this Eulerian point on the zero-velocity surface. In the case of equal masses, the calculations are simpler (the Eulerian points are determined elementarily $\varphi_{1,2,3} = 0, \pm 2\pi/3$) and do not require finding the roots of the fifth-degree polynomial.

Let $J \neq 0$, then in the case of equal masses on the z-axis

$$V(0,0,\xi_3) - \frac{J^2}{2\xi_3} = 3/\sqrt{\xi_3} - \frac{J^2}{2\xi_3} = 1/2 \quad \rightarrow$$
$$\xi_3 \in \left[\left(3 - \sqrt{9 - J^2}\right)^2, \left(3 + \sqrt{9 - J^2}\right)^2\right]. \tag{3.20}$$

The roots of this equation exist only if $|J| \leqslant 3$ (if h is any negative number, then if $|J| \leqslant 3/\sqrt{2|h|}$), otherwise there are no roots on the z-axis, see figs. 3.15–3.17.

Thus, if $|J| \leqslant 3/\sqrt{2|h|}$, we have two points on the z-axis that correspond to the given h and J to two zero-velocity surfaces. Both of these points are positive, as both the product and the sum of the roots are positive. Therefore, in this case, the z-axis intersects the zero-velocity surfaces twice in the positive direction and, since we have an obvious symmetry relative to the equatorial plane, twice in the negative direction.

Now let us look at the structure of the zero-velocity surfaces in the direction of the x-axis:

$$V(\xi_1,0,0) - \frac{J^2}{2\xi_1} = 1/\sqrt{2\xi_1} + 2/\sqrt{\xi_1/2} - \frac{J^2}{2\xi_1} = 1/2 \quad \rightarrow$$
$$\xi_1 \in \left[\left(5 - \sqrt{25 - 2\,J^2}\right)^2/2, \left(5 + \sqrt{25 - 2\,J^2}\right)^2/2\right]. \tag{3.21}$$

As with the roots on the z-axis, when $J \leqslant 5\sqrt{2}$ (or $J \leqslant 5/(2\sqrt{|h|})$), there are two positive roots, and therefore the x-axis intersects the zero-velocity surfaces twice in the positive direction. Since in the case of equal masses we have rotational symmetry by $k2\pi/3$, the rays of the other two Euler points also intersect these surfaces twice when $J \leqslant 5\sqrt{2}$. Thus, if $J \leqslant 3$, any ray intersecting the outer surface, which closely resembles the surface in fig. 3.13, will also intersect the inner surface. Motion is possible outside the inner surface and inside the outer surface.

The inner zero-velocity surface for $J = 2.38$ is shown in fig. 3.14. The top and bottom points of this surface are determined by the smallest root of (3.20), which exists if $J \leqslant 3$. The farthest point of the surface, lying in the equatorial plane, is determined by the smallest root of (3.21), which exists if $J \leqslant 5\sqrt{2} \approx 3.5355$. Regarding the rays of double collisions, according to Sundman's results [67—69], if $|J| > 0$, then ρ is separated from zero by some constant $\bar{\rho}$, i.e., $\rho \geqslant \bar{\rho}$. Thus, the vertices of the "funnels" are located on the lines of double collisions but do not reach the point of triple collision, as can be seen in fig. 3.14.

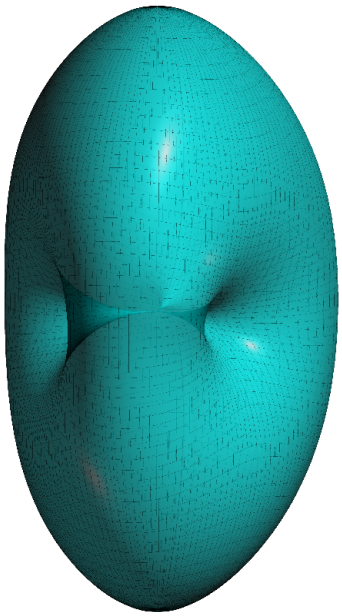

Figure 3.14 – Inner zero-velocity surface at $J = 2.99$

The properties of the inner zero-velocity surface are not examined in detail. It is likely that if the solution point enters one of the funnels, thus approaching a double collision, then according to Sundman, as $t \to \infty$, it will escape into one of the branches, moving off to infinity. In our case, this means $\rho \to \infty$.

Let us now observe how the zero-velocity surface changes with varying J. Figures 3.15–3.17 show the zero-velocity surfaces for $J = 2.99$, $J = 3.2$, and $J = 4.5$. The topology of the permissible motion regions varies in these cases. For $|J| < 3$, this region is bounded by an outer surface with three branches, similar to the surface at $J = 0$ (if the origin is considered a punctured point; in the figures, the blue line corresponds to the cross-section of the zero-velocity surface for $J = 0$), and an inner surface whose cross-section in the plane $\xi_3 = 0$ resembles a trefoil, while the cross-section in the plane $\xi_2 = 0$ is symmetric about the equator and elongated along the x-axis. This cross-section depends on the meridian; if the masses are unequal, the cross-section should be taken along another meridian (passing through the line of the corresponding Euler configuration). However, in the examples provided, the masses will differ only slightly. In figure 3.15, the inner surface is clearly visible. When $|J| = 3$, the inner and outer surfaces have two common points, and for $3 < |J| < 5/\sqrt{2} \approx 3.53553$, a hole appears in the central part of the surface with three branches.

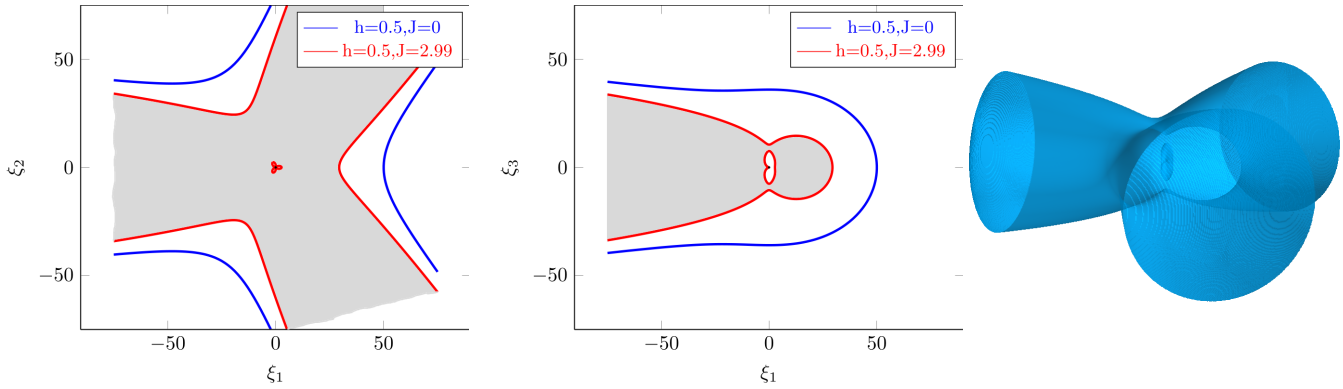

Figure 3.15 – Zero-velocity surface at $J = 2.99$ (right) and its cross-sections by the equatorial plane $\xi_3 = 0$ (left) and the meridian plane $\xi_2 = 0$.

For $|J| < 3$, the inner surface is compact, as shown in figure 3.14. It is evident that it has a singular point at the origin. The surface is depicted as semi-transparent, and the three “funnels” are clearly visible.

For $J = 5/\sqrt{2}$, each branch only has two common points with the neighboring branches, excluding the punctured point at the origin. Beyond this, for $J > 5/\sqrt{2}$, we have three separate branches.

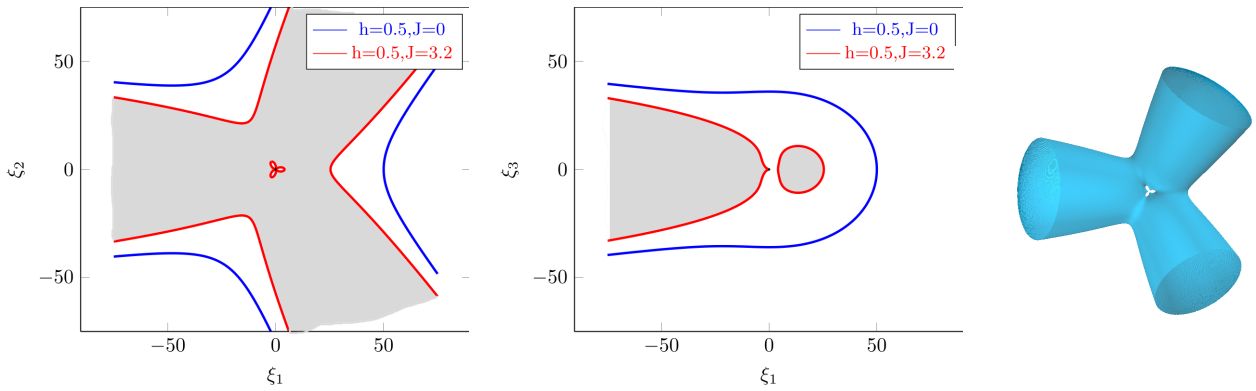

Figure 3.16 – Zero-velocity surface at $J = 3.2$ (right) and its cross-sections by the equatorial plane $\xi_3 = 0$ (left) and the meridian plane $\xi_2 = 0$.

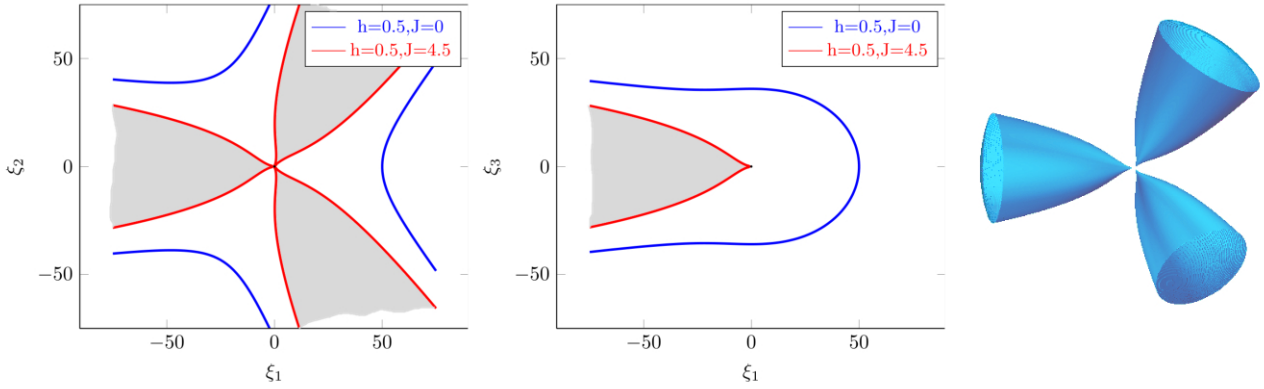

Figure 3.17 – Zero-velocity surface at $J = 4.5$ (right) and its cross-sections by the equatorial plane $\xi_3 = 0$ (left) and the meridian plane $\xi_2 = 0$.

We encounter three topologically different types of zero-velocity surfaces or three different topological regions of possible motion. The first is the inner surface (compact) shown in fig. 3.14, and the outer surface, whose three arms correspond to the three regions of hierarchical motion, where two bodies are close to each other and the third is significantly farther away (fig. 3.15). As the constant angular momentum $0 < J < 3$ changes, the inner region (where motion is impossible) increases, and the outer region decreases. At $J = 3$, the inner and outer surfaces touch, resulting in a surface with a "hole"–an equilateral configuration with $J > 3$ is unreachable, but the exchange of components, i.e., the transition from one arm to another, is quite possible (see fig. 3.16). With further increases in J, $3 < J < 5/\sqrt{2}$, the "hole" grows until, finally, at $J = 5/\sqrt{2}$, each of the three arms has only one common point with the neighboring arms, and for $J > 5/\sqrt{2}$, the region of possible motion splits into three separate regions (fig. 3.17). Motion is possible within each of these regions, but it is

impossible to move from one region to the adjacent one, resulting in a hierarchical system.

Such a simplified structure arises only for three equal masses. In this case, the three special points corresponding to the positive root of polynomial (1.18) are reached simultaneously; more precisely, the polynomials coincide for the three different permutations of the bodies.

Now, let us consider the case of unequal masses. For example, let $m_1 = 2m_2 = 4m_3 = 12/7$. The double collision rays are positioned, as in the case of equal masses, in the equatorial plane, but there is no symmetry concerning rotations by $2k\pi/3$. The sections and surfaces, analogous to the equal mass case, are shown in fig. 3.18–3.22.

For $J = 0$, the topology of the surface is the same as in the case of equal masses: the origin is a punctured point, and the three branches extend to infinity along with the three double collision rays. However, the thickness of the branches now varies: the thinnest branch is directed along the ray of the double collision of the two smallest masses, the thickest branch along the ray of the double collision of the two largest masses, and the third branch is directed along the ray of collisions of the smallest and the largest mass.

The coordinates of the special points (L_4 and L_5) are given by expression (1.13). In the case of equal masses, these points correspond to the poles, which is why we determined the intersection of the surface with the z-axis. In the case of unequal masses, we determined the intersection of the ray (1.13) with our surface and obtained the value (3.19). Thus, for the special point L_4, we have the equation:

$$\frac{(m_1m_2 + m_1m_3 + m_2m_3)^{3/2}}{\sqrt{\rho}\sqrt{m_1 + m_2 + m_3}} + h - \frac{J^2}{2\rho} = 0, \tag{3.22}$$

which has the solution:

$$\sqrt{\rho} = (\pm\sqrt{\frac{(m_1m_2 + m_1m_3 + m_2m_3)^3}{m_1 + m_2 + m_3} + 2J^2h} - \frac{(m_1m_2 + m_1m_3 + m_2m_3)^{3/2}}{\sqrt{m_1 + m_2 + m_3}})/2h,$$

that is,

$$\rho \in \left[\left(\frac{(m_1m_2 + m_1m_3 + m_2m_3)^{3/2}}{\sqrt{m_1 + m_2 + m_3}} - \sqrt{\frac{(m_1m_2 + m_1m_3 + m_2m_3)^3}{m_1 + m_2 + m_3} + 2J^2h} \right)^2 /4h^2 ,\right.$$

$$\left. \left(\frac{(m_1m_2 + m_1m_3 + m_2m_3)^{3/2}}{\sqrt{m_1 + m_2 + m_3}} + \sqrt{\frac{(m_1m_2 + m_1m_3 + m_2m_3)^3}{m_1 + m_2 + m_3} + 2J^2h} \right)^2 /4h^2 \right] .$$

Thus, we obtain a result similar to that for equal masses (if we set $m_1 = m_2 = m_3 = 1$, then the special point at $J = 3$ exists). In the case of unequal masses, the solution exists if ($h = -1/2$):

$$J^2 \leqslant \frac{(m_1m_2 + m_1m_3 + m_2m_3)^3}{m_1 + m_2 + m_3},$$

In the case $m_1 = 2m_2 = 4m_3 = 12/7$, the constant $J \leqslant 3 \cdot 6^{3/2}/7^{3/2}$. For larger J, as in the case of equal masses, we get a “hole.”

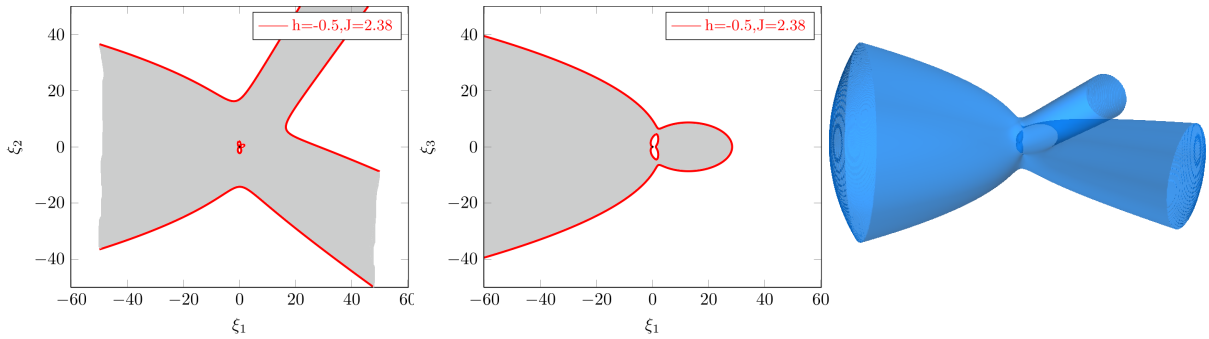

Figure 3.18 – Zero velocity surface at $J = 2.38$ (right) and its sections in the equatorial plane $\xi_3 = 0$ (left) and the meridian plane $\xi_2 = 0$ ($m_1 = 2m_2 = 4m_3 = 12/7$)

The inner surface is similar to the surface 3.14, but lacks the $2\pi/3$ rotation symmetry. The axes of the “funnels” are directed along the rays of double collisions, and the maximum distances in the equatorial plane correspond to the special points. For these points, the calculations are also simple. The main difficulty in obtaining the values for the Euler points is that it requires solving the fifth-degree polynomial (1.18). While it is not difficult to find the root of the polynomial numerically, closed-form expressions like those for the Lagrangian points are not available. Once the direction is

known (i.e., the root is obtained numerically), the distance ρ is determined by solving a quadratic equation, as was done for the case of equal masses or for the Lagrangian points.

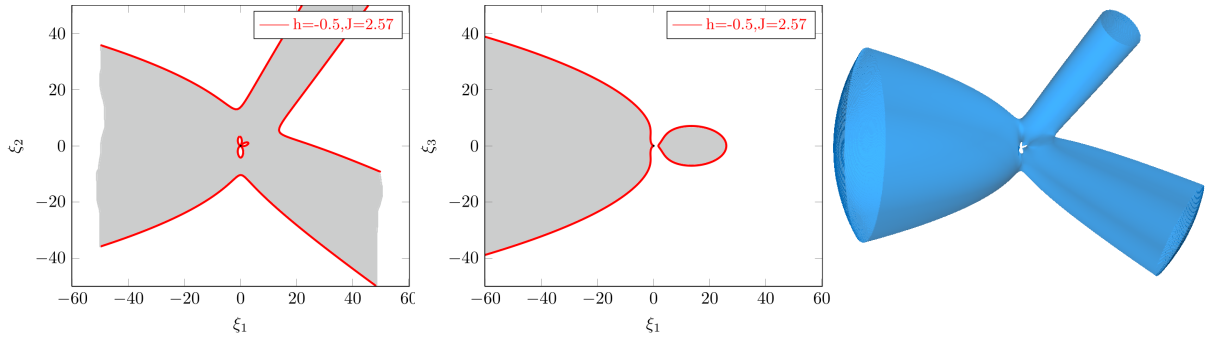

Figure 3.19 – Zero velocity surface at $J = 2.57$ (right) and its sections in the equatorial plane $\xi_3 = 0$ (left) and the meridian plane $\xi_2 = 0$ ($m_1 = 2m_2 = 4m_3 = 12/7$)

Figure 3.18 shows the region of possible motion for the value of J, where this region is bounded by two surfaces. The inner surface is compact and topologically similar to the surface 3.14. The outer surface, as in the case of equal masses, has three arms, with the axes of these arms coinciding with the corresponding rays of double collisions: the axis of the largest arm is directed along the ray of double collisions of the largest masses, the smallest along the ray of double collisions of the smallest masses, and the medium-sized along the ray of double collisions of the largest and smallest masses. Motion is possible only between the surfaces.

Increasing J, let $J = 2.57$ ($> 3 \cdot 6^{3/2}/7^{3/2}$). Equation (3.22) has no solution, thus, the rays of the Lagrangian configurations (1.13) do not intersect the zero velocity surface, which is clearly visible in Fig. 3.19. The rays of the Lagrangian configurations in the case of unequal masses are not directed towards the poles, so to make this noticeable in the section of the possible motion region in the meridian plane, the value of J is chosen to be sufficiently large (but such that the topological picture is preserved).

As J increases further, the hole enlarges, and at a certain value of J, two branches—the branch associated with the collision ray of the larger masses and the branch with the collision ray of the largest and smallest masses–touch at a common

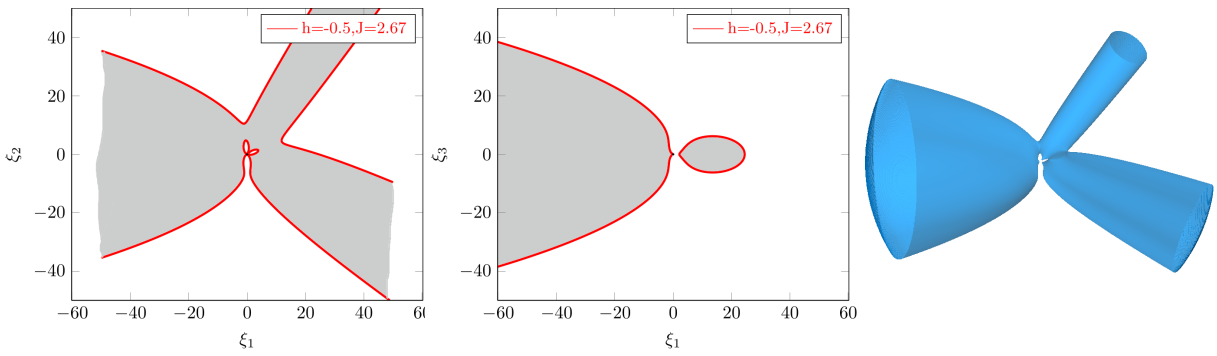

Figure 3.20 – Zero velocity surface at $J = 2.67$ (right) and its sections in the equatorial plane $\xi_3 = 0$ (left) and the meridian plane $\xi_2 = 0$ ($m_1 = 2m_2 = 4m_3 = 12/7$)

point; this is the point of the Euler collinear configuration L_1. As J increases further, these branches cease to be connected, and the point (ξ_1,ξ_2,ξ_3) from one branch can only reach the other branch through the third branch associated with the collision ray of the smallest masses. This type of zero velocity surface is shown in Fig. 3.20.

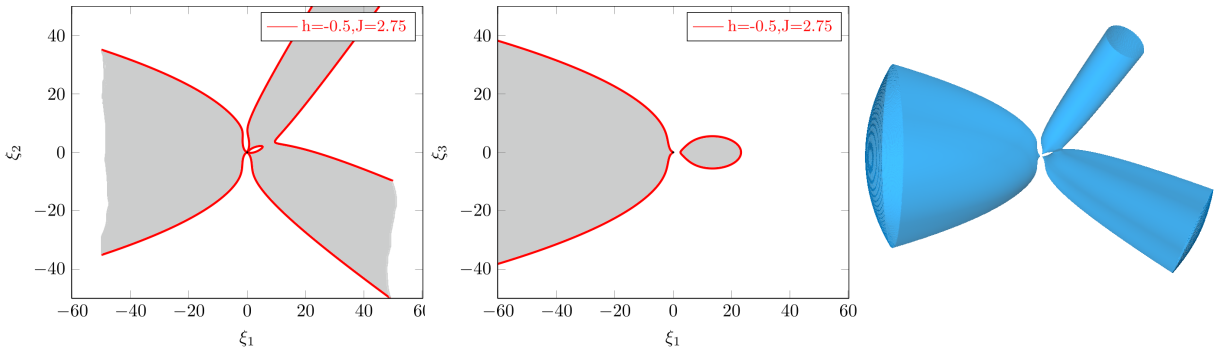

Figure 3.21 – Zero velocity surface at $J = 2.75$ (right) and its sections in the equatorial plane $\xi_3 = 0$ (left) and the meridian plane $\xi_2 = 0$ ($m_1 = 2m_2 = 4m_3 = 12/7$)

If we continue to increase J, there will come a moment when the branch with the largest masses will have only one common point with the branch of the smallest masses. This point corresponds to the Euler collinear configuration L_2. For larger J, the branch of the largest masses becomes disconnected from the other two branches. A point located in this branch cannot reach the others and will remain there indefinitely, although motion between the other two branches is still possible (see Fig. 3.21).

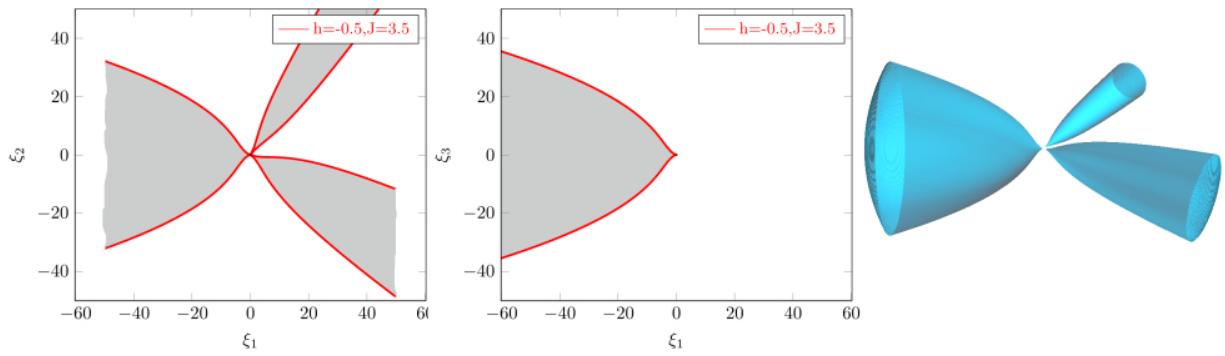

Figure 3.22 – Zero velocity surface at $J = 3.5$ (right) and its sections in the equatorial plane $\xi_3 = 0$ (left) and the meridian plane $\xi_2 = 0$ ($m_1 = 2m_2 = 4m_3 = 12/7$)

Finally, as we continue to increase J, we will reach a point where the two remaining connected branches will have only one common point (the last remaining Euler point L_3). For larger values of J, we obtain three disconnected branches. A point located in one of these branches will remain there indefinitely (see Figure 3.22).

Thus, if the energy constant is negative (for example, $h = -1/2$), there are five topologically distinct regions of possible motion, depending on the value of the angular momentum constant J. The type of region changes when J reaches values corresponding to the Lagrange points $L_{4,5}$, L_3, L_2, and L_1. The situation is analogous to the one shown in Fig. 3.5 for the circular restricted three-body problem. Indeed, in the latter case, we have three disconnected regions of possible motion, just like in the first case shown in Fig. 3.5. In the penultimate case, there are two disconnected regions (the second region in Fig. 3.5), and in the third case, there is one. It should be noted that the zero velocity surfaces in the circular restricted three-body problem are constructed in a rotating coordinate system, while in our case, they are in the shape space.

It is possible to construct the region of possible motion not only in the case of negative energy. For example, in the case of $h = 0$, the inequality

$$\frac{J^2}{2\rho} \leqslant V(\xi_1,\xi_2,\xi_3)$$

holds. For equal masses, along the applicate axis, the inequality $\xi_3 \geqslant J^2/6$ is obtained, and along the abscissa axis, $\xi_1 \geqslant J^2/(5\sqrt{2})$. For positive values of $h > 0$, assuming

$h = 1/2$ for equal masses along the applicate axis, the inequality $\xi_3 \geqslant 9 + J^2 - 3$ holds, and along the abscissa axis, $\xi_1 \geqslant (\sqrt{25 + 2J^2} - 5)/\sqrt{2}$. For non-negative energy constants, the region of possible motion is limited by only one surface, which is very similar to the surface shown in Fig. 3.14, and motion is possible outside this surface.

To summarize the description of the regions of possible motion in the general three-body problem, it is important to emphasize that in the general three-body problem, there are five topologically different types of zero-velocity surfaces, which separate the regions of possible motion from the regions where motion is impossible. These five topologically different types of surfaces, known as Hill surfaces, are also well-known in the restricted circular three-body problem. Hill surfaces are constructed not in an inertial frame but in a rotating coordinate system, which allows for a qualitative analysis of the solutions to the problem. The same can be said for the general (planar) three-body problem. In this case, we construct zero-velocity surfaces in shape space, and these constructed surfaces also enable us to qualitatively analyze the existing solutions, considering the same five different surfaces.

Chapter 4. Lemaitre Regularization

The equations of motion in the N-body problem have singularities: if any of the mutual distances between the bodies becomes zero, i.e., a collision occurs, then the right-hand sides become infinite. In the case of three bodies, collisions can be either between two bodies only (three different collisions depending on which pair collides) or a collision of all three bodies. The latter, apart from occurring less frequently than binary collisions, also has a number of interesting features. Firstly, based on the initial conditions, it can be immediately determined whether a triple collision can occur at all. Sundman's theorem states that "a complete collapse of the system cannot occur if the angular momentum of the system is not zero." Moreover, in this case, the size of the system is separated from zero by a certain constant. The size of the system can be taken as either the square root of the moment of inertia $\sqrt{I} = \rho$, the greatest mutual distance, or the perimeter of the triangle. Secondly, by a change of variables, it is possible to eliminate the singularity of binary collisions, or *regularize* the equations of the problem.

The concept of regularization (solutions of the equations of the N-body problem) first appeared with Sundman. As Sundman demonstrated, binary collisions that may occur in the solution of the three-body problem can be regularized, i.e., the solution can be extended *beyond* the collision by introducing a new independent variable $u = \int_{t_0}^{t} \frac{dt}{r}$. This is precisely how Sundman constructed the solution in the form of series that converge for $-\infty < t < \infty$.

Around the same time, Levi-Civita [33—37] developed a simple method of regularization, which involves the substitution of both dependent and independent variables. Initially, this was the regularization of the two-body problem, which was then extended to the restricted three-body problem, first to the planar case and later (after 50 years!!!) to the spatial case through the efforts of P. Kustaanheimo, E. Stiefel, and others. It turned out that regularization not only allows the continuation of the solution beyond collisions but also significantly improves the efficiency of numerical integration of trajectories that are close to collisions.

The Levi-Civita regularization of the two-body problem involves two variable substitutions. By identifying the position of the body (x,y) with the complex number $z = x + i\,y$, Levi-Civita defined a new dependent variable $\zeta = z^2$. This transformation can be simply explained by considering the limiting case of the two-body problem as $e \to 1$ (see Fig. 4.1).

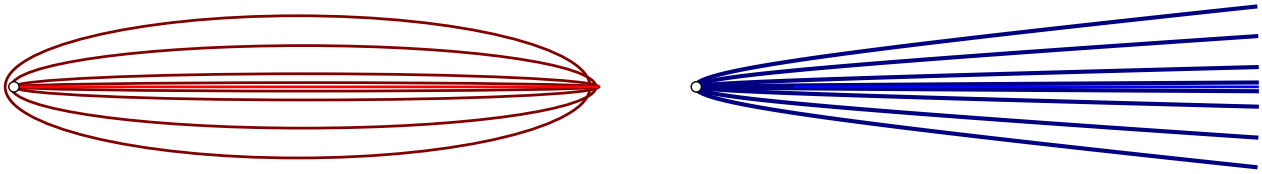

Figure 4.1 – Binary collision at time $t = 0$ as the limiting case when $e \to 1$. Left: elliptic trajectories, right: hyperbolic trajectories

As seen in Fig. 4.1, in the limiting case, the trajectory at the point of collision turns by π, as if it reflects off the second body (white point) and moves in the opposite direction. Thus, we have a singularity in the solution, where the velocity of the body approaches ∞ before the collision and goes from $-\infty$ in the opposite direction after the collision. This singularity can be eliminated by doubling the angle, so that the limiting trajectory continues without changing direction, effectively changing direction by 2π. Levi-Civita proposed a simple transformation

$$\zeta = z^2. \tag{4.1}$$

or, in real coordinates ($\zeta = \zeta_1 + i\,\zeta_2$, $z = z_1 + i\,z_2$)

$$\begin{aligned} \zeta_1 &= z_1^2 - z_2^2 \\ \zeta_2 &= 2 z_1 z_2, \end{aligned}$$

and it is easy to verify that $\zeta_1^2 + \zeta_2^2 = (z_1^2 + z_2^2)^2$. It is clear that the transformation (4.1) doubles the angles at $z = 0$ and the considered singularity is removed. We can derive the estimates:

$$\begin{aligned} r &\sim t^{2/3} \\ v &\sim t^{-1/3} \end{aligned} \tag{4.2}$$

Another singularity remains, where the force function becomes infinitely large at the collision. This singularity is removed by introducing a new independent variable τ

instead of t:

$$r\,d\tau = dt. \tag{4.3}$$

Then

$$\frac{d}{dt} = \frac{1}{r}\frac{d}{d\tau} \quad \text{and} \quad \frac{d^2}{dt^2} = \frac{1}{r^3}\left(r\frac{d^2}{d\tau^2} - \frac{dr}{d\tau}\frac{d}{d\tau}\right).$$

Substituting the new dependent and independent variables into the equations of the two-body problem and replacing the square of the velocity from the area integral, we get the equations of motion in these new variables:

$$z'' + \omega^2 z = 0, \quad \omega = \sqrt{|h|/2}, \tag{4.4}$$

which is the equation of a mathematical pendulum.

Such a simple regularization, extended to the spatial case and the problem of three or more bodies, has, since the time of Kustaanheimo and Stiefel, improved numerical integration methods in celestial mechanics, making them more efficient.

For numerical applications, it is sufficient to regularize the problem for each collision sequentially within the framework of the two-body problem or the restricted three-body problem. For qualitative studies of the general three-body problem, this is not enough. It is necessary to regularize all collisions in the problem, i.e., a *global* regularization is required, which eliminates all double collisions simultaneously. Methods of global regularization have been developed by Birkhoff, Thiele, Lemaitre, Waldvogel, Heggie, and others. !!!

The most interesting for this work is Lemaitre's regularization. The concept of shape space (though not the term itself) appeared in celestial mechanics as early as 1952 in Lemaitre's works [30—32]. Lemaitre proposed a method of global regularization of the general three-body problem, in which the configuration of the bodies plays a central role. Lemaitre's regularization of the planar three-body problem allows to introduce a convenient (and in degenerate cases of collinear and isosceles orbits, simple) parameterization, enabling the numerical construction and study of their properties. In the shape space, size and configuration are separated: size is determined by the distance to the origin, and configuration by the position on the shape sphere.

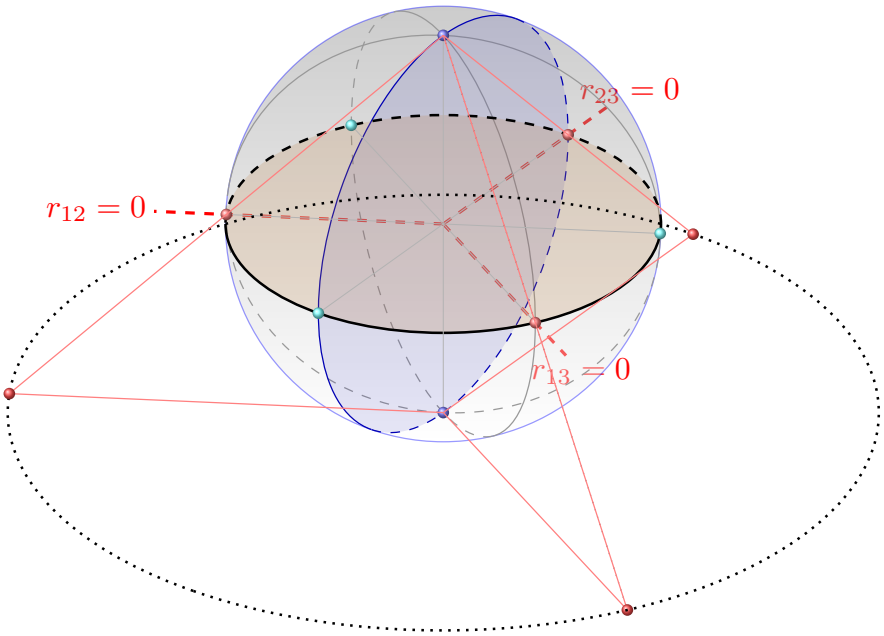

Figure 4.2 – Shape plane in the case of equal masses

Lemaitre's formulas are quite cumbersome; for simplicity, we will further consider the case of three equal masses. Qualitatively, the picture will not change, moreover, as mentioned in 1.2, the points of double collisions can be placed in such points for equal masses by the fractional-linear transformation (1.12). The configurations of double collisions are determined in the case of equal masses by the rays passing through three points of the shape sphere (radius 1/2): $(-1/2,0,0)$, $(1/4, -\sqrt{3}/4,0)$, $(1/4,\sqrt{3}/4,0)$, or on the shape plane as -1, $1/2 - \sqrt{3}/2$, $1/2 + \sqrt{3}/2$.

To eliminate the singularities of double collisions, it is sufficient to apply the transformation only to the shape sphere or, by identifying the sphere with the complex plane (e.g., using stereographic projection, see Fig. 4.2), transform the complex plane, which we will call the *shape plane*.

In Fig. 4.2, the projection of the equator of the shape sphere with a radius of 1/2 is the unit circle. The points of double collisions are projected onto equidistant points of this circle.

The Lemaitre transformation is given by:

$$\zeta = z\frac{\sqrt{8} + z^3}{1 - \sqrt{8}z^3}, \tag{4.5}$$

where z is a point on the regularized plane, and ζ is a point on the original plane (i.e., a point corresponding to a point on the shape sphere).

Table 9 – Double collision points (singularities of the potential function V)

Collision	regularized extended plane z	ζ
C_{12}	$\frac{\sqrt{2}-\sqrt{6}}{2}$ $\frac{\sqrt{2}+\sqrt{6}}{2}$	-1
C_{13}	$-\frac{\sqrt{2}}{2}\left(\frac{1}{2}+\frac{\sqrt{3}}{2}\right)+\frac{\sqrt{6}}{2}\left(\frac{1}{2}+\frac{\sqrt{3}}{2}\right)\imath$ $\frac{\sqrt{2}}{2}\left(-\frac{1}{2}+\frac{\sqrt{3}}{2}\right)-\frac{\sqrt{6}}{2}\left(-\frac{1}{2}+\frac{\sqrt{3}}{2}\right)\imath$	$\frac{1}{2}-\frac{\sqrt{3}}{2}\imath$
C_{23}	$-\frac{\sqrt{2}}{2}\left(\frac{1}{2}+\frac{\sqrt{3}}{2}\right)-\frac{\sqrt{6}}{2}\left(\frac{1}{2}+\frac{\sqrt{3}}{2}\right)\imath$ $\frac{\sqrt{2}}{2}\left(-\frac{1}{2}+\frac{\sqrt{3}}{2}\right)+\frac{\sqrt{6}}{2}\left(-\frac{1}{2}+\frac{\sqrt{3}}{2}\right)\imath$	$\frac{1}{2}+\frac{\sqrt{3}}{2}\imath$

The Lemaitre transformation (4.5) is a four-sheeted map, with each point on the shape sphere having four pre-images, excluding the double collision points, where the mapping is two-sheeted.

The inverse transformation is given by the following expression:

$$z_i = \pm\frac{\sqrt{\pm 2(\zeta+1)\sqrt{\zeta^2-\zeta+1}+2\zeta^2+\zeta-1}}{\sqrt{2}} \mp \frac{\sqrt{\zeta^2-\zeta+1}}{\sqrt{2}} - \frac{\zeta}{\sqrt{2}} \tag{4.6}$$

Here, the sign of the second term is chosen to be opposite to the sign of the first term in radical expression.

The original double collision points are -1, $1/2-\sqrt{3}/2\,i$, and $1/2+\sqrt{3}/2\,i$. Each of these has two pre-images on the regularized plane, as shown in Table 9.

Table 9 lists the pre-images of the double collision points under the Lemaitre transformation.

From (1.6), it is evident that collinear configurations (degenerate triangles) fill the equatorial plane. To analyze collinear orbits, it suffices to examine the pre-images of the equator, that is, the unit circle of the original shape plane. Thus, we will look for the images on the regularized sphere that yield:

$$|\zeta|^2 = \zeta\bar{\zeta} = 1.$$

Direct calculations lead to the equation:

$$\Big((x+\sqrt{2})^2+y^2-3\Big)\Big((x-\sqrt{2}/2)^2+(y-\sqrt{6}/2)^2-3\Big)\Big((x-\sqrt{2}/2)^2+(y+\sqrt{6}/2)^2-3\Big)=0$$

Thus, the equator has three pre-images–circles of radius $\sqrt{3}$, rotated relative to each other by $2\pi/3$, as shown in Fig. 4.3:

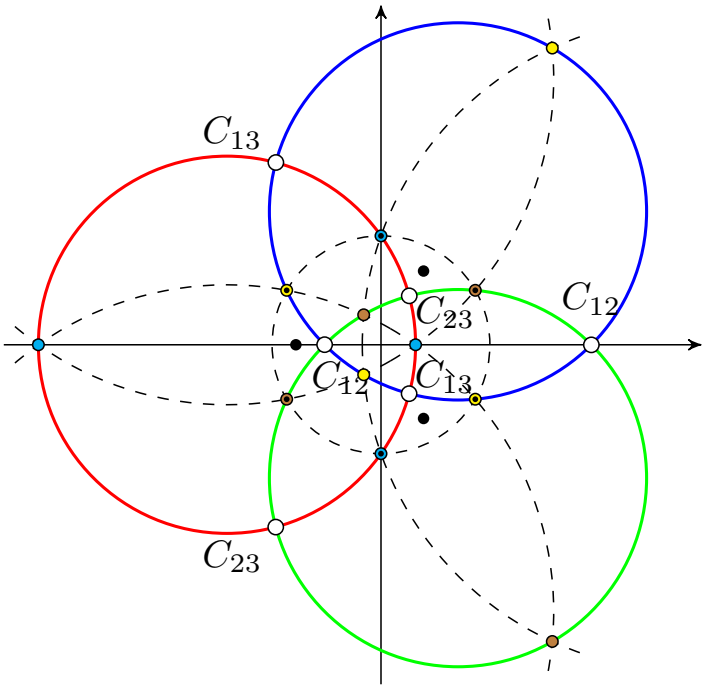

Figure 4.3 – Pre-images of the equator on the regularized plane

The red circle corresponds to collinear configurations where body 3 is between bodies 1 and 2, the blue circle corresponds to configurations where body 1 is between bodies 2 and 3, and the green circle corresponds to configurations where body 2 is between bodies 1 and 3. On the regularized plane, there are six points of double collisions (the mapping is two-sheeted at collision points), which are represented by white circles. These are the intersection points of the circles: red and blue, two points C_{13}; red and green, two points C_{23}; and blue and green, two points C_{12}. In other points, the mapping is four-sheeted, and we have, for instance, 12 Euler points, four on each of the circles: cyan circles on the red circle, yellow on the blue, and brown on the green. Interestingly, these 12 Euler points lie on four circles, with six points on each: on the red circle, there

are four blue points; on the green circle, there are four brown points; and on the blue circle, there are four yellow points. Six of these Euler points also lie on the unit circle, marked with small black dots. This unit circle, as well as parts of circles with a radius of 3, on which Euler points are also located (six points on each circle), are shown with dashed lines in Fig. 4.3. The figure also shows three black points that do not lie on the mentioned circles, which are the fixed points of the Lemaitre mapping (excluding zero and the infinitely remote point). The pre-images of the Lagrange point L_4: the infinitely remote point and the three cube roots of $1/\sqrt{8}$, and the points of L_5: zero and the three cube roots of $-\sqrt{8}$ (which are the centers of our circles: red, blue, and green).

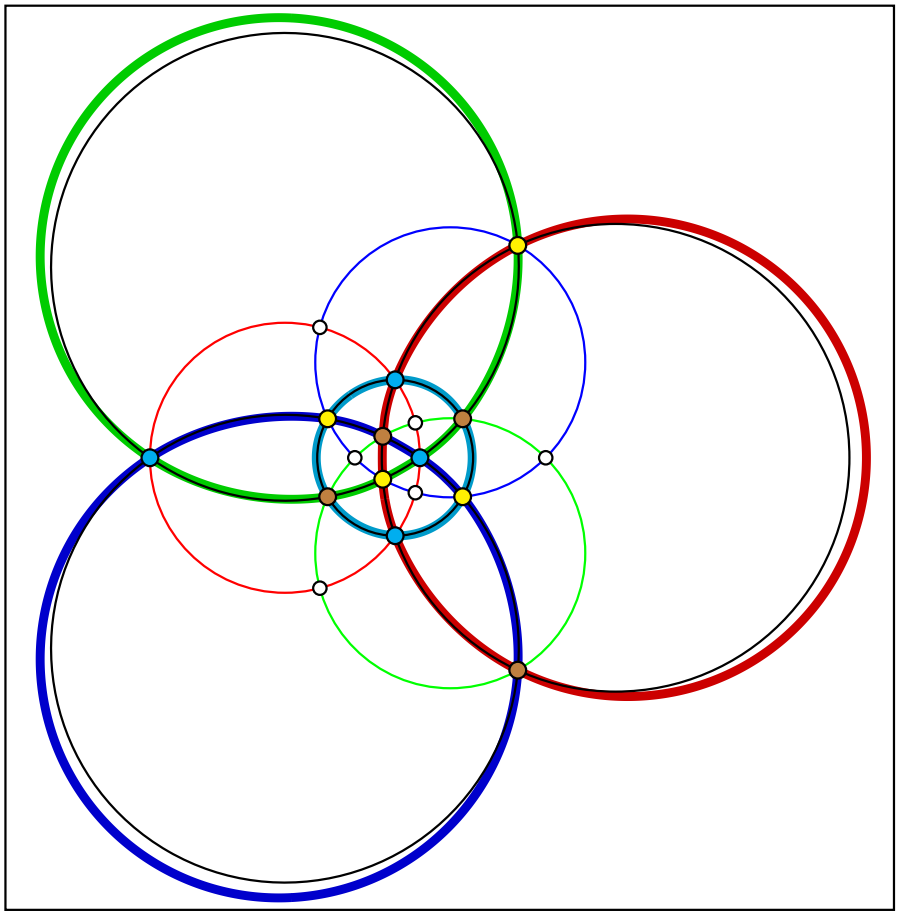

Figure 4.4 – Trajectory of the “figure-eight” on the regularized plane

Thus, on the four dashed circles, the six Euler points are traversed in the following order: L_1, L_2, L_3, L_1, L_2, L_3. This is the order in which the Euler points are traversed on the “figure-eight” orbit. In Fig. 4.4, the four pre-images of the “figure-eight” are depicted with thick lines. Since the figure-eight passes through the Euler points six times in one period, it crosses each point L_1, L_2, L_3 twice. The Euler points corresponding

to the orbit's image lie on one circle, so the orbit's images are close to a circle, which is evident on the larger circles where these points are unevenly distributed. On the unit circle, the Euler points are evenly distributed, and the corresponding pre-image of the "figure-eight" almost coincides with the unit circle, alternately going outside and remaining inside the circle. For comparison, the corresponding circles are shown with thin black lines.

In collinear motion, one of the bodies is always between the other two. As a result of the collision, it reflects off the outer body and begins moving in the opposite direction. This is the singularity of the solution. Let us see what happens on the regularized plane. Recall that, according to section 3.2, the collision trajectory crosses the collision line orthogonally, meaning that the direction of motion at the collision point changes by π. With regularization, this angle doubles, so the direction of motion at the collision does not change.

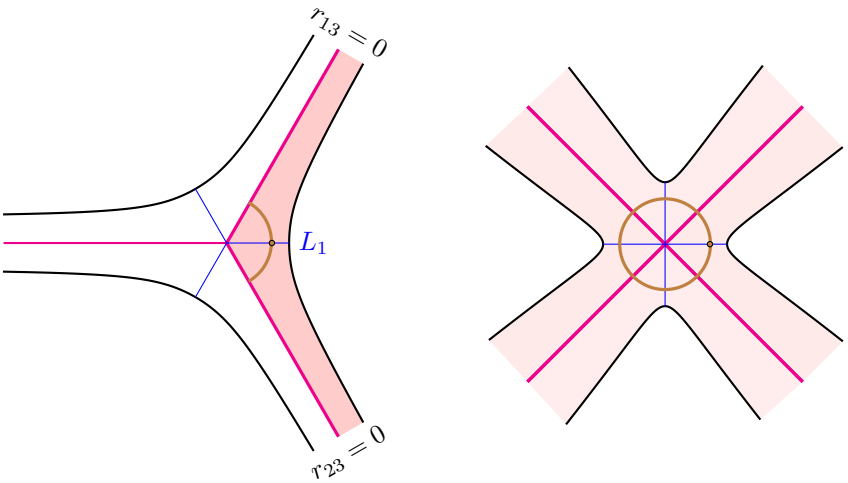

Figure 4.5 – Collinear trajectory in the original and regularized shape spaces

Figure 4.5 shows the collinear problem's trajectory in the original shape space and the regularized shape space. Collinear orbits are divided into three different types depending on which body is between the other two. It is easy to see that our three pre-images of the equator correspond to these three types. Indeed, the red circle in Fig. 4.3 corresponds to orbits where the third body moves between the first and second, passing through two collision points C_{13} and two points C_{23}. The same property holds for the other two circles: the blue circle passes through two points C_{12} and two points C_{13}, and the green one through C_{12} and C_{23}. Since the Lemaitre transformation only

affects the shape sphere and does not depend on the size of the configuration, we can depict the trajectory in the regularized plane. If the regularized shape plane is transformed back to the shape sphere, the red, blue, and green circles transform into great circles on the shape sphere. The inclination of these great circles' planes to the primary plane (equator) is $\arccos\sqrt{3}/3 \approx 54.7^\circ$, and these planes are rotated around the z-axis relative to each other by $2\pi/3$. Thus, for collinear orbits, we can draw the original ($\xi_3 = 0$) and regularized planes and the trajectories in them. These are the planes in which collinear trajectories are drawn: on the left in the $\xi_1\xi_2$ space and on the right in the corresponding regularized space.

The collinear trajectory in the left part of Fig. 4.5 approaches the collision line $r_{13} = 0$ (or $r_{23} = 0$) orthogonally and "reflects" from it; at the collision point, the direction of the point's velocity changes by π. In the right part of the figure, the point orthogonally crosses the collision line. The regions of possible motion are bounded by the zero-velocity curve. In the non-regularized case, the region of possible motion is also bounded by the collision lines. These regions are highlighted in pink.

In the other two cases, when body 1 is in the middle between bodies 2 and 3 (blue circle) or when body 2 is between bodies 1 and 3 (green circle), the qualitative picture remains the same; in the non-regularized case, it will only be rotated by $2\pi/3$.

Chapter 5. Degenerate Trajectories

There are numerous astronomical problems where it is useful to apply degenerate (collinear or isosceles) orbits, such as describing the motion of three colliding galaxies or the motion of three colliding black holes. Utilizing the properties of isosceles solutions and applying regularization methods to the numerical modeling of the three-body problem (considering close encounters) is significantly important if the corresponding orbits are stable. Degenerate orbits in the three-body problem have lower dimensionality and therefore are simpler than higher-dimensional problems. However, they allow the study of the properties of the general problem (in particular, regularization). Many works are dedicated to such studies, including [7; 42; 43; 58—62; 75; 77]. This chapter examines degenerate trajectories in shape space [84; 85].

5.1 Collinear Trajectories

5.1.1 Equations of Motion

In the collinear case, the motion in shape space occurs in the plane $\xi_3 = 0$ (and the spherical coordinate $\theta = 0$), and the angular momentum constant is zero, $J = 0$. This greatly simplifies the system. Then the kinetic energy is:

$$T = \frac{\dot{\xi}_1^2 + \dot{\xi}_2^2}{8\sqrt{\xi_1^2 + \xi_2^2}},$$

and if we introduce polar coordinates

$$\begin{aligned} \xi_1 &= \varrho^2 \cos\varphi, \\ \xi_2 &= \varrho^2 \sin\varphi, \\ \varrho^2 &= \rho = \sqrt{\xi_1^2 + \xi_2^2}, \end{aligned} \tag{5.1}$$

then the kinetic energy takes the form

$$T = \frac{1}{2}\left(\dot{\varrho}^2 + \frac{1}{4}\varrho^2\dot{\varphi}^2\right). \tag{5.2}$$

Without loss of generality, we limit ourselves to the case where body 3 is between body 1 and body 2. The force function ($m_1 = m_2 = m_3 = 1$) is easily calculated, taking into account that in the considered case $-\pi/3 \leqslant \varphi \leqslant \pi/3$ and, since the configuration is collinear, $r_{12} = r_{13} + r_{23}$. Then, from the expression for the force function (1.15) we get

$$\begin{aligned} V &= \frac{1}{r_{12}} + \frac{1}{r_{13}} + \frac{1}{r_{23}} \\ &= \frac{1}{\varrho}\left(\frac{1}{\sqrt{1+\cos\varphi}} + \frac{1}{\sqrt{1-\cos(\varphi-\pi/3)}} + \frac{1}{\sqrt{1-\cos(\varphi-5\pi/3)}}\right) \\ &= \frac{1}{\varrho}\frac{1+4\cos\varphi}{\sqrt{1+\cos\varphi}(2\cos\varphi-1)} = \frac{D(\varphi)}{\varrho}, \end{aligned} \tag{5.3}$$

and the energy integral

$$2h = \dot{\varrho}^2 + \frac{1}{4}\varrho^2\dot{\varphi}^2 - 2V = \dot{\varrho}^2 + \frac{1}{4}\varrho^2\dot{\varphi}^2 - 2\frac{D(\varphi)}{\varrho}. \tag{5.4}$$

The region of possible motion in coordinates ϱ,φ is given by:

$$\frac{D(\varphi)}{\varrho} = \frac{1}{\varrho}\frac{1+4\cos\varphi}{\sqrt{1+\cos\varphi}(2\cos\varphi-1)} \geqslant -h,$$

and the zero velocity curve (for $h = -1/2$) is given by the equation:

$$\varrho = \frac{2(1+4\cos\theta)}{\sqrt{1+\cos\theta}(2\cos\theta-1)}. \tag{5.5}$$

Given the Lagrangian $L = T + V$, we can also write the equations of motion:

$$\begin{aligned} \dot{\varrho} &= v \\ \dot{v} &= \tfrac{1}{4}\varrho\dot{\varphi}^2 - \tfrac{1}{\varrho^2}D(\varphi) = \frac{D(\varphi)}{\varrho^2} + \frac{h}{\varrho} - \frac{v^2}{\varrho}, \\ \dot{\varphi} &= \varpi, \\ \dot{\varpi} &= \frac{4}{\varrho^3}D_\varphi - \frac{2}{\rho}v\varpi. \end{aligned} \tag{5.6}$$

In the interval $[-\pi/3,\pi/3]$, the function $D(\varphi)$ has a singularity at $\varphi = \pm\pi/3$. From the previous chapter, we know how to regularize it: using Lemaitre's transformation, we

reflect the equator of the shape space onto a (red) circle. In this case, the collision points C_{13} and C_{23} each map to a pair of points on the regularized plane. As seen in Fig. 4.3, the collision points (white circles) are distributed non-uniformly on the preimage circle, so the obvious parameterization of the circle $(z+\sqrt{2})\overline{(z+\sqrt{2})}-3=0$ by the expression

$$z = -\sqrt{2} + \sqrt{3}\cos\psi + i\,\sqrt{3}\sin\psi$$

leads to overly cumbersome expressions. Using a fractional linear transformation to place the Euler points evenly on the red circle, the points $(\sqrt{3}-\sqrt{2},0)$, $(0,1)$, $(-\sqrt{3}-\sqrt{2},0)$, $(0,-1)$ are transformed to $(\sqrt{3}-\sqrt{2},0)$, $(-\sqrt{2},\sqrt{3})$, $(-\sqrt{3}-\sqrt{2},0)$, $(-\sqrt{2},-\sqrt{3})$, i.e., they will lie on this same circle at points $E = k\pi/2$, and the collision points will also be at four points: $\pi/4 + k\pi/2$, $k = 0,1,2,3,\ldots$.

As a result of the fractional linear transformation, we obtain the parameterization of the chosen preimage of the equator in the regularized plane:

$$z_E = \frac{\cos E}{\sqrt{3}+\sqrt{2}\cos E} + i\,\frac{\sqrt{3}\sin E}{\sqrt{3}+\sqrt{2}\cos E} \tag{5.7}$$

When E varies from zero to 2π, z traces the entire (red) circle. Thus, in the original space, we replace the spherical coordinates (ϱ,φ) with coordinates ϱ,E. $\varrho = \sqrt{\rho}$ is chosen simply to ensure that the unit of length for this coordinate matches that of familiar unit of length; the coordinate ϱ does not change and remains the same in both the original and regularized spaces. The relationship between the angular coordinate φ in the original space and the angular coordinate E in the regularized space is obtained from Lemaitre's transformation (4.5):

$$\cos\varphi + i\,\sin\varphi = z_E \frac{\sqrt{8}+z_E^3}{1-\sqrt{8}z_E^3}\,,$$

Substituting (5.7) into this, we get:

$$\begin{aligned} \cos\varphi &= \frac{5+\cos 4E}{7-\cos 4E}\,, \\ \sin\varphi &= \frac{4\sqrt{3}\sin 2E}{7-\cos 4E}\,. \end{aligned} \tag{5.8}$$

It is easy to see that the minimum value of $\cos\varphi$ is 1/2 and is achieved at $E = \pi/4 + k\pi/2$, while the maximum value, 1, is achieved at $E = k\pi/2$. The minimum value of

$\sin\varphi$ is $-\sqrt{3}/2$ and occurs at $E = \pi/4 + (2k+1)\pi/2$, while the maximum value, $\sqrt{3}/2$, occurs at $E = \pi/4 + k\pi$. Thus, φ lies in the interval $[-\pi/3,\pi/3]$.

Note. The transformations (5.7) can be obtained not only from the condition of uniformity of the double collision points but also simply by analogy with the hodographs of velocities considered at the beginning of Chapter 1.

Now we derive the necessary expressions. The mutual distances:

$$\begin{aligned} r_{12}^2 &= \varrho^2 \frac{12}{7-\cos 4E}, \\ r_{13}^2 &= \varrho^2 \frac{3(1+\sin 2E)^2}{7-\cos 4E}, \\ r_{23}^2 &= \varrho^2 \frac{3(1-\sin 2E)^2}{7-\cos 4E}, \end{aligned} \tag{5.9}$$

As expected, $r_{12} \neq 0$ (if $\varrho \neq 0$) since, in the case under consideration, body 3 is located between bodies 1 and 2. The distances r_{23} and r_{13} alternately become zero at $E = \pi/4,3\pi/4,5\pi/4,7\pi/4$. With the mutual distances (5.9) for the potential function, we obtain the expression:

$$V = \frac{1}{r_{12}} + \frac{1}{r_{13}} + \frac{1}{r_{23}} = \frac{1}{\varrho} \frac{\sqrt{7-\cos 4E}\,(9+\cos 4E)}{2\sqrt{3}(1+\cos 4E)} = \frac{D(E)}{\varrho}, \tag{5.10}$$

which has a singularity at the points $E = \pi/4 + k\pi/2$, when r_{13} or r_{23} equals zero.

Now, let us write the Hamiltonian $H = T - V$ in terms of the variables ϱ and E. We need to express $\dot{\varphi}$ in terms of $\dot{E}$. Differentiating the equalities (5.8) with respect to t, squaring, and adding them, we get:

$$\dot{\varphi}^2 = 96\dot{E}^2 \frac{1+\cos 4E}{(7-\cos 4E)^2}.$$

The kinetic energy in the variables ϱ and E is:

$$T = 1/2 \left(\dot{\varrho}^2 + 24\varrho^2 \frac{(1+\cos 4E)\dot{E}^2}{(7-\cos 4E)^2} \right). \tag{5.11}$$

With the parameterization (5.8), we obtain expressions for the conjugate momenta:

$$\begin{aligned} p_\varrho &= \frac{\partial L}{\partial \dot{\varrho}} = \frac{\partial T}{\partial \dot{\varrho}} = \dot{\varrho}, \\ p_E &= \frac{\partial L}{\partial \dot{E}} = \frac{\partial T}{\partial \dot{E}} = 24\varrho^2 \dot{E} \frac{1+\cos 4E}{(7-\cos 4E)^2}. \end{aligned} \tag{5.12}$$

Finally, the Hamiltonian is written as (the function D is defined in (5.10)):

$$H = 1/2\left(p_\varrho^2 + \frac{(7-\cos 4E)^2 p_E^2}{24\varrho^2(1+\cos 4E)}\right) - V(\varrho,E)$$

The function V is defined in (5.10), and the final expression for the Hamiltonian takes the form:

$$H = 1/2\left(p_\varrho^2 + \frac{(7-\cos 4E)^2 p_E^2}{24\varrho^2(1+\cos 4E)}\right) - \frac{1}{\varrho}\frac{\sqrt{7-\cos 4E}\,(9+\cos 4E)}{2\sqrt{3}(1+\cos 4E)} \tag{5.13}$$

The energy integral $H = h$ and the region of possible motion in the variables ϱ and the (regularized) E is determined by the inequality $V(\varrho,E) \geqslant -h$. Due to the scale symmetry, we can fix, for example, $h = -1/2$, in which case:

$$\varrho \leqslant \frac{\sqrt{7-\cos 4E}\,(9+\cos 4E)}{\sqrt{3}\,(1+\cos 4E)}\,. \tag{5.14}$$

This equality defines the zero-velocity curve in the regularized space. The zero-velocity curves in the space ϱ,φ and in the regularized space ϱ,E are shown in Fig. 4.5.

The collision points $E = \pi/4 + k\pi/2$ and the Hamiltonian H at these points have a singularity. We will exclude it by performing the second part of the regularization, namely, introducing a new independent variable. We use a well-known technique for this (see, for example, [99]). Consider the Hamiltonian

$$H' = u(q)\,(H-h).$$

If $x(\tau)$ is a solution of the problem with such a Hamiltonian, then $x(t)$ is a solution of the problem with the original Hamiltonian H and the energy constant h, where $d\tau/dt = u^{-1}(q)$. Indeed,

$$\begin{aligned}
\frac{dq}{dt} = \frac{dq}{d\tau}\frac{d\tau}{dt} &= u^{-1}(q)\frac{\partial H'}{\partial q} = u^{-1}(q)\frac{\partial u}{\partial q}(H-h) + \frac{\partial H}{\partial q} = \frac{\partial H}{\partial q}\,,\\
\frac{dp}{dt} = \frac{dp}{d\tau}\frac{d\tau}{dt} &= -u^{-1}(q)\frac{\partial H'}{\partial p} = -\frac{\partial H}{\partial p}\,,
\end{aligned}$$

Thus, to find collinear trajectories, we will consider the Hamiltonian

$$\begin{aligned}
&H' = (1+\cos 4E)(H-h) =\\
&= \frac{1}{2}(1+\cos 4E)(p_\rho^2 - 2h) + \frac{(7-\cos 4E)^2 p_E^2}{48\rho^2} - \frac{\sqrt{7-\cos 4E}(9+\cos 4E)}{2\sqrt{3}\rho}\,,
\end{aligned} \tag{5.15}$$

On the collision line $E = \pi/4 + k\pi/2$:

$$p_E^2 = 2\sqrt{6}\varrho. \tag{5.16}$$

5.1.2 Properties of Collinear Trajectories

Some properties have already been discussed above or follow from general properties:

1. In section 1.2, configurations that can remain unchanged were defined. In the collinear case, these are Euler configurations. If at some moment the point is on the Euler line and $\dot{\varphi} = 0$ (in the unregularized case) or $\dot{E} = 0$ (in the regularized case), then the solution is homothetic.
2. Otherwise, the trajectory must intersect both collision lines and Euler configuration lines.
3. Trajectories are orthogonal to the lines of double collisions (see section 3.2).
4. The relationship (5.16) completely determines the initial conditions on the collision line by the value of ϱ_0.
5. Free-fall trajectories (brake-orbits) and the zero-velocity curve have only two common points. This property is a simple consequence of the reversibility of Hamilton's equations in time, provided the Hamiltonian does not explicitly depend on time.
6. The half-width of the possible motion area (in the ϱ,E space) equals (the branch with the double collision ray $E = \pi/4$):

$$w = \frac{\sqrt{7 - \cos 4E}\,(9 + \cos 4E)}{\sqrt{3}(1 + \cos 4E)} |\sin(E - \pi/4)| = \varrho |\sin(E - \pi/4)| \quad (5.17)$$

If considering zero-velocity curves in ϱ,E coordinates, the branches of the zero-velocity curves will have asymptotes parallel to the double collision rays.

The half-width of the possible motion area (in the unregularized ϱ,φ space) equals (the branch with the double collision ray $\varphi = \pi/3$):

$$w = \frac{1 + 4\cos(\varphi)}{\sqrt{1 + \cos\varphi}(2\cos\varphi - 1)} |\sin(\varphi - \pi/3)|. \quad (5.18)$$

The zero-velocity curves have asymptotes parallel to the double collision rays.

These properties are confirmed by analyzing numerically obtained trajectories. Here are a few more such properties:

– Free-fall trajectories (break-orbits) are orthogonal to the zero-velocity curve.
– The maximum ϱ on the collision line coincides with the maximum p_E.
– The intersection of the Euler configuration lines occurs between series of corresponding collisions, consisting of at least one element.
– The width of the possible motion region in the unregularized space approaches a constant value as $\varrho \to \infty$.

5.1.3 Numerical Results

We will numerically solve the equations of motion in the regularized ϱ,E space. The Hamiltonian H' provides:

$$\begin{aligned}
\dot{\varrho} &= \frac{\partial H'}{\partial p_\varrho} &&= (1+\cos 4E)p_\varrho, \\
\dot{E} &= \frac{\partial H'}{\partial p_E} &&= \frac{(7-\cos 4E)^2 p_E}{24\varrho^2}, \\
\dot{p}_\varrho &= -\frac{\partial H'}{\partial \varrho} &&= \frac{(7-\cos 4E)^2 p_E^2}{24\varrho^3} - \frac{\sqrt{7-\cos 4E}\,(9+\cos 4E)}{2\sqrt{3}\varrho^2}, \\
\dot{p}_E &= -\frac{\partial H'}{\partial E} &&= 2\sin 4E(p_\varrho^2 - 2h) \\
& & & \quad -\frac{(7-\cos 4E)\sin 4E\, p_E^2}{6\varrho^2} - \frac{(5-3\cos 4E)\sin 4E}{\sqrt{3}\sqrt{7-\cos 4E}\,\varrho}.
\end{aligned} \tag{5.19}$$

The energy integral:

$$\left(h - \frac{1}{2}p_\varrho^2\right)(1+\cos 4E) = \\ = -\frac{\sqrt{7-\cos 4E}(9+\cos 4E)}{2\sqrt{3}\varrho} + \frac{(7-\cos 4E)^2 p_E^2}{48\varrho^2}. \tag{5.20}$$

We consider collinear trajectories (with $h < 0$), therefore any trajectory intersects (all) the rays of double collisions. We will set initial conditions on the collision ray $E = \pi/4$. According to property 3 of section 5.1.2, $p_{\varrho_0} = 0$, and according to property 4, $p_E = 2\sqrt{6}\varrho$, thus by specifying only one quantity ϱ_0 on the collision ray, we obtain all initial conditions: ϱ_0, $E = \pi/4$, $p_\varrho = 0$, $p_E = 2\sqrt{6}\varrho$. Hence, the value ϱ_0 at the moment $t_0(=0)$ fully determines the motion.

Choosing initial conditions on any other line, besides ϱ_0 on this line, we need to set another quantity, for example, p_ϱ, the remaining quantity, p_E, can be obtained from the energy integral. For example, consider the line $E = 0$, for the case of equal masses considered here, this is the line of Euler's configuration, Schubart's orbits intersect this line orthogonally, i.e., we can assume $p_\varrho = 0$ and from the energy integral we get the inequality

$$p_{E_0}^2 \leqslant \frac{4\varrho_0(5\sqrt{2} - 2\varrho_0)}{3}.$$

Thus, if the orbit intersects the line $E = 0$ orthogonally ($p_\varrho = 0$), the maximum value of the squared momentum p_E on the line $E = 0$ is 25/3.

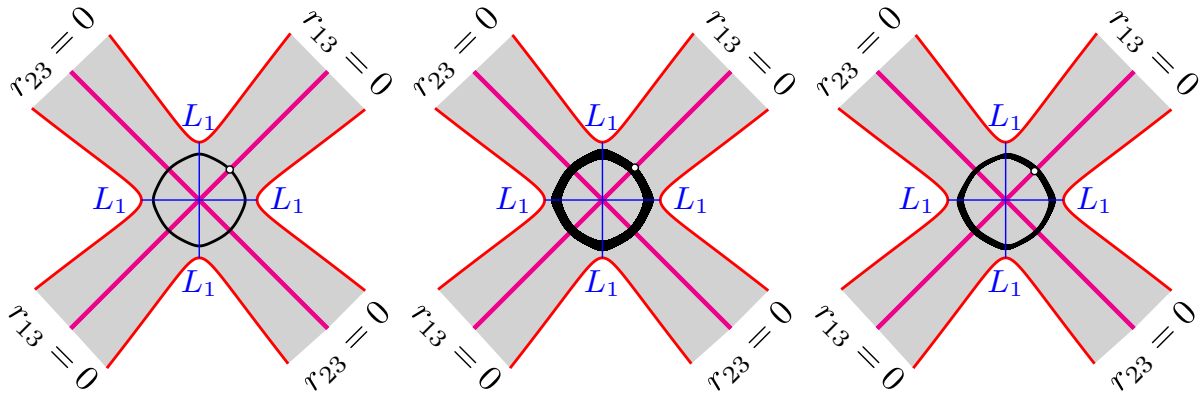

Figure 5.1 – Schubart orbits: $\varrho_0 = 2.63652337$ (left), one hundred periods of the orbit with $\varrho_0 = 2.8$ (center), and the orbit with $\varrho_0 = 2.5$ (right).

Let us start with the classical Schubart orbit, first obtained by Schubart in [61], but the interest in this problem persists (see, for example, [75]). Without loss of generality, we fix the value of the constant energy, $h = -1$; trajectories with a different (negative) constant h) are obtained using the scaling symmetry (1.1). We will set the initial conditions on the double collision ray, for example, on the ray $E = \pi/4$, then according to property 3 of section 5.1.2 $p_{\varrho_0} = 0$, and according to property 4 $p_E = 2\sqrt{6}\varrho$, thus, the initial conditions are fully defined, and by specifying only the value ϱ_0 we can numerically integrate the equations of motion (5.19).

In Figure 5.1, three obtained trajectories similar to the Schubart orbit are shown. Initial conditions are taken on the double collision line $E = \pi/4$ with $\varrho_0 = 2.63652337$ (left), $\varrho_0 = 2.8$ (center), and $\varrho_0 = 2.5$ (right).

The Schubart orbit was constructed with the initial value $\varrho_0 = 2.63652337$ on the collision ray $E = \pi/4$. The orbit is symmetric with respect to the Euler rays and the double collision rays, alternately intersecting the collision lines $E = \pi/4$, $E = 3\pi/4$, $E = 5\pi/4$, and $E = 7\pi/4$ (or in the reverse order), and between intersections of the collision lines, it crosses the Euler line orthogonally once. Although integration was carried out over the entire period, it would have been sufficient to integrate over 1/8 of the period, continuing the orbit by symmetry.

If the initial value ϱ on the collision ray is in the interval $\varrho_0 \in (2.4,2.84)$, the resulting orbits are very similar to the classical Schubart orbit, and this orbit changes little even over long periods. The second ($\varrho_0 = 2.8$) and third ($\varrho_0 = 2.5$) orbits in Fig. 5.1 were integrated over 100 revolutions. The shape of these orbits varies only slightly, but in the figures, such orbits appear as if drawn with a thick line. The first orbit in Fig. 5.2 represents one period of the orbit with $\varrho_0 = 2.42871$; it is evident that the shape of the orbit is similar to the Schubart orbit, but the symmetry relative to the vertical axis is broken.

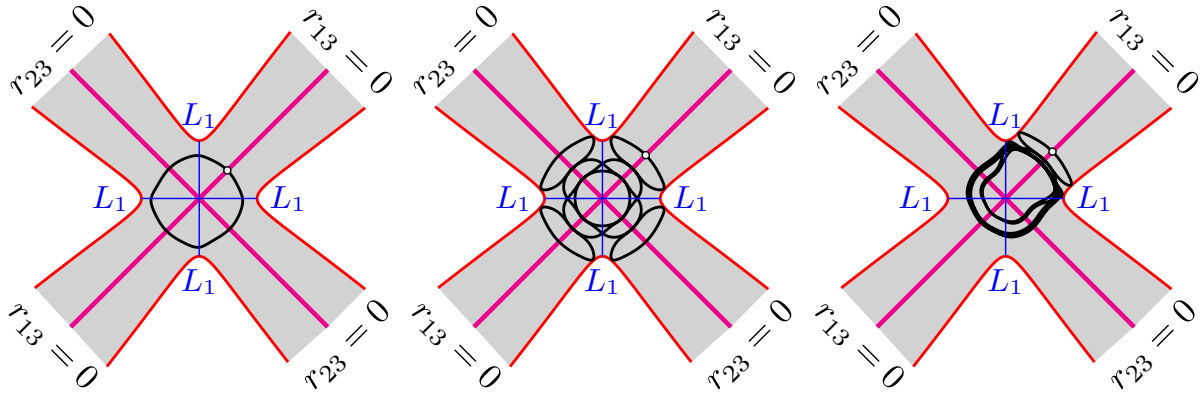

Figure 5.2 – Schubart orbits: $\varrho_0 = 2.42871$ (left), symmetric periodic orbit with $\varrho_0 = 3.74532$ (center), and orbit with $\varrho_0 = 4.04999$ (right).

Note that all Schubart-type orbits are located in the central part of the possible motion region and do not enter the branches of this region. However, if the initial point is taken in one of the branches of the possible motion region, a periodic orbit can be found, for example, with $\varrho_0 = 3.74532$, as shown by the second orbit in Figure 5.2.

Several *remarks* are necessary here: first, the orbit closely resembles the zero-velocity curve, so closely that in the figure it may appear that the orbit has common

points with the zero-velocity curve. This is not the case; the curves are simply close, and in addition, according to property 5, there can only be two common points, whereas in the figure there are eight such "suspicious" points; second, the trajectory intersects each of the four collision rays five times, once at the given ϱ and four more times at points, or rather at two seemingly coincident points. This also cannot be the case; otherwise, the uniqueness of the differential equations' solution would be violated. In reality, these intersections are so close that they are indistinguishable in the figure.

The orbit with $\varrho_0 = 3.74532$ intersects the double collision rays at the following five points: $\varrho_0 = 3.74532$, $\varrho_1 \approx \varrho_1' \approx 2.59$, and $\varrho_2 \approx \varrho_2' \approx 1.70$. The order of intersections of the orbit with the double collision rays is as follows: $(\varrho_0,\pi/4)$, $(\varrho_1,\pi/4)$, $(\varrho_2,7\pi/4)$, $(\varrho_2',5\pi/4)$, $(\varrho_1',3\pi/4)$, $(\varrho_0,3\pi/4)$, $(\varrho_1,3\pi/4)$, $(\varrho_2,\pi/4)$, $(\varrho_2',7\pi/4)$, $(\varrho_1',5\pi/4)$, $(\varrho_0,5\pi/4)$, $(\varrho_1,5\pi/4)$, $(\varrho_2,3\pi/4)$, $(\varrho_2',\pi/4)$, $(\varrho_1',7\pi/4)$, $(\varrho_0,7\pi/4)$, $(\varrho_1,7\pi/4)$, $(\varrho_2,5\pi/4)$, $(\varrho_2',3\pi/4)$, $(\varrho_1',\pi/4)$.

The remarks made for the previous orbit also apply to the third orbit in Fig. 5.2, which is a periodic orbit shaped like a bell.

Choosing the initial point on the collision ray allows for the variation of only one variable, ϱ, which simplifies the task of selecting initial conditions. In many classical works, break orbits have been considered, [9; 28; 39; 75], i.e., orbits having common points with the zero-velocity curve. If the initial conditions are set on this curve, the velocity values are already determined as zero. As is well known, there can be only two such points, so the trajectory connects these points, the orbit is periodic, and the period is equal to twice the time taken to travel from one point to the other.

Four orbits (three shown in Fig. 5.3, and the fourth in Fig. 5.4 on the left) are break-orbits, but the initial conditions were chosen on the Euler line with a velocity perpendicular to this line. The orbits are symmetric relative to the Euler line. The first orbit resembles Schubart's orbit, but unlike Schubart's orbit, it is not closed, or it "closes" on the zero-velocity curve. On the collision rays $E = \pm\pi/4$, the value $\varrho \approx 1.91$, and on the rays $E = \pm 3\pi/4$ $\varrho \approx 2.71$.

The remarks above also apply to break-orbits; hence, the apparent tangency of the orbits to the zero-velocity curves is indeed only apparent. The orbits in these points

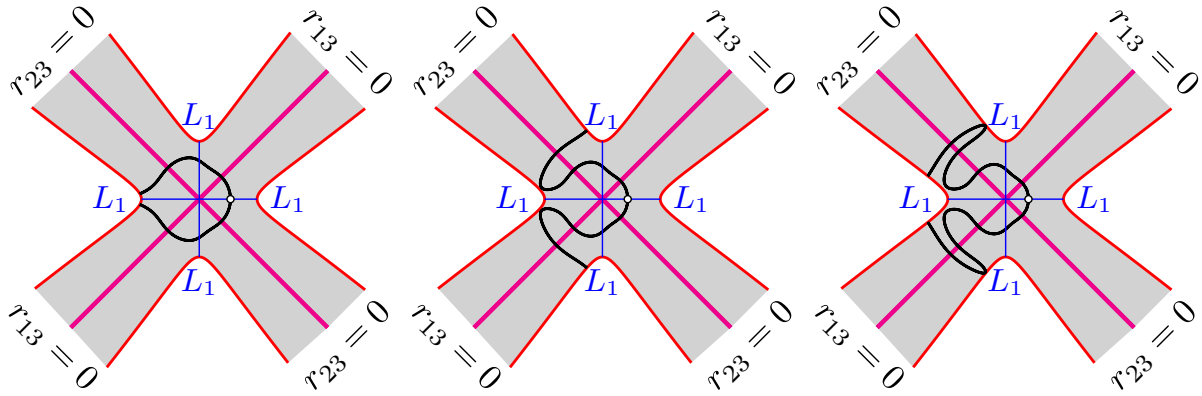

Figure 5.3 – Collinear break-orbits, with the initial point taken on the ray $E = 0$: $\varrho_0 = 1.910687$ (left), $\varrho_0 = 1.544146$ (center), and orbit with $\varrho_0 = 1.395115$ (right).

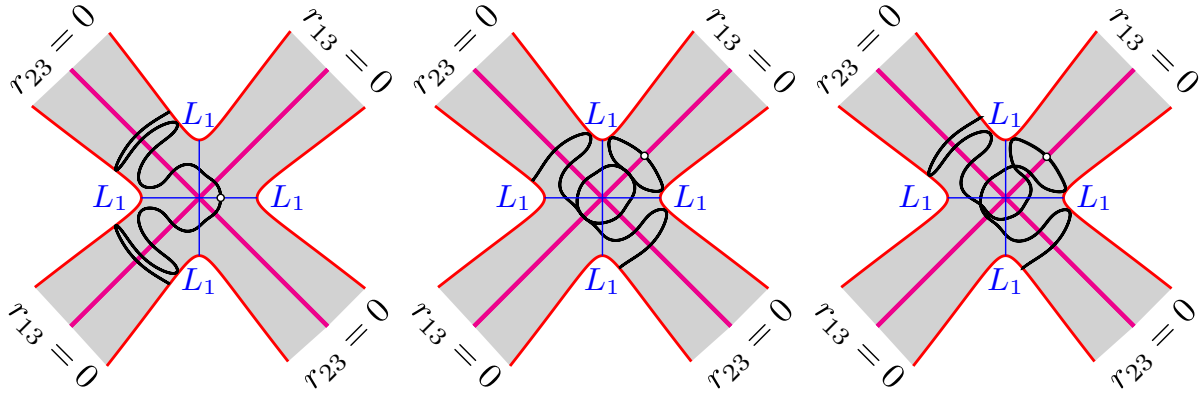

Figure 5.4 – Collinear break-orbits, the initial point of the first orbit on the ray $E = 0$: $\varrho_0 = 1.310462$ (left), the initial point of the next two orbits on the double collision ray $E = \pi/4$: $\varrho_0 = 3.632104$ (center), and orbit with $\varrho_0 = 3.545146$ (right).

are merely very close to the zero-velocity curve. The orbit with $\varrho_0 = 3.632104$ in Fig. 5.4 also has apparent self-intersections on the rays $E = \pi/4$ and $E = 5\pi/4$; these intersections actually occur not on the collision rays. The structure of such intersections is well illustrated by the orbit with $\varrho_0 = 3.545146$, where the intersection with the ray $E = \pi/4$ (and $E = 5\pi/4$) occurs in two nearby points.

Note that ϱ_0 for Schubart-like orbits lies within the range $(2.4,2.6)$, although even within this range, orbits of different types, including chaotic ones, can emerge.

Chaos. Recall that according to properties 3 and 4, we can specify only one value ϱ_0 on the collision ray, then for the remaining values determining the orbit, we have

$E = \pi/4$, $p_\varrho = 0$, $p_E = 2\sqrt{6}\varrho$. Thus, the value ϱ_0 at the moment $t_0(= 0)$ fully determines the motion.

Let $\mathfrak{T} = \{\varrho \,|\, 0 \leqslant \varrho < \infty\}$ be the set of positive real values, and $\mathfrak{E} = \{(\varrho,p_E) \,|\, \varrho < \sqrt{5}/\sqrt{2},p_E^2 \leqslant \frac{4\rho(5\sqrt{2}-2\rho)}{3}\}$, define the mapping $\mathfrak{g} : \mathfrak{T} \to \mathfrak{E}$. The mapping $\mathfrak{g}$ translates the initial condition on the collision ray $E = \pi/4$ to the initial condition on $E = 0$. The set $\mathfrak{T}$ is one-dimensional, while the set $\mathfrak{E}$ is two-dimensional.

The mapping $\mathfrak{T}$ translates the one-dimensional set $(0,\infty)$ into the two-dimensional set $\mathfrak{E}$. There is some analogy to the Peano mapping, which translates the interval $[0,1]$ into the square $[0,1] \times [0,1]$.

All obtained orbits are plotted with an accuracy of 4-5 decimal places. This accuracy is sufficient to make them appear closed (i.e., periodic), but to achieve this appearance, the initial value ρ_0 must be specified with greater precision (up to 8-9 or even 11-12 digits). Only with such precision will the orbit possibly close after one more period. A slight change in the initial value ρ_0 either leads to an orbit that transitions into another branch of the possible motion area or to an orbit that densely fills this area. Figure 5.5 shows three orbits whose initial conditions (on the ray $E = \pi/4$) differ in the fifth decimal place: $\varrho_0 = 2.32427$ (left), $\varrho_0 = 2.32428$ (center), and $\varrho_0 = 2.32433$ (right).

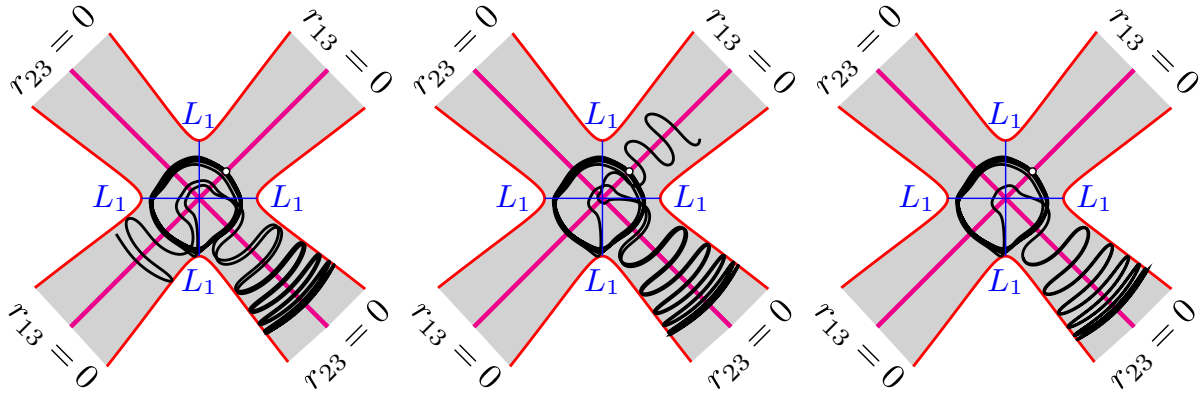

Figure 5.5 – Three collinear orbits with initial values ϱ_0 (on the ray $E = 0$) differing in the fifth decimal place: $\varrho_0 = 2.32427$, $\varrho_0 = 2.32428$, and $\varrho_0 = 2.32433$.

Thus, a small change in the initial conditions leads to significantly different orbits.

Each orbit can be identified with the collisions that occur on it. Table 10 lists for each orbit:

1. the initial value ϱ_0 (on the collision ray or on the Euler configuration ray),
2. the period (in units of regularized time),
3. the set of collisions $\mathfrak{C}$ (a, b, c, d – rays $E = k\pi/4$, $k = 1 \ldots 4$)
4. the set of collisions $\mathfrak{C}_c$ (non-regularized plane).

Table 10 – Order of collisions in collinear orbits

	ϱ_0	T	$\mathfrak{C}$	$\mathfrak{C}_c$
1	2.63652	7.825149	a-b-c-d	2(1-2)
2	2.42871	7.836607	a-b-c-d	2(1-2)
3	3.74532	38.727258	$3(a)$-d-c-$3(b)$-a-d- -$3(c)$-b-a-$3(d)$-c-b	2(3(1)-2-1-3(2)-1-2)
4	4.04999	49.128483	$2(a)$-6(a-d-c-b)	2(1)-12(1-2)
5	*1.91069	14.826108	b-a-d-c :r	2(2-1) :r
6	*1.54415	24.526192	$2(b)$-a-d-$2(c)$:r	2(2)-1-2-2(1) :r
7	*1.39512	36.340492	$3(b)$-a-d-$3(c)$:r	3(2)-1-2-3(1) :r
8	*1.31046	49.673768	$4(b)$-a-d-$4(c)$:r	4(2)-1-2-4(1) :r
9	3.63210	43.822858	$2(b)$-c-d-$3(a)$-b-c-$2(d)$:r	2(2)-1-2-3(1)-2-1-2(2) :r
10	3.54515	49.815710	$3(b)$-c-d-$3(a)$-b-c-$2(d)$:r	3(2)-1-2-3(1)-2-1-2(2) :r

In this table, orbits 5-10 are free-fall orbits and are marked with the symbol ":r". For these orbits, the sequence of collisions is shown only for the first half of the period, the second half being traversed in reverse order.

The initial value ϱ_0 is taken either on the collision ray $E = \pi/4$ or on the ray $E = 0$. In the latter case, only symmetric orbits are considered for $p_{\varrho_0} = 0$, and such orbits are marked with the symbol "*". Repeating segments of sequences are enclosed in parentheses, with the number of repetitions indicated before the opening parenthesis.

The sequences determine the type of orbit. By analogy with the Sitnikov problem, we can assume that these sequences can have any finite length and consist of any permissible transitions. Note that after crossing ray a, there may be a crossing with ray b or d, but not with c. The mapping $\mathfrak{g}$ provides the first step in constructing a Poincaré

section in the (ϱ,p_E) plane, thus mapping the points $(0,\infty)$ of the ray $E = \pi/4$ onto this plane. Subsequently, one or more collisions occur (i.e., crossings of collision rays), followed by another crossing of the Euler configuration ray ($E = k\pi/2$), mapping a 1-dimensional set onto a 2-dimensional set, analogous to a Peano curve.

Thus, the significant dependence on initial conditions and the dimensionality of the initial conditions space demonstrate the chaotic nature of collinear motions in the general three-body problem.

5.2 Isosceles Trajectories

In the previous section, collinear orbits of the three-body problem were considered. The appropriate parameterization of the problem in the Lemaitre regularized shape space allowed us to obtain a number of orbits and analyze their properties. We will apply the same approach to isosceles orbits.

If the two masses at the base of the triangle, m_1 and m_2, are equal, and the third mass at the vertex, m_3, is arbitrary, then choosing initial conditions with appropriate symmetry will keep this isosceles configuration unchanged at any moment in time [108].

Isosceles solutions of the three-body problem have been studied by Broucke [4], Simo and Martinez [66], and others. It is clear that if triple collisions are excluded, only collisions of the bodies at the base of the isosceles triangle are possible. This case is even simpler than in collinear motion, where the middle body collides alternately with one and then the other end body. As in the previous case, we will use Lemaitre's regularization [31].

5.2.1 Equations of Motion

In the isosceles problem, the motion occurs in the meridian $\varphi = 0$ (if the mass m_3 is at the apex of the isosceles triangle), and the two equal masses, m_1 and m_2, are at the base of the triangle. For simplicity, as before, we will consider all masses to be equal, although in this case it is not necessary; it is sufficient for the masses at the base to be equal.

In the isosceles case, the motion in the shape space occurs in the plane $\xi_2 = 0$ ($m_1 = m_2$) with the spherical coordinate $\varphi = 0$, and the angular momentum constant equals zero, $J = 0$. The kinetic energy is given by:

$$T = \frac{\dot{\xi}_1^2 + \dot{\xi}_3^2}{8\sqrt{\xi_1^2 + \xi_3^2}},$$

and if we introduce polar coordinates:

$$\begin{aligned} \xi_1 &= \varrho^2 \cos\theta, \\ \xi_3 &= \varrho^2 \sin\theta, \end{aligned} \tag{5.21}$$

the kinetic energy takes the form:

$$T = \frac{1}{2}\left(\dot{\varrho}^2 + \frac{1}{4}\varrho^2\dot{\theta}^2\right). \tag{5.22}$$

Note that here, for the isosceles case, the angle θ ranges from 0 to 2π.

The expression for the potential function in this case is:

$$\begin{aligned} V &= 1/r_{12} + 2/r_{13} = \\ &= \frac{1}{\varrho}\left(\frac{1}{\sqrt{1+\cos\theta}} + \frac{2}{\sqrt{1-1/2\cos(\theta)}}\right) \\ &= \frac{1}{\varrho}\frac{2\sqrt{1+\cos\theta} + \sqrt{1-1/2\cos\theta}}{\sqrt{1+\cos\theta}\sqrt{1-1/2\cos\theta}} = \frac{D(\theta)}{\varrho}, \end{aligned} \tag{5.23}$$

and the energy integral is:

$$2h = \dot{\varrho}^2 + \frac{1}{4}\varrho^2\dot{\theta}^2 - 2V = \dot{\varrho}^2 + \frac{1}{4}\varrho^2\dot{\theta}^2 - 2\frac{D(\theta)}{\rho}. \tag{5.24}$$

From here, we obtain the region of possible motion:

$$\frac{D(\theta)}{\varrho} = \frac{1}{\varrho}\frac{2\sqrt{1+\cos\theta}+\sqrt{1-1/2\cos\theta}}{\sqrt{1+\cos\theta}\sqrt{1-1/2\cos\theta}} \geqslant -h. \tag{5.25}$$

The potential function has a singularity at $\theta = \pi$. This singularity, as in the case of collinear orbits, can be regularized using Lemaitre's transformation (4.5). The preimage of the meridian $\xi_2 = 0$ is either the line $\mathrm{Re}z = 0$ or the circle:

$$\left(z - \frac{1}{\sqrt{2}}\right)\left(\overline{z} - \frac{1}{\sqrt{2}}\right) = \frac{3}{2} \tag{5.26}$$

Thus, in the regularized space, the preimage of the meridian of the shape sphere, which corresponds to isosceles motion, is the red circle in Fig. 5.6. Points on this circle, as well as points on the meridian, correspond to configurations where m_1 and m_2 are at the base of the triangle. The meridian naturally intersects the equator at two points, which are Euler points. The blue and green circles correspond to meridians representing isosceles configurations where m_1 and m_3 (green circle) and m_2 and m_3 are at the base of the triangle. Collision points are marked with white circles, and Euler points with cyan, yellow, and brown circles, as in Fig. 4.3. Naturally, collision points and Euler points in Figs. 4.3 and 5.6 coincide. The preimages of the meridian are rotated relative to the preimages of the equator by π, and the radii of the corresponding circles are $\sqrt{3/2}$. Each circle has two points of double collisions (of the same pair of bodies at the base of the triangle) and two Euler points (the body at the apex is between the bodies at the base of the triangle).

As we did in the collinear case (5.7), let us choose a parameterization of the (red) circle so that the collision points and Euler points on it are distributed uniformly. In this case, we obtain the following parameterization:

$$z_E = \frac{\sqrt{2}\cos E}{\sqrt{3}-\cos E} + i\,\frac{\sqrt{3}\sin E}{\sqrt{3}-\cos E}\,. \tag{5.27}$$

We get:

$$\begin{aligned} \mathrm{Re}\; z_E &= \frac{3\cos 2E + 4\sqrt{3}\cos E - 3}{3\cos 2E - 4\sqrt{3}\cos E - 3}, \\ \mathrm{Im}\; z_E &= 0, \end{aligned} \tag{5.28}$$

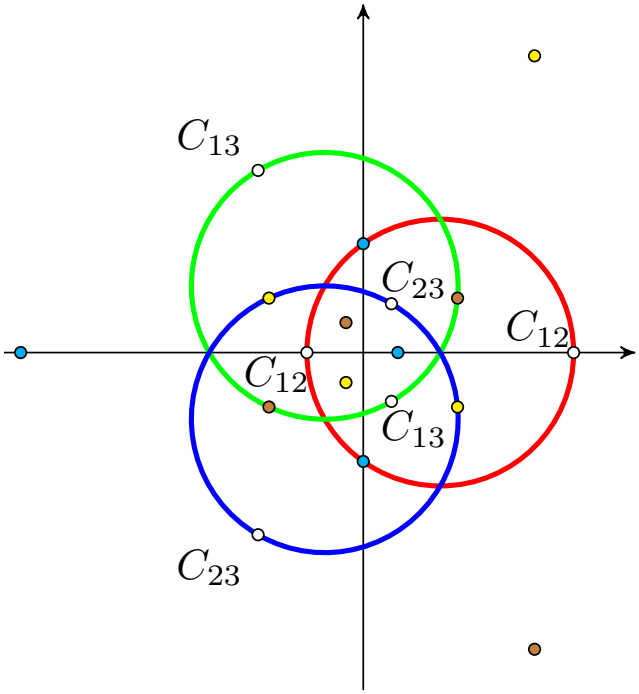

Figure 5.6 – Preimages of meridians on the regularized plane

which is quite natural since we are considering the preimage of the meridian $\xi_2 = 0$. However, in the meridian plane, we have polar coordinates (5.21), so:

$$\begin{aligned} \cos\theta &= \frac{2\mathrm{Re}\, z_E}{1+(\mathrm{Re}\, z_E)^2} = \frac{(\cos 2E - 5)(1+3\cos 2E)}{3\cos^2 2E + 2\cos 2E + 11}\,, \\ \sin\theta &= \frac{(\mathrm{Re}\, z_E)^2 - 1}{1+(\mathrm{Re}\, z_E)^2} = \frac{-8\sqrt{3}\sin E \sin 2E}{3\cos^2 2E + 2\cos 2E + 11}\,, \end{aligned} \tag{5.29}$$

and mutual distances:

$$\begin{aligned} r_{12} &= \varrho\,\frac{\sqrt{6}(1-\cos 2E)}{\sqrt{3\cos^2 2E + 2\cos 2E + 11}}\,, \\ r_{13} = r_{23} &= \varrho\,\frac{\sqrt{3}(3+\cos 2E)}{\sqrt{2(3\cos^2 2E + 2\cos 2E + 11)}}\,. \end{aligned} \tag{5.30}$$

With these mutual distances, we obtain the following expression for the potential function:

$$V = \frac{1}{r_{12}} + \frac{1}{r_{13}} + \frac{1}{r_{23}} = \frac{1}{\varrho}\,\frac{\sqrt{3\cos^2 2E + 2\cos 2E + 11}\,(7 - 3\cos 2E)}{\sqrt{6}(1-\cos 2E)(3+\cos 2E)} = \frac{D(E)}{\varrho}\,, \tag{5.31}$$

which has a singularity at the points $E = k\pi$ when r_{12} equals zero.

Let us now write the Hamiltonian $H = T - V$ for the isosceles problem in the variables ϱ, E. It is necessary to express $\dot\theta$ through $\dot E$. Differentiating equations (5.29)

with respect to t, squaring them, and summing, we get:

$$\dot{\theta}^2 = 96\dot{E}^2 \frac{(1-\cos 2E)(3+\cos 2E)^2}{\sqrt{3\cos^2 2E + 2\cos 2E + 11}}$$

The kinetic energy of the isosceles problem in the variables ϱ,E is:

$$T = 1/2 \left(\dot{\varrho}^2 + 24\varrho^2\dot{E}^2 \frac{(1-\cos 2E)(3+\cos 2E)^2}{(3\cos^2 2E + 2\cos 2E + 11)^2} \right) , \tag{5.32}$$

With the parameterization (5.27), we get the expressions for the conjugate momenta:

$$\begin{aligned} p_\varrho &= \frac{\partial T}{\partial \dot{\varrho}} = \dot{\varrho}, \\ p_E &= \frac{\partial T}{\partial \dot{E}} = 24\varrho^2\dot{E} \frac{(1-\cos 2E)(3+\cos 3E)^2}{(3\cos^2 2E + 2\cos 2E + 11)^2} , \end{aligned} \tag{5.33}$$

Finally, the Hamiltonian is written as:

$$H = 1/2 \left(p_\varrho^2 + \frac{(3\cos^2 2E + 2\cos 2E + 11)^2 p_E^2}{24\varrho^2(1-\cos 2E)(3+\cos 2E)^2} \right) - V(\varrho,E)$$

The function V for the isosceles case is defined in (5.31), and the final expression for the Hamiltonian of the isosceles problem is:

$$\begin{aligned} H = 1/2 \left(p_\varrho^2 + \frac{(3\cos^2 2E + 2\cos 2E + 11)^2 p_E^2}{24\varrho^2(1-\cos 2E)(3+\cos 2E)^2} \right) \\ - \frac{1}{\varrho} \frac{\sqrt{3\cos^2 2E + 2\cos 2E + 11}\,(7-3\cos 2E)}{\sqrt{6}(1-\cos 2E)(3+\cos 2E)} , \end{aligned} \tag{5.34}$$

The energy integral $H = h$ and the region of possible motion in terms of ϱ and the (regularized) E are determined by the inequality $V(\varrho,E) \geqslant -h$. For $h = -1$, we have:

$$\varrho \leqslant \frac{\sqrt{3\cos^2 2E + 2\cos 2E + 11}\,(7-3\cos 2E)}{\sqrt{6}(1-\cos 2E)(3+\cos 2E)} , \tag{5.35}$$

This equation defines the zero velocity curve in the regularized space. The region of possible motion in the regularized plane (ϱ,E) is bounded by the zero velocity curve only, which in this case consists of two branches. The Euler points correspond to $E = \pm\pi/2$, and the point on the curve closest to the origin is achieved at $E = k\pi \pm \arccos(1/3)$.

At the collision points $E = k\pi$, the Hamiltonian H has a singularity. As in the collinear case, we will eliminate this by performing the second part of the regularization, namely, by introducing a new Hamiltonian:

$$H' = (1 - \cos 2E)(H - h) = \\ = \frac{1}{2}(1 - \cos 2E)(p_\rho^2 - 2h) + \frac{(3\cos^2 2E + 2\cos 2E + 11)^2 p_E^2}{24\varrho^2(3 + \cos 2E)^2} \\ - \frac{1}{\varrho}\frac{\sqrt{3\cos^2 2E + 2\cos 2E + 11}\,(7 - 3\cos 2E)}{\sqrt{6}(3 + \cos 2E)}, \quad (5.36)$$

On the collision line $E = k\pi$:

$$p_E^2 = 2\sqrt{6}\varrho. \quad (5.37)$$

5.2.2 Properties of Isosceles Trajectories

Some properties are similar to those already discussed in Section 5.1.2.

1. In Section 1.2, configurations that can remain invariant were identified. In the isosceles case, such an Euler configuration, if $\dot{E} = 0$ (in the non-regularized case $\dot{\theta} = 0$), represents a homothetic configuration, with motion ending in a triple collision.
2. Otherwise, the trajectory must intersect both collision lines and Euler lines.
3. Trajectories are orthogonal to the double collision lines (see Section 3.2), a property of all collision trajectories, already mentioned for collinear trajectories.
4. The relation (5.37) fully determines the initial conditions on the collision line based on the value of ϱ_0.
5. Free-fall trajectories (brake orbits) and the zero-velocity curve have only two common points.
6. The half-width of the possible motion area (in the ϱ,E space) is given by:

$$w = \frac{\sqrt{3\cos^2 2E + 2\cos 2E + 11}\,(7 - 3\cos 2E)}{\sqrt{6}(1 - \cos 2E)(3 + \cos 2E)}|\sin E| = \varrho|\sin E| \quad (5.38)$$

7. Intersection of Euler configuration lines occurs between series of corresponding collisions, consisting of at least one element.

The value ϱ_0 at the moment t_0 fully determines our motion, since $p_\varrho = 0$ (orthogonality), $E = 0$ or π (in the non-regularized case $\theta = \pi$), and p_E is determined from property 4 by formula (5.37). Choosing initial conditions on any other line, we would have to specify two values, the third would be determined by this line, and the fourth from the energy integral. If we choose, for example, the line $E = \pi/2$ (or $3\pi/2$), i.e., the Euler configuration in the case of equal masses $m_1 = m_2$, then besides ϱ_0, we must also specify p_ϱ. And if the orbit intersects the Euler line orthogonally ($p_\varrho = 0$), then from the energy integral we have

$$p_E^2 \leqslant \frac{4\varrho(5\sqrt{2} - 2\varrho)}{3},$$

and the maximum value of p_E^2 on the $\pi/2$ ray in this case is 25/3.

Similarly to the case of collinear orbits, we can define the mapping $\mathfrak{g} : \{(0,\infty)\} \to \{0 < \varrho \leqslant 5/\sqrt{2},\, p_E^2 \leqslant 4\varrho(5\sqrt{2} - 2\varrho)/3\}$, which maps the one-dimensional set $\mathbb{R}^+$ to a two-dimensional one, indicating the chaotic nature of the motion.

5.2.3 Numerical results

As with the collinear orbits, we will solve the equations of motion in the regularized space ϱ,E numerically. The Hamiltonian H' from (5.36) gives:

$$\begin{aligned}
\dot{\varrho} = \frac{\partial H'}{\partial p_\varrho} &= (1-\cos 2E)\, p_\varrho, \\
\dot{E} = \frac{\partial H'}{\partial p_E} &= \frac{(3\cos^2 2E + 2\cos 2E + 11)^2 p_E}{24(3+\cos 2E)^2 \varrho^2}, \\
\dot{p}_\varrho = -\frac{\partial H'}{\partial \varrho} &= \frac{(3\cos^2 2E + 2\cos 2E + 11)^2 p_E^2}{24(3+\cos 2E)^2 \varrho^3} \\
&\quad - \frac{(7-3\cos 2E)\sqrt{3\cos^2 2E + 2\cos 2E + 11}}{\sqrt{6}(3+\cos 2E)\varrho^2}, \\
\dot{p}_E = -\frac{\partial H'}{\partial E} &= -\sin 2E(p_\varrho - 2h) + \\
&\quad \frac{(3\cos^2 2E + 2\cos 2E + 11)(3\cos^2 2E + 18\cos 2E - 5)\sin 2E\, p_E^2}{12(3+\cos 2E)^3 \varrho^2} + \\
&\quad \frac{2(9\cos^3 2E + 57\cos^2 2E + -29\cos 2E + 155)\sin 2E}{\sqrt{6}(3+\cos 2E)^2\sqrt{3\cos^2 2E + 2\cos 2E + 11}\varrho},
\end{aligned} \tag{5.39}$$

and the energy integral (5.36).

Any isosceles trajectory with $h < 0$ intersects the double collision rays. We will set the initial conditions on the collision ray $E = 0$. By property 3 of the previous section $p_{\varrho_0} = 0$, and by property 4 (same section) $p_E = 2\sqrt{6}\varrho$, therefore, by setting only one value ϱ_0 on the collision ray, we obtain all the initial conditions: ϱ_0, $E = 0$, $p_\varrho = 0$, $p_E = 2\sqrt{6}\varrho$. Thus, the value ϱ_0 at time $t_0(= 0)$ fully determines the motion.

If we choose the initial conditions on any other line, except ϱ_0, we must set one more value, for example, p_ϱ, the remaining value p_E can be obtained from the energy integral. For the case of equal masses considered here, let us take the line $E = \pi/2$, this is the line of Euler configuration, symmetrical orbits intersect this line orthogonally, i.e., we can set $p_\varrho = 0$ and from the energy integral we get the equal-

ity

$$2h - p_\varrho^2 = -\frac{5\sqrt{2}}{\varrho} + \frac{3p_E^2}{4\varrho^2}\,.$$

Thus, if the orbit intersects the line $E = \pi/2$ orthogonally ($p_\varrho = 0$), then the maximum value of the impulse square p_E on the line $E = \pi/2$ is $5/\sqrt{-3h}$.

Let us start with the Broucke orbit, discussed in [4; 77]. As with collinear orbits, without loss of generality, we fix the value of the energy constant, $h = -1$; trajectories with other (negative) energy constants h can be obtained by using the scaling symmetry (1.1). We will set the initial conditions on the double collision ray, for example, on the ray $E = 0$, then according to property 3 $p_{\varrho_0} = 0$, and according to property 4 $p_E = 2\sqrt{6}\varrho$, thus, the initial conditions are fully determined, and by setting only the value ϱ_0, we can numerically integrate the equations of motion (5.39).

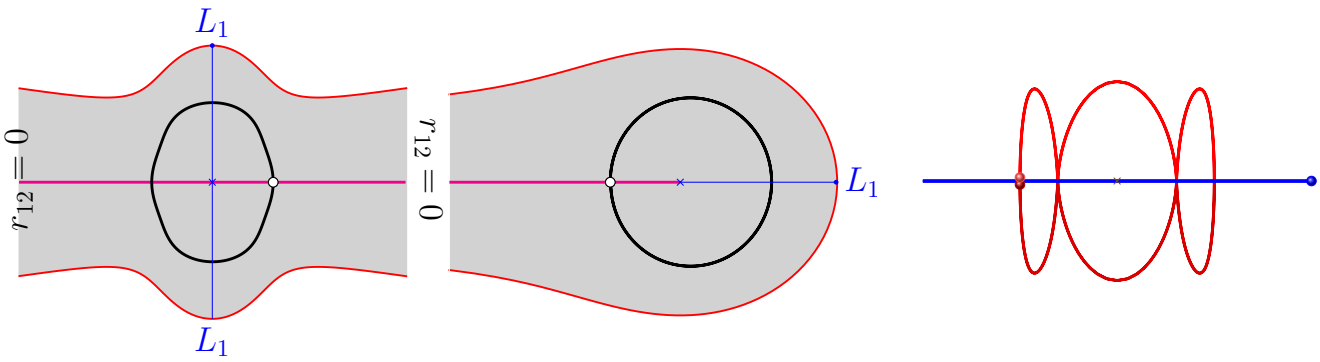

Figure 5.7 – Broucke orbit, on the left in the regularized plane, in the center in the non-regularized plane, on the right trajectories of all points on the plane

The trajectory shown in Figure 5.7 resembles the Broucke orbit. The initial conditions are taken on the double collision line $E = 0$ with $\varrho_0 = 1.57576$: on the left in the regularized coordinates ϱ,E, in the center, the same orbit in the non-regularized coordinates ϱ,θ, with the initial points marked by white circles, the double collision line in magenta, the Euler configurations as blue lines, the feasible region shaded in gray, and the zero velocity curves in red. On the right are the trajectories of all three points of this orbit in the plane (x,y): the blue point moves along the horizontal line, while the two red points lie at the base of the isosceles triangle, with the initial position

of all points on the line. To separate the two red points, they are shown after a short time interval from the start.

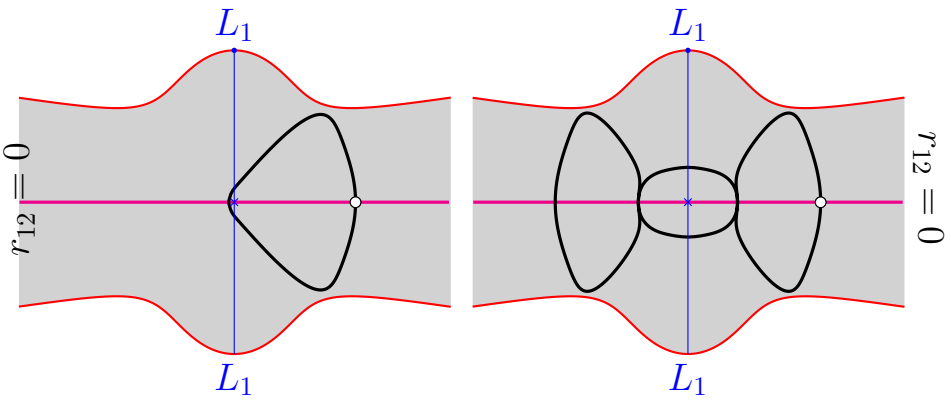

Figure 5.8 – Orbits with $\varrho_0 = 2.82483$ (left) and $\varrho_0 = 3.08990$ (right) in the regularized plane

Increasing ϱ_0, the orbits shown in Figs. 5.8–5.11 are obtained.

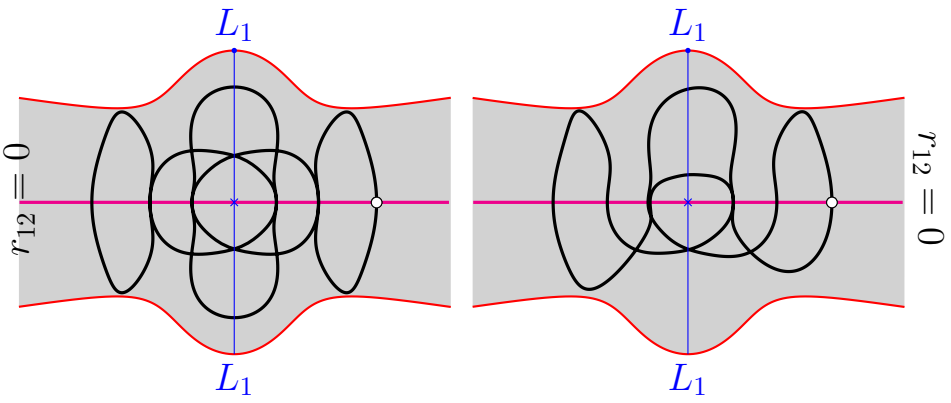

Figure 5.9 – Orbit with $\varrho_0 = 3.31543$ (left) and $\varrho_0 = 3.35228$ (right) in the regularized plane

The observations made for collinear orbits in Section 5.1.3 apply to isosceles orbits as well.

The initial points of the orbits in Figs. 5.8–5.10 lie on the double collision line, marked by a white circle.

The last figure shows two break-orbits, with the initial point on the zero velocity curve marked by a white circle.

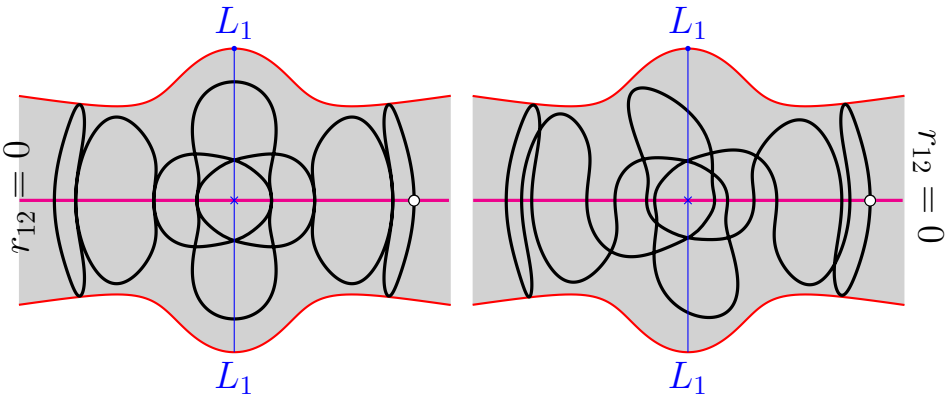

Figure 5.10 – Orbit with $\varrho_0 = 4.18797$ (left) and $\varrho_0 = 4.24520$ (right) in the regularized plane

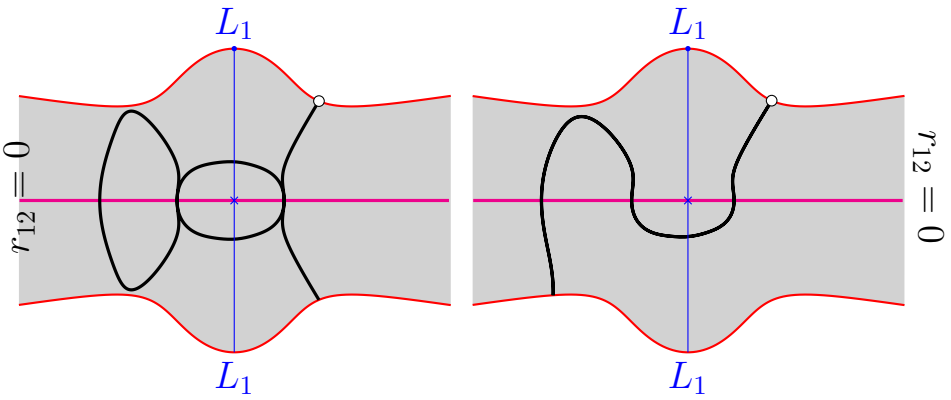

Figure 5.11 – Break-orbit with $E_0 = 0.864900$ (left) and $E_0 = 0.872985$ (right) in the regularized plane

Table 11 – Collision order in isosceles orbits

	ρ_0/E_0 $(*)$	T	$\mathfrak{C}$
1	1.57576	9.49965	a-b
2	2.82483	12.22611	a-b
3	3.08990	33.84638	$2(a)$-$3(b)$-a
4	3.31543	55.74503	$2(a)$-b-a-$3(b)$-a-b-(a)
5	3.35228	42.28584	$2(a)$-b-a-$3(b)$-a-b-(a)
6	4.18797	94.03594	$3(a)$-b-a-$5(b)$-a-b-$3(a)$
7	4.24520	94.77880	$3(a)$-b-a-$5(b)$-a-b-$3(a)$
8	*0.86490	26.42871	a-$3(b)$-a :r
9	*0.87299	17.56025	a-$2(b)$:r

The four columns of Table 11 contain the same information as the corresponding columns of Table 10. Note that orbits 4 and 5 and orbits 6 and 7 have identical collision sets, and the corresponding pairs of orbits are topologically similar.

Conclusion

Considering the motions of the general three body problem in the form space, we use integrals of motion. From the very beginning, with the help of appropriate symmetries, we get rid of «extra dimensions», leaving only the configuration of the problem of three bodies, its size and shape. Thus, we have a three-dimensional space of congruent triangles defining the configuration of three bodies. The three-dimensionality of this space makes it possible to simplify the analysis of solutions, and at least simply visualize the space of solutions. If the solution of the problem in the form space is known, we can use the quadrature to find the angle of inclination of this triangle to a fixed axis, and, therefore, restore the position of our triangle.

The study of periodic orbits in the form space allows us to conclude that at least some of them have a simple form on the form sphere: the trajectories (topologically) are a circle in the center of which lies either a singular point $\mathcal{C}_i$, or an Eulerian point $\mathcal{E}_i$. However, the figure-eight has a completely different appearance: the trajectory cicles the form sphere twice along the equator, deviating from the equator in one direction or another, and on the regularized plane corresponding to the form sphere, one of the (four) images of the figure-eight is a single quasi-circle, since it passes through six images of three Eulerian points lying on the unit circles.

The shape space surprisingly makes it possible to construct easy the zero-velocity surfaces, and, therefore, areas of possible motion. This task, to build a zero velocity surface, has been set before, but in the form space a simple solution is obtained. In addition, we can simply imagine the resulting three-dimensional surface. It turns out that the zero-velocity surfaces of the general three-body problem have a lot in common with the zero-velocity surfaces of the circular restricted problem (Hill surfaces). In both cases, the surface depends on one parameter. For a circular restricted problem, such a parameter is the value of the Jacobi constant (energy), for a general problem, the energy constant can be fixed due to the scale symmetry, and the constant of the areas J can be chosen as a parameter (in Hill's problem, this constant is fixed by choosing the average

motion n of a rotating coordinate system). As in the circular restricted problem, there are five topologically different types of zero velocity surface in the general three-body problem. As $|J|$ increases, at first the surface consists of an outer one, three branches of which are directed along three collision rays, and an inner one, in the case of $J = 0$ this is the origin of the coordinates, then the inner surface grows and eventually touches the outer surface (at points L_{45}), with the further growth of $|J|$ at the points E_i, the branches are separated in turn, and finally, all three disconnected branches are obtained.

The Lemaitre transform allows you to simply regularize degenerate orbits. Using the given parameterizations, we regularize the Hamiltonian, and solve the equations of motion, which have no singularities, numerically. At the same time, the properties of the solutions allow us to conclude that the motion is chaotic. The corresponding orbits are given for collinear and isosceles configurations.

The consistent representation of the motion of the general problem of three bodies in the space of forms greatly facilitates the analysis of the properties of the motion of the problem of three bodies.

The author is grateful to all the staff of the Department of Celestial Mechanics of St. Petersburg State University for their support and the atmosphere without which this work could hardly have been done. I would like to express special gratitude to K. V. Kholshevnikov, who headed the department for 50 years, who showed keen interest and sometimes participated in the work, alas, who left before its completion.

Bibliography

1. *Albouy, A.* The problem of n bodies and mutual distances [Text] / A. Albouy, A. Chenciner // Inventiones mathematicae. — 1998. — Jan. — Vol. 131. — P. 151—184.
2. *Barutello, V.* Symmetry groups of the planar 3-body problem and action–minimizing trajectories [Text] / V. Barutello, D. L. Ferrario, S. Terracini // arXiv Mathematics e-prints. — 2004. — Apr. — math/0404514. — arXiv: math/0404514 [math.DS].
3. *Broucke, R.* On relative periodic solutions of the planar general three-body problem. [Text] / R. Broucke // Celestial Mechanics. — 1975. — Aug. — Vol. 12, no. 3. — P. 303—313.
4. *Broucke, R.* On the isosceles triangle configuration in the planar general three-body problem. [Text] / R. Broucke // Astronomy and Astrophysics. — 1979. — Mar. — Vol. 73, no. 3. — P. 303—313.
5. *Broucke, R.* Periodic orbits in the planar general three body problem [Text] / R. Broucke, D. Boggs // Celestial Mechanics. — 1975. — Oct. — Vol. 11, no. 1. — P. 13—38.
6. *Broucke, R.* A note on relative motion in the general three-body problem [Text] / R. Broucke, D. Lass // Celestial Mechanics. — 1973. — Vol. 8, no. 1. — P. 5—10.
7. *Broucke, R.* Numerical explorations of the rectilinear problem of three bodies [Text] / R. Broucke, D. E. Walker // Celestial Mechanics. — 1980. — Vol. 21, no. 1. — P. 73—81.
8. *Butikov, E. I.* The velocity hodograph for an arbitrary Keplerian motion [Text] / E. I. Butikov // European Journal of Physics. — 2000. — July. — Vol. 21, no. 4. — P. 297—302.
9. *Chen, N.-C.* Periodic brake orbits in the planar isosceles three-body problem [Текст] / N.-C. Chen // Non-linearity. — 2013. — Т. 26, № 10. — С. 2875. — URL: https://dx.doi.org/10.1088/0951-7715/26/10/2875.

10. *Chenciner, A.* Symmetries and “simple” solutions of the classical n-body problem [Text] / A. Chenciner. — 2006. — Mar.

11. *Chenciner, A.* The ”form” of a triangle [Text] / A. Chenciner // Rendiconti di Matematica e delle sue Applicazioni. Serie VII. — 2007. — Jan. — Vol. 27.

12. *Chenciner, A.* Three body problem [Text] / A. Chenciner // Scholarpedia. — 2007. — Jan. — Vol. 2. — P. 2111.

13. *Chenciner, A.* The Lagrange reduction of the N-body problem, a survey [Text] / A. Chenciner // Acta Mathematica Vietnamica. — 2011. — Nov. — Vol. 38.

14. *Chenciner, A.* A Walk Through the New Methods of Celestial Mechanics [Text] / A. Chenciner // Springer Proceedings in Mathematics and Statistics. — 2013. — Jan. — Vol. 54.

15. *Chenciner, A.* Poincaré and the Three-Body Problem [Text] / A. Chenciner // Progress in Mathematical Physics. — 2015. — Oct. — Vol. 67. — P. 51—149.

16. *Chenciner, A.* A remarkable periodic solution of the three-body problem in the case of equal masses [Text] / A. Chenciner, R. Montgomery // Annals of Mathematics. — 2000. — Vol. 152, no. 3. — P. 881—901.

17. *Davoust, E.* A manifold of periodic orbits in the planar general three-body problem with equal masses [Text] / E. Davoust, R. Broucke // Astronomy and Astrophysics. — 1982. — Vol. 112, no. 2. — P. 305—320.

18. *Dmitrašinović, V.* Topological dependence of Kepler’s third law for collisionless periodic three-body orbits with vanishing angular momentum and equal masses [Text] / V. Dmitrašinović, M. Šuvakov // Physics Letters A. — 2015. — Sept. — Vol. 379, no. 36. — P. 1939—1945. — arXiv: 1507.08096 [physics.class-ph].

19. *Euler, L.* De motu rectilineo trium corporum se mutuo attrahentum [Text] / L. Euler // Novi Comm. Acad. Sci. Imp. Petrop. — 1767. — Vol. 11. — P. 144—151.

20. *Henon, M.* Families of periodic orbits in the three-body problem [Text] / M. Henon // Celestial Mechanics. — 1974. — Vol. 10, no. 3. — P. 375—388.

21. *Henon, M.* A family of periodic solutions of the planar three-body problem, and their stability [Text] / M. Henon // Celestial Mechanics. — 1976. — Vol. 13, no. 3. — P. 267—285.

22. *Hsiang, W.-Y.* Kinematic geometry of triangles and the study of the three-body problem [Text] / W.-Y. Hsiang, E. Straume // Lobachevskii J. Math. — 2007. — Vol. 25. — P. 9—130.

23. *Hsiang, W.-Y.* Global geometry of 3-body motions with vanishing angular momentum. I [Text] / W.-Y. Hsiang, E. Straume // Chin. Ann. Math., Ser. B. — 2008. — Vol. 29, no. 1. — P. 1—54.

24. *Hsiang, W.-Y.* Global geometry of planary 3-body motions [Text] / W.-Y. Hsiang, E. Straume // Acta Appl. Math. — 2008. — Vol. 101, no. 1—3. — P. 105—119.

25. *Janković, M. R.* Angular momentum and topological dependence of Kepler's Third Law in the Broucke-Hadjidemetriou-Hénon family of periodic three-body orbits [Text] / M. R. Janković, V. Dmitrašinović // Phys. Rev. Lett. — 2016. — May. — Vol. 116. — arXiv: 1604.08358v1 [physics.class-ph].

26. *Janković, M. R.* A guide to hunting periodic three-body orbits with non-vanishing angular momentum [Text] / M. R. Janković, V. Dmitrašinović, M. Šuvakov // Computer Physics Communications. — 2020. — May. — Vol. 250. — P. 107052.

27. *Kol, B.* Natural dynamical reduction of the three-body problem [Text] / B. Kol // Cel. Mech. and Dynamical Astron. — 2023. — Vol. 135, no. 3.

28. *Kuwabara, K.* An extension of the Free-Fall Problem [Text] / K. Kuwabara, K. Tanikawa // Few-Body Problem: Theory and Computer Simulations. — University of Turku, Finland, 2006. — P. 29.

29. *Lagrange, J.-L.* Essai sur le Probléme des Trois Corps [Text] / J.-L. Lagrange // Prix de l'Académie Royale des Sciences de Paris. — 1772. — Vol. IX, no. 6. — P. 292.

30. *Lemaitre, G.* Coordonnées Symétriques dans le Problème des Trois Corps [Text] / G. Lemaitre // Bulletin de l'Académie Royale de Belgique (classe des sciences). — 1952. — Vol. 38. — 582 - 592 and 1218 —1234.

31. *Lemaitre, G.* Regularization of the three-body problem [Text] / G. Lemaitre // Vistas in Astronomy. — 1955. — Vol. 1. — P. 207—215.

32. *Lemaitre, G.* The Three Body Problem [Text] / G. Lemaitre // NASA Contractor Report. — 1964. — Vol. 110. — P. 60.

33. *Levi-Civita, T.* Condition du choc dans le problème restreint des trois corps. [Text] / T. Levi-Civita // C. R. Hebd. Acad. Sci. Paris. — 1903. — Vol. 136. — P. 221—223.

34. *Levi-Civita, T.* Sur les trajectoires singulières du problème restreinte des trois corps [Text] / T. Levi-Civita // C. R. Hebd. Acad. Sci. Paris. — 1903. — Vol. 136. — P. 82—84.

35. *Levi-Civita, T.* Sur les trajectoires singulières du problème restreinte des trois corps [Text] / T. Levi-Civita // Annal. Mat. Pura. Appl.Paris. — 1903. — Vol. 9, no. 3. — P. 1—32.

36. *Levi-Civita, T.* Sur la régularisation du problème des trois corps [Text] / T. Levi-Civita // C. R. Hebd. Acad. Sci. Paris. — 1916. — Vol. 162. — P. 625—628.

37. *Levi-Civita, T.* Sur la régularization du problème de trois corps [Text] / T. Levi-Civita // Acta Mathematica. — 1921. — Vol. 42. — P. 144—151.

38. *Lewis, D. C.* Comments on the Sundman inequality [Text] / D. C. Lewis // Second Complilation of papers on trajectory analysis and guidance theory. — NASA, Electronics Research Center, 1968. — P. 129—139.

39. *Li, X.* Collisionless periodic orbits in the free-fall three-body problem [Text] / X. Li, S. Liao // New Astron. — 2019. — July. — Vol. 70. — P. 22—26. — arXiv: 1805.07980 [nlin.CD].

40. *Marchal, C.* On the final evolution of the n-body problem [Text] / C. Marchal, D. Saari // Journal of Differential Equations. — 1976. — Vol. 20. — P. 150—186.

41. *Marchal, C.* Hill Regions for the General Three-Body Problem [Text] / C. Marchal, D. G. Saari // Celestial Mechanics. — 1975. — Sept. — Vol. 12, no. 2. — P. 115—129.

42. *Mikkola, S.* A numerical investigation of the one-dimensional newtonian three-body problem [Text] / S. Mikkola, J. Hietarinta // Celestial Mechanics and Dynamical Astronomy. — 1989. — Vol. 46, no. 1. — P. 1—18.

43. *Mikkola, S.* Algorithmic regularization of the few-body problem [Text] / S. Mikkola, K. Tanikawa // MNRAS. — 1999. — Dec. — Vol. 310, no. 3. — P. 745—749.

44. *Moeckel, R.* A topological existence proof for the Schubart orbits in the collinear three-body problem [Text] / R. Moeckel // Discrete and Continuous Dynamical Systems. Series B. — 2008. — Oct. — Vol. 10. — P. 609.

45. *Moeckel, R.* Symmetric regularization, reduction and blow-up of the planar three-body problem [Text] / R. Moeckel, R. Montgomery // Pacific Journal of Mathematics. — 2013. — Mar. — Vol. 262. — P. 129.

46. *Montgomery, R.* Infinitely many syzygies [Text] / R. Montgomery // Archive for Rational Mechanics and Analysis. — 2002. — Apr. — Vol. 162, no. 4. — P. 311—330.

47. *Montgomery, R.* The Three-Body Problem and the Shape Sphere [Text] / R. Montgomery // The American Mathematical Monthly. — 2015. — Vol. 122, no. 4. — pp. 299—321. — URL: https://www.jstor.org/stable/10.4169/amer.math.monthly.122.04.299 (visited on 10/13/2023).

48. *Moore, C.* Braids in classical dynamics [Text] / C. Moore // Phys. Rev. Lett. — 1993. — Jan. — Vol. 70, issue 24. — P. 3675—3679.

49. *Nauenberg, M.* Periodic orbits for three particles with finite angular momentum [Text] / M. Nauenberg // Physics Letters A. — 2001. — Dec. — Vol. 292, no. 1/2. — P. 93—99. — arXiv: nlin/0112003 [nlin.CD].

50. *Orlov, V. V.* Periodic orbits in the free-fall three-body problem [Text] / V. V. Orlov, V. A. Titov, L. A. Shombina // Astronomy Reports. — 2016. — Vol. 60, no. 12. — P. 1083—1089.

51. *Palais, R. S.* The principle of symmetric criticality [Text] / R. S. Palais // Communications in Mathematical Physics. — 1979. — Oct. — Vol. 69, no. 1. — P. 19—30.

52. Periodic Solutions about the Collinear Lagrangian Solution in the General Problem of Three Bodies [Text] / R. Broucke [et al.] // Celestial Mechanics. — 1981. — May. — Vol. 24, no. 1. — P. 63—82.

53. *Poincaré, H.* Sur les solutions périodiques et le principe de moindre action [Text] / H. Poincaré // Compte Rundu Math. Acad. Sci. Paris. — 1896. — Vol. 123. — P. 915—918.

54. *Prada, I.* The Planar Three-Body Problem, Symmetries and Periodic Orbits [Text] / I. Prada, L. Jimenez-Lara // Qualitative Theory of Dynamical Systems. — 2009. — Vol. 8. — P. 419—442.

55. *Saari, D. G.* A Visit to the Newtonian N-Body Problem via Elementary Complex Variables [Text] / D. G. Saari // The American Mathematical Monthly. — 1990. — Vol. 97, no. 2. — P. 105—119. — URL: http://www.jstor.org/stable/2323910 (visited on 08/04/2023).

56. *Saari, D. G.* Expanding Gravitational Systems [Text] / D. G. Saari // Transactions of the American Mathematical Society. — 1971. — Vol. 156. — P. 219—240. — URL: http://www.jstor.org/stable/1995609 (visited on 10/20/2023).

57. *Saari, D. G.* From Rotations and Inclinations to Zero Configurational Velocity Surfaces [Text] / D. G. Saari // Celestial Mechanics. — 1984. — Vol. 33.

58. *Saito, M. M.* Collinear three body problem with non-equal masses by symbol dynamics [Text] / M. M. Saito, K. Tanikawa // Over the resonance, 35th Symposium on Celestial Mechanics / ed. by E. Kokubo, H. Arakida, T. Yamamoto. — 01/2003. — P. 324—331.

59. *Saito, M. M.* Structure change of the Poincaré section due to the mass change in the rectilinear three-body problem [Text] / M. M. Saito, K. Tanikawa // A fool in space. Proceedings of the 36th Symposium on Celestial Mechanics / ed. by K. Tanikawa [et al.]. — 01/2004. — P. 68—74.

60. *Saito, M. M.* The rectilinear three-body problem using symbol sequence I. Role of triple collision [Text] / M. M. Saito, K. Tanikawa // Celestial Mechanics and Dynamical Astronomy. — 2007. — Vol. 98, no. 2. — P. 95—120.

61. *Schubart, J.* Numerische Aufscuchung periodischer Lösungen im Dreikörperproblem [Text] / J. Schubart // Astronomische Nachrichten. — 1956. — Vol. 283, no. 1. — P. 17—22.

62. *Schubart, J.* Orbits of real and fictitious asteroids studied by integration [Text] / J. Schubart // Astron. Astrophys. Suppl. Ser. — 1994. — Vol. 104. — P. 391—399.

63. *Simó, C.* New Families of Solutions in N-Body Problems [Text] / C. Simó // European Congress of Mathematics / ed. by C. Casacuberta [et al.]. — Basel : Birkhäuser Basel, 2001. — P. 01—115.

64. *Simó, C.* Periodic orbits of the planar N-body problem with equal masses and all bodies on the same path [Text] / C. Simó // The Restless Universe / ed. by B. A. Steves, A. J. Maciejewski. — 01/2001. — P. 265—284.

65. *Simó, C.* Dynamical properties of the figure eight solution of the three-body problem [Text] / C. Simó // Contemp. Math. — 2002. — Jan. — Vol. 1. — P. 209.

66. *Simó, C.* Qualitative study of the planar isosceles three-body problem [Text] / C. Simó, R. Martinez // Celestial Mechanics. — 1987. — Mar. — Vol. 41. — P. 179—251.

67. *Sundman, K.* Recherches sur le probleme de trois corps [Text] / K. Sundman // Acta Societatis Scientiarum Fennicae. — 1907. — Vol. 34, no. 6.

68. *Sundman, K.* Nouvelles recherches sur le probleme de trois corps [Text] / K. Sundman // Acta Societatis Scientiarum Fennicae. — 1909. — Vol. 35, no. 9.

69. *Sundman, K.* Mémoire sur le problème de trois corps [Text] / K. Sundman // Acta Mathematica. — 1912. — Vol. 36. — P. 105—179.

70. *Šuvakov, M.* Numerical search for periodic solutions in the vicinity of the figure-eight orbit: slaloming around singularities on the shape sphere [Text] / M. Šuvakov // Celestial Mechanics and Dynamical Astronomy. — 2014. — Aug. — Vol. 119, no. 3/4. — P. 369—377. — arXiv: 1312.7002 [physics.class-ph].

71. *Šuvakov, M.* Approximate action-angle variables for the figure-eight and periodic three-body orbits [Text] / M. Šuvakov, V. Dmitrašinović // Phys. Rev. E. — 2011. — May. — Vol. 83, no. 5. — P. 056603. — arXiv: 1106.3413 [math-ph].

72. *Šuvakov, M.* Three Classes of Newtonian Three-Body Planar Periodic Orbits [Text] / M. Šuvakov, V. Dmitrašinović // Phys. Review Letter. — 2013. — Mar. — Vol. 110, no. 11. — P. 114301. — arXiv: 1303.0181 [physics.class-ph].

73. *Šuvakov, M.* A guide to hunting periodic three-body orbits [Text] / M. Šuvakov, V. Dmitrašinović // American Journal of Physics. — 2014. — June. — Vol. 82, no. 6. — P. 609—619.

74. *Szebeheli, V.* Complete Solution of a General Problem of Three Bodies [Text] / V. Szebeheli, P. C. Frederick // Astronomical Journal. — 1967. — Vol. 72, no. 7. — P. 876—883.

75. The Broucke–Hénon orbit and the Schubart orbit in the planar three-body problem with two equal masses [Text] / W. Kuang, T. Ouyang, Z. Xie, D. Yan // Nonlinearity. — 2019. — Vol. 32, no. 12. — P. 4639.

76. The orbits and masses of satellites of Pluto [Text] / M. Brozović [et al.] // Icarus. — 2015. — Vol. 246, no. 11. — P. 317—329.

77. The rectilinear three-body problem [Text] / V. V. Orlov [et al.] // Celestial Mechanics and Dynamical Astronomy. — 2008. — Feb. — Vol. 100, no. 2. — P. 93—120.

78. *Titov, V.* Three-body problem periodic orbits with vanishing angular momentum [Text] / V. Titov // Astronomische Nachrichten. — 2015. — Vol. 336, no. 3. — P. 271—275.

79. *Titov, V.* Some solutions of the general three body problem in form space [Text] / V. Titov // 8th Polyakhov's Reading. Vol. 1959 / ed. by E. Kustova [et al.]. — United States : American Institute of Physics, 2018.

80. *Titov, V. B.* Groups of transformations of phase trajectories in the two-body problem. [Text] / V. B. Titov // Astronomiya i geodeziya. — 1985. — Vol. 13. — P. 11—21.

81. *Titov, V. B.* Isoenergetic transformations in the two-body problem [Text] / V. B. Titov // Leningradskii Universitet Vestnik Matematika Mekhanika Astronomiia. — 1986. — P. 116—118.

82. *Titov, V. B.* On a geometric method for determining an unperturbed orbit from observations using group transformations [Text] / V. B. Titov // Kinematics and physics of celestial bodies. — 1987. — Vol. 3, no. 4. — P. 26—29.

83. *Titov, V.* Symmetrical periodic orbits in the three body problem - the variational approach [Text] / V. Titov // Few-Body Problem: Theory and Computer Simulations. — University of Turku, Finland, 2006. — P. 9.

84. *Titov, V.* Some properties of Lemaitre regularization. II isosceles trajectories and figure-eight [Text] / V. Titov // Astronomische Nachrichten. — 2022. — Vol. 343, no. 3. — e14006.

85. *Titov, V. B.* Some properties of Lemaitre regularization: Collinear trajectories [Text] / V. B. Titov // Astronomische Nachrichten. — 2021. — Mar. — Vol. 342, no. 3. — P. 588—597.

86. *Vanderbei, R.* Linear Programming: Foundations and Extensions [Text] / R. Vanderbei // Journal of the Operational Research Society. — 1998. — Mar. — Vol. 49. — P. 93—98.

87. *Vanderbei, R.* New Orbits for the n-Body Problem [Text] / R. Vanderbei // Annals of the New York Academy of Sciences. — 2004. — May. — Vol. 1017, no. 1. — P. 422—433.

88. *Vashkovjak, M. A.* On the stability of circular asteroid orbits in an N-planetary system [Text] / M. A. Vashkovjak // Celestial Mechanics. — 1976. — Vol. 13. — P. 313—324.

89. *Antonov, V. A.* Elements of the theory of gravitational potential and some cases of its explicit expression [Текст] / V. A. Antonov, I. I. Nikiforov, K. V. Kholshevnikov. — SPb : SPbGU, 2008. — 227 с.

90. *Arnold, V. I.* Mathematical aspects of classical and celestial mechanics [Текст] / V. I. Arnold, V. V. Kozlov, A. I. Neistadt // The Results of Science and Technology. The series Modern problems of Mathematics. Fundamental directions. — 1985. — Т. 3. — С. 5—304.

91. *Birkhoff, D.* Dynamical systems [Текст] / D. Birkhoff. — Ijevsk : Publ.: “Udmurt University”, 1999. — 408 с.

92. *Vashkovyak, M. A.* A method for calculating secular perturbations of asteroid orbits [Текст] / M. A. Vashkovyak // Space researches. — 1986. — Т. 24, № 4. — С. 513—526.

93. *Golubev, V. G.* On some estimates in the unbounded three-body problem in the case when the motion of one of the pairs of bodies is absolutely stable according to Hill [Текст] / V. G. Golubev // Reports of the USSR Academy of Sciences. — 1978. — Т. 240, № 4. — С. 798—801.

94. *Golubev, V. G.* The three body problem in celestial mechanics [Текст] / V. G. Golubev, E. A. Grebenikov. — М. : Publ. MGU, 1985. — 240 с.

95. *Lukyanov, L. G.* The analogue of zero-velocity surfaces in bounded elliptical, parabolic and hyperbolic three-body problems [Текст] / L. G. Lukyanov // Letters to AJ. — 2010. — Т. 36, № 11. — С. 869—880.

96. *Lukyanov, L. G.* Lections on celestial mechanics [Текст] / L. G. Lukyanov, G. I. Shirmin. — Almaaty, 2009. — 227 с.

97. *Marchal, K.* Three body problem [Текст] / K. Marchal. — М.–Ijevsk : Institute of computer researces, 2004. — 640 с.

98. A Problem Found in the Position Shift Norm of a Celestial Body in Dynamical Astronomy [Текст] / K. V. Kholshevnikov [и др.] // Astronomy Reports. — 2020. — Т. 64, № 4. — С. 369—373.

99. *Pars, L. A.* Analytical dynamics [Текст] / L. A. Pars. — Moscow : Nauka, 1971. — 636 с.

100. *Saari, D.* Collisions, rings , and other Newtonian N-body problems [Текст] / D. Saari. — М.-Ijevsk : Institute of computer researches, 2009. — 280 с.

101. *Szebehely, V.* Orbit theory: A restricted three-body problem [Текст] / V. Szebehely. — М. : Nauka, 1982. — 656 с.

102. *Subbotin, M. F.* Introduction to Theoretical Astronomy [Текст] / M. F. Subbotin. — М. : Nauka, 1968. — 800 с.

103. *Titov, V. B.* Periodic orbits of general three body problem with zero angular moment [Text] / V. B. Titov // Russian Journal of Nonlinear Dynamics. — 2012. — Vol. 8, no. 2. — P. 377—389.

104. *Titov, V.* The regions of possible motion in the general three bodies problem [Text] / V. Titov // Zap. nauchn. sem. POMI. — 2022. — Vol. 517. — P. 225—249.

105. *Titov, V.* Zero-Velocity Surface in the General Three-Body-Problem [Text] / V. Titov // Vestnik St. Petersburg University, Mathematics. — 2023. — Vol. 56, no. 1. — P. 125—133.

106. *Thai, V.* Investigation of the planar unrestricted three-body problem [Текст] / V. Thai // Applied Mathematics and Mechanics. — 1996. — Т. 60, № 3. — С. 355—374.

107. Deflecting an Asteroid with a Low-Thrust Tangential Engine to the Orbit [Текст] / K. V. Kholshevnikov [и др.] // Astronomy Reports. — 2020. — Т. 64, № 9. — С. 785—794.

108. *Wintner, A.* Analytical foundations of celestial mechanics [Текст] / A. Wintner. — M. : Nauka, 1967. — 524 с.

109. *Kholshevnikov, K. V.* Minimal Velocity Surface in a Restricted Circular Three-Body Problem [Текст] / K. V. Kholshevnikov, V. B. Titov // Vestnik St. Petersburg University, Mathematics. — 2020. — Т. 53, № 4. — С. 473—479.

110. *Chenciner, A.* Four lections on N body problem [Текст] / A. Chenciner // Pollard G. Mathematical introduction in celestial mechanics. — M.–Ijevsk : Institute of computer researches, 2012. — С. 146—187.

Appendix A

Models for optimization with the language AMPL

Listing A.1 `Eight.mod` of model for searching the solution “figure-eight”.

Listing A.1 Eight.mod

```
# Models for searching solution figure-eight

param N;  # Nuber of masses
param n;  # Number of terms in Fourier series
param m;  # Number of nodes for integral calculation

param pi := 4*atan(1); # Just \pi;

set Bodies := {1..N};
param masses {i in Bodies}; # The values of masses

set Times := {0..m-1} circular;

set C3X := {1..n} diff {3..n by 3};
set C3Y := {1..n} diff {3..n by 3};

# The moments of time for coordinate calculations
# differ from each other by 2\pi/3
param theta {i in Bodies, t in Times} :=
      if (i = 1) then t*2*pi/m            # body 1
      else
        if (i = 2) then t*2*pi/m + 2*pi/3 # body 2
           else
             t*2*pi/m + 4*pi/3;           # body 3
param dt := 2*pi/m;  # Step value for integral calculation

var as {k in C3X}; # Coefficients of Fourier seties terms (by sine) for x
var bs {k in C3Y}; # Coefficients of Fourier series terms (by cosine for y

# Coordinates and velocity
```

```
var x {i in Bodies, t in Times} =
     sum{k in C3X} as[k]*sin(k*theta[i,t]);
var y {i in Bodies, t in Times} =
     sum{k in C3Y} bs[k]*sin(k*theta[i,t]);

var xdot {i in Bodies, t in Times} =
   sum {k in CX3} as[k]*k*cos(k*theta[i,t]);
var ydot {i in Bodies, t in Times} =
   sum {k in CY3} bs[k]*k*cos(k*theta[i,t]);

# Kinetic energi for t_i=2(i-1)\pi/m
var K {t in Times} = 0.5*sum {i in Bodies}
                    masses[i]*(xdot[i,t]^2 + ydot[i,t]^2);

# Potential energy for t_i=2(i-1)\pi/m
var P {t in Times}
 = - sum {i in Bodies, ii in Bodies: ii>i }
  masses[i]*masses[ii]/sqrt((x[i,t]-x[ii,t])^2+(y[i,t]-y[ii,t])^2);

# Goal function: integral K-P
minimize A: sum {t in Times} (K[t] - P[t])*dt;
# Constraints: at initial moment the bodies are located on x-axis
subject to inity1 : y[1,0] = 0;
subject to inity2 : y[2,0] = 0;
```

Listing A.2 `2-1.mod` of model for searching 2-1 choreograpfies.

Listing A.2 2-1.mod

```
# Model for searching solution with 2-1 choreography

param N;  # Nuber of masses
param n;  # Number of terms in Fourier series
param m;  # Number of nodes for integral calculation

param pi := 4*atan(1); # Just the value of \pi;
param masses {i in Bodies}; # Masses
param omega;

set Bodies := {1..N};
set Bodies_minus_1 := {1..N-1};
```

```
set Times := {0..m-1} circular;

# time moments for body 1 and 2 coordinates calculations
# differ from each other by \pi
param theta {i in Bodies, t in Times} :=
                      t*2*pi/m + (if i == 2 then pi else 0);
param dt := 2*pi/m; # Step value for integral calculation

var a0; # Free term of Fourier series for x
var ac {k in 1..n}; # Coefficients Fourier (by cosine) for x
var as {k in 1..n}; # Coefficients Fourier (by sine) for x
var b0; # Free term of Fourier series for y
var bc {k in 1..n}; # Coefficients Fourier (by cosine) for y
var bs {k in 1..n}; # Coefficients Fourier (by sine) for y

# Coordinates and velosity
# in rotating plane
var xrot {i in Bodies, t in Times} =
  if (i in Bodies_minus_1) then
     a0+sum{k in 1..n} (ac[k]*cos(k*theta[i,t]) + as[k]*sin(k*theta[i,t]))
  else
   -(sum{j in Bodies_minus_1} (masses[j]*xrot[j,t]))/masses[N];
var yrot {i in Bodies, t in Times} =
  if (i in Bodies_minus_1) then
     b0+sum{k in 1..n} (bc[k]*cos(k*theta[i,t]) + bs[k]*sin(k*theta[i,t]))
  else
   -(sum{j in Bodies_minus_1} (masses[j]*yrot[j,t]))/masses[N];

# Coordinates and velosity
# in inertial system
var x {i in Bodies, t in Times} = xrot[i,t]*cos(omega*theta[1,t])
                                        - yrot[i,t]*sin(omega*theta[1,t]);
var y {i in Bodies, t in Times} = xrot[i,t]*sin(omega*theta[1,t])
                                        + yrot[i,t]*cos(omega*theta[1,t]);

var xrotdot {i in Bodies, t in Times} =
  if (i in Bodies_minus_1) then
  sum {k in 1..n} (-ac[k]*k*sin(k*theta[i,t]) + as[k]*k*cos(k*theta[i,t]))
  else
```

```
   -(sum{j in Bodies_minus_1} (masses[j]*xrotdot[j,t]))/masses[N];
var yrotdot {i in Bodies, t in Times} =
  if (i in Bodies_minus_1) then
  sum {k in 1..n} (-bc[k]*k*sin(k*theta[i,t]) + bs[k]*k*cos(k*theta[i,t]))
  else
   -(sum{j in Bodies_minus_1} (masses[j]*yrotdot[j,t]))/masses[N];

var xdot {i in Bodies, t in Times} = xrotdot[i,t]*cos(omega*theta[1,t])
                                   - yrotdot[i,t]*sin(omega*theta[1,t])
                                   - omega * y[i,t];
var ydot {i in Bodies, t in Times} = xrotdot[i,t]*sin(omega*theta[1,t])
                                   + yrotdot[i,t]*cos(omega*theta[1,t])
                                   + omega * x[i,t];

# Kinetic energy at t_i=2(i-1)\pi/m
var K {t in Times} = 0.5*sum {i in Bodies}
                              masses[i]*(xdot[i,t]^2 + ydot[i,t]^2);
# Force function
var P {t in Times}
 = - sum {i in Bodies, ii in Bodies: ii>i }
      if ((x[i,t]-x[ii,t])^2+(y[i,t]-y[ii,t])^2 <= 0.01 ) then 1000
      else
      masses[i]*masses[ii]/sqrt((x[i,t]-x[ii,t])^2+(y[i,t]-y[ii,t])^2);

minimize A: sum {t in Times} (K[t] - P[t])*dt;
# Constraints: in initial moment all bodies are on x-axis
subject to inity1: y[1,0] = 0;
subject to inity2: y[2,0] = 0;
```

Listing A.3 `ISO.mod` of model for searching the orbits with isosceles symmetry.

Listing A.3 ISO.mod

```
# Construct the model

param N;  # Nuber of masses
param n;  # Number of terms in Fourier series
param m;  # Number of nodes for integral calculation

param pi := 4*atan(1); # Just the \pi value;
#param mh : m/2;
```

```
set Bodies := {1..N};
set Bodies_minus_1 := {1..N-1};

set Times := {0..m} circular;

set HarmX := {1..n};
set HarmY := {1..n};

param masses {i in Bodies}; # Massses

param dt := 2*pi/m;
param theta {t in Times} := t*dt;

var b0;

var ac {k in HarmX};
var as {k in HarmX};
var bc {k in HarmY};
var bs {k in HarmY};

var x {i in Bodies, t in Times} =
  if (i in Bodies_minus_1) then
     if (i == 1) then
       sum{k in HarmX} (ac[k]*cos(k*theta[t]) + as[k]*sin(k*theta[t]))
     else
       sum{k in HarmX} (ac[k]*cos(k*theta[t]) - as[k]*sin(k*theta[t]))
  else
   -(sum{j in Bodies_minus_1} (masses[j]*x[j,t]))/masses[N];
var y {i in Bodies, t in Times} =
  if (i in Bodies_minus_1) then
   if (i == 1) then
      b0+sum{k in HarmY} (bc[k]*cos(k*theta[t]) + bs[k]*sin(k*theta[t]))
     else
      -b0-sum{k in HarmY} (bc[k]*cos(k*theta[t]) - bs[k]*sin(k*theta[t]))
  else
   -(sum{j in Bodies_minus_1} (masses[j]*y[j,t]))/masses[N];

var xdot {i in Bodies, t in Times} =
```

```
  if (i in Bodies_minus_1) then
     if (i == 1) then
        sum{k in HarmX} (-ac[k]*k*sin(k*theta[t])+as[k]*k*cos(k*theta[t]))
     else
        -sum{k in HarmX} (ac[k]*k*sin(k*theta[t])+as[k]*k*cos(k*theta[t]))
  else
   -(sum{j in Bodies_minus_1} (masses[j]*xdot[j,t]))/masses[N];

var ydot {i in Bodies, t in Times} =
  if (i in Bodies_minus_1) then
     if (i == 1) then
       sum{k in HarmY} (-bc[k]*k*sin(k*theta[t])+bs[k]*k*cos(k*theta[t]))
     else
       sum{k in HarmY} (bc[k]*k*sin(k*theta[t])+bs[k]*k*cos(k*theta[t]))
  else
   -(sum{j in Bodies_minus_1} (masses[j]*ydot[j,t]))/masses[N];

var K {t in Times} = 0.5*sum {i in Bodies}
                   masses[i]*(xdot[i,t]^2 + ydot[i,t]^2);

var P {t in Times}
 = - sum {i in Bodies_minus_1, ii in Bodies: ii>i }
      if ((x[i,t]-x[ii,t])^2+(y[i,t]-y[ii,t])^2 <= 0.00000001 ) then
        1000000
      else
      masses[i]*masses[ii]/sqrt((x[i,t]-x[ii,t])^2+(y[i,t]-y[ii,t])^2);

minimize A: sum {t in Times} (K[t] - P[t])*dt;
subject to y3init:  y[3,0] = 0.0;
subject to y3hinit: y[3,mh] = 0.0;
```

Listing A.4 `Line.mod` of model for searching the orbits with line symmetry.

Listing A.4 Line.mod

```
# Construct the model

param N; # Nuber of masses
param n; # Number of terms in Fourier series
param m; # Number of nodes for integral calculation
```

```
param pi := 4*atan(1); # Just the \pi;
param omega;

set Bodies := {1..N};
set Bodies_minus_1 := {1..N-1};
set Times := {0..m-1} circular;

param masses {i in Bodies}; # Masses

param theta {i in Bodies, t in Times} := t*2*pi/m;
param dt := 2*pi/m;

var a0 {i in Bodies};

var ac {i in Bodies_minus_1, k in 1..n};
var bs {i in Bodies_minus_1, k in 1..n};

var xrot {i in Bodies, t in Times} =
  if (i in Bodies_minus_1) then
     a0[i]+sum{k in 1..n} (ac[i,k]*cos(k*theta[i,t]))
  else
   -(sum{j in Bodies_minus_1} masses[j]*(xrot[j,t]))/masses[N];
var yrot {i in Bodies, t in Times} =
  if (i in Bodies_minus_1) then
     sum{k in 1..n} ( bs[i,k]*sin(k*theta[i,t]))
  else
   -(sum{j in Bodies_minus_1} masses[j]*(yrot[j,t]))/masses[N];

var x {i in Bodies, t in Times} = xrot[i,t]*cos(omega*theta[i,t])
                                        - yrot[i,t]*sin(omega*theta[i,t]);
var y {i in Bodies, t in Times} = xrot[i,t]*sin(omega*theta[i,t])
                                        + yrot[i,t]*cos(omega*theta[i,t]);

var xrotdot {i in Bodies, t in Times} =
  if (i in Bodies_minus_1) then
   sum {k in 1..n} (-ac[i,k]*k*sin(k*theta[i,t]))
  else
   -(sum{j in Bodies_minus_1} masses[j]*(xrotdot[j,t]))/masses[N];

```

```
var yrotdot {i in Bodies, t in Times} =
  if (i in Bodies_minus_1) then
   sum {k in 1..n} (  bs[i,k]*k*cos(k*theta[i,t]))
  else
   -(sum{j in Bodies_minus_1} masses[j]*(yrotdot[j,t]))/masses[N];

var xdot {i in Bodies, t in Times} = xrotdot[i,t]*cos(omega*theta[i,t])
                                        - yrotdot[i,t]*sin(omega*theta[i,t
   ])
                                        - omega * y[i,t];
var ydot {i in Bodies, t in Times} = xrotdot[i,t]*sin(omega*theta[i,t])
                                        + yrotdot[i,t]*cos(omega*theta[i,t
   ])
                                        + omega * x[i,t];

var K {t in Times} = 0.5*sum {i in Bodies} masses[i]*(xdot[i,t]^2 + ydot[i,t
   ]^2);

var P {t in Times}
 = - sum {i in Bodies, ii in Bodies: ii>i }
      if ((x[i,t]-x[ii,t])^2+(y[i,t]-y[ii,t])^2 <= 0.01 ) then
        1000
      else
      masses[i]*masses[ii]/sqrt((x[i,t]-x[ii,t])^2+(y[i,t]-y[ii,t])^2);

minimize A: sum {t in Times} (K[t] - P[t])*dt;
subject to inity0 {i in Bodies} : y[i,0] = 0;
```

Appendix B

Periodic trajectories of the chapter 2

Coordinates are given in a rotating coordinate system, to obtain an orbit in a barycentric system, you just need to rotate them by an angle $\omega\ t$, the initial data is given in a barycentric coordinate system, they can be directly used as initial conditions for numerical integration.

B.1 Figure-eight ($\omega = 0$)

The masses are equal to each other: $m_1 = m_2 = m_3 = 1$.

Solution:

$$\begin{aligned}
x_1(t) &= 1.0958785\sin t - 0.0252775\sin 5t - 0.0058497\sin 7t \\
&\quad +0.0004212\sin 11t + 0.0001224\sin 13t - 0.0000114\sin 17t \\
&\quad -0.0000036\sin 19t + 0.0000004\sin 23t, \\
y_1(t) &= 0.3372826\sin 2t + 0.0557118\sin 4t - 0.0029908\sin 8t \\
&\quad -0.0008022\sin 10t + 0.0000676\sin 14t + 0.0000206\sin 16t \\
&\quad -0.0000021\sin 20t - 0.0000007\sin 22t. \\
x_2(t) &= x_2(t + 2\pi/3) \\
y_2(t) &= y_2(t + 2\pi/3) \\
x_3(t) &= x_3(t + 4\pi/3) \\
y_3(t) &= y_3(t + 4\pi/3)
\end{aligned} \tag{B.1}$$

The value of the action functional (A), the constant energy (E) and the constant of angular momentum (J):

$$A = 24.37193, \quad E = -1.29297, \quad J = 0$$

B.2 Choreographies 2-1

Here are all the solutions-choreographies 2-1, listed in the table. 2.

All orbits, except the last three, were calculated with masses $m_1 = m_2 = 0.95$, $m_3 = 1.1$, Coordinates in the main system are given for the first body, the second body moves along the same orbit with a lag (π), coordinates of the third body are determined from the condition $m_1\mathbf{r}_1 + m_2\mathbf{r}_2 + m_3\mathbf{r}_3 = 0$

1. $A = 10.61083$, angular velocity of rotation of the base system: $\omega = 1/5$ (fig. 2.7l)

$$
\begin{aligned}
x_1(t) &= 1.5565760 \\
&\quad +0.7065140\cos(t) + 0.0008633\cos(2t) + 0.0010532\cos(3t) \\
&\quad +0.0000084\cos(4t) + 0.0000077\cos(5t) + 0.0000001\cos(6t) \\
&\quad +0.0000001\cos(7t) \\
y_1(t) &= -0.7254535\sin(t) + 0.0004847\sin(2t) - 0.0011753\sin(3t) \\
&\quad +0.0000064\sin(4t) - 0.0000096\sin(5t) + 0.0000001\sin(6t) \\
&\quad -0.0000001\sin(7t), \\
x_2(t) &= x_1(t+\pi), \\
y_2(t) &= y_1(t+\pi), \\
0 &= m_1x_1(t) + m_2x_2(t) + m_3x_3(t) \quad , \\
0 &= m_1y_1(t) + m_2y_2(t) + m_3y_3(t) \quad .
\end{aligned}
$$

$$E = -0.562922, \quad J = 1.73204 \quad .$$

Initial conditions:

$$
\begin{pmatrix} x_1 \\ y_1 \\ \dot{x}_1 \\ \dot{y}_1 \end{pmatrix} = \begin{pmatrix} 2.2650228 \\ 0 \\ 0 \\ -0.2750278 \end{pmatrix} \quad \begin{pmatrix} x_2 \\ y_2 \\ \dot{x}_2 \\ \dot{y}_2 \end{pmatrix} = \begin{pmatrix} 0.8498728 \\ 0 \\ 0 \\ 0.8999983 \end{pmatrix} \quad \begin{pmatrix} x_3 \\ y_3 \\ \dot{x}_3 \\ \dot{y}_3 \end{pmatrix} = \begin{pmatrix} -2.6901372 \\ 0 \\ 0 \\ -0.5397473 \end{pmatrix}
$$

2. $A = 11.87886$, $\omega = 1/3$ (fig. 2.8l)

$$\begin{aligned}
x_1(t) &= 1.1158617 \\
&+0.7759119\cos(t) + 0.0037554\cos(2t) + 0.0018298\cos(3t) \\
&+0.0000866\cos(4t) + 0.0000256\cos(5t) + 0.0000033\cos(6t) \\
&+0.0000005\cos(7t) + 0.0000002\cos(8t) \\
y_1(t) &= -0.8251039\sin(t) + 0.0018789\sin(2t) - 0.0026518\sin(3t) \\
&+0.0000651\sin(4t) - 0.0000546\sin(5t) + 0.0000028\sin(6t) \\
&-0.0000018\sin(7t) + 0.0000001\sin(8t).
\end{aligned}$$

$$E = -0.630193, \quad J = 1.34061 \qquad .$$

Initial conditions:

$$\begin{pmatrix} x_1 \\ y_1 \\ \dot{x}_1 \\ \dot{y}_1 \end{pmatrix} = \begin{pmatrix} 1.8974750 \\ 0 \\ 0 \\ -0.1968177 \end{pmatrix} \quad \begin{pmatrix} x_2 \\ y_2 \\ \dot{x}_2 \\ \dot{y}_2 \end{pmatrix} = \begin{pmatrix} 0.3419393 \\ 0 \\ 0 \\ 0.9513610 \end{pmatrix} \quad \begin{pmatrix} x_3 \\ y_3 \\ \dot{x}_3 \\ \dot{y}_3 \end{pmatrix} = \begin{pmatrix} -1.9340397 \\ 0 \\ 0 \\ -0.6516511 \end{pmatrix}$$

3. $A = 12.41405$, $\omega = 2/5$ (fig. 2.6l)

$$\begin{aligned}
x_1(t) &= 0.9925978 \\
&-0.8163328\cos(t) + 0.0064762\cos(2t) - 0.0018448\cos(3t) \\
&+0.0002080\cos(4t) - 0.0000225\cos(5t) + 0.0000112\cos(6t) \\
&+0.0000001\cos(7t) + 0.0000007\cos(8t) + 0.0000001\cos(9t), \\
y_1(t) &= 0.8851767\sin(t) + 0.0030578\sin(2t) + 0.0035224\sin(3t) \\
&+0.0001561\sin(4t) + 0.0001051\sin(5t) + 0.0000093\sin(6t) \\
&+0.0000051\sin(7t) + 0.0000006\sin(8t) + 0.0000003\sin(9t).
\end{aligned}$$

$$E = -0.658586, \quad J = 1.22042 \qquad .$$

Initial conditions:

$$\begin{pmatrix} x_1 \\ y_1 \\ \dot{x}_1 \\ \dot{y}_1 \end{pmatrix} = \begin{pmatrix} 0.1810941 \\ 0 \\ 0 \\ 0.9755469 \end{pmatrix} \quad \begin{pmatrix} x_2 \\ y_2 \\ \dot{x}_2 \\ \dot{y}_2 \end{pmatrix} = \begin{pmatrix} 1.8174939 \\ 0 \\ 0 \\ -0.1625086 \end{pmatrix} \quad \begin{pmatrix} x_3 \\ y_3 \\ \dot{x}_3 \\ \dot{y}_3 \end{pmatrix} = \begin{pmatrix} -1.7260533 \\ 0 \\ 0 \\ -0.7021694 \end{pmatrix}$$

4. $A = 12.43822$, $\omega = 1/5$ (fig. 2.7r)

$$\begin{aligned}
x_1(t) &= 1.5519058 \\
&\quad +0.5347713\cos(t) + 0.0006602\cos(2t) + 0.0024871\cos(3t) \\
&\quad +0.0000045\cos(4t) + 0.0000291\cos(5t) + 0.0000005\cos(7t), \\
y_1(t) &= 0.5602807\sin(t) - 0.0005190\sin(2t) + 0.0025517\sin(3t) \\
&\quad -0.0000037\sin(4t) + 0.0002981\sin(5t) + 0.0000005\sin(7t).
\end{aligned}$$

$$E = -0.659868, \quad J = 3.17929 \qquad .$$

Initial conditions:

$$\begin{pmatrix} x_1 \\ y_1 \\ \dot{x}_1 \\ \dot{y}_1 \end{pmatrix} = \begin{pmatrix} 2.0898586 \\ 0 \\ 0 \\ 0.9850069 \end{pmatrix} \quad \begin{pmatrix} x_2 \\ y_2 \\ \dot{x}_2 \\ \dot{y}_2 \end{pmatrix} = \begin{pmatrix} 1.0152828 \\ 0 \\ 0 \\ -0.3660844 \end{pmatrix} \quad \begin{pmatrix} x_3 \\ y_3 \\ \dot{x}_3 \\ \dot{y}_3 \end{pmatrix} = \begin{pmatrix} -2.6817130 \\ 0 \\ 0 \\ -0.5345240 \end{pmatrix}$$

5. $A = 13.13826$, $\omega = 1/2$ (fig. 2.4l)

$$\begin{aligned}
x_1(t) &= 0.8613454 \\
&\quad -0.8866020\cos(t) + 0.0128924\cos(2t) - 0.0009447\cos(3t) \\
&\quad +0.0006383\cos(4t) + 0.0000584\cos(5t) + 0.0000527\cos(6t) \\
&\quad +0.0000095\cos(7t) + 0.0000052\cos(8t) + 0.0000012\cos(9t) \\
&\quad +0.0000006\cos(10t) + 0.0000002\cos(11t), \\
y_1(t) &= 0.9901696\sin(t) - 0.0055727\sin(2t) + 0.0051002\sin(3t) \\
&\quad +0.0004791\sin(4t) + 0.0002584\sin(5t) + 0.0000443\sin(6t) \\
&\quad +0.0000208\sin(7t) + 0.0000046\sin(8t) + 0.0000020\sin(9t) \\
&\quad +0.0000005\sin(10t) + 0.0000002\sin(11t).
\end{aligned}$$

$$E = -0.697007, \quad J = 1.09433 \qquad .$$

Initial conditions:

$$\begin{pmatrix} x_1 \\ y_1 \\ \dot{x}_1 \\ \dot{y}_1 \end{pmatrix} = \begin{pmatrix} -0.0125428 \\ 0 \\ 0 \\ 1.0140278 \end{pmatrix} \quad \begin{pmatrix} x_2 \\ y_2 \\ \dot{x}_2 \\ \dot{y}_2 \end{pmatrix} = \begin{pmatrix} 1.7624120 \\ 0 \\ 0 \\ -0.1123521 \end{pmatrix} \quad \begin{pmatrix} x_3 \\ y_3 \\ \dot{x}_3 \\ \dot{y}_3 \end{pmatrix} = \begin{pmatrix} -1.5112507 \\ 0 \\ 0 \\ -0.7787200 \end{pmatrix}$$

6. $A = 14.90941$, $\omega = 1/3$ (fig. 2.8m)

$$\begin{aligned}
x_1(t) &= 1.1041275 \\
&\quad +0.4688262\cos(t) + 0.0023857\cos(2t) + 0.0089485\cos(3t) \\
&\quad +0.0000370\cos(4t) + 0.0003487\cos(5t) + 0.0000012\cos(6t) \\
&\quad +0.0000175\cos(7t) + 0.0000010\cos(9t), \\
y_1(t) &= 0.5501636\sin(t) - 0.0020831\sin(2t) + 0.0091862\sin(3t) \\
&\quad -0.0000305\sin(4t) + 0.0003544\sin(5t) - 0.0000010\sin(6t) \\
&\quad +0.0000177\sin(7t) + 0.0000010\sin(9t).
\end{aligned}$$

$$E = -0.790968, \quad J = 2.76171 \qquad .$$

Initial conditions:

$$\begin{pmatrix} x_1 \\ y_1 \\ \dot{x}_1 \\ \dot{y}_1 \end{pmatrix} = \begin{pmatrix} 1.5846935 \\ 0 \\ 0 \\ 1.1035653 \end{pmatrix} \quad \begin{pmatrix} x_2 \\ y_2 \\ \dot{x}_2 \\ \dot{y}_2 \end{pmatrix} = \begin{pmatrix} 0.6284095 \\ 0 \\ 0 \\ -0.3744532 \end{pmatrix} \quad \begin{pmatrix} x_3 \\ y_3 \\ \dot{x}_3 \\ \dot{y}_3 \end{pmatrix} = \begin{pmatrix} -1.9113163 \\ 0 \\ 0 \\ -0.6296877 \end{pmatrix}$$

7. $A = 16.03507$, $\omega = 2/5$ (fig. 2.6r)

$$\begin{aligned}
x_1(t) &= 0.9760527 \\
&\quad +0.4294736\cos(t) + 0.0037296\cos(2t) + 0.0146659\cos(3t) \\
&\quad +0.0000816\cos(4t) + 0.0009135\cos(5t) + 0.0000038\cos(6t) \\
&\quad +0.0000723\cos(7t) + 0.0000002\cos(8t) + 0.0000065\cos(9t) \\
&\quad +0.0000006\cos(11t), \\
y_1(t) &= 0.5557843\sin(t) - 0.0034112\sin(2t) + 0.0149548\sin(3t) \\
&\quad -0.0000681\sin(4t) + 0.0009213\sin(5t) - 0.0000031\sin(6t) \\
&\quad +0.0000727\sin(7t) - 0.0000002\sin(8t) + 0.0000065\sin(9t) \\
&\quad +0.0000006\sin(11t).
\end{aligned}$$

$$E = -0.850687, \quad J = 2.61695 \qquad .$$

Initial conditions:

$$\begin{pmatrix} x_1 \\ y_1 \\ \dot{x}_1 \\ \dot{y}_1 \end{pmatrix} = \begin{pmatrix} 1.4250005 \\ 0 \\ 0 \\ 1.1687159 \end{pmatrix} \quad \begin{pmatrix} x_2 \\ y_2 \\ \dot{x}_2 \\ \dot{y}_2 \end{pmatrix} = \begin{pmatrix} 0.5347356 \\ 0 \\ 0 \\ -0.3990521 \end{pmatrix} \quad \begin{pmatrix} x_3 \\ y_3 \\ \dot{x}_3 \\ \dot{y}_3 \end{pmatrix} = \begin{pmatrix} -1.6924993 \\ 0 \\ 0 \\ -0.6647096 \end{pmatrix}$$

8. $A = 16.57031$, $\omega = 1/3$ (fig. 2.8r)

$$\begin{aligned} x_1(t) &= 0.18354047 \\ &\quad +1.4040182\cos(t) - 0.0784666\cos(2t) + 0.0122495\cos(3t) \\ &\quad -0.0023966\cos(4t) + 0.0005415\cos(5t) - 0.0001285\cos(6t) \\ &\quad +0.0000327\cos(7t) - 0.0000085\cos(8t) + 0.0000023\cos(9t) \\ &\quad -0.0000006\cos(10t) + 0.0000002\cos(11t), \\ y_1(t) &= -1.3893845\sin(t) + 0.0786710\sin(2t) - 0.0120628\sin(3t) \\ &\quad +0.0023984\sin(4t) - 0.0005354\sin(5t) + 0.0001284\sin(6t) \\ &\quad -0.0000324\sin(7t) + 0.0000085\sin(8t) - 0.0000023\sin(9t) \\ &\quad +0.0000006\sin(10t) - 0.0000002\sin(11t). \end{aligned}$$

$$E = -0.879082, \quad J = 2.46683 \qquad .$$

Initial conditions:

$$\begin{pmatrix} x_1 \\ y_1 \\ \dot{x}_1 \\ \dot{y}_1 \end{pmatrix} = \begin{pmatrix} 1.5193840 \\ 0 \\ 0 \\ -0.7542570 \end{pmatrix} \quad \begin{pmatrix} x_2 \\ y_2 \\ \dot{x}_2 \\ \dot{y}_2 \end{pmatrix} = \begin{pmatrix} -1.3143048 \\ 0 \\ 0 \\ 1.1581786 \end{pmatrix} \quad \begin{pmatrix} x_3 \\ y_3 \\ \dot{x}_3 \\ \dot{y}_3 \end{pmatrix} = \begin{pmatrix} -0.1771139 \\ 0 \\ 0 \\ -0.3488413 \end{pmatrix}$$

9. $A = 17.61955$, $\omega = 1/2$ (fig. 2.4r)

$$\begin{aligned}
x_1(t) &= 0.8360497 \\
&\quad +0.3582472\cos(t) + 0.0063098\cos(2t) + 0.0275002\cos(3t) \\
&\quad +0.0002191\cos(4t) + 0.0031197\cos(5t) + 0.0000169\cos(6t) \\
&\quad +0.0004428\cos(7t) + 0.0000018\cos(8t) + 0.0000706\cos(9t) \\
&\quad +0.0000002\cos(10t) + 0.0000121\cos(11t) + 0.0000022\cos(13t) \\
&\quad +0.0000004\cos(15t), \\
y_1(t) &= 0.5793870\sin(t) - 0.0060786\sin(2t) + 0.0274387\sin(3t) \\
&\quad -0.0001875\sin(4t) + 0.0030922\sin(5t) - 0.0000140\sin(6t) \\
&\quad +0.0004389\sin(7t) - 0.0000015\sin(8t) + 0.0000701\sin(9t) \\
&\quad -0.0000002\sin(10t) + 0.0000120\sin(11t) + 0.0000022\sin(13t) \\
&\quad +0.0000004\sin(15t).
\end{aligned}$$

$$E = -0.934746, \quad J = 2.43060 \qquad .$$

Initial conditions:

$$\begin{pmatrix} x_1 \\ y_1 \\ \dot{x}_1 \\ \dot{y}_1 \end{pmatrix} = \begin{pmatrix} 1.2319928 \\ 0 \\ 0 \\ 1.2840272 \end{pmatrix} \quad \begin{pmatrix} x_2 \\ y_2 \\ \dot{x}_2 \\ \dot{y}_2 \end{pmatrix} = \begin{pmatrix} 0.4532024 \\ 0 \\ 0 \\ -0.4674394 \end{pmatrix} \quad \begin{pmatrix} x_3 \\ y_3 \\ \dot{x}_3 \\ \dot{y}_3 \end{pmatrix} = \begin{pmatrix} -1.4553959 \\ 0 \\ 0 \\ -0.7052349 \end{pmatrix}$$

10. $A = 19.78460$, $\omega = 1/3$ (fig. 2.11l)

$$\begin{aligned}
x_1(t) &= 1.1030882 \\
&\quad +0.3202534\cos(3t) + 0.0000811\cos(6t) + 0.0001972\cos(9t) \\
&\quad +0.0000003\cos(12t) + 0.0000005\cos(15t), \\
y_1(t) &= -0.3232173\sin(3t) + 0.0000492\sin(6t) - 0.0002045\sin(9t) \\
&\quad +0.0000002\sin(12t) - 0.0000006\sin(15t).
\end{aligned}$$

$$E = -1.049612, \quad J = 1.57727 \qquad .$$

Initial conditions:

$$\begin{pmatrix} x_1 \\ y_1 \\ \dot{x}_1 \\ \dot{y}_1 \end{pmatrix} = \begin{pmatrix} 1.4236209 \\ 0 \\ 0 \\ -0.4966677 \end{pmatrix} \quad \begin{pmatrix} x_2 \\ y_2 \\ \dot{x}_2 \\ \dot{y}_2 \end{pmatrix} = \begin{pmatrix} 0.7827184 \\ 0 \\ 0 \\ 1.2327027 \end{pmatrix} \quad \begin{pmatrix} x_3 \\ y_3 \\ \dot{x}_3 \\ \dot{y}_3 \end{pmatrix} = \begin{pmatrix} -1.9054749 \\ 0 \\ 0 \\ -0.6356666 \end{pmatrix}$$

11. $A = 21.89957$, $\omega = 1/3$ (fig. 2.11r)

$$\begin{aligned} x_1(t) &= 1.1022720 \\ &\quad +0.2756116\cos(3t) + 0.0000699\cos(6t) + 0.0003117\cos(9t) \\ &\quad +0.0000002\cos(12t) + 0.0000011\cos(15t), \\ y_1(t) &= +0.2791050\sin(3t) - 0.0000511\sin(6t) + 0.0003169\sin(9t) \\ &\quad -0.0000002\sin(12t) + 0.0000011\sin(15t). \end{aligned}$$

$$E = -1.049612, \quad J = 1.57727 \qquad .$$

Initial conditions:

$$\begin{pmatrix} x_1 \\ y_1 \\ \dot{x}_1 \\ \dot{y}_1 \end{pmatrix} = \begin{pmatrix} 1.3782665 \\ 0 \\ 0 \\ 1.2992926 \end{pmatrix} \quad \begin{pmatrix} x_2 \\ y_2 \\ \dot{x}_2 \\ \dot{y}_2 \end{pmatrix} = \begin{pmatrix} 0.8264177 \\ 0 \\ 0 \\ -0.5650222 \end{pmatrix} \quad \begin{pmatrix} x_3 \\ y_3 \\ \dot{x}_3 \\ \dot{y}_3 \end{pmatrix} = \begin{pmatrix} -1.9040455 \\ 0 \\ 0 \\ -0.6541426 \end{pmatrix}$$

12. $A = 25.74992$, $\omega = 1/3$ (fig. 2.10l)

$$\begin{aligned} x_1(t) &= 1.1014946 \\ &\quad +0.2213003\cos(5t) + 0.0000143\cos(10t) + 0.0000560\cos(15t), \\ y_1(t) &= -0.2220820\sin(5t) + 0.0000090\sin(10t) - 0.0000569\sin(15t). \end{aligned}$$

$$E = -1.36608, \quad J = 1.65989.$$

Initial conditions:

$$\begin{pmatrix} x_1 \\ y_1 \\ \dot{x}_1 \\ \dot{y}_1 \end{pmatrix} = \begin{pmatrix} 1.3228653 \\ 0 \\ 0 \\ -0.6702237 \end{pmatrix} \quad \begin{pmatrix} x_2 \\ y_2 \\ \dot{x}_2 \\ \dot{y}_2 \end{pmatrix} = \begin{pmatrix} 0.8801525 \\ 0 \\ 0 \\ 1.4047370 \end{pmatrix} \quad \begin{pmatrix} x_3 \\ y_3 \\ \dot{x}_3 \\ \dot{y}_3 \end{pmatrix} = \begin{pmatrix} -1.9026063 \\ 0 \\ 0 \\ -0.6343523 \end{pmatrix}$$

13. $A = 27.53447$, $\omega = 1/3$ (fig. 2.10r)

$$\begin{aligned} x_1(t) &= 1.1012493 \\ &\quad +0.2023926\cos(5t) + 0.0000131\cos(10t) + 0.0000734\cos(15t), \\ y_1(t) &= +0.2032551\sin(5t) - 0.0000092\sin(10t) + 0.0000742\sin(15t). \end{aligned}$$

$$E = -1.46075, \quad J = 2.51159.$$

Initial conditions:

$$\begin{pmatrix} x_1 \\ y_1 \\ \dot{x}_1 \\ \dot{y}_1 \end{pmatrix} = \begin{pmatrix} 1.3037285 \\ 0 \\ 0 \\ 1.4518695 \end{pmatrix} \quad \begin{pmatrix} x_2 \\ y_2 \\ \dot{x}_2 \\ \dot{y}_2 \end{pmatrix} = \begin{pmatrix} 0.8987962 \\ 0 \\ 0 \\ -0.7178872 \end{pmatrix} \quad \begin{pmatrix} x_3 \\ y_3 \\ \dot{x}_3 \\ \dot{y}_3 \end{pmatrix} = \begin{pmatrix} -1.9021805 \\ 0 \\ 0 \\ -0.6338938 \end{pmatrix}$$

The next three orbits were calculated with slightly changed masses $m_1 = m_2 = 1.05$, $m_3 = 0.9$.

14. $A = 12.20094$, $\omega = 1/3$ (fig. 2.9l)

$$\begin{aligned} x_1(t) &= 0.9144752 \\ &\quad +0.8086164\cos(t) + 0.0033078\cos(2t) + 0.0015123\cos(3t) \\ &\quad +0.0000802\cos(4t) + 0.0000162\cos(5t) + 0.0000032\cos(6t) \\ &\quad +0.0000001\cos(7t) + 0.0000002\cos(8t), \\ y_1(t) &= -0.8503844\sin(t) + 0.0016401\sin(2t) - 0.0022576\sin(3t) \\ &\quad +0.0000603\sin(4t) - 0.0000438\sin(5t) + 0.0000027\sin(6t) \\ &\quad -0.0000015\sin(7t) + 0.0000001\sin(8t). \end{aligned}$$

$$E = -0.647280, \quad J = 0.98928 \qquad .$$

Initial conditions:

$$\begin{pmatrix} x_1 \\ y_1 \\ \dot{x}_1 \\ \dot{y}_1 \end{pmatrix} = \begin{pmatrix} 1.7280117 \\ 0 \\ 0 \\ -0.2778443 \end{pmatrix} \quad \begin{pmatrix} x_2 \\ y_2 \\ \dot{x}_2 \\ \dot{y}_2 \end{pmatrix} = \begin{pmatrix} 0.1077216 \\ 0 \\ 0 \\ 0.8968330 \end{pmatrix} \quad \begin{pmatrix} x_3 \\ y_3 \\ \dot{x}_3 \\ \dot{y}_3 \end{pmatrix} = \begin{pmatrix} -2.1416888 \\ 0 \\ 0 \\ -0.7221535 \end{pmatrix}$$

15. $A = 15.79177$, $\omega = 1/3$ (fig. 2.9l)

$$
\begin{aligned}
x_1(t) &= 0.9041779 \\
&\quad +0.4924818\cos(t) + 0.0020992\cos(2t) + 0.0075928\cos(3t) \\
&\quad +0.0000306\cos(4t) + 0.0002459\cos(5t) + 0.0000009\cos(6t) \\
&\quad +0.0000103\cos(7t) + 0.0000005\cos(9t), \\
y_1(t) &= +0.5616499\sin(t) - 0.0018295\sin(2t) + 0.0078238\sin(3t) \\
&\quad -0.0000254\sin(4t) + 0.0002515\sin(5t) - 0.0000008\sin(6t) \\
&\quad +0.0000105\sin(7t) + 0.0000005\sin(9t).
\end{aligned}
$$

$$E = -0.837779, \quad J = 2.68412 \qquad .$$

Initial conditions:

$$
\begin{pmatrix} x_1 \\ y_1 \\ \dot{x}_1 \\ \dot{y}_1 \end{pmatrix} = \begin{pmatrix} 1.4066400 \\ 0 \\ 0 \\ 1.0515721 \end{pmatrix} \quad \begin{pmatrix} x_2 \\ y_2 \\ \dot{x}_2 \\ \dot{y}_2 \end{pmatrix} = \begin{pmatrix} 0.4059774 \\ 0 \\ 0 \\ -0.4548974 \end{pmatrix} \quad \begin{pmatrix} x_3 \\ y_3 \\ \dot{x}_3 \\ \dot{y}_3 \end{pmatrix} = \begin{pmatrix} -2.1147204 \\ 0 \\ 0 \\ -0.6961205 \end{pmatrix}
$$

16. $A = 16.61662$, $\omega = 1/3$ (fig. 2.9r)

$$
\begin{aligned}
x_1(t) &= 0.2077809 \\
&\quad +1.3038070\cos(t) - 0.0914475\cos(2t) + 0.0203737\cos(3t) \\
&\quad -0.0056247\cos(4t) + 0.0018176\cos(5t) - 0.0006076\cos(6t) \\
&\quad +0.0002209\cos(7t) - 0.0000809\cos(8t) + 0.0000312\cos(9t) \\
&\quad -0.0000120\cos(10t) + 0.0000048\cos(11t) - 0.0000019\cos(12t) \\
&\quad +0.0000008\cos(13t) - 0.0000003\cos(14t) + 0.0000001\cos(15t), \\
y_1(t) &= -1.2788394\sin(t) + 0.0918660\sin(2t) - 0.0197013\sin(3t) \\
&\quad +0.0056294\sin(4t) - 0.0017723\sin(5t) + 0.0006071\sin(6t) \\
&\quad -0.0002166\sin(7t) + 0.0000807\sin(8t) - 0.0000307\sin(9t) \\
&\quad +0.0000120\sin(10t) - 0.0000047\sin(11t) + 0.0000019\sin(12t) \\
&\quad -0.0000008\sin(13t) + 0.0000003\sin(14t) - 0.0000001\sin(15t).
\end{aligned}
$$

$$E = -0.647280, \quad J = 0.98928 \qquad .$$

Initial conditions:

$$\begin{pmatrix} x_1 \\ y_1 \\ \dot{x}_1 \\ \dot{y}_1 \end{pmatrix} = \begin{pmatrix} 1.4362621 \\ 0 \\ 0 \\ -0.6592213 \end{pmatrix} \quad \begin{pmatrix} x_2 \\ y_2 \\ \dot{x}_2 \\ \dot{y}_2 \end{pmatrix} = \begin{pmatrix} -1.2162501 \\ 0 \\ 0 \\ 1.1539316 \end{pmatrix} \quad \begin{pmatrix} x_3 \\ y_3 \\ \dot{x}_3 \\ \dot{y}_3 \end{pmatrix} = \begin{pmatrix} -0.2566807 \\ 0 \\ 0 \\ -0.5771620 \end{pmatrix}$$

B.3 Line symmetry

Here are all the solutions listed in the table. 3 and 4.

All orbits of the table 3 were calculated with masses $m_1 = 0.99$, $m_2 = 1.01$, $m_3 = 1.0$. The coordinates of the bodies m_1 and m_2 in the main system are given for the first and second bodies, the coordinates of the third body are determined from the condition $m_1\mathbf{r}_1 + m_2\mathbf{r}_2 + m_3\mathbf{r}_3 = 0$.

1. $A = 11.42286$, angular velocity of rotation of the base system: $\omega = 1/4$ (fig. 2.15l)

$$\begin{aligned}
x_1(t) &= 2.4587995 \\
&\quad +0.0000127\cos(t) + 0.0030937\cos(2t) + 0.0000034\cos(3t) \\
&\quad +0.0000446\cos(4t) + 0.0000001\cos(5t) + 0.0000011\cos(6t), \\
y_1(t) &= -0.0000051\sin(t) + 0.0016594\sin(2t) + 0.0000023\sin(3t) \\
&\quad +0.0000337\sin(4t) + 0.0000001\sin(5t) + 0.0000009\sin(6t), \\
x_2(t) &= -1.2109403 \\
&\quad -0.7430792\cos(t) - 0.0015371\cos(2t) - 0.0012838\cos(3t) \\
&\quad -0.0000225\cos(4t) - 0.0000121\cos(5t) - 0.0000005\cos(6t) \\
&\quad -0.0000002\cos(7t) \\
y_2(t) &= 0.7693911\sin(t) - 0.0007815\sin(2t) + 0.0015435\sin(3t) \\
&\quad -0.0000154\sin(4t) + 0.0000178\sin(5t) - 0.0000004\sin(6t) \\
&\quad +0.0000003\sin(7t), \\
0 &= m_1x_1(t) + m_2x_2(t) + m_3x_3(t) \quad , \\
0 &= m_1y_1(t) + m_2y_2(t) + m_3y_3(t) \quad .
\end{aligned}$$

$$E = -0.606002, \quad J = 1.36301 \quad .$$

Initial conditions:

$$\begin{pmatrix} x_1 \\ y_1 \\ \dot{x}_1 \\ \dot{y}_1 \end{pmatrix} = \begin{pmatrix} 2.4619552 \\ 0 \\ 0 \\ 0.6189505 \end{pmatrix} \quad \begin{pmatrix} x_2 \\ y_2 \\ \dot{x}_2 \\ \dot{y}_2 \end{pmatrix} = \begin{pmatrix} -1.9568757 \\ 0 \\ 0 \\ 0.2832669 \end{pmatrix} \quad \begin{pmatrix} x_3 \\ y_3 \\ \dot{x}_3 \\ \dot{y}_3 \end{pmatrix} = \begin{pmatrix} -0.4608912 \\ 0 \\ 0 \\ -0.8988605 \end{pmatrix}$$

2. $A = 12.04740$, $\omega = 1/3$ (fig. 2.16m)

$$\begin{aligned}
x_1(t) &= -1.0254852 \\
&\quad -0.7947362\cos(t) - 0.0035637\cos(2t) - 0.0016920\cos(3t) \\
&\quad -0.0000839\cos(4t) - 0.0000210\cos(5t) - 0.0000033\cos(6t) \\
&\quad -0.0000003\cos(7t) - 0.0000002\cos(8t), \\
y_1(t) &= 0.8409185\sin(t) - 0.0018340\sin(2t) + 0.0024956\sin(3t) \\
&\quad -0.0000664\sin(4t) + 0.0000502\sin(5t) - 0.0000029\sin(6t) \\
&\quad +0.0000017\sin(7t) - 0.0000001\sin(8t), \\
x_2(t) &= 2.0201695 \\
&\quad -0.0000351\cos(t) + 0.0070285\cos(2t) - 0.0000099\cos(3t) \\
&\quad +0.0001658\cos(4t) - 0.0000006\cos(5t) + 0.0000065\cos(6t) \\
&\quad + 0.0000003\cos(8t), \\
y_2(t) &= 0.0000227\sin(t) + 0.0035024\sin(2t) - 0.0000064\sin(3t) \\
&\quad +0.0001246\sin(4t) - 0.0000005\sin(5t) + 0.0000055\sin(6t) \\
&\quad + 0.0000003\sin(8t), \\
&\quad E = -0.639135, \quad J = 1.19429 \qquad .
\end{aligned}$$

Initial conditions:

$$\begin{pmatrix} x_1 \\ y_1 \\ \dot{x}_1 \\ \dot{y}_1 \end{pmatrix} = \begin{pmatrix} -1.8255858 \\ 0 \\ 0 \\ 0.2361876 \end{pmatrix} \quad \begin{pmatrix} x_2 \\ y_2 \\ \dot{x}_2 \\ \dot{y}_2 \end{pmatrix} = \begin{pmatrix} 2.0273250 \\ 0 \\ 0 \\ 0.6833141 \end{pmatrix} \quad \begin{pmatrix} x_3 \\ y_3 \\ \dot{x}_3 \\ \dot{y}_3 \end{pmatrix} = \begin{pmatrix} -0.2402684 \\ 0 \\ 0 \\ -0.9239731 \end{pmatrix}$$

3. $A = 12.06332$, $\omega = 1/3$ (fig. 2.16r)

$$
\begin{aligned}
x_1(t) &= 1.0155882 \\
&\quad +0.8003048\cos(t) + 0.0035375\cos(2t) + 0.0016793\cos(3t) \\
&\quad +0.0000834\cos(4t) + 0.0000203\cos(5t) + 0.0000033\cos(6t) \\
&\quad +0.0000003\cos(7t) + 0.0000002\cos(8t), \\
y_1(t) &= -0.8463483\sin(t) + 0.0018780\sin(2t) - 0.0024914\sin(3t) \\
&\quad +0.0000693\sin(4t) - 0.0000502\sin(5t) + 0.0000031\sin(6t) \\
&\quad -0.0000017\sin(7t) + 0.0000002\sin(8t), \\
x_2(t) &= 1.0149040 \\
&\quad -0.7845275\cos(t) + 0.0035518\cos(2t) - 0.0016657\cos(3t) \\
&\quad +0.0000844\cos(4t) - 0.0000211\cos(5t) + 0.0000033\cos(6t) \\
&\quad -0.0000003\cos(7t) + 0.0000002\cos(8t), \\
y_2(t) &= 0.8296341\sin(t) + 0.0016554\sin(2t) + 0.0024293\sin(3t) \\
&\quad +0.0000569\sin(4t) + 0.0000482\sin(5t) + 0.0000024\sin(6t) \\
&\quad +0.0000016\sin(7t) + 0.0000001\sin(8t), \\
&\quad E = -0.639979, \quad J = 1.17690 \qquad .
\end{aligned}
$$

Initial conditions:

$$
\begin{pmatrix} x_1 \\ y_1 \\ \dot{x}_1 \\ \dot{y}_1 \end{pmatrix} = \begin{pmatrix} 1.8212172 \\ 0 \\ 0 \\ -0.2429600 \end{pmatrix} \quad \begin{pmatrix} x_2 \\ y_2 \\ \dot{x}_2 \\ \dot{y}_2 \end{pmatrix} = \begin{pmatrix} 0.2323290 \\ 0 \\ 0 \\ 0.9181714 \end{pmatrix} \quad \begin{pmatrix} x_3 \\ y_3 \\ \dot{x}_3 \\ \dot{y}_3 \end{pmatrix} = \begin{pmatrix} -2.0376573 \\ 0 \\ 0 \\ -0.6868227 \end{pmatrix}
$$

4. $A = 12.07962$, $\omega = 1/3$ (fig. 2.16l)

$$
\begin{aligned}
x_1(t) &= -2.0408068 \\
&\quad +0.0000360\cos(t) - 0.0071516\cos(2t) + 0.0000100\cos(3t) \\
&\quad -0.0001696\cos(4t) + 0.0000006\cos(5t) - 0.0000067\cos(6t) \\
&\quad - 0.0000003\cos(8t), \\
y_1(t) &= -0.0000230\sin(t) - 0.0035606\sin(2t) + 0.0000065\sin(3t) \\
&\quad -0.0001275\sin(4t) + 0.0000005\sin(5t) - 0.0000056\sin(6t) \\
&\quad - 0.0000003\sin(8t), \\
x_2(t) &= 1.0050042 \\
&\quad -0.7901169\cos(t) + 0.0035262\cos(2t) - 0.0016534\cos(3t) \\
&\quad +0.0000838\cos(4t) - 0.0000205\cos(5t) + 0.0000033\cos(6t) \\
&\quad -0.0000003\cos(7t) + 0.0000002\cos(8t), \\
y_2(t) &= 0.8350880\sin(t) + 0.0016988\sin(2t) + 0.0024251\sin(3t) \\
&\quad +0.0000597\sin(4t) + 0.0000481\sin(5t) + 0.0000026\sin(6t) \\
&\quad +0.0000016\sin(7t) + 0.0000001\sin(8t), \\
&\quad E = -0.640844, \quad J = 1.15915 \qquad .
\end{aligned}
$$

Initial conditions:

$$
\begin{pmatrix} x_1 \\ y_1 \\ \dot{x}_1 \\ \dot{y}_1 \end{pmatrix} = \begin{pmatrix} -2.0480884 \\ 0 \\ 0 \\ -0.6903640 \end{pmatrix} \quad \begin{pmatrix} x_2 \\ y_2 \\ \dot{x}_2 \\ \dot{y}_2 \end{pmatrix} = \begin{pmatrix} 0.2168265 \\ 0 \\ 0 \\ 0.9185445 \end{pmatrix} \quad \begin{pmatrix} x_3 \\ y_3 \\ \dot{x}_3 \\ \dot{y}_3 \end{pmatrix} = \begin{pmatrix} 1.8086127 \\ 0 \\ 0 \\ -0.2442696 \end{pmatrix}
$$

5. $A = 13.15385$, $\omega = 1/2$ (fig. 2.13l)

$$
\begin{aligned}
x_1(t) &= -0.0001858 \\
&\quad +1.5847082\cos(t) + 0.0000014\cos(2t) + 0.0177719\cos(3t) \\
&\quad -0.0000383\cos(4t) + 0.0011124\cos(5t) - 0.0000059\cos(6t) \\
&\quad +0.0000996\cos(7t) - 0.0000009\cos(8t) + 0.0000105\cos(9t) \\
&\quad -0.0000001\cos(10t) + 0.0000012\cos(11t) + 0.0000001\cos(13t), \\
y_1(t) &= -1.5705460\sin(t) - 0.0000203\sin(2t) - 0.0174552\sin(3t) \\
&\quad +0.0000369\sin(4t) - 0.0010953\sin(5t) + 0.0000058\sin(6t) \\
&\quad -0.0000983\sin(7t) + 0.0000009\sin(8t) - 0.0000103\sin(9t) \\
&\quad +0.0000001\sin(10t) - 0.0000012\sin(11t) - 0.00000013\sin(13t), \\
x_2(t) &= 0.9549088 \\
&\quad -0.7802503\cos(t) - 0.0447622\cos(2t) - 0.0086749\cos(3t) \\
&\quad -0.0018774\cos(4t) - 0.0005381\cos(5t) - 0.0001487\cos(6t) \\
&\quad -0.0000477\cos(7t) - 0.0000147\cos(8t) - 0.0000050\cos(9t) \\
&\quad -0.0000016\cos(10t) - 0.0000006\cos(11t) - 0.0000002\cos(12t) \\
&\quad -0.0000001\cos(13t), \\
y_2(t) &= 0.7732548\sin(t) + 0.0502034\sin(2t) + 0.0085143\sin(3t) \\
&\quad +0.0020465\sin(4t) + 0.0005292\sin(5t) + 0.0001578\sin(6t) \\
&\quad +0.0000471\sin(7t) + 0.0000153\sin(8t) + 0.0000049\sin(9t) \\
&\quad +0.0000017\sin(10t) + 0.0000006\sin(11t) + 0.0000002\sin(12t) \\
&\quad +0.0000001\sin(13t), \\
&\quad E = -0.697833, \quad J = 0.92132 \qquad .
\end{aligned}
$$

Initial conditions:

$$
\begin{pmatrix} x_1 \\ y_1 \\ \dot{x}_1 \\ \dot{y}_1 \end{pmatrix} = \begin{pmatrix} 1.6034742 \\ 0 \\ 0 \\ -0.8272969 \end{pmatrix} \quad \begin{pmatrix} x_2 \\ y_2 \\ \dot{x}_2 \\ \dot{y}_2 \end{pmatrix} = \begin{pmatrix} 0.1185873 \\ 0 \\ 0 \\ 0.9707998 \end{pmatrix} \quad \begin{pmatrix} x_3 \\ y_3 \\ \dot{x}_3 \\ \dot{y}_3 \end{pmatrix} = \begin{pmatrix} -1.7072126 \\ 0 \\ 0 \\ -0.1614839 \end{pmatrix}
$$

6. $A = 13.15566$, $\omega = 1/2$ (fig. 2.13m)

$$
\begin{aligned}
x_1(t) &= \quad 0.7853020 \\
&\quad +0.9185030\cos(t) + 0.0123788\cos(2t) + 0.0007174\cos(3t) \\
&\quad +0.0006392\cos(4t) - 0.0000785\cos(5t) + 0.0000553\cos(6t) \\
&\quad -0.0000119\cos(7t) + 0.0000058\cos(8t) - 0.0000015\cos(9t) \\
&\quad +0.0000007\cos(10t) - 0.0000002\cos(11t), \\
y_1(t) &= -1.0156340\sin(t) + 0.0054098\sin(2t) - 0.0048317\sin(3t) \\
&\quad +0.0004925\sin(4t) - 0.0002508\sin(5t) + 0.0000477\sin(6t) \\
&\quad -0.0000211\sin(7t) + 0.0000052\sin(8t) - 0.0000022\sin(9t) \\
&\quad +0.0000006\sin(10t) - 0.0000002\sin(11t), \\
x_2(t) &= \quad 0.7841421 \\
&\quad -0.9006572\cos(t) + 0.0120906\cos(2t) - 0.0007959\cos(3t) \\
&\quad +0.0006083\cos(4t) + 0.0000640\cos(5t) + 0.0000507\cos(6t) \\
&\quad +0.0000098\cos(7t) + 0.0000051\cos(8t) + 0.0000012\cos(9t) \\
&\quad +0.0000006\cos(10t) + 0.0000002\cos(11t), \\
y_2(t) &= \quad 0.9959087\sin(t) + 0.0050418\sin(2t) + 0.0046806\sin(3t) \\
&\quad +0.0004424\sin(4t) + 0.0002357\sin(5t) + 0.0000414\sin(6t) \\
&\quad +0.0000191\sin(7t) + 0.0000044\sin(8t) + 0.0000019\sin(9t) \\
&\quad +0.0000005\sin(10t) + 0.0000002\sin(11t).
\end{aligned}
$$

$$E = -0.697930, \quad J = 0.93926.$$

Initial conditions:

$$
\begin{pmatrix} x_1 \\ y_1 \\ \dot{x}_1 \\ \dot{y}_1 \end{pmatrix} = \begin{pmatrix} 1.7175102 \\ 0 \\ 0 \\ -0.1596739 \end{pmatrix} \quad \begin{pmatrix} x_2 \\ y_2 \\ \dot{x}_2 \\ \dot{y}_2 \end{pmatrix} = \begin{pmatrix} -0.1044804 \\ 0 \\ 0 \\ 0.9711650 \end{pmatrix} \quad \begin{pmatrix} x_3 \\ y_3 \\ \dot{x}_3 \\ \dot{y}_3 \end{pmatrix} = \begin{pmatrix} -1.5948099 \\ 0 \\ 0 \\ -0.8228197 \end{pmatrix}
$$

7. $A = 13.15748$, $\omega = 1/2$ (fig. 2.13r)

$$
\begin{aligned}
x_1(t) &= \quad 0.9604700 \\
&\quad +0.7961963\cos(t) - 0.0459191\cos(2t) + 0.0089418\cos(3t) \\
&\quad -0.0019496\cos(4t) + 0.0005612\cos(5t) - 0.0001564\cos(6t) \\
&\quad +0.0000504\cos(7t) - 0.0000156\cos(8t) + 0.0000053\cos(9t) \\
&\quad -0.0000017\cos(10t) + 0.0000006\cos(11t) - 0.0000024\cos(12t) \\
&\quad +0.0000001\cos(13t), \\
y_1(t) &= -0.7891726\sin(t) + 0.0515043\sin(2t) - 0.0087900\sin(3t) \\
&\quad +0.0021245\sin(4t) - 0.0005532\sin(5t) + 0.0001658\sin(6t) \\
&\quad -0.0000498\sin(7t) + 0.0000163\sin(8t) - 0.0000053\sin(9t) \\
&\quad +0.0000018\sin(10t) - 0.0000006\sin(11t) + 0.0000002\sin(12t) \\
&\quad -0.0000001\sin(13t), \\
x_2(t) &= \quad 0.0001820 \\
&\quad -1.5681865\cos(t) - 0.0000020\cos(2t) - 0.0174586\cos(3t) \\
&\quad +0.0000379\cos(4t) - 0.0010860\cos(5t) + 0.0000058\cos(6t) \\
&\quad -0.0000967\cos(7t) + 0.0000009\cos(8t) - 0.0000101\cos(9t) \\
&\quad -0.0000001\cos(10t) - 0.0000012\cos(11t) - 0.0000001\cos(13t), \\
y_2(t) &= \quad 1.5543089\sin(t) + 0.0000206\sin(2t) + 0.0171498\sin(3t) \\
&\quad -0.0000365\sin(4t) + 0.0010694\sin(5t) - 0.0000057\sin(6t) \\
&\quad +0.0000954\sin(7t) - 0.0000008\sin(8t) + 0.0000100\sin(9t) \\
&\quad -0.0000001\sin(10t) + 0.0000011\sin(11t) + 0.0000001\sin(13t).
\end{aligned}
$$

$$E = -0.698026, \quad J = 0.95484.$$

Initial conditions:

$$
\begin{pmatrix} x_1 \\ y_1 \\ \dot{x}_1 \\ \dot{y}_1 \end{pmatrix} = \begin{pmatrix} 1.7181831 \\ 0 \\ 0 \\ 0.1530319 \end{pmatrix} \quad \begin{pmatrix} x_2 \\ y_2 \\ \dot{x}_2 \\ \dot{y}_2 \end{pmatrix} = \begin{pmatrix} -1.5866144 \\ 0 \\ 0 \\ 0.8184230 \end{pmatrix} \quad \begin{pmatrix} x_3 \\ y_3 \\ \dot{x}_3 \\ \dot{y}_3 \end{pmatrix} = \begin{pmatrix} -0.0985207 \\ 0 \\ 0 \\ -0.9781088 \end{pmatrix}
$$

8. $A = 14.08066$, $\omega = 1/3$ (fig. 2.17l)

$$
\begin{aligned}
x_1(t) &= -1.1631410 \\
&\quad -0.6647223\cos(t) + 0.0797437\cos(2t) - 0.0219619\cos(3t) \\
&\quad +0.0070258\cos(4t) - 0.0027062\cos(5t) + 0.0010668\cos(6t) \\
&\quad -0.0004591\cos(7t) + 0.0001984\cos(8t) - 0.0000983\cos(9t) \\
&\quad +0.0000411\cos(10t) - 0.0000193\cos(11t) + 0.0000091\cos(12t) \\
&\quad -0.0000044\cos(13t) + 0.0000021\cos(14t) - 0.0000010\cos(15t) \\
&\quad +0.0000005\cos(16t) - 0.0000002\cos(17t) + 0.0000001\cos(18t), \\
y_1(t) &= 0.6442871\sin(t) - 0.0834186\sin(2t) + 0.0211970\sin(3t) \\
&\quad -0.0071504\sin(4t) + 0.0026322\sin(5t) - 0.0010730\sin(6t) \\
&\quad +0.0004490\sin(7t) - 0.0001984\sin(8t) + 0.0000886\sin(9t) \\
&\quad -0.0000410\sin(10t) + 0.0000190\sin(11t) - 0.0000090\sin(12t) \\
&\quad +0.0000043\sin(13t) - 0.0000021\sin(14t) + 0.0000010\sin(15t) \\
&\quad -0.0000005\sin(16t) + 0.0000002\sin(17t) - 0.0000001\sin(18t), \\
x_2(t) &= 1.1416635 \\
&\quad -0.6630044\cos(t) - 0.0784310\cos(2t) - 0.0213022\cos(3t) \\
&\quad -0.0067024\cos(4t) - 0.0025495\cos(5t) - 0.0009880\cos(6t) \\
&\quad -0.0004200\cos(7t) - 0.0001784\cos(8t) - 0.0000802\cos(9t) \\
&\quad -0.0000358\cos(10t) - 0.0000167\cos(11t) - 0.0000077\cos(12t) \\
&\quad -0.0000037\cos(13t) - 0.0000017\cos(14t) - 0.0000008\cos(15t) \\
&\quad -0.0000004\cos(16t) - 0.0000002\cos(17t) - 0.0000001\cos(18t), \\
y_2(t) &= 0.6431607\sin(t) + 0.0821494\sin(2t) + 0.0205555\sin(3t) \\
&\quad +0.0068393\sin(4t) + 0.0024777\sin(5t) + 0.0009966\sin(6t) \\
&\quad +0.0004103\sin(7t) + 0.0001789\sin(8t) + 0.0000786\sin(9t) \\
&\quad +0.0000359\sin(10t) + 0.0000164\sin(11t) + 0.0000077\sin(12t) \\
&\quad +0.0000036\sin(13t) + 0.0000017\sin(14t) + 0.0000008\sin(15t) \\
&\quad +0.0000004\sin(16t) + 0.0000002\sin(17t) + 0.0000001\sin(18t).
\end{aligned}
$$

$E = -0.747002, \quad J = 0.85327.$

Initial conditions:

$$\begin{pmatrix} x_1 \\ y_1 \\ \dot{x}_1 \\ \dot{y}_1 \end{pmatrix} = \begin{pmatrix} -1.7650184 \\ 0 \\ 0 \\ -0.0670958 \end{pmatrix} \quad \begin{pmatrix} x_2 \\ y_2 \\ \dot{x}_2 \\ \dot{y}_2 \end{pmatrix} = \begin{pmatrix} 0.3679402 \\ 0 \\ 0 \\ 1.0432386 \end{pmatrix} \quad \begin{pmatrix} x_3 \\ y_3 \\ \dot{x}_3 \\ \dot{y}_3 \end{pmatrix} = \begin{pmatrix} 1.3757486 \\ 0 \\ 0 \\ -0.9872443 \end{pmatrix}$$

9. $A = 14.55725$, $\omega = 1/4$ (fig. 2.15m)

$$\begin{aligned}
x_1(t) \;=\;& 1.2760193 \\
& +0.6246577\cos(t) - 0.0998114\cos(2t) - 0.0319161\cos(3t) \\
& -0.0119562\cos(4t) + 0.0052425\cos(5t) - 0.0023848\cos(6t) \\
& +0.0011667\cos(7t) - 0.0005786\cos(8t) - 0.0002994\cos(9t) \\
& -0.0001559\cos(10t) + 0.0000835\cos(11t) - 0.0000448\cos(12t) \\
& +0.0000246\cos(13t) - 0.0000135\cos(14t) + 0.0000075\cos(15t) \\
& -0.0000042\cos(16t) + 0.0000024\cos(17t) - 0.0000013\cos(18t) \\
& +0.0000008\cos(19t) - 0.0000004\cos(20t) + 0.0000002\cos(21t) \\
& -0.0000001\cos(22t) + 0.0000001\cos(23t), \\
y_1(t) \;=\;& -0.5923739\sin(t) + 0.1005616\sin(2t) - 0.0303686\sin(3t) \\
& +0.0118430\sin(4t) - 0.0050473\sin(5t) + 0.0023532\sin(6t) \\
& -0.0011319\sin(7t) + 0.0005706\sin(8t) - 0.0002920\sin(9t) \\
& +0.0001538\sin(10t) - 0.0000817\sin(11t) + 0.0000443\sin(12t) \\
& -0.0000241\sin(13t) + 0.0000133\sin(14t) - 0.0000074\sin(15t) \\
& +0.0000041\sin(16t) - 0.0000023\sin(17t) + 0.0000013\sin(18t) \\
& -0.0000007\sin(19t) + 0.0000004\sin(28t) - 0.0000002\sin(15t) \\
& +0.0000001\sin(22t) - 0.0000001\sin(23t),
\end{aligned}$$

$$
\begin{aligned}
x_2(t) \;=\;& 0.0014364 \\
& -1.2297834\cos(t) - 0.0003099\cos(2t) - 0.0624906\cos(3t) \\
& +0.0001018\cos(4t) - 0.0102059\cos(5t) + 0.0000473\cos(6t) \\
& -0.0022582\cos(7t) + 0.0000179\cos(8t) - 0.0005761\cos(9t) \\
& +0.0000065\cos(10t) - 0.0001597\cos(11t) + 0.0000024\cos(12t) \\
& -0.0000467\cos(13t) + 0.0000009\cos(14t) - 0.0000142\cos(15t) \\
& +0.0000003\cos(16t) - 0.0000044\cos(17t) + 0.0000001\cos(18t) \\
& -0.0000014\cos(19t) - 0.0000005\cos(21t) - 0.0000002\cos(23t), \\
y_2(t) \;=\;& 1.1667228\sin(t) + 0.0003923\sin(2t) + 0.0594739\sin(3t) \\
& -0.0000882\sin(4t) + 0.0098267\sin(5t) - 0.0000442\sin(6t) \\
& +0.0021910\sin(7t) - 0.0000171\sin(8t) + 0.0005619\sin(9t) \\
& -0.0000063\sin(10t) + 0.0001563\sin(11t) - 0.0000023\sin(12t) \\
& +0.0000459\sin(13t) - 0.0000008\sin(14t) + 0.0000140\sin(15t) \\
& -0.0000003\sin(16t) + 0.0000044\sin(17t) - 0.0000001\sin(18t) \\
& +0.0000014\sin(19t) + 0.0000005\sin(21t) + 0.0000002\sin(23t).
\end{aligned}
$$

$$E = -0.772286, \quad J = 0.88706.$$

Initial conditions:

$$
\begin{pmatrix} x_1 \\ y_1 \\ \dot{x}_1 \\ \dot{y}_1 \end{pmatrix} = \begin{pmatrix} 1.8244692 \\ 0 \\ 0 \\ 0.0050039 \end{pmatrix} \quad \begin{pmatrix} x_2 \\ y_2 \\ \dot{x}_2 \\ \dot{y}_2 \end{pmatrix} = \begin{pmatrix} -1.3042376 \\ 0 \\ 0 \\ 1.0911701 \end{pmatrix} \quad \begin{pmatrix} x_3 \\ y_3 \\ \dot{x}_3 \\ \dot{y}_3 \end{pmatrix} = \begin{pmatrix} -0.4889446 \\ 0 \\ 0 \\ -1.1070357 \end{pmatrix}
$$

10. $A = 16.64808$, $\omega = 1/3$ (fig. 2.17r)

$$
\begin{aligned}
x_1(t) &= 0.4151006 \\
&\quad +0.0060072\cos(t) - 0.1803505\cos(2t) - 0.0001234\cos(3t) \\
&\quad -0.0086797\cos(4t) - 0.0000239\cos(5t) - 0.0007333\cos(6t) \\
&\quad -0.0000037\cos(7t) - 0.0000763\cos(8t) - 0.0000006\cos(9t) \\
&\quad -0.0000089\cos(10t) - 0.0000001\cos(11t) - 0.0000011\cos(12t) \\
&\quad - 0.0000001\cos(14t), \\
y_1(t) &= -0.0060556\sin(t) + 0.1810340\sin(2t) + 0.0001214\sin(3t) \\
&\quad +0.0086872\sin(4t) + 0.0000238\sin(5t) + 0.0007330\sin(6t) \\
&\quad +0.0000037\sin(7t) + 0.0000763\sin(8t) + 0.0000006\sin(9t) \\
&\quad +0.0000089\sin(10t) + 0.0000001\sin(11t) + 0.0000011\sin(12t) \\
&\quad + 0.0000001\sin(14t), \\
x_2(t) &= -0.2031046 \\
&\quad -1.3442445\cos(t) + 0.0882836\cos(2t) - 0.0173181\cos(3t) \\
&\quad +0.0042252\cos(4t) - 0.0011999\cos(5t) + 0.0003547\cos(6t) \\
&\quad -0.0001134\cos(7t) + 0.0000367\cos(8t) - 0.0000125\cos(9t) \\
&\quad +0.0000042\cos(10t) - 0.0000015\cos(11t) + 0.0000005\cos(12t) \\
&\quad -0.0000002\cos(13t) + 0.0000001\cos(14t), \\
y_2(t) &= 1.3232201\sin(t) - 0.0886276\sin(2t) + 0.0168853\sin(3t) \\
&\quad -0.0042298\sin(4t) + 0.0011773\sin(5t) - 0.0003546\sin(6t) \\
&\quad +0.0001118\sin(7t) - 0.0000367\sin(8t) + 0.0000123\sin(9t) \\
&\quad -0.0000042\sin(10t) + 0.0000015\sin(11t) - 0.0000005\sin(12t) \\
&\quad +0.0000002\sin(13t) - 0.0000001\sin(14t).
\end{aligned}
$$

$$E = -0.883208, \quad J = 2.39407.$$

Initial conditions:

$$
\begin{pmatrix} x_1 \\ y_1 \\ \dot{x}_1 \\ \dot{y}_1 \end{pmatrix} = \begin{pmatrix} 0.2311059 \\ 0 \\ 0 \\ 0.4734246 \end{pmatrix} \quad \begin{pmatrix} x_2 \\ y_2 \\ \dot{x}_2 \\ \dot{y}_2 \end{pmatrix} = \begin{pmatrix} -1.4730897 \\ 0 \\ 0 \\ 0.6930001 \end{pmatrix} \quad \begin{pmatrix} x_3 \\ y_3 \\ \dot{x}_3 \\ \dot{y}_3 \end{pmatrix} = \begin{pmatrix} 1.2590257 \\ 0 \\ 0 \\ -1.1686205 \end{pmatrix}
$$

11. $A = 16.76478$, $\omega = 1/3$ (fig. 2.18l)

$$
\begin{aligned}
x_1(t) &= -1.0153453 \\
&\quad -0.4446981\cos(2t) - 0.0003014\cos(4t) - 0.0004725\cos(6t) \\
&\quad -0.0000021\cos(8t) - 0.0000024\cos(10t), \\
y_1(t) &= 0.4526167\sin(2t) - 0.0001909\sin(4t) + 0.0005114\sin(6t) \\
&\quad -0.0000020\sin(8t) + 0.0000029\sin(10t), \\
x_2(t) &= 2.0004571 \\
&\quad -0.0000019\cos(2t) + 0.0006089\cos(4t) - 0.0000005\cos(6t) \\
&\quad +0.0000045\cos(8t), \\
y_2(t) &= 0.0000003\sin(2t) + 0.0003516\sin(4t) - 0.0000003\sin(6t) \\
&\quad +0.0000035\sin(8t).
\end{aligned}
$$

$$E = -0.889400, \quad J = 1.37020.$$

Initial conditions:

$$
\begin{pmatrix} x_1 \\ y_1 \\ \dot{x}_1 \\ \dot{y}_1 \end{pmatrix} = \begin{pmatrix} -1.4608219 \\ 0 \\ 0 \\ 0.4206104 \end{pmatrix} \quad \begin{pmatrix} x_2 \\ y_2 \\ \dot{x}_2 \\ \dot{y}_2 \end{pmatrix} = \begin{pmatrix} 2.0010682 \\ 0 \\ 0 \\ 0.6684559 \end{pmatrix} \quad \begin{pmatrix} x_3 \\ y_3 \\ \dot{x}_3 \\ \dot{y}_3 \end{pmatrix} = \begin{pmatrix} -0.5748652 \\ 0 \\ 0 \\ -1.0915448 \end{pmatrix}
$$

12. $A = 17.80747$, $\omega = 1/4$ (fig. 2.15r)

$$
\begin{aligned}
x_1(t) \;=\;& 0.6171166 \\
& +0.0057823\cos(t) - 0.2541723\cos(2t) - 0.0002086\cos(3t) \\
& -0.0293197\cos(4t) - 0.0001083\cos(5t) - 0.0056887\cos(6t) \\
& -0.0000397\cos(7t) - 0.0013469\cos(8t) - 0.0000140\cos(9t) \\
& -0.0003546\cos(10t) - 0.0000049\cos(11t) - 0.0000997\cos(12t) \\
& -0.0000017\cos(13t) - 0.0000293\cos(14t) - 0.0000006\cos(15t) \\
& -0.0000089\cos(16t) - 0.0000002\cos(17t) - 0.0000028\cos(18t) \\
& -0.0000001\cos(19t) - 0.0000009\cos(20t) - 0.0000003\cos(22t), \\
y_1(t) \;=\;& -0.0060241\sin(t) + 0.2522087\sin(2t) + 0.0001864\sin(3t) \\
& +0.0289724\sin(4t) + 0.0001041\sin(5t) + 0.0056214\sin(6t) \\
& +0.0000387\sin(7t) + 0.0013320\sin(8t) + 0.0000137\sin(9t) \\
& +0.0003510\sin(10t) + 0.0000048\sin(11t) + 0.0000988\sin(12t) \\
& +0.0000017\sin(13t) + 0.0000291\sin(14t) + 0.0000006\sin(15t) \\
& +0.0000088\sin(16t) + 0.0000002\sin(17t) + 0.0000028\sin(18t) \\
& +0.0000001\sin(19t) + 0.0000009\sin(20t) + 0.0000003\sin(22t), \\
x_2(t) \;=\;& -0.3018093 \\
& -1.1797243\cos(t) + 0.1244470\cos(2t) - 0.0382480\cos(3t) \\
& +0.0142880\cos(4t) - 0.0061867\cos(5t) + 0.0027551\cos(6t) \\
& -0.0013335\cos(7t) + 0.0006484\cos(8t) - 0.0003320\cos(9t) \\
& +0.0001697\cos(10t) - 0.0000899\cos(11t) + 0.0000474\cos(12t) \\
& -0.0000257\cos(13t) + 0.0000139\cos(14t) - 0.0000076\cos(15t) \\
& +0.0000042\cos(16t) - 0.0000023\cos(17t) + 0.0000013\cos(18t) \\
& -0.0000007\cos(19t) + 0.0000004\cos(20t) - 0.0000002\cos(21t) \\
& +0.0000001\cos(22t),
\end{aligned}
$$

$$
\begin{aligned}
y_2(t) \;=\;& 1.1333803\sin(t) - 0.1235162\sin(2t) + 0.0360720\sin(3t)\\
& -0.0141249\sin(4t) + 0.0059292\sin(5t) - 0.0027238\sin(6t)\\
& +0.0012902\sin(7t) - 0.0006415\sin(8t) + 0.0003232\sin(9t)\\
& -0.0001680\sin(10t) + 0.0000879\sin(11t) - 0.0000470\sin(12t)\\
& +0.0000252\sin(13t) - 0.0000138\sin(14t) + 0.0000075\sin(15t)\\
& -0.0000042\sin(16t) + 0.0000023\sin(17t) - 0.0000013\sin(18t)\\
& +0.0000007\sin(19t) - 0.0000004\sin(20t) + 0.0000002\sin(21t)\\
& -0.0000001\sin(22t).\\
& E=-0.944715, \quad J=2.06327.
\end{aligned}
$$

Initial conditions:

$$
\begin{pmatrix} x_1 \\ y_1 \\ \dot{x}_1 \\ \dot{y}_1 \end{pmatrix} = \begin{pmatrix} 0.3314955 \\ 0 \\ 0 \\ 0.7484256 \end{pmatrix} \quad \begin{pmatrix} x_2 \\ y_2 \\ \dot{x}_2 \\ \dot{y}_2 \end{pmatrix} = \begin{pmatrix} -1.3853849 \\ 0 \\ 0 \\ 0.6107577 \end{pmatrix} \quad \begin{pmatrix} x_3 \\ y_3 \\ \dot{x}_3 \\ \dot{y}_3 \end{pmatrix} = \begin{pmatrix} 1.0710582 \\ 0 \\ 0 \\ -1.3578066 \end{pmatrix}
$$

13. $A = 20.59152$, $\omega = 1/3$ (fig. 2.18m)

$$
\begin{aligned}
x_1(t) \;=\;& -1.0129392\\
& -0.3270151\cos(3t) - 0.0000730\cos(6t) - 0.0001847\cos(9t)\\
& -0.0000003\cos(12t) - 0.0000005\cos(15t),\\
y_1(t) \;=\;& 0.3297934\sin(3t) - 0.0000516\sin(6t) + 0.0001917\sin(9t)\\
& -0.0000003\sin(12t) + 0.0000005\sin(15t),\\
x_2(t) \;=\;& 1.9957611\\
& -0.0000004\cos(3t) + 0.0001514\cos(6t) - 0.0000001\cos(9t)\\
& +0.0000006\cos(12t),\\
y_2(t) \;=\;& 0.0000917\sin(6t) - 0.0000001\sin(9t)\\
& +0.0000005\sin(12t).\\
& E=-1.09241, \quad J=1.45497.
\end{aligned}
$$

Initial conditions:

$$\begin{pmatrix} x_1 \\ y_1 \\ \dot{x}_1 \\ \dot{y}_1 \end{pmatrix} = \begin{pmatrix} -1.3402127 \\ 0 \\ 0 \\ 0.5440633 \end{pmatrix} \quad \begin{pmatrix} x_2 \\ y_2 \\ \dot{x}_2 \\ \dot{y}_2 \end{pmatrix} = \begin{pmatrix} 1.9959126 \\ 0 \\ 0 \\ 0.6658596 \end{pmatrix} \quad \begin{pmatrix} x_3 \\ y_3 \\ \dot{x}_3 \\ \dot{y}_3 \end{pmatrix} = \begin{pmatrix} -0.6890612 \\ 0 \\ 0 \\ -1.2111409 \end{pmatrix}$$

The five orbits of the table 4 represent the orbit of B.3 ($m_1 = 0.99$, $m_2 = 1.01$, $m_3 = 1.0$, $\omega = 1/2$), but the masses of the bodies change: the sum of the masses remains the same $m_1 + m_2 + m_3 = 3$, the mass of the third body is the same $m_3 = 1.0$, and the masses of the first two bodies change. The initial orbit is shown in fig. 2.13, the next orbits are in Fig.2.14.

2. $m_1 = 0.95$, $A = 13.15312$.

$$
\begin{aligned}
x_1(t) &= -0.9718961 \\
&\quad +0.8281011\cos(t) + 0.0482772\cos(2t) + 0.0094930\cos(3t) \\
&\quad +0.0021012\cos(4t) + 0.0006103\cos(5t) + 0.0001729\cos(6t) \\
&\quad +0.0000562\cos(7t) + 0.0000177\cos(8t) + 0.0000061\cos(9t) \\
&\quad +0.0000020\cos(10t) + 0.0000007\cos(11t) + 0.0000002\cos(12t) \\
&\quad +0.0000001\cos(13t), \\
y_1(t) &= -0.8210266\sin(t) - 0.0541559\sin(2t) - 0.0093615\sin(3t) \\
&\quad -0.0022883\sin(4t) - 0.0006044\sin(5t) - 0.0001831\sin(6t) \\
&\quad -0.0000558\sin(7t) - 0.0000184\sin(8t) - 0.0000060\sin(9t) \\
&\quad -0.0000021\sin(10t) - 0.0000007\sin(11t) - 0.0000003\sin(12t) \\
&\quad -0.0000001\sin(13t), \\
x_2(t) &= -0.0008726 \\
&\quad -1.5351842\cos(t) + 0.0000157\cos(2t) - 0.0168301\cos(3t) \\
&\quad -0.0001851\cos(4t) - 0.0010354\cos(5t) - 0.0000282\cos(6t) \\
&\quad -0.0000914\cos(7t) - 0.0000041\cos(8t) - 0.0000095\cos(9t) \\
&\quad -0.0000006\cos(10t) - 0.0000011\cos(11t) - 0.0000001\cos(12t) \\
&\quad -0.0000001\cos(13t), \\
y_2(t) &= 1.5218700\sin(t) - 0.0001061\sin(2t) + 0.0165361\sin(3t) \\
&\quad +0.0001785\sin(4t) + 0.0010197\sin(5t) + 0.0000276\sin(6t) \\
&\quad +0.0000902\sin(7t) + 0.0000040\sin(8t) + 0.0000094\sin(9t) \\
&\quad +0.0000006\sin(10t) + 0.0000011\sin(11t) + 0.0000001\sin(12t) \\
&\quad +0.0000001\sin(13t).
\end{aligned}
$$

$$E = -0.697795, \quad J = 1.01964.$$

Initial conditions:

$$
\begin{pmatrix} x_1 \\ y_1 \\ \dot{x}_1 \\ \dot{y}_1 \end{pmatrix} = \begin{pmatrix} -0.0830573 \\ 0 \\ 0 \\ -1.0128514 \end{pmatrix} \quad \begin{pmatrix} x_2 \\ y_2 \\ \dot{x}_2 \\ \dot{y}_2 \end{pmatrix} = \begin{pmatrix} -1.5542266 \\ 0 \\ 0 \\ 0.8008997 \end{pmatrix} \quad \begin{pmatrix} x_3 \\ y_3 \\ \dot{x}_3 \\ \dot{y}_3 \end{pmatrix} = \begin{pmatrix} 1.7108424 \\ 0 \\ 0 \\ 0.1212641 \end{pmatrix}
$$

3. $m_1 = 0.9$, $A = 13.12580$.

$$
\begin{aligned}
x_1(t) &= 0.9867797 \\
&+0.8680048\cos(t) - 0.0513121\cos(2t) + 0.0102168\cos(3t) \\
&-0.0023053\cos(4t) + 0.0006774\cos(5t) - 0.0001959\cos(6t) \\
&+0.0000644\cos(7t) - 0.0000207\cos(8t) + 0.0000072\cos(9t) \\
&-0.0000025\cos(10t) + 0.0000009\cos(11t) - 0.0000003\cos(12t) \\
&+0.0000001\cos(13t), \\
y_1(t) &= -0.8608759\sin(t) + 0.0575678\sin(2t) - 0.0101159\sin(3t) \\
&+0.0025087\sin(4t) - 0.0006746\sin(5t) + 0.0002072\sin(6t) \\
&-0.0000644\sin(7t) + 0.0000215\sin(8t) - 0.0000072\sin(9t) \\
&+0.0000025\sin(10t) - 0.0000009\sin(11t) + 0.0000003\sin(12t) \\
&-0.0000001\sin(13t), \\
x_2(t) &= 0.0016527 \\
&-1.4940039\cos(t) - 0.0000447\cos(2t) - 0.0160397\cos(3t) \\
&+0.0003588\cos(4t) - 0.0009761\cos(5t) + 0.0000539\cos(6t) \\
&-0.0000859\cos(7t) + 0.0000077\cos(8t) - 0.0000090\cos(9t) \\
&+0.0000011\cos(10t) - 0.0000010\cos(11t) + 0.0000002\cos(12t) \\
&-0.0000001\cos(13t), \\
y_2(t) &= 1.4813854\sin(t) + 0.0002184\sin(2t) + 0.0157628\sin(3t) \\
&-0.0003464\sin(4t) + 0.0009613\sin(5t) - 0.0000528\sin(6t) \\
&+0.0000848\sin(7t) - 0.0000076\sin(8t) + 0.0000089\sin(9t) \\
&-0.0000011\sin(10t) + 0.0000010\sin(11t) - 0.0000002\sin(12t) \\
&+0.0000001\sin(13t).
\end{aligned}
$$

$$E = -0.697795, \quad J = 1.01964.$$

Initial conditions:

$$
\begin{pmatrix} x_1 \\ y_1 \\ \dot{x}_1 \\ \dot{y}_1 \end{pmatrix} = \begin{pmatrix} 1.8119145 \\ 0 \\ 0 \\ 0.1374498 \end{pmatrix} \quad \begin{pmatrix} x_2 \\ y_2 \\ \dot{x}_2 \\ \dot{y}_2 \end{pmatrix} = \begin{pmatrix} -1.5090859 \\ 0 \\ 0 \\ 0.7782846 \end{pmatrix} \quad \begin{pmatrix} x_3 \\ y_3 \\ \dot{x}_3 \\ \dot{y}_3 \end{pmatrix} = \begin{pmatrix} 0.0292715 \\ 0 \\ 0 \\ -0.9798179 \end{pmatrix}
$$

4. $m_1 = 0.8$, $A = 12.99779$.

$$
\begin{aligned}
x_1(t) &= 1.0187407 \\
&\quad +0.9479065\cos(t) - 0.0577004\cos(2t) + 0.0117944\cos(3t) \\
&\quad -0.0027693\cos(4t) + 0.0008342\cos(5t) - 0.0002517\cos(6t) \\
&\quad +0.0000849\cos(7t) - 0.0000285\cos(8t) + 0.0000102\cos(9t) \\
&\quad -0.0000036\cos(10t) + 0.0000013\cos(11t) - 0.0000005\cos(12t) \\
&\quad +0.0000002\cos(13t), \\
y_1(t) &= -0.9406877\sin(t) + 0.0647474\sin(2t) - 0.0117738\sin(3t) \\
&\quad +0.0030097\sin(4t) - 0.0008400\sin(5t) + 0.0002656\sin(6t) \\
&\quad -0.0000858\sin(7t) + 0.0000295\sin(8t) - 0.0000103\sin(9t) \\
&\quad +0.0000037\sin(10t) - 0.0000013\sin(11t) + 0.0000005\sin(12t) \\
&\quad -0.0000002\sin(13t), \\
x_2(t) &= 0.0029512 \\
&\quad -1.4118860\cos(t) - 0.0001321\cos(2t) - 0.0144396\cos(3t) \\
&\quad +0.0006700\cos(4t) - 0.0008701\cos(5t) + 0.0000982\cos(6t) \\
&\quad -0.0000782\cos(7t) + 0.0000138\cos(8t) - 0.0000085\cos(9t) \\
&\quad +0.0000020\cos(10t) - 0.0000010\cos(11t) + 0.0000003\cos(12t) \\
&\quad -0.0000001\cos(13t), \\
y_2(t) &= 1.4006287\sin(t) + 0.0004513\sin(2t) + 0.0141919\sin(3t) \\
&\quad -0.0006474\sin(4t) + 0.0008564\sin(5t) - 0.0000961\sin(6t) \\
&\quad +0.0000771\sin(7t) - 0.0000136\sin(8t) + 0.0000084\sin(9t) \\
&\quad -0.0000020\sin(10t) + 0.0000010\sin(11t) - 0.0000003\sin(12t) \\
&\quad +0.0000001\sin(13t).
\end{aligned}
$$

$$E = -0.689554, \quad J = 1.23654.$$

Initial conditions:

$$
\begin{pmatrix} x_1 \\ y_1 \\ \dot{x}_1 \\ \dot{y}_1 \end{pmatrix} = \begin{pmatrix} 1.9186183 \\ 0 \\ 0 \\ 0.1217978 \end{pmatrix} \quad \begin{pmatrix} x_2 \\ y_2 \\ \dot{x}_2 \\ \dot{y}_2 \end{pmatrix} = \begin{pmatrix} -1.4236802 \\ 0 \\ 0 \\ 0.7338794 \end{pmatrix} \quad \begin{pmatrix} x_3 \\ y_3 \\ \dot{x}_3 \\ \dot{y}_3 \end{pmatrix} = \begin{pmatrix} 0.1735216 \\ 0 \\ 0 \\ -0.9780935 \end{pmatrix}
$$

5. $m_1 = 0.7$, $A = 12.77091$.

$$
\begin{aligned}
x_1(t) &= 1.0540227 \\
&\quad +1.0279285\cos(t) - 0.0645670\cos(2t) + 0.0135723\cos(3t) \\
&\quad -0.0033221\cos(4t) + 0.0010283\cos(5t) - 0.0003239\cos(6t) \\
&\quad +0.0001124\cos(7t) - 0.0000393\cos(8t) + 0.0000145\cos(9t) \\
&\quad -0.0000054\cos(10t) + 0.0000020\cos(11t) - 0.0000008\cos(12t) \\
&\quad +0.0000003\cos(13t) - 0.0000001\cos(14t), \\
y_1(t) &= -1.0206325\sin(t) + 0.0724560\sin(2t) - 0.0136616\sin(3t) \\
&\quad +0.0036066\sin(4t) - 0.0010464\sin(5t) + 0.0003415\sin(6t) \\
&\quad -0.0001147\sin(7t) + 0.0000408\sin(8t) - 0.0000147\sin(9t) \\
&\quad +0.0000055\sin(10t) - 0.0000021\sin(11t) + 0.0000008\sin(12t) \\
&\quad -0.0000003\sin(13t) + 0.0000001\sin(14t), \\
x_2(t) &= 0.0039121 \\
&\quad -1.3300580\cos(t) - 0.0002462\cos(2t) - 0.0128062\cos(3t) \\
&\quad +0.0009266\cos(4t) - 0.0007788\cos(5t) + 0.0001331\cos(6t) \\
&\quad -0.0000741\cos(7t) + 0.0000187\cos(8t) - 0.0000088\cos(9t) \\
&\quad +0.0000027\cos(10t) - 0.0000012\cos(11t) + 0.0000004\cos(12t) \\
&\quad -0.0000002\cos(13t) + 0.0000001\cos(14t), \\
y_2(t) &= 1.3201375\sin(t) + 0.0006813\sin(2t) + 0.0125823\sin(3t) \\
&\quad -0.0008961\sin(4t) + 0.0007657\sin(5t) - 0.0001302\sin(6t) \\
&\quad +0.0000729\sin(7t) - 0.0000184\sin(8t) + 0.0000086\sin(9t) \\
&\quad -0.0000027\sin(10t) + 0.0000012\sin(11t) - 0.0000004\sin(12t) \\
&\quad +0.0000002\sin(13t) - 0.0000001\sin(14t).
\end{aligned}
$$

$$E = -0.677518, \quad J = 1.35872.$$

Initial conditions:

$$
\begin{pmatrix} x_1 \\ y_1 \\ \dot{x}_1 \\ \dot{y}_1 \end{pmatrix} = \begin{pmatrix} 2.0284225 \\ 0 \\ 0 \\ 0.1081788 \end{pmatrix} \quad \begin{pmatrix} x_2 \\ y_2 \\ \dot{x}_2 \\ \dot{y}_2 \end{pmatrix} = \begin{pmatrix} -1.3389798 \\ 0 \\ 0 \\ 0.6896437 \end{pmatrix} \quad \begin{pmatrix} x_3 \\ y_3 \\ \dot{x}_3 \\ \dot{y}_3 \end{pmatrix} = \begin{pmatrix} 0.3207779 \\ 0 \\ 0 \\ -0.9722619 \end{pmatrix}
$$